A THEORETICAL STUDY OF THE CONDENSATION OF PURE VAPORS, GAS-VAPOR MIXTURES, AND BINARY VAPOR MIXTURES IN LAMINAR FLOW IN THE ENTRANCE REGION OF A VERTICAL TUBE

A THESIS

Presented to

The Faculty of the Graduate Division

by

William A. Burns, Jr.

In Partial Fulfillment

of the Requirements for the Degree

Doctor of Philosophy

in the School of Chemical Engineering

Georgia Institute of Technology

December, 1965

In presenting the dissertation as a partial fulfillment of the requirements for an advanced degree from the Georgia Institute of Technology, I agree that the Library of the Institute shall make it available for inspection and circulation in accordance with its regulations governing materials of this type. I agree that permission to copy from, or to publish from, this dissertation may be granted by the professor under whose direction it was written, or, in his absence, by the Dean of the Graduate Division when such copying or publication is solely for scholarly purposes and does not involve potential financial gain. It is understood that any copying from, or publication of, this dissertation which involves potential financial gain will not be allowed without written permission.

3/17/65
b

A THEORETICAL STUDY OF THE CONDENSATION OF PURE VAPORS, GAS-VAPOR MIXTURES, AND BINARY VAPOR MIXTURES IN LAMINAR FLOW IN THE ENTRANCE REGION OF A VERTICAL TUBE

Approved:

Chairman

Date Approved by Chairman: 1/7/66

TO JUDY

ACKNOWLEDGMENTS

The author expresses his appreciation to his thesis advisor, Dr. Henderson C. Ward, for suggesting the problem and for his interest and helpful suggestions during this study. The constructive criticisms of Dr. William M. Newton and Dr. Charles W. Gorton, who served on the reading committee, are gratefully acknowledged.

Dr. Jack W. Whatley has discussed many of the ideas presented in this thesis with the author. Mr. Craig Wemmers has assisted the author in the preparation of figures and tables.

The large amount of computer time required by this study was made available by the Rich Electronic Computer Center.

The author is grateful for the financial assistance provided by the Dow Chemical Company Fellowship and the Ethyl Corporation Fellowship. In addition, Dr. Homer V. Grubb provided several teaching assistantships and part-time employment between quarters. Finally, both the author's parents and his wife's parents provided financial aid.

The author's wife, Judy W. Burns, typed the preliminary draft. Her interest and encouragement contributed greatly to the completion of this work.

TABLE OF CONTENTS

	Page
ACKNOWLEDGMENTS	iii
LIST OF TABLES	v
LIST OF FIGURES	xii
NOMENCLATURE	xvii
SUMMARY	xxi
CHAPTER	
I. INTRODUCTION	1
II. MATHEMATICAL DESCRIPTION OF THE PROBLEMS	15
III. CONDENSATION OF A PURE VAPOR	28
IV. CONDENSATION OF A VAPOR AND NONCONDENSABLE GAS MIXTURE	69
V. CONDENSATION OF A BINARY VAPOR MIXTURE	93
VI. CONCLUSIONS AND RECOMMENDATIONS	113
APPENDICES	
A. THE NUMERICAL SOLUTION OF THE MATHEMATICAL MODELS	116
B. OUTLINES OF THE COMPUTER PROGRAMS	166
C. COMPUTER PROGRAMS	175
D. PHYSICAL PROPERTIES	235
E. PURE VAPOR CONDENSATION RESULTS	238
F. GAS-VAPOR CONDENSATION RESULTS	264
G. BINARY VAPOR CONDENSATION RESULTS	285
LITERATURE CITED	300
VITA	305

LIST OF TABLES

Table		Page
1.	Correlation of Heat Transfer Results: Condensation of Pure Vapors	60
2.	Correlation of Carpenter Results (39): Condensation of Pure Vapors	64
3.	Comparison of Experimental Data With Predicted Results: Condensation of Pure Vapors	66
4.	Physical Properties of Pure Vapors and Air-Vapor Mixtures	236
5.	Physical Properties of Binary Vapor Mixtures	237
6.	Condensation of Water Vapor, Summary of Results: $D' = 0.03825$ Ft., $\Delta T' = 5^\circ$ F, $Pr_\ell = 1.79$, $C_p'\Delta T'/\lambda' = 0.00519$	239
7.	Condensation of Water Vapor, Summary of Results: $D' = 0.03825$ Ft., $\Delta T' = 10^\circ$ F, $Pr_\ell = 1.79$, $C_p'\Delta T'/\lambda' = 0.0104$	240
8.	Condensation of Water Vapor, Summary of Results: $D' = 0.03825$ Ft., $\Delta T' = 20^\circ$ F, $Pr_\ell = 1.79$, $C_p'\Delta T'/\lambda' = 0.0208$	241
9.	Condensation of Water Vapor, Summary of Results: $D' = 0.16667$ Ft., $\Delta T' = 5^\circ$ F, $Pr_\ell = 1.79$, $C_p'\Delta T'/\lambda' = 0.00519$	242
10.	Condensation of Water Vapor, Summary of Results: $D' = 0.16667$ Ft., $\Delta T' = 10^\circ$ F, $Pr_\ell = 1.79$, $C_p'\Delta T'/\lambda' = 0.0104$	243
11.	Condensation of Water Vapor, Summary of Results: $D' = 0.16667$ Ft., $\Delta T' = 20^\circ$ F, $Pr_\ell = 1.79$, $C_p'\Delta T'/\lambda' = 0.0208$	244
12.	Condensation of Ethanol Vapor, Summary of Results: $D' = 0.03825$ Ft., $\Delta T' = 5^\circ$ F, $Pr_\ell = 8.03$, $C_p'\Delta T'/\lambda' = 0.00924$	245

Table — Page

13. Condensation of Ethanol Vapor, Summary of Results: $D' = 0.03825$ Ft., $\Delta T' = 10^{\circ}$ F, $Pr_{\ell} = 8.03$, $C_p'\Delta T'/\lambda' = 0.0185$ 246

14. Condensation of Ethanol Vapor, Summary of Results: $D' = 0.03825$ Ft., $\Delta T' = 20^{\circ}$ F, $Pr_{\ell} = 8.03$, $C_p'\Delta T'/\lambda' = 0.0370$ 247

15. Condensation of Ethanol Vapor, Summary of Results: $D' = 0.16667$ Ft., $\Delta T' = 5^{\circ}$ F, $Pr_{\ell} = 8.03$, $C_p'\Delta T'/\lambda' = 0.00924$ 248

16. Condensation of Ethanol Vapor, Summary of Results: $D' = 0.16667$ Ft., $\Delta T' = 10^{\circ}$ F, $Pr_{\ell} = 8.03$, $C_p'\Delta T'/\lambda' = 0.0185$ 249

17. Condensation of Ethanol Vapor, Summary of Results: $D' = 0.16667$ Ft., $\Delta T' = 20^{\circ}$ F, $Pr_{\ell} = 8.03$, $C_p'\Delta T'/\lambda' = 0.0370$ 250

18. Condensation of Trichloroethylene Vapor, Summary of Results: $D' = 0.03825$ Ft., $\Delta T' = 5^{\circ}$ F, $Pr_{\ell} = 3.26$, $C_p'\Delta T'/\lambda' = 0.0118$ 251

19. Condensation of Trichloroethylene Vapor, Summary of Results: $D' = 0.03825$ Ft., $\Delta T' = 10^{\circ}$ F, $Pr_{\ell} = 3.26$, $C_p'\Delta T'/\lambda' = 0.0236$ 252

20. Condensation of Trichloroethylene Vapor, Summary of Results: $D' = 0.03825$ Ft., $\Delta T' = 20^{\circ}$ F, $Pr_{\ell} = 3.26$, $C_p'\Delta T'/\lambda' = 0.0471$ 253

21. Condensation of Trichloroethylene Vapor, Summary of Results: $D' = 0.16667$ Ft., $\Delta T' = 10^{\circ}$ F, $Pr_{\ell} = 2.26$, $C_p'\Delta T'/\lambda' = 0.0236$ 254

22. Radial and Axial Velocity Profiles in the Vapor Phase: Trichloroethylene, $D' = 0.03825$ Ft., $\Delta T' = 10^{\circ}$ F, $\bar{u}' = 100$ Ft./sec., $Re_g = 122213$, $Pr_{\ell} = 3.26$, $C_p'\Delta T'/\lambda' = 0.0236$ 255

23. Velocity and Temperature Profiles in the Liquid Phase: Trichloroethylene, $D' = 0.03825$ Ft., $\Delta T' = 10^{\circ}$ F, $\bar{u}' = 100$ ft./sec., $Re_g = 122213$, $Pr_{\ell} = 3.26$, $C_p'\Delta T'/\lambda' = 0.0236$ 256

Table		Page
24.	Radial and Axial Velocity Profiles in the Vapor Phase: Water, $D' = 0.03825$ Ft., $\Delta T' = 5^{\circ}$ F, $\bar{u}' = 10$ ft./sec., $Re_g = 1692$, $Pr_\ell = 1.79$, $C_p'\Delta T'/\lambda' = 0.00519$	258
25.	Velocity and Temperature Profiles in the Liquid Phase: Water, $D' = 0.03825$ Ft., $\Delta T' = 5^{\circ}$ F, $\bar{u}' = 10$ ft./sec., $Re_g = 1692$, $Pr_\ell = 1.79$, $C_p'\Delta T'/\lambda' = 0.00519$	259
26.	Radial and Axial Velocity Profiles in the Vapor Phase: Water, $D' = 0.16667$ Ft., $\Delta T' = 5^{\circ}$ F, $\bar{u}' = 100$ ft./sec., $Re_g = 73{,}739$, $Pr_\ell = 1.79$, $C_p'\Delta T'/\lambda' = 0.00519$	261
27.	Radial and Axial Velocity Profiles in the Vapor Phase: Water, $D' = 0.03825$ Ft., $\Delta T' = 5^{\circ}$ F, $\bar{u}' = 100$ ft./sec., $Re_g = 16{,}923$, $Pr_\ell = 1.79$, $C_p'\Delta T'/\lambda' = 0.00519$	262
28.	Radial and Axial Velocity Profiles in the Vapor Phase: Ethanol, $D' = 0.03825$ Ft., $\Delta T' = 10^{\circ}$ F, $\bar{u}' = 200$ ft./sec., $Re_g = 82{,}802$, $Pr_\ell = 8.03$ $C_p'\Delta T'/\lambda' = 0.0185$	263
29.	Condensation of Water Vapor from a Water Vapor and Air Mixture, Summary of Results: $D' = 0.16667$ Ft., $\bar{u}' = 100$ ft./sec., $Re_g = 73739$, $Pr_\ell = 1.79$, $Sc_g = 0.500$ . . .	265
30.	Condensation of Water Vapor From a Water Vapor and Air Mixture, Summary of Results: $D' = 0.16667$ Ft., $\bar{u}' = 25$ ft./sec., $Re_g = 18435$, $Pr_\ell = 1.79$, $Sc_g = 0.500$ . . .	266
31.	Condensation of Water Vapor From a Water Vapor and Air Mixture, Summary of Results: $D' = 0.16667$ Ft., $\bar{u}' = 25$ ft./sec., $Re_g = 18435$, $Pr_\ell = 1.79$, $Sc_g = 0.500$ . . .	267
32.	Condensation of Water Vapor From a Water Vapor and Air Mixture, Summary of Results: $D' = 0.16667$ ft., $\bar{u}' = 2.5$ ft./sec., $Re_g = 1843$, $Pr_\ell = 1.79$, $Sc_g = 0.500$ . . .	268
33.	Condensation of Water Vapor From a Water Vapor and Air Mixture, Summary of Results: $D' = 0.16667$ ft., $\bar{u}' = 25$ ft./sec., $Re_g = 18435$, $Pr_\ell = 1.79$, $Sc_g = 0.600$ . . .	269
34.	Condensation of Water Vapor From a Water Vapor and Air Mixture, Summary of Results: $D' = 0.16667$ ft., $\bar{u}' = 2.5$ ft./sec., $Re_g = 1843$, $Pr_\ell = 1.79$, $Sc_g = 0.600$ . . .	270

Table		Page
35.	Condensation of Water Vapor From a Water Vapor and Air Mixture, Summary of Results: $D' = 0.03825$ ft., $\bar{u}' =$ 25 ft./sec., $Re_g = 4231$, $Pr_\ell = 1.79$, $Sc_g = 0.500$	271
36.	Condensation of Ethanol Vapor From an Ethanol Vapor and Air Mixture, Summary of Results: $D' = 0.16667$ ft., $\bar{u}' =$ 200 ft./sec., $Re_g = 360793$, $Pr_\ell = 8.03$, $Sc_g = 0.537$ . . .	272
37.	Condensation of Ethanol Vapor From an Ethanol Vapor and Air Mixture, Summary of Results: $D' = 0.16667$ ft., $\bar{u}' =$ 100 ft./sec., $Re_g = 180397$, $Pr_\ell = 8.03$, $Sc_g = 0.537$ . . .	273
38.	Condensation of Ethanol Vapor From an Ethanol Vapor and Air Mixture, Summary of Results: $D' = 0.16667$ ft., $\bar{u}' =$ 25 ft./sec., $Re_g = 45099$, $Pr_\ell = 8.03$, $Sc_g = 0.537$	274
39.	Condensation of Ethanol Vapor From an Ethanol Vapor and Air Mixture, Summary of Results: $D' = 0.16667$ ft., $\bar{u}' =$ 25 ft./sec., $Re_g = 45099$, $Pr_\ell = 8.03$, $Sc_g = 0.537$	275
40.	Condensation of Ethanol Vapor From an Ethanol Vapor and Air Mixture, Summary of Results: $D' = 0.3825$ ft., $\bar{u}' =$ 25 ft./sec., $Re_g = 10350$, $Pr_\ell = 8.03$, $Sc_g = 0.537$	276
41.	Velocity, Concentration and Temperature Profiles in the Vapor Phase: Water Vapor and Air, $D' = 0.16667$ ft., $\bar{u}' = 25$ ft./sec., $Re_g = 18435$, $Pr_\ell =$ 1.79, $T_o' = 212^\circ$ F, $T_w' = 202^\circ$ F, $W_{air_o} \cong 0.05$, $Sc_g =$ 0.600	277
42.	Velocity, Concentration and Temperature Profiles in the Vapor Phase: Water Vapor and Air, $D' = 0.03825$ ft., $\bar{u}' = 25$ ft./sec., $Re_g = 4231$, $Pr_\ell =$ 1.79, $T_o' = 212^\circ$ F, $T_w' = 202^\circ$ F, $W_{air_o} \cong 0.05$, $Sc_g =$ 0.500	278
43.	Velocity, Concentration and Temperature Profiles in the Vapor Phase: Water Vapor and Air, $D' = 0.16667$ ft., $\bar{u}' = 2.5$ ft./sec., $Re_g = 1843$, $Pr_\ell =$ 1.79, $T_o' = 212^\circ$ F, $T_w' = 207^\circ$ F, $W_{air_o} = 0.01$, $Sc_g =$ 0.600	279
44.	Velocity and Temperature Profiles in the Liquid Phase: Water Vapor and Air, $D' = 0.16667$ ft., $T_o' = 212^\circ$ F, $T_w' = 207^\circ$ F, $Sc_g = 0.600$, $W_{air_o} = 0.01$	280

Table | Page

45. Velocity, Concentration and Temperature Profiles in the Vapor Phase: Ethanol Vapor and Air, $D' = 0.16667$ ft., $\bar{u}' = 25$ ft./sec., $Re_g = 45099$, $Pr_\ell = 8.08$, $T_o' = 173.3^\circ$ F, $T_w' = 153.3^\circ$ F, $W_{air_o} = 0.05$, $Sc_g = 0.537$ 281

46. Velocity, Concentration and Temperature Profiles in the Vapor Phase: Ethanol Vapor and Air, $D' = 0.16667$ ft., $\bar{u}' = 100$ ft./sec., $Re_g = 180397$, $Pr_\ell = 8.03$, $T_o' = 173.3^\circ$ F, $T_w' = 153.3^\circ$F, $W_{air_o} = 0.01$, $Sc_g = 0.537$ 282

47. Velocity, Concentration and Temperature Profiles in the Vapor Phase: Ethanol Vapor and Air, $D' = 0.16667$ ft., $\bar{u}' = 25$ ft./sec., $Re_g = 45099$, $Pr_\ell = 8.03$, $T_o' = 173.3^\circ$ F, $T_w' = 163.3^\circ$F, $W_{air_o} = 0.05$, $Sc_g = 0.537$ 283

48. Velocity and Temperature Profiles in the Liquid Phase: Ethanol Vapor and Air, $D' = 0.16667$ ft., $\bar{u}' = 25$ ft./sec., $Re_g = 45099$, $Pr_\ell = 8.03$, $T_o' = 173.3^\circ$ F, $T_w' = 163.3^\circ$F, $Sc_g = 0.537$, $W_{air_o} = 0.05$ 284

49. Condensation of Ethanol-Water Vapors, Summary of Results: $D' = 0.03825$ ft., $\bar{u}' = 25$ ft./sec., $Re_g = 4941$, $Pr_\ell = 4.17$, $Sc_g = 0.927$, $Sc_\ell = 276$, $T_{dp}'^g = 206.25^\circ$ F, $T_{bp}' = 186.5^\circ$ F, a = Ethanol 286

50. Condensation of Ethanol-Water Vapors, Summary of Results: $D' = 0.03825$ ft., $\bar{u}' = 50$ ft./sec., $Re_g = 9882$, $Pr_\ell = 4.17$, $Sc_g = 0.927$, $Sc_\ell = 276$, $T_{dp}'^g = 206.25^\circ$ F, $T_{bp}' = 186.5^\circ$ F, a = Ethanol 287

51. Condensation of Ethanol-Water Vapors, Summary of Results: $D' = 0.03825$ ft., $\bar{u}' = 100$ ft./sec., $Re_g = 19763$, $Pr_\ell = 4.17$, $Sc_g = 0.927$, $Sc_\ell = 276$, $T_{dp}'^g = 206.25^\circ$ F, $T_{bp}' = 186.5^\circ$ F, a = Ethanol 288

52. Condensation of Ethanol-Water Vapors, Summary of Results: $D' = 0.03825$ ft., $Pr_\ell = 4.17$, a = Ethanol, $W_{a_o} = 0.50$, $Sc_g = 0.762$, $Sc_\ell = 276$, $T_{dp}' = 197.2^\circ$ F, $T_{bp}' = 179.9^\circ$ F, $\Delta T' = 25.2^\circ$ F. 289

53. Condensation of Ethanol-Water Vapors, Summary of Results: $D' = 0.03825$ ft., $\bar{u}' = 100$ ft./sec., $Re_g = 30726$, $Pr_\ell = 4.17$, $Sc_g = 0.596$, $Sc_\ell = 276$, $T'_{dp} = 180.9^\circ$ F, $T_{bp}' = 175.5^\circ$ F, a = Ethanol 290

Table		Page
54.	Condensation of Benzene-Toluene Vapors, Summary of Results: $D' = 0.03825$ ft., $\bar{u}' = 2$ ft./sec., $Re_g = 2270$, $Pr_\ell = 4.11$, $Sc_g = 0.633$, $Sc_\ell = 8.79$, $T'_{dp} = 193.1^\circ$ F, $T'_{bp} = 184.7^\circ$ F, a = Toluene	291
55.	Condensation of Benzene-Toluene Vapors, Summary of Results: $D' = 0.03825$ ft., $\bar{u}' = 25$ ft./sec., $Re_g = 28378$, $Pr_\ell = 4.11$, $Sc_g = 0.633$, $Sc_\ell = 8.79$, $T'_{dp} = 193.1^\circ$ F, $T'_{bp} = 184.7^\circ$ F, a = Toluene	292
56.	Condensation of Benzene-Toluene Vapors, Summary of Results: $D' = 0.16667$ ft., $\bar{u}' = 25$ ft./sec., $Re_g = 123650$, $Pr_\ell = 4.11$, $Sc_g = 0.633$, $Sc_\ell = 8.79$, $T'_{dp} = 193.1^\circ$ F, $T'_{bp} = 184.7^\circ$ F, a = Toluene	293
57.	Condensation of Benzene-Toluene Vapors, Summary of Results: $D' = 0.03825$ ft., $Pr_\ell = 4.11$, a = Toluene, $W_{a_o} = 0.50$, $Sc_g = 0.621$, $Sc_\ell = 8.79$, $T'_{dp} = 207.3^\circ$ F, $T'_{bp} = 195.8^\circ$ F, $\Delta T' = 27.3^\circ$ F	294
58.	Condensation of Benzene-Toluene Vapors, Summary of Results: $D' = 0.03825$ ft., $\bar{u}' = 25$ ft./sec., $Re_g = 29581$, $Pr_\ell = 4.11$, $Sc_g = 0.608$, $Sc_\ell = 8.79$, $T'_{dp} = 219.9^\circ$ F, $T'_{bp} = 210.5^\circ$ F, a = Toluene	295
59.	Velocity, Temperature, and Concentration Profiles in the Liquid Phase: Ethanol-Water, $D' = 0.03825$ ft., $\bar{u}' = 100$ ft./sec., $Re_g = 19763$, $Pr_\ell = 4.17$, $W_{EtOH_o} = 0.25$, $T'_o = T'_{dp} = 206.25^\circ$ F, $T'_w = 182^\circ$ F, $Sc_g = 0.927$, $Sc_\ell = 276$, C = Weight fraction ethanol, q = Interface.	296
60.	Velocity, Concentration and Temperature Profiles in the Vapor Phase: Ethanol-Water, $D' = 0.03825$ ft., $\bar{u}' = 100$ ft./sec., $Re_g = 19763$, $Pr_\ell = 4.17$, $T'_o = 206.25^\circ$ F, $T'_w = 182^\circ$ F, $W_{EtOH_o} = 0.25$, $Sc_g = 0.927$, $Sc_\ell = 276$, C = Weight fraction ethanol . . .	297

Table | Page

61. Velocity, Temperature, and Concentration Profiles in the Liquid Phase: Benzene-Toluene, $D' = 0.03825$ ft., $\bar{u}' = 25$ ft./sec., $Re_g = 28967$, $Pr_\ell = 4.11$, $W_{Tol_o} = 0.50$, $T'_o = T'_{dp} = 207.3^\circ$ F, $T'_w = 180^\circ$ F, $Sc_g = 0.621$, $Sc_\ell = 8.79$, C = Weight fraction toluene, q = Interface 298

62. Velocity, Concentration and Temperature Profiles in the Vapor Phase: Benzene-Toluene, $D' = 0.03825$ ft., $\bar{u}' = 25$ ft./sec., $Re_g = 28967$, $Pr_\ell = 4.11$, $T'_o = 207.3^\circ$ F, $T'_w = 180^\circ$ F, $W_{Tol_o} = 0.50$, $Sc_g = 0.621$, $Sc_\ell = 8.79$, C = Weight fraction toluene 299

LIST OF FIGURES

Figure		Page
1.	Schematic Representation of the Mathematical Model	16
2.	Axial Velocity Profiles in the Vapor Phase: Water, $\Delta T' = 5^{\circ}$ F, $D' = 0.03825$ ft., $\bar{u}' = 10$ ft./sec.	30
3.	Centerline Velocity as a Function of Temperature drop Through the Liquid Film: Water, $D' = 0.03825$ ft., $\bar{u}' = 10$ ft./sec.	31
4.	Radial Velocity Profiles in the Vapor Phase: Water, $\Delta T' = 5^{\circ}$ F, $D' = 0.03825$ ft., $\bar{u}' = 10$ ft./sec.	33
5.	Axial and Radial Velocity Profiles Near the Gas-Liquid Interface: Water, $\Delta T' = 5^{\circ}$ F, $D' = 0.03825$ ft., $\bar{u}' =$ 10 ft./sec.	34
6.	Comparison of Liquid Axial Velocity Profiles with Simple Models: Water, $\Delta T' = 5^{\circ}$ F, $D' = 0.03825$ ft., $\bar{u}' =$ 10 ft./sec.	36
7.	Axial Velocity Profiles in the Vapor Phase: Trichloroethylene, $\Delta T' = 10^{\circ}$ F, $D' = 0.03825$ ft., $\bar{u}' =$ 100 ft./sec.	38
8.	Radial Velocity Profiles in the Vapor Phase: Trichloroethylene, $\Delta T' = 10^{\circ}$ F, $D' = 0.03825$ ft., $\bar{u}' = 100$ ft./sec.	39
9.	Axial and Radial Velocity Profiles Near the Gas-Liquid Interface: Trichloroethylene, $\Delta T' = 10^{\circ}$ F, $D' = 0.03825$ ft., $\bar{u}' = 100$ ft./sec.	41
10.	Comparison of Liquid Axial Velocity Profiles with Simple Models: Trichloroethylene, $\Delta T' = 10^{\circ}$ F, $D' = 0.03825$ ft., $\bar{u}' = 100$ ft./sec.	42
11.	Effect of Vapor Entrance Velocity on Liquid Film Thickness: Trichloroethylene, $\Delta T' = 10^{\circ}$ F, $D' = 0.03825$ ft. .	44
12.	Comparison of Film Thickness with Nusselt Model: Water, $\Delta T' = 20^{\circ}$ F, $D' = 0.03825$ ft., $\bar{u}' = 100$ ft./sec.	45

Figure Page

13. Pressure Drop During Condensation: Trichloroethylene, $\Delta T' = 5^{\circ}$ F, $D' = 0.03825$ ft. 46

14. Correlation of Interfacial Shear Stress: $\Delta T' = 10^{\circ}$ F . . 49

15. Average and Local Heat Transfer Ratios as Functions of Length: Water, $\Delta T' = 20^{\circ}$ F, $D' = 0.03825$ ft., $\bar{u}' = 100$ ft./sec. 51

16. Effect of Condenser Length and Entering Velocity on Heat Transfer: Water, $\Delta T' = 20^{\circ}$ F, $D' = 0.03825$ ft. . . 54

17. Effect of $z'\Delta T'$ on Heat Transfer: Trichloroethylene . . 55

18. Comparison of Carpenter Data with Numerical Results for a Tube 8.3 Feet Long and 0.03825 Feet in Diameter: Numerical Results with $\Delta T' = 20^{\circ}$ F and Carpenter Data at Various Temperature Drops 57

19. Detailed Comparison of Carpenter Data with Numerical Results for a Tube 8.3 Feet Long and 0.03825 Feet in Diameter: Water. 58

20. Importance of Length Froude Number as a Correlating Factor: Ethanol. 62

21. Effect of Noncondensable Concentration on Centerline Velocity: Water Vapor and Air, $D' = 0.16667$ ft., $\bar{u}' = 25$ ft./sec., $Re_g = 18435$, $Sc_g = 0.500$, $T'_o = 212^{\circ}$ F, $T'_w = 207^{\circ}$ F 71

22. Concentration Profile in the Vapor Phase: Water Vapor and Air, $D' = 0.16667$ ft., $\bar{u}' = 25$ ft./sec., $Re_g = 18435$, $Sc_g = 0.500$, $T'_o - T'_w = 5^{\circ}$ F, $W_{air_o} = 0.01$ 73

23. Effect of Velocity on Interfacial Concentration: Ethanol Vapor and Air, $D' = 0.16667$ ft., $Sc_g = 0.537$, $W_{air_o} = 0.01$, $T'_o = 173.3^{\circ}$ F, $T'_w = 163.3$ 74

24. Interfacial Concentration as a Function of Available Temperature Drop: Ethanol Vapor and Air, $D' = 0.16667$ ft., $\bar{u}' = 25$ ft./sec., $Re_g = 45099$, $Sc_g = 0.537$, $W_{air_o} = 0.05$, $T'_o = 173.3^{\circ}$ F. 75

25. Interface Temperature as a Function of Available Temperature Drop: Ethanol Vapor and Air, $D' = 0.16667$ ft., $\bar{u}' = 25$ ft./sec., $Re_g = 45099$, $Sc_g = 0.537$, $W_{air_o} = 0.05$, $T'_o = 173.3^{\circ}$ F 77

Figure Page

26. Effect of Noncondensable Concentration on Liquid Film Thickness: Water Vapor and Air, $D' = 0.16667$ ft., $\bar{u}' = 25$ ft./sec., $Re_g = 18435$, $Sc_g = 0.500$, $T'_o = 212^o$ F, $T'_w = 202^o$ F. 78

27. Effect of Noncondensable Concentration on Pressure Drop: Water Vapor and Air, $D' = 0.16667$ ft., $\bar{u}' = 25$ ft./sec., $Re_g = 18435$, $Sc_g = 0.600$, $T'_o = 212^o$ F, $T'_w = 202^o$ F . . . 80

28. Effect of Noncondensable Concentration on Average Heat Transfer Coefficients: Water Vapor and Air, $D' = 0.16667$ ft., $\bar{u}' = 25$ ft./sec., $Re_g = 18435$, $Sc_g = 0.500$, $T'_o = 212^o$ F, $T'_w = 202^o$ F 82

29. Effect of Noncondensable Concentration on Local Heat Transfer Coefficients: Water Vapor and Air, $D' = 0.16667$ ft., $\bar{u}' = 25$ ft./sec., $Re_g = 18435$, $Sc_g = 0.500$, $T'_o = 212^o$ F, $T'_w = 202^o$ F 83

30. Effect of Schmidt Number on Average Heat Transfer Coefficients: Water Vapor and Air, $D' = 0.16667$ ft., $\bar{u}' = 25$ ft./sec., $Re_g = 18435$, $T'_o = 212^o$ F, $T'_w = 202^o$ F, $W_{air_o} = 0.020$ 85

31. Effect of Condenser Length and Entering Velocity on Heat Transfer: Ethanol Vapor and Air, $D' = 0.16667$ ft., $T'_o = 173.3^o$F, $T'_w = 163.3^o$F, $W_{air_o} = 0.01$ 86

32. Effect of Available Temperature Drop on Heat Transfer: Ethanol Vapor and Air, $D' = 0.16667$ ft., $Sc_g = 0.537$, $z' = 8$ feet 88

33. Comparison of Calculation Methods: Water Vapor and Air, $\bar{u} = 25$ ft./sec., $D' = 0.16667$ ft., $T'_o = 212^o$ F, $T'_w = 202^o$ F, $W_{air_o} = 0.05$, $Sc_g = 0.5$, $Re_g = 18,435$ 90

34. Concentration Profiles in the Vapor Phase: Benzene-Toluene, $D' = 0.03825$ ft., $\bar{u}' = 100$ ft./sec., $Re_g = 115867$, $W_{Tol_o} = 0.50$, $T'_o = 207.3^o$ F, $T'_w = 180^o$ F 96

35. Concentration Profiles in the Liquid Phase: Benzene-Toluene, $D' = 0.03825$ ft., $\bar{u}' = 100$ ft./sec., $Re_g = 115867$, $W_{Tol_o} = 0.50$, $T'_o = 207.3^o$ F, $T'_w = 180^o$ F 97

36. Effects of Wall Temperature and Length on the Interface Temperature: Ethanol-Water, $D' = 0.03825$ ft., $\bar{u}' = 100$ ft./sec., $Re_g = 19763$, $W_{EtOH_o} = 0.25$ 99

Figure Page

37. Effects of Entrance Velocity and Length on the Interface Temperature: Ethanol-Water, $D' = 0.03825$ ft., $W_{EtOH_o} = 0.25$ $T'_w = 192^\circ$ F 100

38. Comparison of Temperature Base for Heat Transfer Coefficients: Benzene-Toluene, $D' = 0.03825$ ft., $\bar{u}' = 25$ ft./sec., $Re_g = 28967$, $W_{Tol} = 0.50$, $T'_o = T'_{dp} = 207.3^\circ$ F, $T'_{bp} = 195.8^\circ$ F, $T'_w = 180^\circ$ F 102

39. Effect of Entrance Concentration on Heat Transfer Coefficients (Based on $T'_{dp}-T'_w$): Ethanol-Water, $z'\Delta T' = 40$. 104

40. Effect of Temperature Drop on Heat Transfer Coefficient: Ethanol-Water, $D' = 0.03825$ ft., $\bar{u}' = 100$ ft./sec., $Re_g = 19{,}763$, $z' = 1.0$ ft.. 107

41. Comparison of Calculation Methods: Ethanol-Water, $D' = 0.03825$ ft., $\bar{u}' = 100$ ft./sec., $Re_g = 19763$, $W_{EtOH_o} = 0.25$, $T'_o = T'_{dp} = 206.25^\circ$ F, $T'_{bp} = 186.5^\circ$ F, $T'_w = 182^\circ$ F 110

42. Comparison of Heat Transfer Coefficient Predictions, Ethanol-Water, $D' = 0.03825$ ft., $\bar{u}' = 100$ ft./sec., $W_{EtOH_o} = 0.25$, $z' = 4$ ft., $Re_g = 19763$. 112

43. Diagram of Finite Difference Grid System 119

44. Difference Scheme for Motion, Energy, and Diffusion Equations 121

45. Difference Scheme for Continuity Equation 121

46. Diagram of Grid System Near Interface 123

47. Pressure and Velocity Matrix 149

48. Diffusion Equation for Component b in the Gas Phase . . . 153

49. Diffusion Equation for Component c in the Liquid Phase. . 153

50. Effect of Starting Position on Heat Transfer Results: Ethanol, $\Delta T' = 20^\circ$ F, $\bar{u}' = 200$ ft./sec., $D' = 0.019125$ ft 161

Figure Page

51. Effect of Starting Position on Interfacial Shear: Ethanol, $\Delta T' = 20^{\circ}$ F, $\overline{u}' = 200$ ft./sec., $D' =$ 0.019125 ft. 162

NOMENCLATURE

This table contains the definitions of the symbols used throughout this work. It does not contain symbols defined and used locally within the body of this work. Dimensional variables are primed to distinguish them from dimensionless variables.

Symbol	Definition
A'	area, ft.^{2}
C_p'	heat capacity, BTU/lb.-$^\circ$F.
D'	tube inner diameter, ft.
D_{ab}'	diffusion coefficient, ft.^{2}/sec.
e'	enthalpy, BTU/lb.
Ek	Eckert number, $\bar{u}'^2/C_p'(T_o' - T_w')$.
$\bar{f}$	Fanning friction factor of vapor phase.
f	dummy function.
Fr	Froude number, $\bar{u}'^2/g'D'$.
Fr_L	length Froude number, $\bar{u}'^2/g'z'$.
g'	acceleration due to gravity in the z direction, 32.174 ft./sec.^{2}
G_m'	average value of mass velocity of vapor, lb./sec.-ft.^{2}
he	radial step size, $R_{i+1}-R_i$.
h_m'	average heat transfer coefficient, BTU/sec.-ft.^{2}-$^\circ$F.
$h_{m_{Nu}}'$	average heat transfer coefficient derived by Nusselt, defined by equation (I-10), BTU/sec.-ft.^{2}-$^\circ$F.

Symbol	Definition
h'_m ratio	ratio of h'_m to $h'_{m_{Nu}}$
h'_{loc}	local heat transfer coefficient, BTU/sec.-ft.^{2}-^oF.
$h'_{loc_{Nu}}$	local heat transfer coefficient derived by Nusselt, defined by equation (I-9), BTU/sec.-ft.^{2}-^oF.
h'_{loc} ratio	ratio of h'_{loc} to $h'_{loc_{Nu}}$.
hw	radial step size, R_i-R_{i-1}.
$\underline{i}$	unit vector in the z direction.
$\underline{j}$	unit vector in the r direction.
k'	thermal conductivity, BTU/sec.-ft.-^oF.
N'	mass flux, lb./sec.-ft.^{2}
$\underline{N}'$	mass flux vector, defined by equation (A-80).
$\underline{n}$	normal vector, defined by equation (A-79).
P	dimensionless pressure drop, $(p'-p'_o)/\rho'\bar{u}'^2$.
p'	pressure, psia.
Pr	Prandtl number, $\mu' C'_p/k'$.
Q'	heat flow, BTU/sec.
R	dimensionless radius, $2r'/D'$.
ΔR	radial step size, defined locally.
r	radial direction.
r'	radius, ft.
$\Delta r'$	dimensional radial step size, $r'_{q+1}-r'_q$.
Re	Reynolds number, $\rho' D' \bar{u}'/\mu'$.
$\Delta s'$	dimensional grid arc size, $(\Delta r'^2 + \Delta z'^2)^{\frac{1}{2}}$.
Sc	Schmidt number, $\mu'/\rho' D'_{ab}$.
T	dimensionless temperature, $(T'-T'_w)/(T'_o-T'_w)$.

Symbol	Definition
T'	temperature, ^{o}F.
$\Delta T'$	$T'_o - T'_w$, ^{o}F.
$\underline{t}$	tangent vector, defined by equation (A-74).
U	dimensionless axial velocity, $v'_z / \bar{u}'$.
$\underline{U}'$	velocity vector, defined by equation (A-75).
$\bar{u}'$	average entrance velocity, ft./sec.
V	dimensionless radial velocity, $v'_r / \bar{u}'$.
v'_r	radial velocity, ft./sec.
v'_z	axial velocity, ft./sec.
W	weight fraction.
x'	distance from wall, ft.
Z	dimensionless tube length, $2z'/D'$.
ΔZ	axial step size, $Z_{j+1} - Z_j$.
Z^*	dimensionless tube length, $z'/D'Re$.
z	axial direction.
z'	tube length, ft.
$\Delta z'$	dimensional axial step size, $z'_{j+1} - z'_j$.
ZI	value of Z^* used as starting position in computer program.

Greek Symbols

Γ'	liquid film flow rate per unit width of wall, lb./sec.-ft.
δ'	liquid film thickness, ft.
λ'	latent heat of condensation, BTU/lb.
μ'	viscosity, lb./sec.-ft.

Symbol	Definition
ρ'	density, lb./ft.^{3}
τ'	interfacial shear stress, lb./ft.-sec.^{2}
τ^*	dimensionless interfacial stress, defined by equation (A-131).
Φ'	physical property group, defined by equation (III-1), BTU/sec.-ft.^{2}-$^\circ$F.
Subscripts	
a	condensable vapor.
b	noncondensable gas.
bp	bubble point of entering vapor.
c	condensable vapor.
dp	dew point of entering vapor.
g	vapor phase value.
i	radial grid coordinate.
j	axial grid coordinate.
ℓ	liquid phase value.
$\bar{n}$	normal to the interface.
n + 1	wall grid coordinate.
o	entrance value.
q	interface value or interface grid coordinate.
r	radial direction.
t	tangent to the interface.
w	wall value.
z	axial direction.
1	value at the first axial step.

SUMMARY

Numerical solutions to the laminar boundary layer equations of motion, continuity, energy, and diffusion for pure vapor, gas-vapor, and binary vapor condensation in the entrance region of vertical tubes are presented in this work. Three pure vapors: water, ethanol, and trichloroethylene; two gas-vapor mixtures; air-water, and air-ethanol; and two binary vapor mixtures: ethanol-water, and benzene-toluene are considered. For each system local and average heat transfer coefficients, pressure drop, average liquid concentrations, liquid film thicknesses, interfacial temperatures, and interfacial shear are reported for a variety of entrance velocities, tube lengths, tube diameters and temperature drops. In addition, the development of velocity, temperature, and concentration profiles in both phases is presented for each system as a function of length and radial position. These solutions are compared to experimental data where available and to existing design procedures.

Calculations using the laminar model were made for diameter Reynolds numbers of the entering vapor as high as 488,000. No claim is advanced that the flow is laminar at such Reynolds numbers, but there are reasons to suspect that transition to turbulent flow may occur at diameter Reynolds numbers far greater than 2100 and that the point of transition in the entrance region of a tube may be more dependent on the length Reynolds number than the diameter Reynolds

number. The length necessary for the development of turbulence may be an appreciable portion of condenser length. The effect of the liquid film on the transition of the vapor to turbulent flow is unknown. The film may induce turbulence in the vapor phase, but on the other hand, condensation may provide a stabilizing suction near the wall, thus delaying the formation of turbulence. Numerical solutions at high diameter Reynolds numbers provide insight into experimental results and agree with experimental data for diameter Reynolds numbers of the entering vapor below 30,000. More experimental data are necessary to determine the exact range of applicability of the laminar models.

The solutions to the equations and related boundary conditions were determined numerically by an implicit finite difference "marching" procedure with the aid of a high speed digital computer. The finite difference grid extended from the center of the tube to the wall and covered both phases. The step sizes varied in both the radial and the axial directions. At each axial step one of the grid points fell on the vapor-liquid interface. The axial step size was adjusted for each axial step until the normal heat flux into the liquid at the interface was properly balanced by the normal mass flux across the interface. Systems of equations similar to those used in this work have been shown to be stable and convergent by earlier workers. The results showed good agreement with the laminar, no interfacial shear model of Nusselt (2) when the interfacial shear was small. The numerical solutions also agreed with experimental data for diameter Reynolds numbers of the entering vapor less than 30,000.

A large number of boundary conditions were used with the equations. Some of these were continuity of tangential shear, tangential velocity, temperature, normal mass flux, and normal component flux across the interface. Others were various constant wall temperatures and "flat" velocity, temperature and concentration profiles at the entrance. Vapor-liquid equilibrium was assumed at the interface. The numerical scheme used to solve the equations and boundary conditions could be easily adapted to other condensation problems such as the condensation of superheated vapor, or the variation of wall temperature with length, or the use of parabolic velocity profiles at the entrance.

In pure vapor condensation the constant property equation of motion was applied to both phases separately, the constant property continuity equation was applied to both phases separately, and the constant property energy equation was applied to the liquid phase. A range of entrance velocities, temperature drops, and tube diameters was considered for the condensation of ethanol, water, and trichloroethylene vapors. The numerical results were compared to the experimental data of Carpenter and Colburn (1). The few points available at low vapor velocities (entering Reynolds numbers less than 30,000) appear to agree within 10 percent. At higher Reynolds numbers turbulence apparently exists causing the heat transfer to be much greater than that predicted by this study. However, the numerical solutions of this study qualitatively predict the dependence of the high velocity data on entrance velocity, tube diameter, tube length, temperature drop, and physical properties.

The numerical results for the average heat transfer coefficient for pure vapor condensation were correlated by a least squares procedure. For length Froude numbers below 10 the results may be adequately described by the Nusselt model, where

$$h'_{m_{Nu}} = \begin{matrix}\text{average Nusselt heat} \\ \text{transfer coefficient}\end{matrix} = 0.943 \left(\frac{k'^3_\ell g' \rho'^2_\ell \lambda'}{\mu'_\ell z' \Delta T'}\right)^{\frac{1}{4}}$$

and

$$Fr_L = \text{length Froude number} = \frac{\bar{u}'^2}{g' z'}$$

For length Froude numbers between 10 and 1000 the average heat transfer coefficient h'_m is given by

$$\frac{h'_m}{h'_{m_{Nu}}} = 0.747 \, (Fr_L)^{0.130}$$

This equation represented the numerical results with an average error of $\pm$ 3.8 percent. For length Froude numbers above 1000 the average heat transfer coefficient is given by

$$\frac{h'_m}{h'_{m_{Nu}}} = 0.188 \, (Fr_L)^{0.335}$$

with an average error of $\pm$ 7.2 percent. These correlations are felt to be good for a wide range of substances because of the use of the Nusselt model in the equations.

In the design of pure vapor condensers the method of Rohsenow, Webber, and Ling (5) appears to be good for both high and low vapor velocities.

In the gas-vapor condensation, density was allowed to vary with concentration. The equation of motion was applied to both phases separately, the energy equation was applied to both phases separately, the variable density equation of continuity was applied to the gas-vapor phase, and the constant density equation of continuity was applied to the liquid phase. The constant property diffusion equation was applied to the gas-vapor phase. Neglecting the variable density terms in the diffusion equation caused the overall mass balance to vary with length. Only those solutions were considered valid where the mass balance varied less than three percent. This compares favorably with an accuracy of five percent reported in the only other theoretical study of laminar gas-vapor condensation in a tube, which was done by Baasel and Smith (25).

A range of entrance velocities, wall temperatures, tube diameters and concentrations were considered for the condensation of water vapor from air-water vapor mixtures and ethanol vapor from air-ethanol vapor mixtures. The entrance composition ranged from 0.1 to 5 weight percent air. The concentration of air was higher at the interface than at the centerline. The presence of air at the interface caused the interface temperature to be lower than the entrance temperature because of the lower partial pressure of condensable vapor at the interface. The interface temperature varied with length as the concentration profile developed. This caused a significant decrease in heat transfer. While no data could be found in the entrance region of vertical tubes for the concentration range studied, the numerical

results qualitatively agreed with the experimental results of Othmer (20) on the dependence of heat transfer on air concentration. In addition, the numerical solutions approached those of pure vapor condensation as the air concentration became small.

The available methods of design for gas-vapor condensers do not include the effect of interfacial shear, which can be quite important for low noncondensable concentrations. The design method of Colburn and Hougen (21) for gas-vapor condensers predicts areas which are substantially smaller than the results of this study for the entering Reynolds numbers considered. Experimental studies should be undertaken to determine the range of applicability of these methods and a new design procedure, which includes the effect of entrance region interfacial shear, should be developed.

In binary vapor condensation the vapor density was allowed to vary with concentration. The equation of motion was applied to both phases separately, the equation of energy was applied to both phases separately, the variable density continuity equation was applied to the vapor phase, the constant density continuity equation was applied to the liquid phase, and the constant property diffusion equation was applied to both phases separately. Neglecting the variable density terms in the diffusion equation caused the overall mass balance to vary a maximum of five percent while the component balances varied a maximum of ten percent. Most runs were well below these maximums.

A number of entrance velocities, wall temperatures, tube diameters, and concentrations were considered for the condensation of

ethanol-water and benzene-toluene mixtures. Ethanol and water form a minimum boiling azeotrope while benzene and toluene form an almost ideal mixture. Vapor-liquid equilibrium was assumed at the interface. The interface temperature ranged between the bubble point and the dew point of the entering mixture and decreased with increasing tube length. The average concentrations in both phases varied widely with length. Diffusional resistances in the liquid were quite small.

There are apparently no data on binary condensation in the entrance region of a vertical pipe to compare with. Available data for other geometries indicate that the heat transfer coefficients for mixtures fall between results for the pure vapors. This behavior was also observed in the numerical solutions of this study. The results of this study indicate that the relative position of the heat transfer coefficient between the pure vapors as a function of concentration is expressed by the Nusselt equation given above when the proper mixture properties are used.

The available methods of design for binary vapor mixtures do not include the effect of shear, which can be quite important. The design method of Kern (29) for binary vapor condensers predicts areas which are smaller than the results of this study for the entering Reynolds numbers considered. Experimental studies should be undertaken to determine the range of applicability of these methods and a new design procedure, which includes the effect of entrance region shear, should be developed.

CHAPTER I

INTRODUCTION

Experimental studies (1) of condensation of a pure vapor in the entrance region of a vertical tube indicate that heat transfer can be much greater than predicted by the Nusselt model (2). Some investigators (3,4,5) have tried to explain these results by including the effect of shear at the vapor-liquid interface by evaluating shear from fully developed, one or two phase turbulent flow expressions and neglecting the fact that shear is much higher in the entrance region than in fully developed flow. Some of these investigators allowed shear to vary with length or used an average value of shear for the entire tube. There are apparently no solutions for gas-vapor or binary vapor condensation which include the effect of interfacial shear and developing profiles in the entrance region of vertical tubes.

This study was undertaken to provide solutions for the condensation of pure vapors, gas-vapor mixtures, and binary vapor mixtures in the entrance region of vertical tubes. These solutions consider how the velocity, temperature, concentration, and shear profiles develop in both phases. The laminar equations of continuity, motion, energy, and diffusion were used in the mathematical model, but calculations were made for diameter Reynolds numbers of the entering vapor as high as 488,000. It is not postulated that the flow is laminar at such diameter

Reynolds numbers, but the transition to turbulent flow may occur at diameter Reynolds numbers far greater than 2100. In addition, the point of transition in the entrance region of a tube may not be dependent on the diameter Reynolds number alone. Shapiro (6) has likened the flow near the entrance of a tube to that over a flat plate, where transition occurs at a length Reynolds number of about 5×10^5. During condensation, as tube length increases, the length Reynolds number of the vapor increases, reaches a maximum and then decreases. The diameter Reynolds number of the vapor decreases with increasing length. The length necessary for the development of turbulence may be an appreciable portion of the entrance length. The liquid film on the wall may possibly induce turbulence in the vapor, or condensation may possibly delay the formation of turbulence by providing a stabilizing suction near the wall. Numerical solutions at high diameter Reynolds numbers provide insight into experimental results and agree with experimental data for diameter Reynolds numbers of the entering vapor less than 30,000. More experimental data are necessary to determine the exact range of applicability of the laminar models.

The following literature survey will review the work of other investigators on liquid film behavior and condensation. A similar review was given by Cronauer (7).

Liquid Film

In film condensation the behavior of the liquid film is very important in determining heat transfer. Less heat transfer occurs through laminar films than through turbulent films of the same thick-

ness. There is some question, however, as to where the transition from laminar to turbulent film flow occurs. A number of investigators have considered the problem.

A simple laminar flow model of liquid flowing down a vertical wall with no shear at the vapor-liquid interface and no end or side effects (8) predicts that the velocity at the interface should be one and one half times the average velocity. Friedman and Miller (9) have shown that the surface velocity is considerably greater than this for film Reynolds numbers greater than 25. For Reynolds numbers greater than 25 they found that ripples were present in the film. By means of dye injection they discovered turbulence at the free interface down to a film Reynolds number of 200.

Measurements made by Stirba and Hurt (10) on mass transfer into liquid films from both the gas and the solid sides strongly indicate that the liquid film was not in laminar flow even for Reynolds numbers as low as 300.

Ripples can be eliminated by wetting agents and the film can remain apparently laminar up to a Reynolds number of approximately 3000. In such cases Emmert and Pigford (11) have found that mass transfer rates then check laminar theory.

It has been postulated by Carpenter and Colburn (1) that the condensate layer becomes turbulent at a much lower value of film Reynolds number if there is significant vapor velocity at the interface. They state, "... the hydrodynamics of a free flowing layer and one with a large frictional force are quite different." This vapor induced tur-

bulence was postulated for film Reynolds numbers as low as 240. They used this reasoning in trying to explain heat transfer data for high vapor velocity condensation.

Cooper, Drew, and McAdams (12) observed that liquid film holdup checks with the simple laminar model up to a Reynolds number of 1800 to 2000. This is the film Reynolds number normally considered as the onset of turbulence in the liquid. Average film thickness checks with theory also although at any one instant the thickness may deviate because of ripples on the surface.

In the absence of high vapor shear the Nusselt model of condensation (2) which includes simple laminar liquid flow provides accurate prediction of heat transfer results for film Reynolds numbers less than 2100. In practical application of the theory the predicted results are multiplied by a small correction factor to include the effect of rippling. Such a procedure is advocated by McCabe and Smith (13).

Pure Vapor Condensation

The classical approach to the condensation of pure vapor on a vertical wall was given by Nusselt (2) in 1916. He assumed:

1) Steady-state, laminar, non rippling liquid film.
2) Resistance to heat transfer exists in the liquid film only.
3) Heat is transferred by conduction in the x direction only.

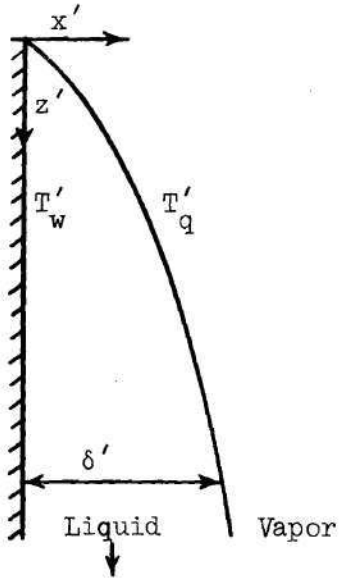

4) The interface and wall temperatures are constant and the temperature varies linearly between them.
5) Only latent heat is transferred. Sensible heat transfer is neglected.
6) Constant physical properties.
7) The acceleration of fluid elements in the film may be neglected in comparison with gravitational and viscous forces.

The equation of motion is

$$\mu'_\ell \frac{d^2 v'_z}{dx'^2} = - \rho'_\ell g' \qquad \text{(I-1)}$$

where primes denote dimensional variables and the subscript "ℓ" denotes a liquid value. This may be integrated twice and the boundary conditions of no shear at the interface and no velocity at the wall may be used to solve for the constants of integration. The result is

$$v'_z = \frac{\rho'_\ell g'}{\mu'_\ell} \left[x'\delta' - \frac{x'^2}{2} \right] \qquad \text{(I-2)}$$

The average velocity of the liquid film is

$$< v'_z > = \frac{1}{\delta'} \int_0^{\delta'} V'_z \, dx' = \frac{\rho'_\ell g'}{\mu'_\ell} \frac{\delta'^2}{3} \qquad \text{(I-3)}$$

The flow rate per unit width of wall, Γ', is

$$\Gamma' = \rho_\ell' < v_z' > \delta' = \frac{\rho_\ell'^2 g'}{\mu_\ell'} \frac{\delta'^3}{3} \tag{I-4}$$

and

$$d\Gamma' = \frac{\rho_\ell'^2 g'}{\mu_\ell'} \delta'^2 \, d\delta' \tag{I-5}$$

The energy balance in the film is

$$- \frac{Q'}{A'} dz' = \frac{k_\ell' \Delta T'}{\delta'} dz' = h_{loc}' \Delta T' \, dz' = \lambda' d\Gamma' = \frac{\lambda' \rho_\ell'^2 g' \delta'^2 d\delta'}{\mu_\ell'} \tag{I-6}$$

The film thickness may be found by

$$\int_0^{z'} \frac{\mu_\ell' k_\ell' \Delta T'}{\lambda' \rho_\ell'^2 g'} dz' = \int_0^{\delta'} \delta'^3 d\delta' \tag{I-7}$$

or

$$\delta' = \left(\frac{4 \mu_\ell' k_\ell' \Delta T' z'}{\lambda' \rho_\ell'^2 g'} \right)^{\frac{1}{4}} \tag{I-8}$$

The local heat transfer coefficient is given by

$$h_{loc}' = \frac{k_\ell'}{\delta'} = \left(\frac{k_\ell'^3 g' \rho_\ell'^2 \lambda'}{4 \mu_\ell' z' \Delta T'} \right)^{\frac{1}{4}} \tag{I-9}$$

The average heat transfer coefficient is given by

$$h_{m_{Nu}}' = \frac{1}{z'} \int_0^{z'} h_{loc}' \, dz' = 0.943 \left(\frac{k_\ell'^3 g' \rho_\ell'^2 \lambda'}{\mu_\ell' z' \Delta T'} \right)^{\frac{1}{4}} \tag{I-10}$$

This may be rearranged to give

$$h_m' \left(\frac{\mu_\ell'^2}{k_\ell'^3 \rho_\ell'^2 g'} \right)^{1/3} = 1.46 \left(\frac{4\Gamma'}{\mu_\ell'} \right)^{-1/3} \tag{I-11}$$

Other investigators have added refinements to the Nusselt theory over the years. Rohsenow (14) considered the nonlinear temperature distribution and the cooling of the liquid film, but neglected the acceleration terms and interfacial shear. Sparrow and Gregg (15) extended the analysis to include the acceleration terms by using boundary layer theory. Koh, Sparrow, and Hartnett (16) extended this analysis to include the interfacial vapor drag of a stagnant vapor phase. These added refinements are usually important only under extreme conditions, such as large values of $C'_{p_\ell} \Delta T'/\lambda'$ or physical properties in the range of liquid metals.

For condensation inside vertical tubes the high interfacial shear can be quite important, causing the liquid film thickness to deviate considerably from that predicted by the Nusselt model.

The condensation of high velocity pure vapors in a vertical tube was investigated experimentally by Carpenter and Colburn (1). The vapor entered a small chamber above the condenser and flowed downward with velocities varying up to almost 600 feet per second. No attempt was made to insure a "flat" entrance profile. The resulting heat transfer was much greater than predicted by equation (I-11) of the Nusselt model. They presented a correlation of their results and postulated that the high vapor shear causes the liquid film to become turbulent at film Reynolds numbers as low as 240.

Several investigators have theoretically attacked condensation in vertical tubes with downward vapor flow. Jakob (3) reported on the earlier attempts by Nusselt (1) to include vapor shear at the inter-

face. He did not allow the vapor velocity to vary with tube length, and evaluated the interfacial shear by using a fully developed, one phase, turbulent flow, friction factor expression. Hartmann (4) performed a similar analysis, but allowed the vapor velocity and shear to vary with tube length. He also used a fully developed, one phase, turbulent flow, friction factor expression to evaluate shear. He presented his heat transfer results graphically and with a correlating equation. He also presented an equation which correlates the results reported by Jakob.

Rohsenow, Webber, and Ling (5) considered the interfacial shear to have a constant value over the length of the condenser. They allowed the liquid film to change from laminar flow to turbulent flow as postulated by Carpenter and Colburn. This transition is a function of the interfacial shear and fluid properties. They presented their results in graphical form. To use their results an average value of shear is estimated from fully developed, one phase, turbulent flow friction factor expressions or from experimental cocurrent gas-liquid flow data.

Gas-Vapor Condensation

There appear to be no data available on the condensation of a vapor and noncondensable gas mixture in the entrance of a tube. Some data are reported (17,18,19) for gas-vapor mixtures in tubes, but the noncondensable concentration was much larger than covered in this study and a long calming section was used before the condenser. Such data and the data of Othmer (20) for the condensation of steam from

steam-air mixtures on a horizontal cylinder indicate that heat transfer decreases markedly as the amount of noncondensable increases.

The classical approach to the design of condensers for turbulent gas-vapor mixtures was given by Colburn and Hougen (21). They postulated that the major resistance to heat transfer is diffusion of the condensable component to the interface and not the liquid layer as in pure vapor condensation. The presence of noncondensable gas at the interface reduces the partial pressure of the condensable component thus reducing the interface temperature. Colburn and Hougen recommend using a point to point method for calculating the necessary heat transfer area. A condensing curve is constructed and from this curve the amount condensed and the heat transferred in each section may be calculated. With an equation summing up the resistances to condensation over a section, the heat transfer coefficient and the interface temperature in that section may be calculated. From these the area of that section is calculated. The Colburn and Hougen method does not include the effects of interfacial shear on the liquid phase. It applies to situations where the vapor phase is controlling. In these situations the effect of interfacial shear is relatively unimportant.

Smith (22) extended the Colburn and Hougen method to include cooling of the condensate layer. This can become important for organic vapors where the latent heat of vaporization is small. For organic vapors the Colburn and Hougen method estimates areas which are slightly too large.

Other stepwise methods have been proposed which offer slight

improvement over the Colburn and Hougen method. Mizushina, Nakajima, and Oshima (17) compare their graphical step by step method and the methods of Hulden (23) and Colburn and Hougen with experimental measurements. For a water-air run with an entering Reynolds number of about 21,000 the method of Mizushina, et al., estimates an area 3.1 percent too large. Colburn and Hougen's method estimates an area 4.6 percent too large while Hulden's method estimates an area 1.5 percent too small. For a benzene-air mixture the three methods estimate areas 3.9 percent too large, 10.8 percent too large, and 3.1 percent too small, respectively. These methods appear to work fairly well for large concentrations of noncondensable gas where the liquid film is not controlling.

Sparrow and Lin (24) and Baasel and Smith (25) have provided mathematical solutions for the condensation of gas-vapor mixtures where the flow was laminar. Sparrow and Lin investigated condensation on a vertical wall immersed in a large body of gas-vapor mixture. Concentrations of up to five weight percent noncondensable were investigated. They did not include interfacial shear effects or allow the interfacial concentration to change with length. The results are presented graphically. Baasel and Smith investigated condensation inside vertical tubes. They assumed parabolic entrance flow and did not consider the flow of liquid in their model. Only the equations of diffusion and continuity in the gas-vapor phase were considered. They did not allow interfacial concentration to vary with length, and considered vapor Reynolds numbers less than 2100. One must know the concentration of

noncondensable at the interface to use the results of their work.

Binary Vapor Condensation

In considering binary vapor condensation, Colburn and Drew (26) postulated equilibrium at the vapor-liquid interface and assumed there was resistance to condensation in both phases. They showed that the interface temperature varied between the dew point and the bubble point of the vapor depending on the various resistances. Their approach is useful in understanding the mechanism of binary condensation, but actually only predicts the composition of the first drop of condensate at the entrance of a condenser.

For making calculations on the total condensation of binary mixtures in a vertical tube where the coolant inlet temperature is below the boiling point of the most volatile components Colburn (27) suggests using the bubble point temperature of the entering vapor as the interface temperature at the top of the condenser and the boiling point of the most volatile component (or azeotrope, if formed) at the bottom of the condenser. This approach is unrealistic when the component balance down the tube is considered.

van Es and Heertjes (28) tried to extend the Colburn and Drew theory to practical calculations for a condenser of finite length. Their relations are restricted to cases where the compositions of the liquid and the vapor do not change with length. This method cannot apply to complete or nearly complete condensation.

Kern (29) recommends using differential condensation to make practical condenser calculations. This approach neglects the presence

of a vapor film and the effects of interfacial shear on the liquid layer. The heat transfer coefficient is calculated by the substitution of liquid mixture properties into the Nusselt equation, equation (I-10).

McAdams (30) recommends using the bubble point temperature of the entering vapor as the interface temperature for the entire length of condenser.

Haselden and Platt (31) have reviewed the existing methods of calculating heat transfer for condensing binary vapors. They find that at large temperature differences, $T'_{dp}-T'_{w} > 50^{o}$ F, the predictions of McAdams, Colburn, and Kern agree. At lower temperature differences they feel that Kern's method is fictitious and that the predictions of McAdams and Colburn are "too conservative for a well designed condenser." The Colburn method is more conservative than the McAdams method. They state that there is no satisfactory design method for low temperature drops.

A number of investigators have made experimental studies of binary vapor condensation to test the Colburn and Drew theory. None of these studies were made in the entrance region of a vertical tube. However, these studies are valuable in determining the interfacial temperature and concentration dependence of heat transfer coefficients.

Wallace and Davison (32) investigated the condensation of ethanol-water mixtures on a horizontal cylinder. Total condensation was achieved in most cases. This provided limited verification of the Colburn and Drew theory. They reported "extreme difficulty" in

maintaining constant inlet composition as the molal percent of water in the vapor increased to about 50. The composition of the vapor was allowed to vary of its own accord or by dilution.

Pressburg and Todd (33) investigated the condensation of five ideal and nonideal pairs of vapors which gave miscible condensates. The vapors condensed on a horizontal cylinder. Almost total condensation was achieved. Their data indicated that the bubble point of the condensate (the same as the entering vapor) was the proper choice for the interface temperature and that heat transfer coefficients when calculated on this basis fell between the results of the pure vapors and showed an approximately linear dependence on molar concentration.

Mirkovich and Missen (34) performed experiments similar to those of Pressburg and Todd. They investigated binary systems which gave both filmwise and nonfilmwise condensation. The nonfilmwise condensation (streaks) occurred for low temperature drops and certain compositions of two of the four solutions investigated. The nonfilmwise condensation caused heat transfer coefficients to be higher than for filmwise condensation. They did not observe linear dependence of heat transfer coefficients with composition, but did conclude that the interface temperature is the bubble point of the entering vapor.

Finally, Cronauer (7) investigated the condensation of three systems of binary vapors. Vapor was condensed on the inside of a vertical tube, but reflux was provided at the top of the tube to provide a wide variation of film Reynolds numbers. There was a calming tube for vapor located above the place of reflux addition and a

cooled calming section below the place where reflux was added. Below this calming section were several two inch test sections. No data on vapor flow rates were given but the vapor rate was usually adjusted until all condensed in the apparatus. The data from this experiment are not felt to be applicable to binary condensation in the entrance region of a tube. The addition of reflux and the calming section prevented the determination of the true effects of fractionation, length, varying vapor friction, etc. However, Cronauer did observe approximately linear dependence of heat transfer coefficients on composition for two of the systems but not for the third.

CHAPTER II

MATHEMATICAL DESCRIPTION OF THE PROBLEMS

Three cases of condensation in the entrance length of a vertical tube will be considered: pure vapor, vapor and noncondensable gas; and binary vapors. A diagram of the physical problem is shown in Fig. 1, and all terms and symbols used in this work are defined in the Nomenclature. The vapor phase is assumed to have uniform velocity, temperature, and concentration profiles at the entrance of the tube. Vapor condenses in a film on the cold inside tube wall, and both phases flow downward under the influence of pressure, gravity, and shear forces.

These problems may be described mathematically. The general, laminar equations of motion, continuity, energy, and diffusion are given by Bird, Stewart, and Lightfoot (8). The following assumptions will be made for each of the three cases of condensation under consideration:

1. Laminar flow exists in both the gas and the liquid phases.
2. The equation of motion in the radial direction may be neglected.
3. No angular velocity or angular dependence of any value exist.
4. Steady-state exists.
5. Momentum transfer by viscous action in the axial direction is negligible.
6. Heat conduction in the axial direction is negligible.

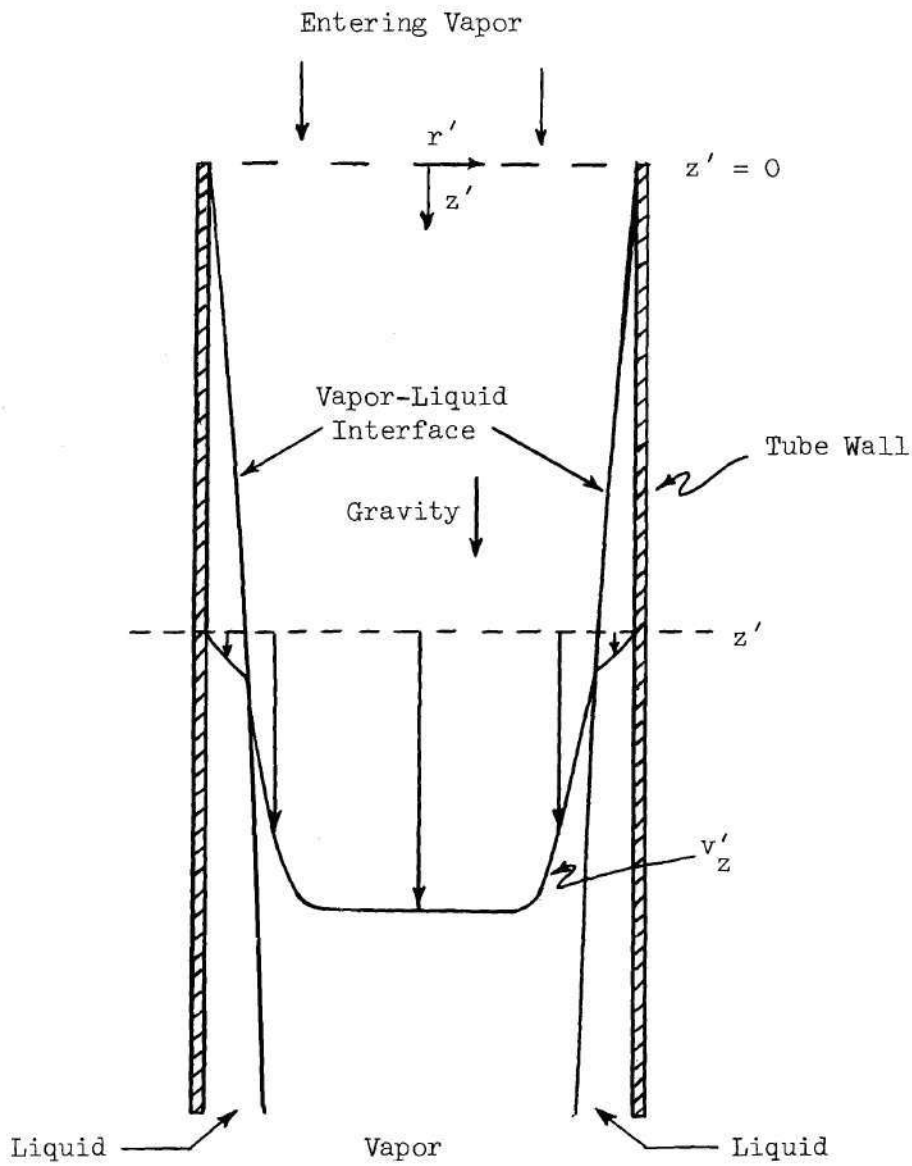

Fig. 1. Schematic Representation of the Mathematical Model

7. Diffusion of mass in the axial direction is negligible.

8. Velocity, concentration, and temperature profiles are uniform at the tube entrance.

Assumptions 2, 5, 6 and 7 may be justified by an order analysis similar to that performed by Lee (35). In applying Lee's analysis to the problem of condensation in the entrance length of a tube, it is assumed that the radial velocity is still an order of magnitude smaller than the axial velocity.

Assumption 1 might preclude the application of these equations to many cases of practical interest where vapor velocities are more than likely in the turbulent region. However, calculations using the laminar model were made for Reynolds numbers of the entering vapor as high as 488,000. No claim is advanced that the flow is laminar at such Reynolds numbers, but the calculations were made nevertheless for the following reasons: 1. There are reasons to suspect that transition to turbulent flow may occur at diameter Reynolds numbers far greater than 2100 and that the point of transition in the entrance region of a tube may not be dependent on the diameter Reynolds number alone. Shapiro (6) states that one phase flow "near the inlet of a tube, where the boundary-layer thickness is small compared with the pipe radius, is more like the flow over a flat plate than like the flow in a pipe." If the fluid enters the tube with little turbulence "the boundary layer may be expected to remain laminar, irrespective of the value of [symbol omitted] diameter Reynolds number; up to values of [symbol omitted] length Reynolds number of about 10^6, the latter representing the Reynolds number of transition for a flat plate."

During condensation, as tube length increases, the length Reynolds number of the vapor increases, passes through a maximum and decreases as total condensation is reached. The diameter Reynolds number of the vapor decreases with increasing length. The length necessary for the development of turbulence may be an appreciable portion of the condenser length. In addition, it is not known what effect the condensate film has on transition. The presence of such a film on the wall may serve to induce turbulence in the vapor or condensation may provide a stabilizing suction near the wall. 2. According to Carpenter and Colburn's hypothesis, the liquid film does not have vapor induced turbulence until it reaches a film Reynolds number of about 240. At the temperature drops investigated in this work a number of feet of tube length is sometimes necessary before the liquid film reaches this flow rate. Therefore, the liquid film, which is a major resistance to heat transfer, may be laminar for a good portion of the entrance length. 3. Numerical solutions at these high vapor velocities utilizing assumption 1 do provide insight into the experimental results of Carpenter and Colburn (1) for pure vapors. 4. These solutions will provide important limiting cases and determine which variables are of importance in correlating experimental data. Calculations using the laminar model could be used with future experimental data to determine where transition occurs.

The equations and boundary conditions for the condensation of a binary vapor are given below. These equations and the boundary conditions will be represented by finite difference approximations and

implicit finite difference "marching" procedures will be used to solve them. A description of these approximations and procedures is given in Appendix A. Brief outlines of the computer programs are given in Appendix B, and the complete computer programs are given in Appendix C.

Condensation of a Pure Vapor

The condensation of a pure vapor may be described by the axial component of the constant property equation of motion applied to both phases separately, the constant density continuity equation applied to both phases separately and the constant property equation of energy applied to the liquid phase. These equations are: the axial component of the equation of motion,

$$v_z' \frac{\partial v_z'}{\partial z'} + v_r' \frac{\partial v_z'}{\partial r'} = - \frac{1}{\rho'} \frac{\partial p'}{\partial z'} + \frac{\mu'}{\rho'} \left(\frac{\partial^2 v_r'}{\partial r'^2} + \frac{1}{r'} \frac{\partial v_z'}{\partial r'} \right) + g' \qquad \text{(II-1)}$$

the equation of continuity,

$$\frac{\partial (r' v_z')}{\partial z'} + \frac{\partial (r' v_r')}{\partial r'} = 0 \qquad \text{(II-2)}$$

and the equation of energy

$$v_z' \frac{\partial T'}{\partial z'} + v_r' \frac{\partial T'}{\partial r'} = \frac{k'}{\rho' C_p'} \frac{\partial^2 T'}{\partial r'^2} + \frac{k'}{\rho' C_p' r'} \frac{\partial T'}{\partial r'} + \frac{\mu'}{\rho' C_p'} \left(\frac{\partial v_z'}{\partial r'} \right)^2 \qquad \text{(II-3)}$$

The order analysis performed by Lee (35) indicates that all viscous dissipation terms and expansion effect terms are small compared to other terms in the equation of energy. However the largest of the viscous dissipation term has been retained in the energy equation above. The physical properties in these equations are evaluated according to the phase the equation is describing.

These equations may be put into dimensionless form for convenience. The equation of motion becomes

$$U\frac{\partial U}{\partial Z} + V\frac{\partial U}{\partial R} = -\frac{\partial P}{\partial Z} + \frac{2}{Re}\left(\frac{\partial^2 U}{\partial R^2} + \frac{1}{R}\frac{\partial U}{\partial R}\right) + \frac{1}{2Fr} \qquad \text{(II-4)}$$

The equation of continuity becomes

$$\frac{\partial (RU)}{\partial Z} + \frac{\partial (RV)}{\partial R} = 0 \qquad \text{(II-5)}$$

Finally, the equation of energy becomes

$$U\frac{\partial T}{\partial Z} + V\frac{\partial T}{\partial R} = \frac{2}{R}\frac{1}{RePr}\frac{\partial T}{\partial R} + \frac{2}{RePr}\frac{\partial^2 T}{\partial R^2} + \frac{2}{ReEk}\left(\frac{\partial U}{\partial R}\right)^2 \qquad \text{(II-6)}$$

The dimensionless variables are defined as:

$$Z = \frac{2z'}{D'}, \qquad R = \frac{2r'}{D'}, \qquad U = \frac{v_z'}{\bar{u}'}, \qquad V = \frac{v_r'}{\bar{u}'}$$

$$Re = \frac{\rho' D' \bar{u}'}{\mu'}, \qquad Pr = \frac{\mu' C_p'}{k'}, \qquad Fr = \frac{\bar{u}'^2}{g' D'}, \qquad P = \frac{p' - p_o'}{\rho_g' \bar{u}'^2},$$

$$T = \frac{T' - T_w'}{T_o' - T_w'}, \qquad Ek = \frac{\bar{u}'^2}{C_p'(T_o' - T_w')}.$$

The primes indicate dimensional quantities, the subscript "w" indicates wall conditions, the subscript "o" indicates entrance conditions, "g" the gas phase, and "$\bar{u}'$" is the average entrance velocity.

In the vapor phase the equation of motion is equation (II-4). In the liquid phase it is necessary to write the pressure term in this equation as

$$-\frac{\rho_g'}{\rho_l'}\frac{\partial P}{\partial Z},$$

The boundary conditions are

(A) At Z = 0 and all R, $P = V = 0$

$T = U = 1$

(B) At R = 1 and all Z, $T = U = V = 0$

(C) At the gas-liquid interface for all Z, $U_{g_t} = U_{\ell_t}$

$\tau'_{g_t} = \tau'_{\ell_t}$

$(N'_g)_{\bar{n}} = (N'_\ell)_{\bar{n}}$

$\lambda'(N'_g)_{\bar{n}} = -k'_\ell\left(\frac{\partial T'}{\partial \bar{n}'}\right)_\ell$

$T_g = T_\ell = 1$

(D) At R = 0 and all Z, $V = \frac{\partial U}{\partial R} = 0$

(E) At all Z, $\int_0^1 = \rho' U R \, dR$ is a constant.

The subscript "g" stands for "gas"; the subscript "ℓ" indicates "liquid"; the subscript "t" stands for "tangetial to the interface"; the subscript "$\bar{n}$" means "normal to the interface". "τ'" stands for shear stress and "N'" for mass flux. The velocity and shear conditions at the interface have been reduced to

$$U_{g_z} = U_{\ell_z} \qquad \text{and} \qquad \tau'_{g_z} = \tau'_{\ell_z}$$

where "z" stands for the axial direction. These assumptions are discussed further in Appendix A.

Condensation of a Vapor from a Noncondensable Gas-Vapor Mixture

The condensation of a vapor from a vapor and noncondensable gas mixture may be described by the axial component of the equation of motion applied to both phases separately, the constant density equation of continuity applied to the liquid phase, the variable density equation of continuity applied to the vapor phase, the constant property equation of energy applied to both phases separately, and the constant property diffusion equation applied to the vapor phase. All properties in these equations are evaluated according to the phase the equations are describing.

The equation of motion for constant viscosity and constant density has been given in equation (II-1). The equation of motion for constant viscosity and variable density would be the same equation with the addition of

$$-\frac{2}{3}\mu' \frac{\partial}{\partial z'}\left(\frac{1}{r'}\frac{\partial}{\partial r'}(r'v_r') + \frac{\partial v_z'}{\partial z'}\right)$$

to the right hand side of the equation. These terms may be neglected compared to the others in the equation. Equation (II-1) is used as the equation of motion for both phases. The density is allowed to vary in the gas as a function of composition and is assumed constant in the liquid.

The variable density equation of continuity, applicable in the gas is

$$\frac{\partial}{\partial r'}(\rho' r' v_r') + \frac{\partial}{\partial z'}(\rho' r' v_z') = 0 \qquad \text{(II-8)}$$

Equation (II-2), the constant density equation of continuity, is used for the liquid phase.

The equation of energy for both phases is given by equation (II-6). Using this equation assumes that the energy carried by inter-diffusion of species is small compared to the latent heat of vaporization.

The constant property equation of diffusion is

$$v'_z \frac{\partial W_a}{\partial z'} + v'_r \frac{\partial W_a}{\partial r'} = D'_{ab} \left(\frac{\partial^2 W_a}{\partial r'^2} + \frac{1}{r'} \frac{\partial W_a}{\partial r'} \right) \qquad \text{(II-9)}$$

where W_a is mass fraction of component a.

The variable density diffusion equation would include

$$+ D'_{ab} \left[\left(\frac{\partial W_a}{\partial r'} \right) \left(\frac{\partial \rho'}{\partial r'} \right) + \left(\frac{\partial W_a}{\partial z'} \right) \left(\frac{\partial \rho'}{\partial z'} \right) \right]$$

on the right hand side of the above equation. These terms were neglected by Sparrow and Lin (24) and Sparrow and Eckert (36) for vertical wall condensation, and by Baasel and Smith (25) for condensation in a vertical tube. Sparrow and Eckert did not allow density to vary in their other equations. They reported poor agreement with experimental data and attributed this difference to free convection which was present in the experiment. Sparrow and Lin showed that by allowing density to vary as a function of concentration in other equations quite satisfactory agreement was achieved with experimental data.

These equations may be made dimensionless using the definitions of the dimensionless variables as given in equation (II-7).

The equation of motion is given by equation (II-4). Using

variable density necessitates the use of radial and axial pressure correction terms similar to the one mentioned in the previous section. These two correction terms are included in the finite difference representation of the equation of motion given in Appendix A.

The equation of continuity for the liquid is given by equation (II-5). For the gas the equation of continuity becomes

$$\frac{\partial}{\partial Z}(\rho' RU) + \frac{\partial}{\partial R}(\rho' RV) = 0 \qquad \text{(II-10)}$$

with dimensional density retained for convenience in computation.

The equation of energy is given by equation (II-6).

The equation of diffusion, equation (II-9), becomes

$$U\frac{\partial W_a}{\partial Z} + V\frac{\partial W_a}{\partial R} = \frac{2}{ScRe}\left(\frac{\partial^2 W_a}{\partial R^2} + \frac{1}{R}\frac{\partial W_a}{\partial R}\right) \qquad \text{(II-11)}$$

where $Sc = \mu'/\rho' D'_{ab}$.

The boundary conditions for this problem are

(A) At $Z = 0$ and all R, $P = V = 0$

$T = U = 1$

$W_a = W_{a_o}$

$W_b = W_{b_o}$

(B) At $R = 1$ and all Z, $T = U = V = 0$

(C) At the gas-liquid interface for all Z, $U_{g_t} = U_{\ell_t}$

$\tau'_{g_t} = \tau'_{\ell_t}$

$$(N'_{a_g})_{\bar{n}} = (N'_{a_\ell})_{\bar{n}}$$

$$\lambda'(N'_{a_g})_{\bar{n}} = -k'_\ell \left(\frac{\partial T'}{\partial \bar{n}}\right)_\ell + k'_g \left(\frac{\partial T'}{\partial \bar{n}'}\right)_g$$

$$T_g = T_\ell$$

$$W_{b_\ell} = (N'_{b_g})_{\bar{n}} = 0$$

(D) At R = 0 and all Z, $V = \frac{\partial W_a}{\partial R} = \frac{\partial W_b}{\partial R} = \frac{\partial T}{\partial R} = \frac{\partial U}{\partial R} = 0$,

(E) At all Z, $\int_0^1 \rho' U R \, dR$ is a constant

$\int_0^1 \rho'_a U R \, dR$ is a constant.

In addition, vapor-liquid equilibrium exists at the interface. "b" refers to the noncondensable gas. As before, the interfacial shear and velocity conditions have been changed to

$$U_{g_z} = U_{\ell_z} \qquad \text{and} \qquad \tau'_{g_z} = \tau'_{\ell_z}$$

The assumptions are discussed further in Appendix A.

Condensation of a Binary Vapor Mixture

The condensation of a binary vapor mixture may be described by the axial component of the equation of motion, equation (II-1), applied to both phases separately, the constant density equation of continuity, equation (II-2), applied to the liquid phase, the variable density equation of continuity, equation (II-8), applied to the vapor phase

with density a function of concentration, the constant property energy equation, equation (II-3), applied to both phases separately, and the constant property diffusion equation, equation (II-9), applied to both phases separately. The physical properties in these equations are evaluated according to the phase the equation is describing.

The dimensionless equations and the discussion of these equations are the same as in the previous section.

The boundary conditions for the condensation of binary vapor mixtures are

(A) At Z = 0 and all R,

$$P = V = 0$$

$$T = U = 1$$

$$W_a = W_{a_o}$$

$$W_c = W_{c_o}$$

(B) At R = 1 and all Z,

$$T = U = V = (N'_a)_r = (N'_c)_r = 0$$

(C) At the gas-liquid interface for all Z,

$$U_{g_t} = U_{\ell_t}$$

$$\tau'_{g_t} = \tau'_{\ell_t}$$

$$(N'_{a_g})_{\bar{n}} = (N'_{a_\ell})_{\bar{n}}$$

$$(N'_{c_g})_{\bar{n}} = (N'_{a_\ell})_{\bar{n}}$$

$$(N'_{a_g} + N'_{c_g})_{\bar{n}} (e'_g - e'_\ell) = -k'_\ell \left(\frac{\partial T'}{\partial \bar{n}'}\right)_\ell + k'_g \left(\frac{\partial T'}{\partial \bar{n}'}\right)_g$$

$$T_g = T_\ell$$

(D) At R = 0 and all Z, $$V = \frac{\partial U}{\partial R} = \frac{\partial W_a}{\partial R} = \frac{\partial W_c}{\partial R} = \frac{\partial T}{\partial R} = 0$$

(E) At all Z, $\int_0^1 \rho' U R \, dR$ is a constant.

$\int_0^1 \rho_a' U R \, dR$ is a constant.

In addition, vapor-liquid equilibrium exists at the interface. Subscripts "a" and "c" refer to the two condensable vapors, and subscript "r" refers to the radial direction.

The interfacial shear and velocity conditions will be changed as in the previous section.

CHAPTER III

CONDENSATION OF A PURE VAPOR

Numerical solutions to equations (II-4), (II-5), and (II-6), and the boundary conditions for pure vapor condensation given in Chapter II are presented in this chapter. Details of the numerical solutions and discussion of their validity may be found in Appendix A. An outline of the computer program used to solve the equations is given in Appendix B, and the complete computer program is given in Appendix C. The physical properties used in these calculations are presented in Appendix D, and the numerical results are presented in tabular form in Appendix E.

Three pure fluids were considered: water, ethanol, and trichloroethylene. A wide range of conditions was covered. Entrance velocity was allowed to vary from two and one-half feet per second to four hundred feet per second. The Reynolds number of the entering gas varied from 846 to 488,854. Five, ten, and twenty degree Fahrenheit temperature drops through the liquid film were considered. Tube diameters of 0.459 inches and 2.0 inches were investigated, and tube lengths were as long as twenty feet. Properties used in the model are those of the liquid and vapor at the boiling point.

Axial and radial velocity profiles, liquid film thickness, pressure drop, interfacial shear, heat transfer results, comparison with experimental data, correlation of heat transfer results, and

comparison with correlations available in the literature are discussed below. "Run" refers to a numerical solution unless otherwise designated.

Velocity Profiles

No attempt was made to generalize the velocity profiles which varied quite a bit with the conditions of each run. Complete radial and axial velocity profiles are presented graphically below for two typical runs. In the first, water vapor enters a 0.03825 foot diameter tube at 10 feet per second. This is equivalent to a diameter Reynolds number of 1692 in the entering vapor. The temperature drop through the liquid film is five degrees Fahrenheit. In the second, trichloroethylene vapor enters a 0.03825 foot diameter tube at 100 feet per second. The diameter Reynolds number of the entering vapor is 122,213. A 10° F temperature drop through the liquid film is considered. These and other runs are presented in Tables 22, 23, 24, 25, 26, 27, and 28 of Appendix E.

The axial velocity profiles in the vapor phase for the water run are presented in Fig. 2. The entering vapor is almost completely condensed in the first foot of condenser length. The point of total condensation is predicted when zero axial velocities are reached.

In one phase laminar flow in the entrance of a tube the centerline velocity increases sharply near the entrance and eventually reaches twice the entrance value. When condensation occurs the centerline velocity is a function of the temperature drop through the liquid film. This may be seen in Fig. 3. The Reynolds number of the entering vapor is 1692 in each case. The entering vapor is condensed in a

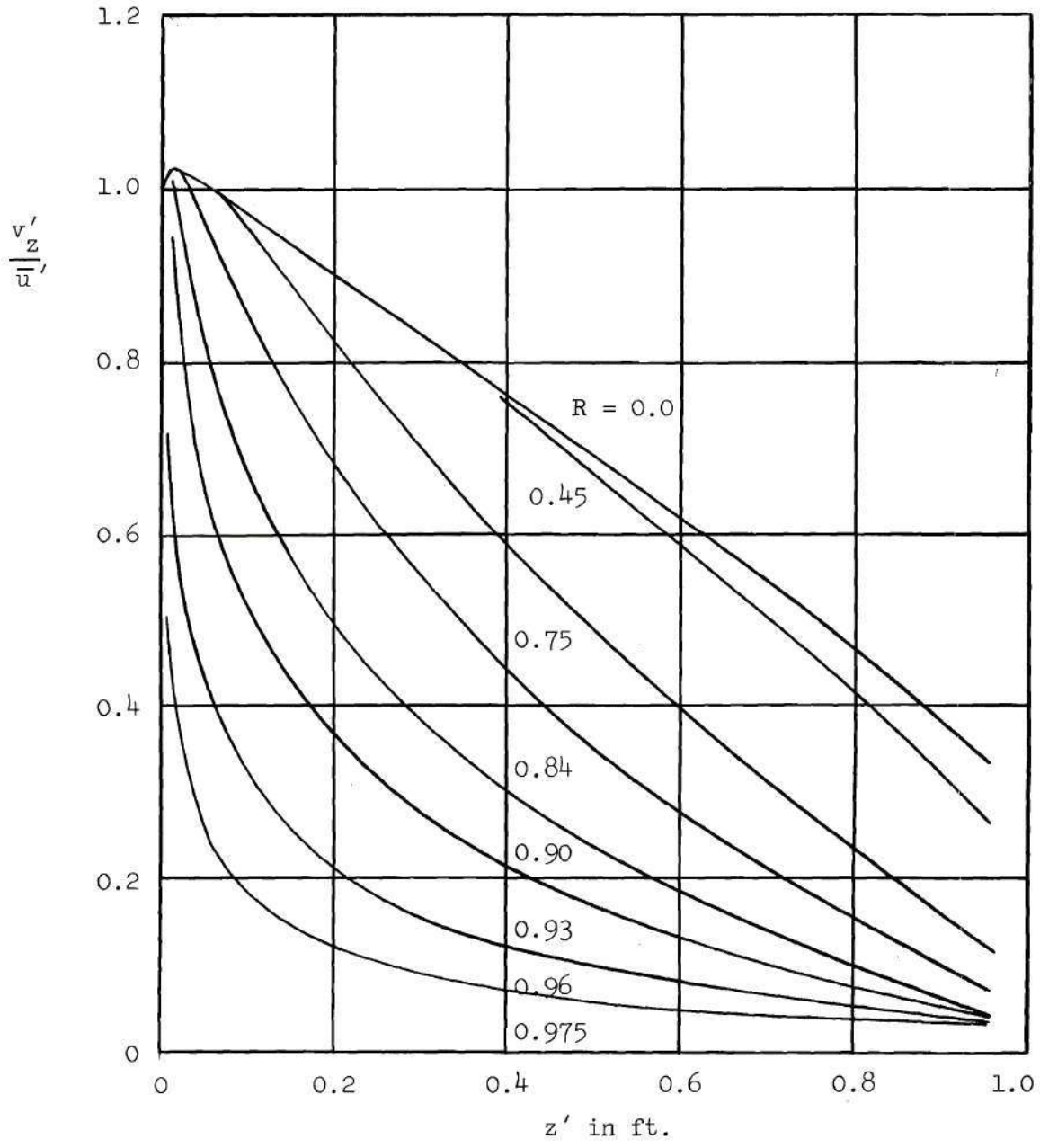

Fig. 2. Axial Velocity Profiles in the Vapor Phase: Water, $\Delta T' = 5^{\circ}$ F, $D' = 0.03825$ ft., $\overline{u}' = 10$ ft./sec.

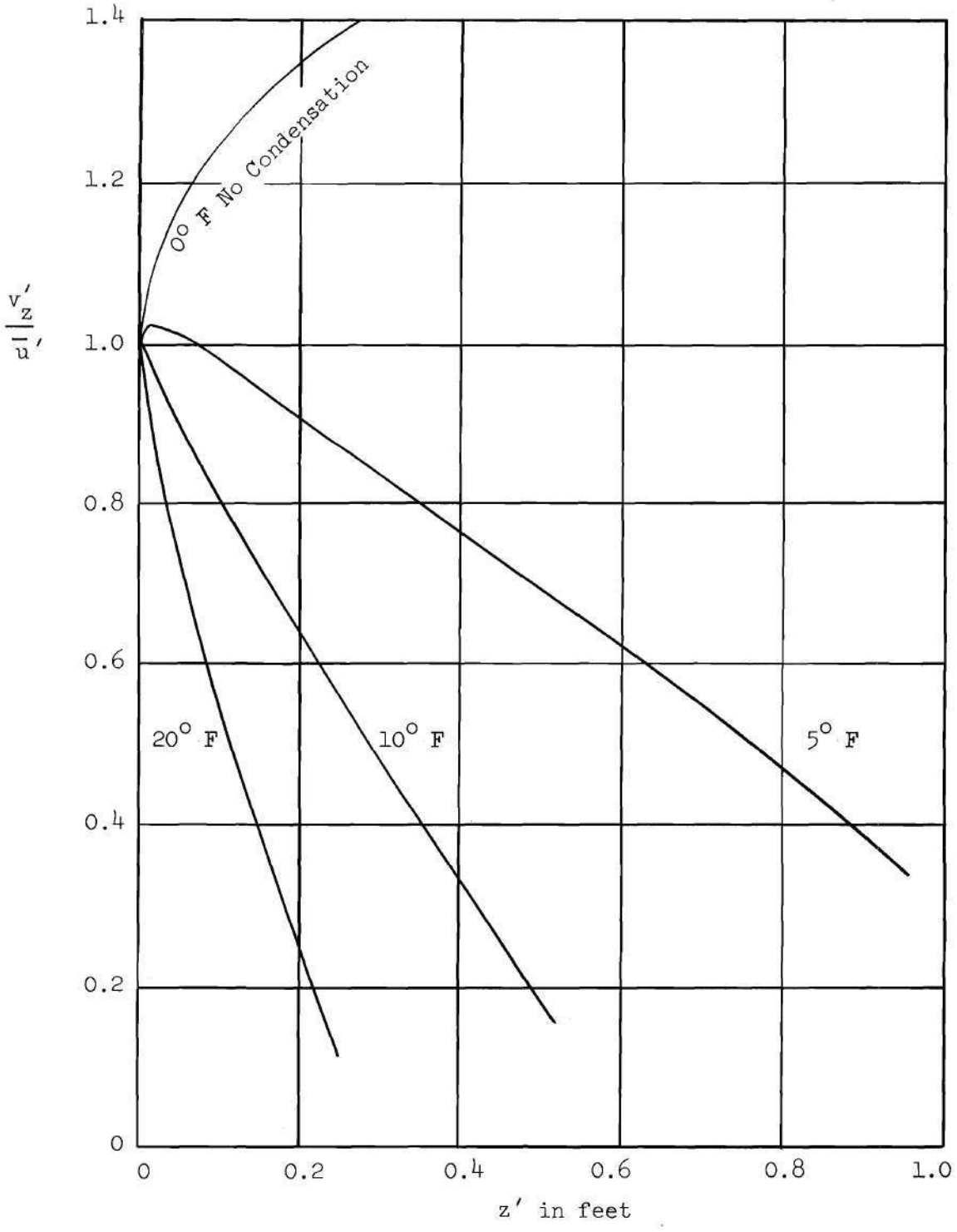

Fig. 3. Centerline Velocity as a Function of Temperature Drop Through the Liquid Film: Water, D′= 0.03825 ft., $\bar{u}'$ = 10 ft./sec.

shorter distance as the temperature drop is increased.

The radial velocity profiles in the vapor for this run are presented in Fig. 4. Close to the entrance the radial velocity is negative over most of the distance between the wall and the center of the tube. Over most of this region there is a linear dependence on radius as there is in one phase entrance flow (37). However, near the vapor-liquid interface the radial velocity becomes positive. The radial velocity of the vapor at the interface is initially high and positive. This interfacial velocity decreases with increasing z'. After a small distance into the tube the radial velocity becomes positive at all radial values. It remains positive for the rest of the tube. The behavior of radial velocity for larger values of z' is reported in Table 24.

A more detailed look at the axial and radial velocity profiles in and about the vapor-liquid interface is shown in Fig. 5. The position of the interface as a function of length is marked on this figure. The vapor phase is above the interface line and the liquid phase is below it. Lines of constant axial and radial velocity are shown on the graph.

The axial velocity is continuous across the interface. This results from the assumption that continuity of velocity tangential to the interface may be approximated by continuity of axial velocity at the interface. This assumption is discussed in Appendix A.

An assumption made in the development of the mathematical model is that $v_r' << v_z'$. It may be seen in Fig. 5 that this is not the case

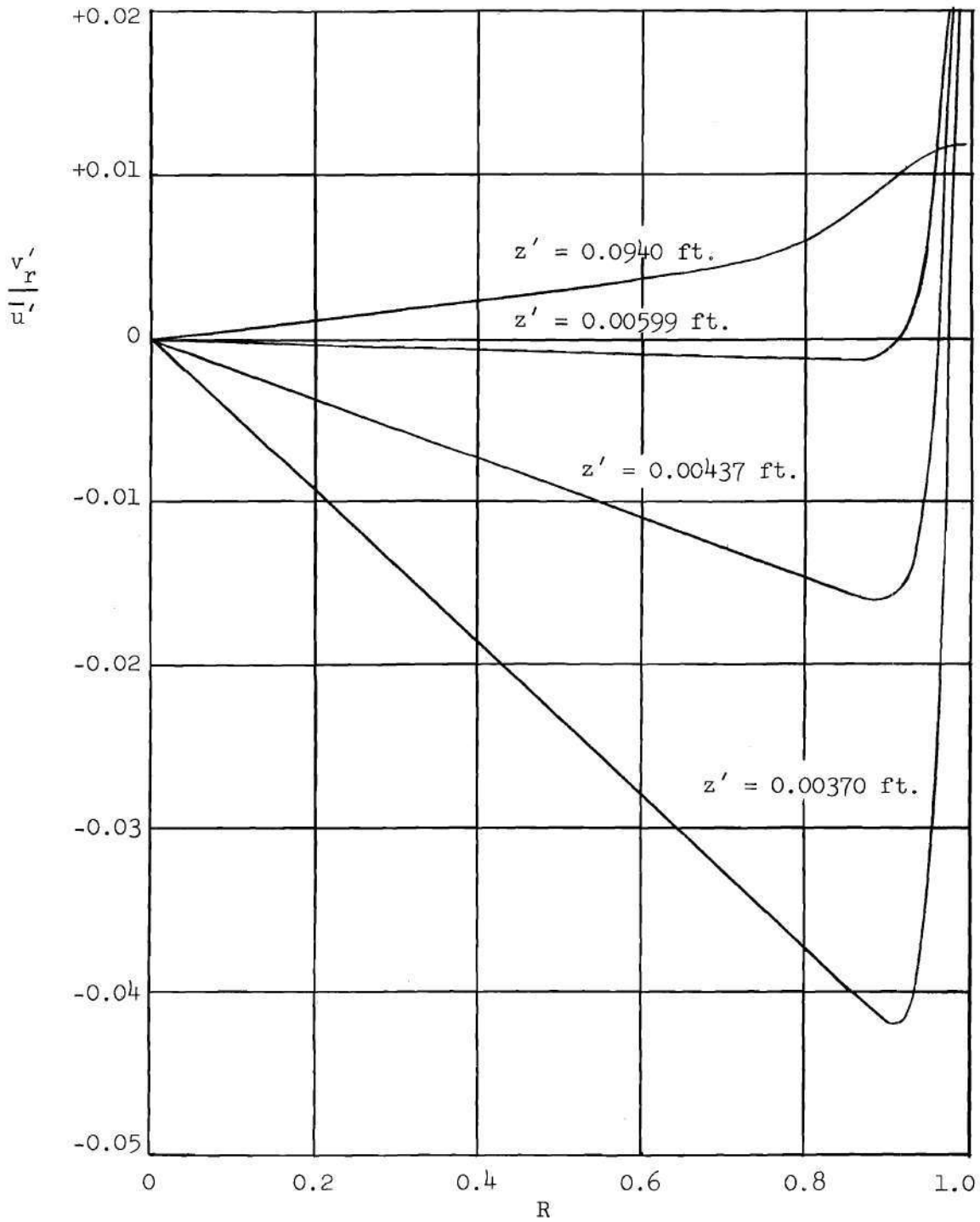

Fig. 4. Radial Velocity Profiles in the Vapor Phase: Water, $\Delta T' = 5^{\circ}$ F, $D' = 0.03825$ ft., $\bar{u}' = 10$ ft./sec.

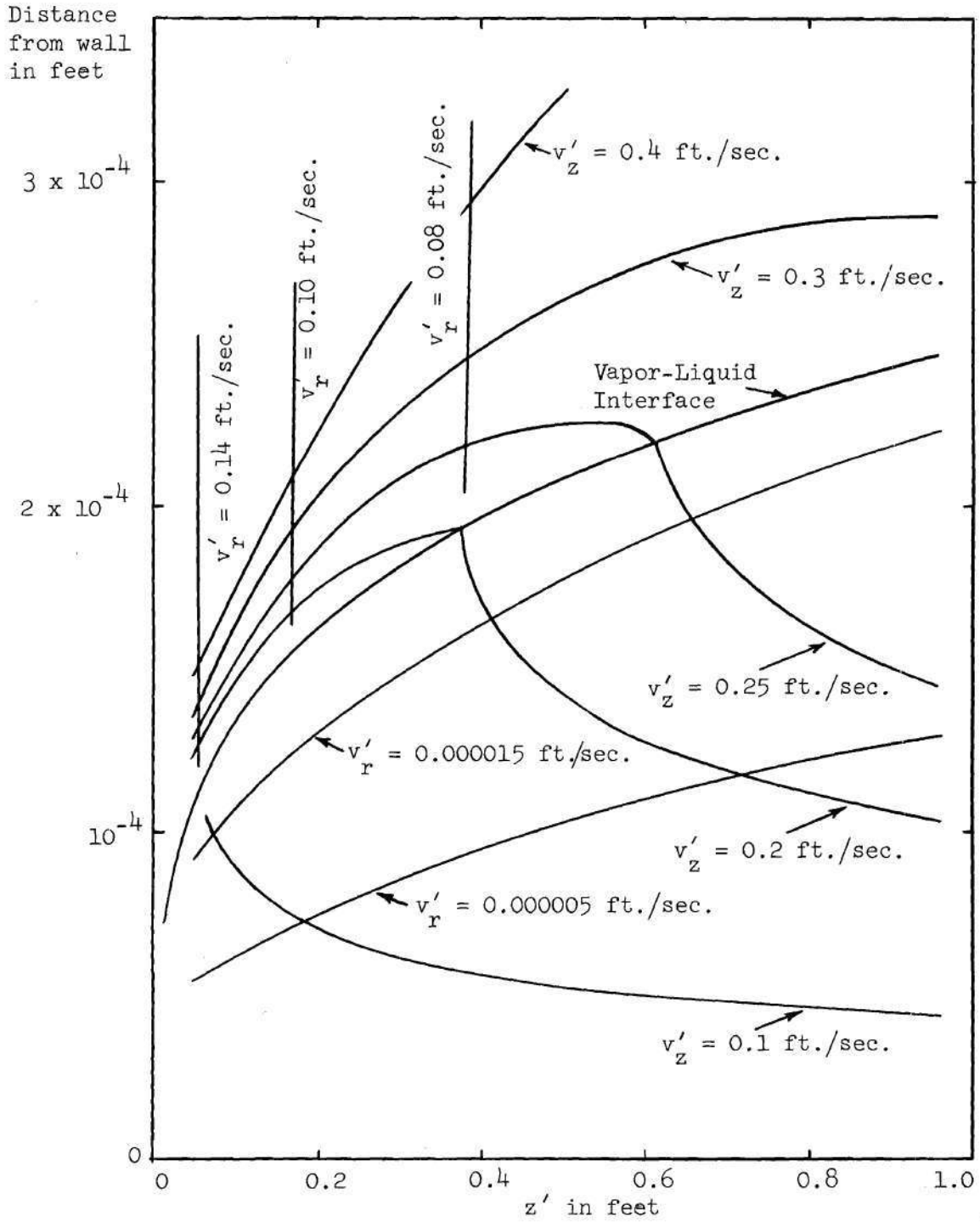

Fig. 5. Axial and Radial Velocity Profiles Near the Gas-Liquid Interface: Water, $\Delta T' = 5^{\circ}$ F, $D' = 0.03825$ ft., $\bar{u}' = 10$ ft./sec.

in the vapor near the interface and near the entrance. This sort of behavior was observed in all runs where the Reynolds number was less than 2100. It was also observed to some degree in runs with an entering velocity of 25 feet per second, particularly for ten and twenty degree temperature drops. It was not observed in runs with higher entering velocities.

The fact that v_r' is of the order of v_z' in the low velocity runs means that the equation of motion in the radial direction should have been included in the mathematical model for these runs. Not including it causes the model to predict slightly higher rates of condensation than it should, but the error should be small because of the small region where the assumption does not hold and the fact that the main resistance to condensation is the liquid film.

The shape of the axial velocity profile in the liquid as a function of length may be seen in Fig. 6. If the interfacial shear was quite large compared to gravity and the pressure gradient, the velocity of the liquid would be a straight line (1). On the other hand, if there was no shear at the vapor-liquid interface, no pressure gradient, the acceleration terms were negligible, and the fluid was flowing down the wall under the influence of gravity alone, the velocity profile would be parabolic as predicted by the Nusselt model (2).

The pressure gradient is quite small over the entire condenser and should have a negligible effect on the shape of the liquid velocity profile. Near the entrance the shear force at the vapor-liquid inter-

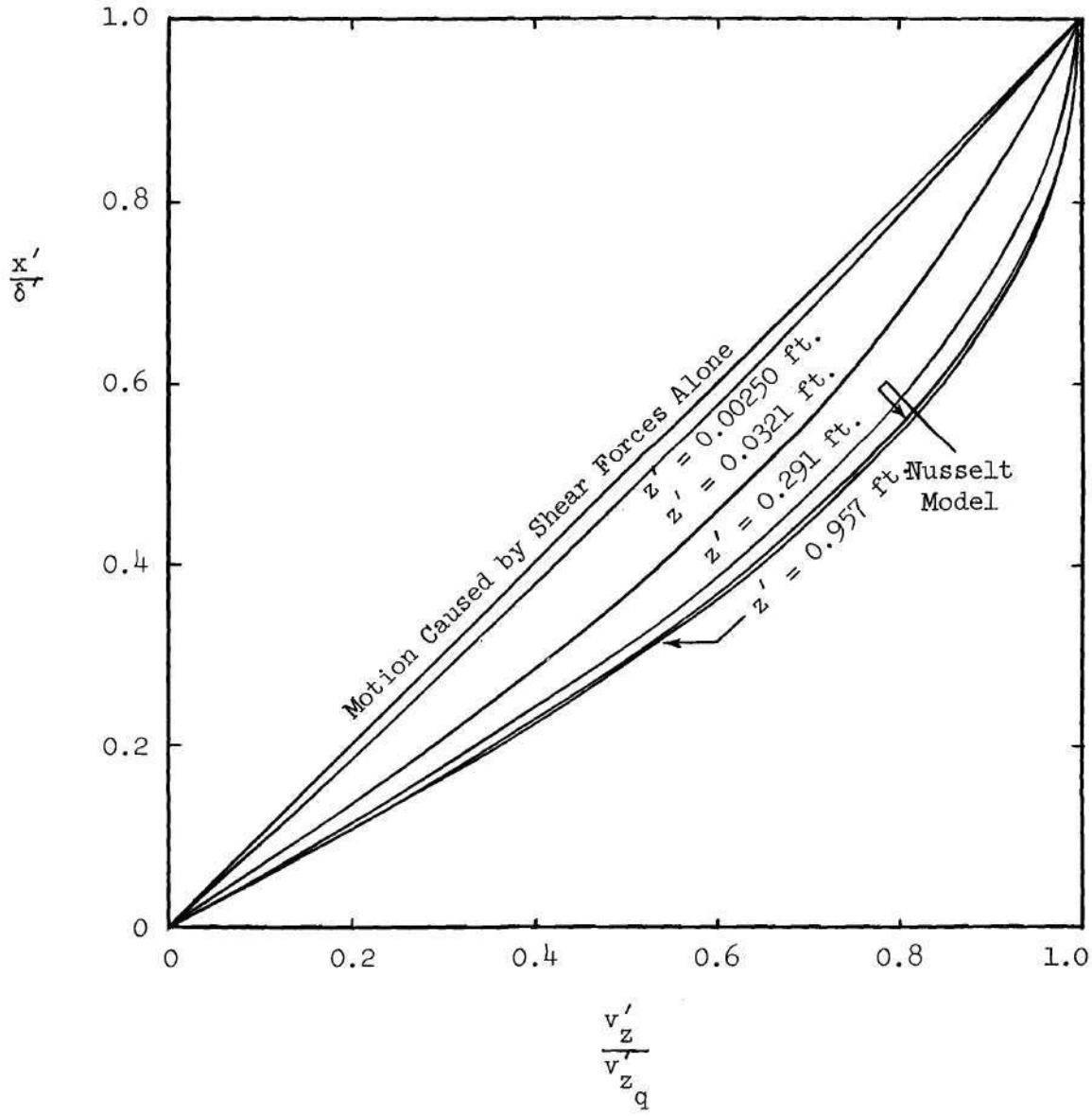

Fig. 6. Comparison of Liquid Axial Velocity Profiles with Simple Models: Water, $\Delta T' = 5^{\circ}$ F, $D' = 0.03825$ ft., $\bar{u}' = 10$ ft./sec.

face is very large. The liquid velocity profile is therefore almost a straight line. The interfacial shear for this numerical solution decreases quickly as the length increases. The profiles approach that of the Nusselt model as the length increases. Near the end of the condenser the profiles become slightly more curved than the Nusselt model. This is caused by the acceleration terms, which were included in this study but not included in the Nusselt model.

In the second run trichloroethylene enters the tube at 100 feet per second, equivalent to an entering diameter Reynolds number of 122,213 for the vapor. The axial velocity profiles in the vapor are shown in Fig. 7. The vapor is not completely condensed in seven feet of condenser length. As in the previous case there is a core of vapor in the center of the tube where axial velocity is independent of radius. In all cases the size of this core decreases with increasing length. The centerline velocity reaches a maximum near the entrance and then decreases slowly with increasing length. Thus, after a very short distance into the tube, condensation is more than offsetting the increase in velocity inherent in one phase entrance flow.

The radial velocity profiles in the vapor phase are presented in Fig. 8 for this case. The shapes of these curves are similar to those of the previous case. The radial velocity becomes positive from the center to the interface after a short distance into the tube, but it is quite small in magnitude.

Except for a small length very near the entrance, the interfacial radial velocity of the vapor is positive and decreases with increasing length. The first few steps into the tube may have negative

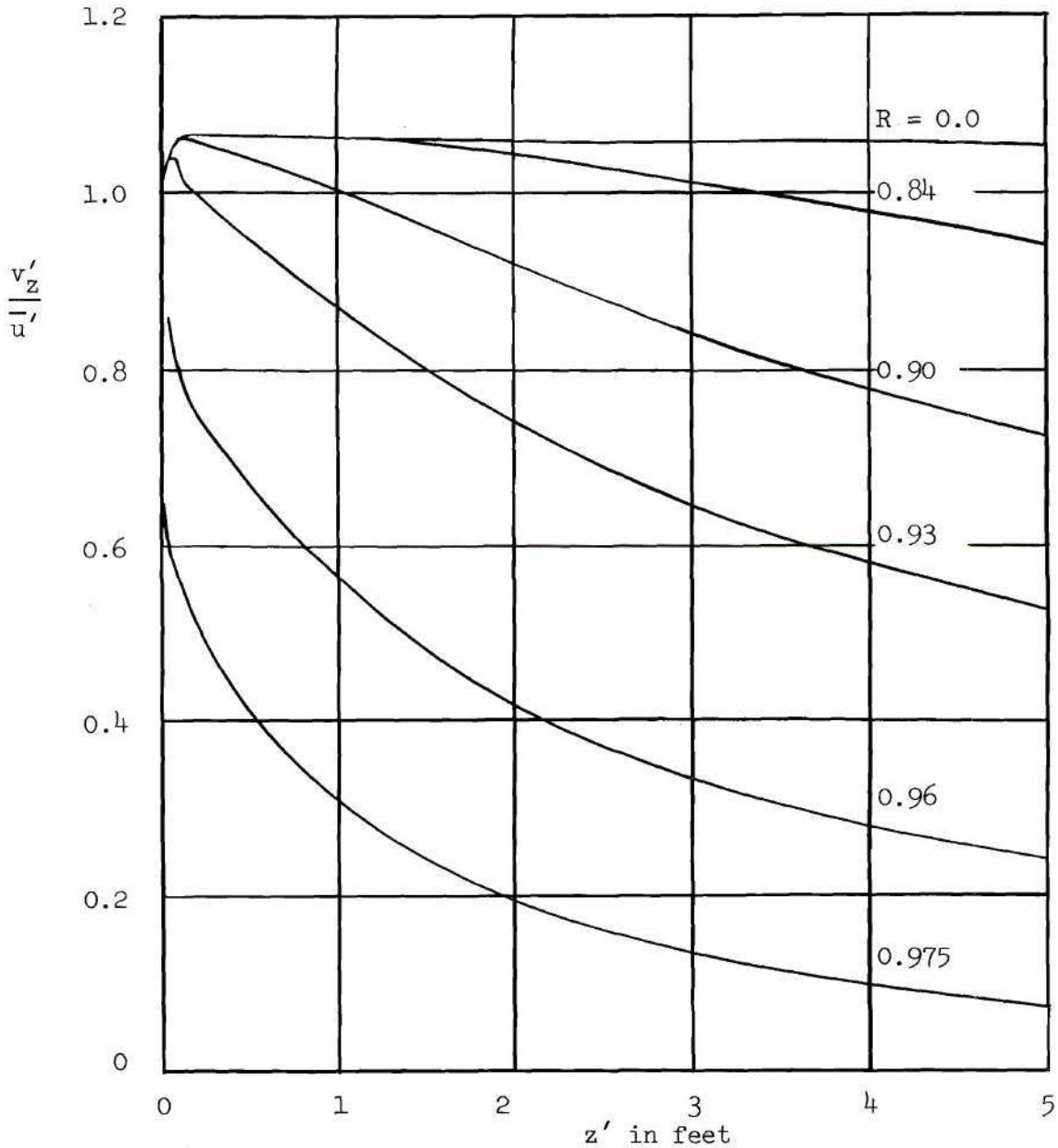

Fig. 7. Axial Velocity Profiles in the Vapor Phase: Trichloroethylene, $\Delta T' = 10^{\circ}$ F, $D' = 0.03825$ ft., $\overline{u'} = 100$ ft./sec.

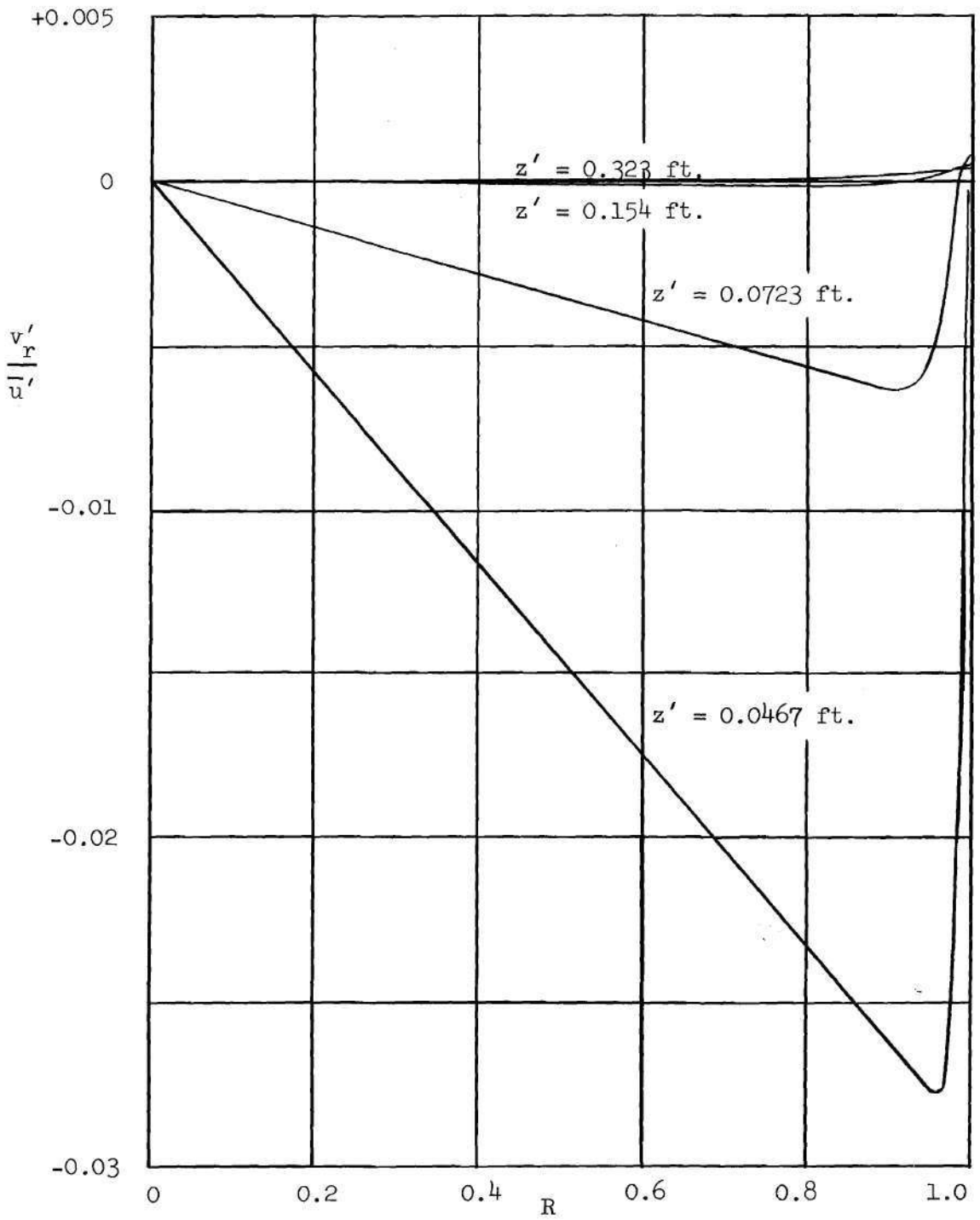

Fig. 8. Radial Velocity Profiles in the Vapor Phase: Trichloroethylene, $\Delta T' = 10^{\circ}$ F, $D' = 0.03825$ ft., $\bar{u}' = 100$ ft./sec.

radial velocities of the vapor at the interface. It is felt that this is a result of some of the more gross approximations that had to be made at the first step to get the numerical procedure running. This effect quickly disappears after the first few steps.

The axial and radial velocity profiles in and about the vapor-liquid interface are shown in Fig. 9. The position of the interface as a function of length is marked as before with the vapor being above this line and the liquid being below it.

It is readily apparent from this graph that $v_r' << v_z'$. This assumption seems to be justified for high entering velocities. The radial velocity in the liquid film is seen to be negative in the first half of the tube and positive in the second half. There were negative values in the previous run but only at very small z.

The axial velocity is continuous across the interface as in all runs. Lines of constant axial velocity in the liquid were not extended into the vapor because of lack of space on the figure.

The shape of the axial velocity profile in the liquid as a function of length is presented in Fig. 10. The interfacial shear does not decrease as quickly as in the previous run and is still quite important for distances more than six feet into the tube.

Liquid Temperature Profiles

Liquid temperature profiles for these two runs are presented in Tables 23 and 25 of Appendix E. These profiles appear to be almost linear with radius.

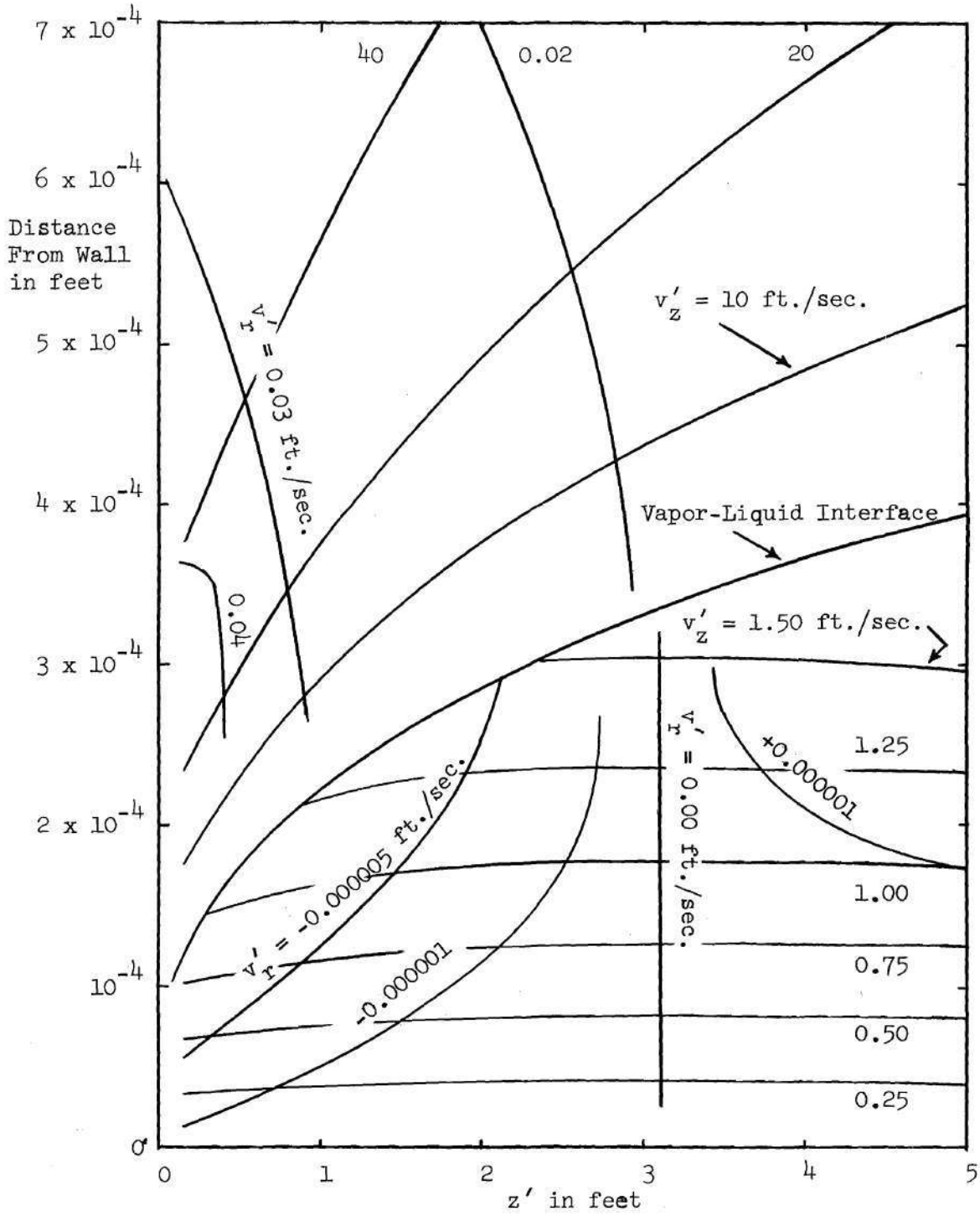

Fig. 9. Axial and Radial Velocity Profiles Near the Gas-Liquid Interface: Trichloroethylene, $\Delta T' = 10^{\circ}$ F, $D' = 0.03825$ ft., $\bar{u}' = 100$ ft./sec.

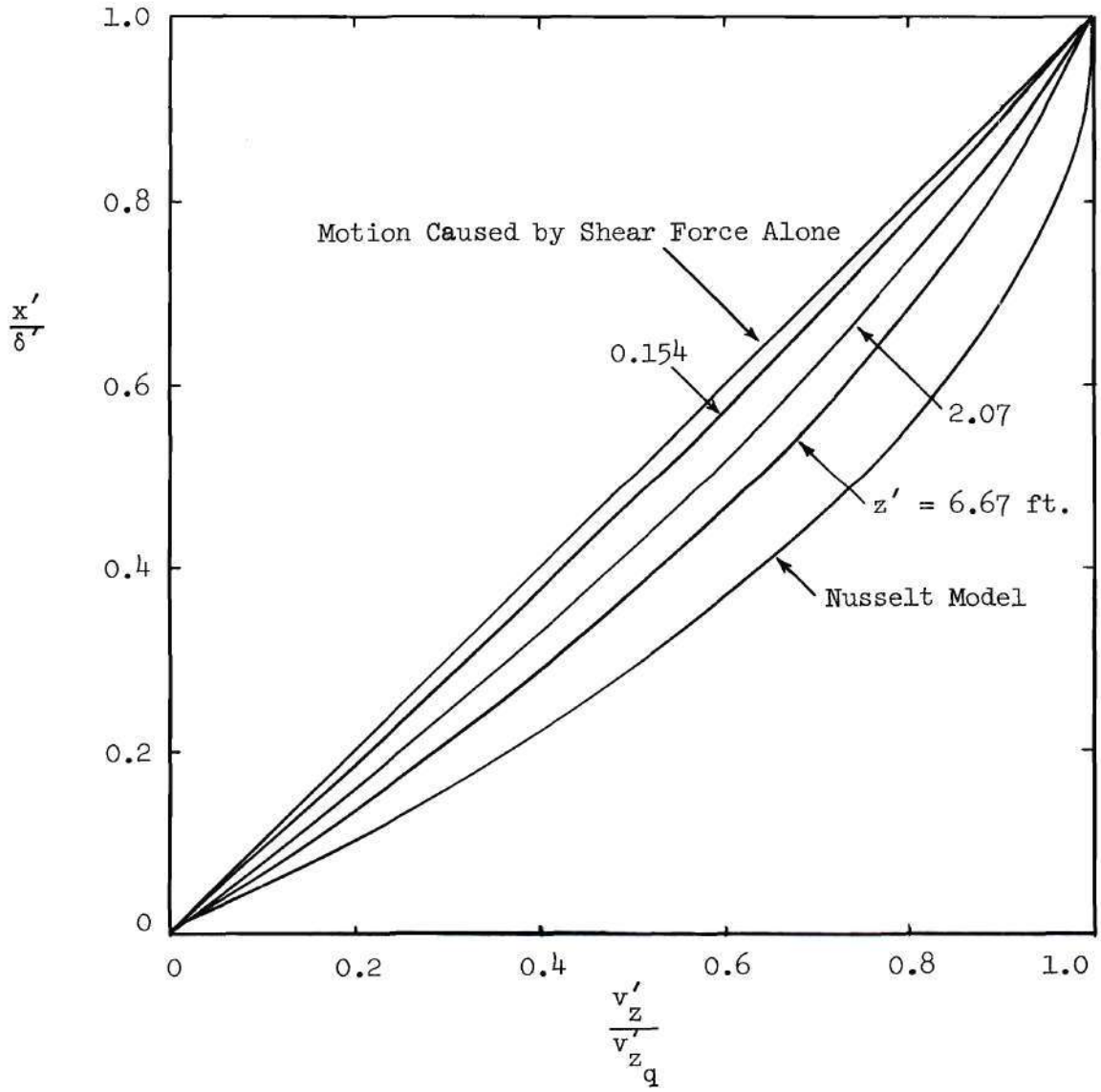

Fig. 10. Comparison of Liquid Axial Velocity Profiles with Simple Models: Trichloroethylene, $\Delta T' = 10^{\circ}$ F, $D' = 0.03825$ ft., $\bar{u}' = 100$ ft./sec.

Liquid Film Thickness

The effect of vapor velocity on liquid film thickness δ' is shown in Fig. 11. Trichloroethylene vapor is being condensed in a 0.03825 foot diameter tube with a temperature drop through the liquid film of ten degrees Fahrenheit. Entering vapor velocity varies from 25 ft./sec. to 400 ft./sec.

It can be seen from Fig. 11 that the greater the entrance vapor velocity, the thinner the liquid film. This is so despite the fact that at any given length the higher the velocity, the greater the flow rate in the liquid film. The greater liquid throughput at higher velocities is caused by higher interfacial shear forces at those velocities.

In Fig. 11 all film thicknesses are less than that predicted by the Nusselt model (2). However, different behavior was observed in other cases, as may be seen in Fig. 12. In this run the interfacial shear is quite high near the entrance, the film is thinner than the Nusselt prediction, and the amount condensed is greater than the Nusselt model predicts. When the interfacial shear drops to the point where gravity predominates, the film gradually becomes thicker than the Nusselt prediction because the amount condensed is greater than the Nusselt prediction.

Pressure Drop

The mathematical model predicts an interesting pressure effect, which is shown in Fig. 13. Initially the pressure decreases with increasing length. A minimum pressure is ultimately reached, and then

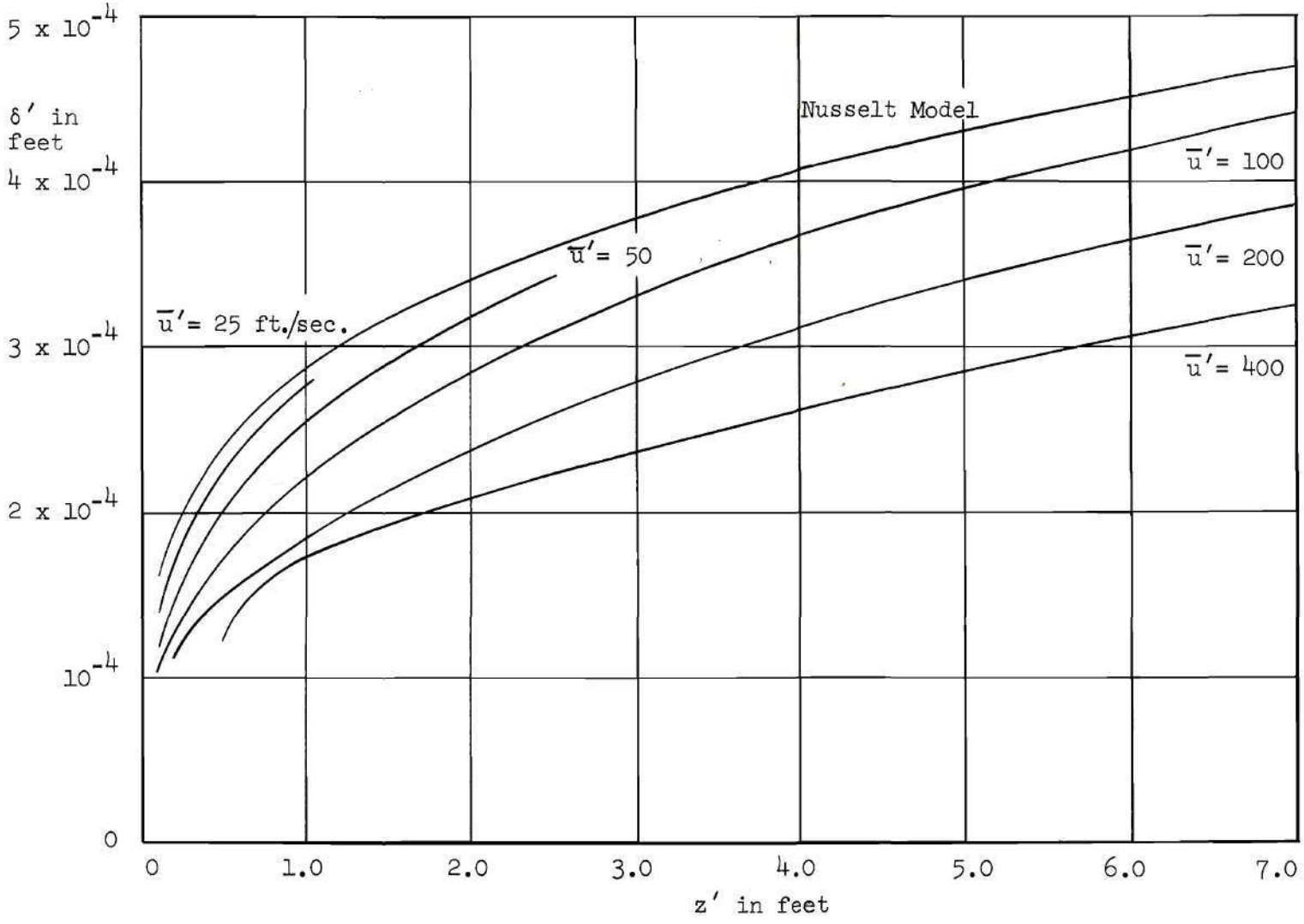

Fig. 11. Effect of Vapor Entrance Velocity on Liquid Film Thickness: Trichloroethylene, $\Delta T' = 10^{\circ}$ F, $D' = 0.03825$ ft.

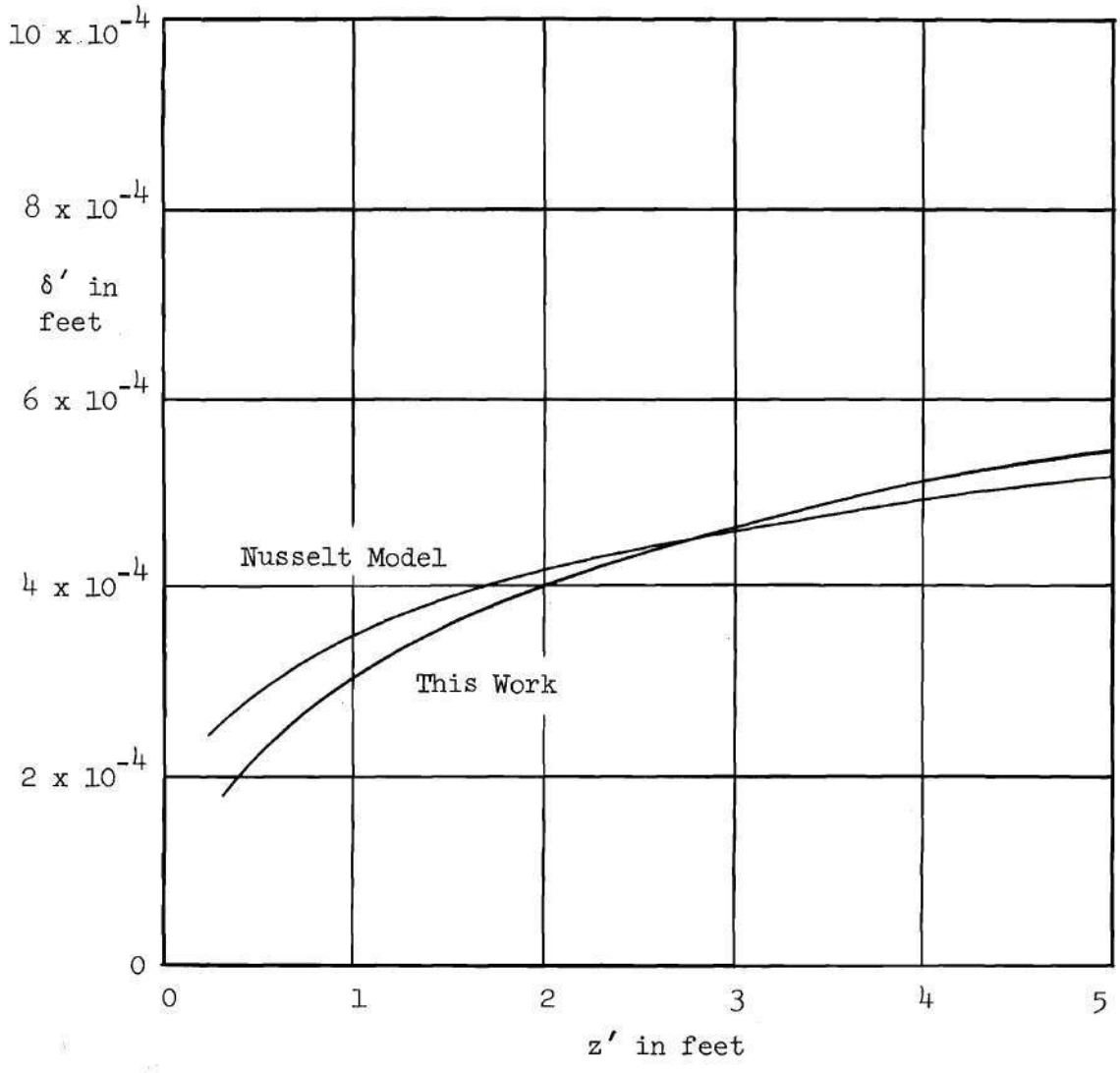

Fig. 12. Comparison of Film Thickness with Nusselt Model: Water, $\Delta T' = 20^{\circ}$ F, $D' = 0.03825$ ft., $\bar{u}' = 100$ ft./sec.

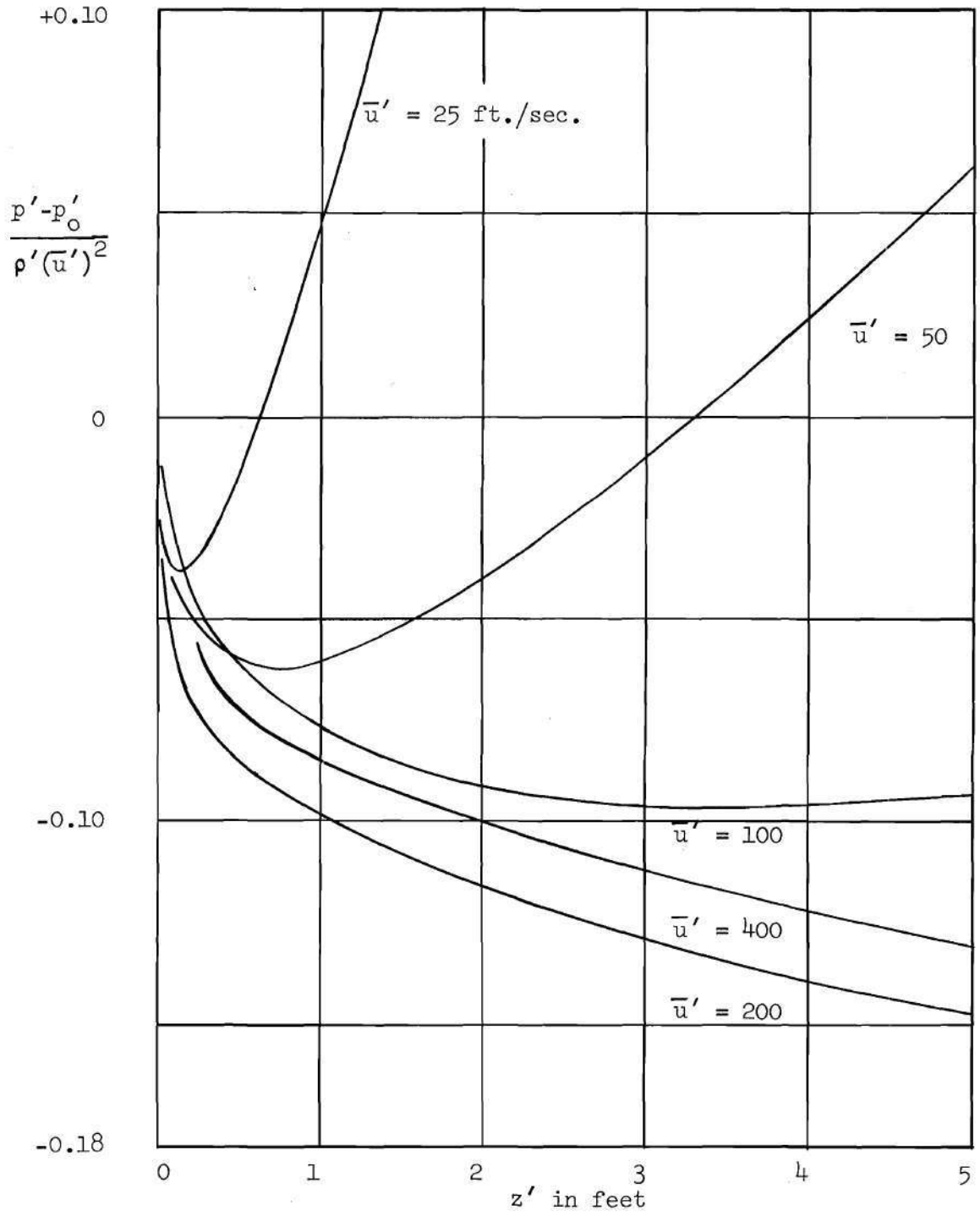

Fig. 13. Pressure Drop During Condensation: Trichloroethylene, $\Delta T' = 5^{\circ}$ F, $D' = 0.03825$ ft.

the pressure starts increasing with increasing length. The pressure eventually becomes greater than the entrance pressure.

This behavior is probably caused by two effects: the high pressure drop normally associated with the entrance region of tubes; and a Bernoulli effect, converting kinetic energy into pressure. The first effect is apparently gradually overcome by the second. The second effect is caused by high velocity vapor with high kinetic energy being condensed into slowly moving liquid with lower kinetic energy.

The pressure presented in Fig. 13 and in the tables of Appendix E is a dimensionless pressure drop, $(p'-p_o')/\rho_g'(\bar{u}')^2$. The pressure drop, when expressed in psi, is usually small. The pressure drops reported in Appendix E are much less than those reported by Carpenter and Colburn (1). This difference may be attributed to possible turbulence and to downstream conditions present in their experiments.

Interfacial Shear

τ^*, the dimensionless shear stress at the vapor-liquid interface reported in Appendix E, is defined in equation (A-131). This is the same dimensionless shear stress used by Rohsenow, Webber, and Ling (5) in their model of condensation. Their model is based on constant shear stress at the interface, and they report heat transfer results for stresses ranging between 0 and 50. In results summarized in Appendix E this same stress ranges between 0.001 and 53.41 with most points falling below 5. However, in this work the interfacial shear is not held constant. It varies quite strongly with distance into the tube, as well as with entering velocity, temperature drop, tube diameter,

and physical properties. As reported in Appendix E it is quite high near the entrance and decreases sharply with increasing tube length. For a given length of condenser it increases with increasing entrance velocity. Near the entrance there seems to be little or no effect of tube diameter, and the shear stress increases with increasing temperature. Farther into the tube it increases with increasing diameter and decreases with increasing temperature drop.

The interfacial shear may be correlated to some degree. Such a correlation is shown in Fig. 14. The dimensionless shear stress divided by the Reynolds number seems to be a function of a dimensionless length, Z^*, for any given diameter, material, and temperature drop. No attempt was made to obtain a more generalized correlation.

Heat Transfer Results

Heat transfer results are presented in Appendix E. The ratio of the local heat transfer coefficient predicted by the mathematical model to the local heat transfer coefficient predicted by equation (I-9) of the Nusselt model is reported as "h'_{loc} ratio." The ratio of the average heat transfer coefficient predicted by the mathematical model to the average heat transfer coefficient predicted by equation (I-10) of the Nusselt model is reported as "h'_m ratio." The average heat transfer coefficient divided by Φ', the condensation number, is also reported. Φ' is defined as

$$\Phi' = \left(\frac{k'^3_\ell \rho'^2_\ell g'}{\mu'^2_\ell}\right)^{1/3} \qquad \text{(III-1)}$$

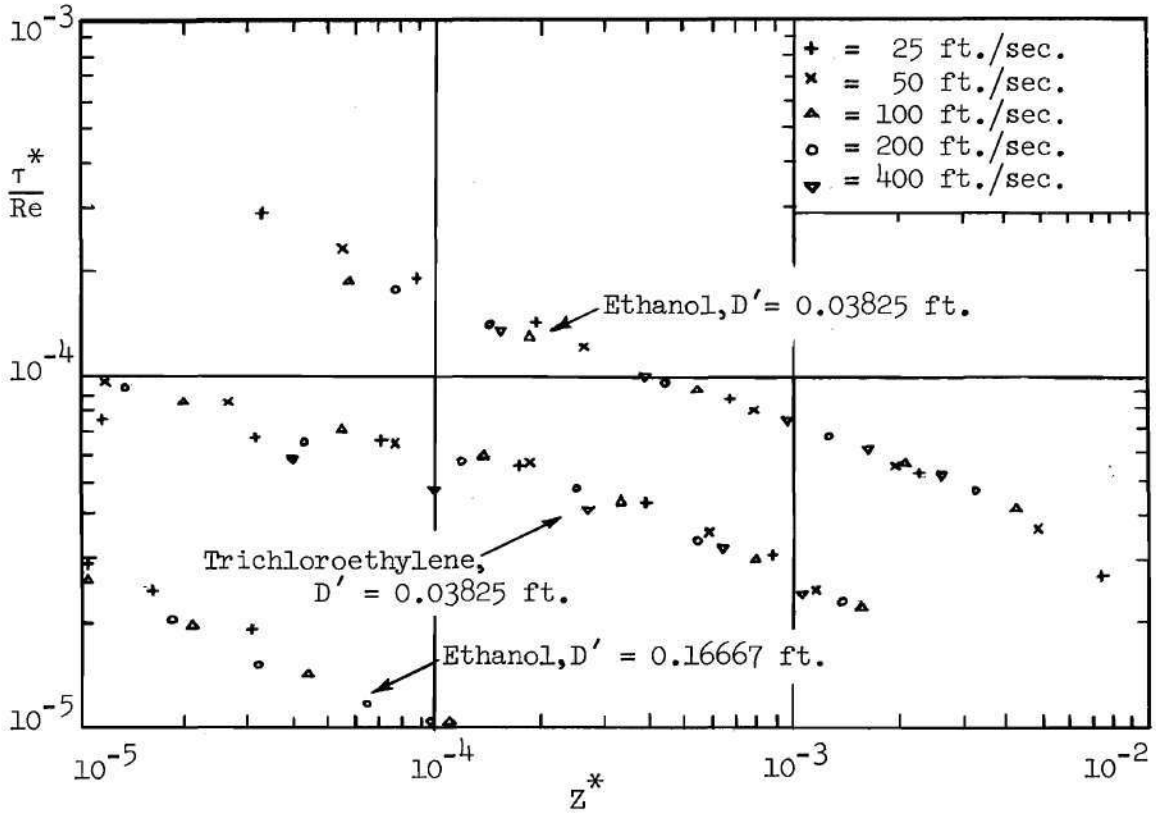

Fig. 14. Correlation of Interfacial Shear Stress: $\Delta T' = 10^{\circ}$ F.

The local and average heat transfer coefficients decrease with increasing length just as the Nusselt model predicts.

The local and average heat transfer ratios for a typical case are presented in Fig. 15. The average heat transfer coefficient is high near the entrance of the tube where the shear is the greatest. It asymptotically approaches the average heat transfer coefficient predicted by the Nusselt model. The average heat transfer coefficients reported in Appendix E are always greater than the Nusselt model would predict them to be and always approach the Nusselt prediction asymptotically. The local heat transfer coefficient is also high near the entrance but less than the average heat transfer coefficient at a given length. The local coefficient becomes lower than the Nusselt model prediction when the liquid film thickness becomes greater than that predicted by Nusselt. The film thickness for this run has been presented in Fig. 12. The film thickness becomes thicker than the Nusselt model at about the same place in the tube that h'_{loc} falls below the Nusselt prediction.

For an entering Reynolds number of 76,000 and a temperature drop of 48.5° F for the condensation of steam in the entrance region of a vertical tube, Jakob (38) has observed that the local heat transfer coefficient can fall below that predicted by his model in which the vapor velocity varied with length but the friction factor at the interface remained constant. He postulates that this may be caused by possible dropwise condensation near the entrance. The greater amount of fluid condensed by dropwise condensation increases the film thickness,

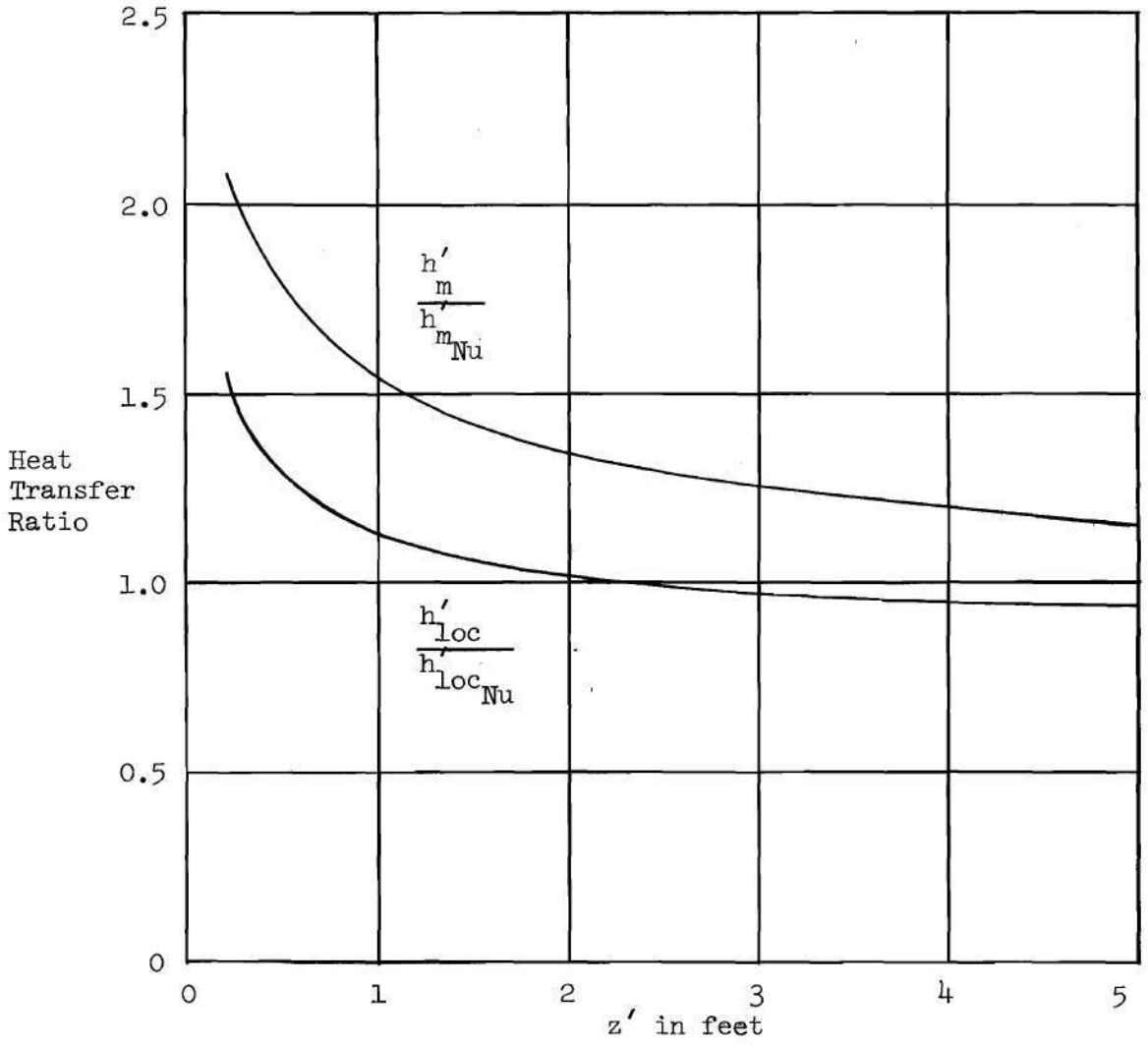

Fig. 15. Average and Local Heat Transfer Ratios as Functions of Length: Water, $\Delta T' = 20^{\circ}$ F, $D' = 0.03825$ ft., $\overline{u}' = 100$ ft./sec.

thus lowering h'_{loc}.

While it may be possible that this is occurring, the behavior of h'_{loc} may also be explained by allowing the entrance region interfacial shear to vary with increasing length as has been done in this study. Initially the shear is quite high, causing more vapor to be condensed. Farther into the tube it becomes much lower; the film becomes thicker than the Nusselt model prediction; and h'_{loc} becomes less than predicted. This may be observed in Figures 12 and 15.

Jakob also observed that the total amount of heat transferred through the wall was always greater than that predicted by theory. This is equivalent to saying that the average heat transfer coefficient was always greater than that predicted by theory. The numerical results of this study agree with this observation.

The effects of entering velocity and tube length on the average heat transfer coefficient are shown in Fig. 16 for water condensing in a 0.03825 foot diameter tube with a ten degree Fahrenheit temperature drop. As tube length increases h'_m decreases and all runs approach the Nusselt prediction. The individual numerical solutions approach the Nusselt curve at greater angles than do the models of Rohsenow, Webber, and Ling (5) and Hartmann (4). Rohsenow, Webber and Ling do not consider interfacial shear to be a function of length but their results indicate that if shear were a function of length the h'_m/Φ' curve would approach the Nusselt prediction at a greater angle. Hartmann does consider variation of shear with length, but his shear is estimated from friction factors for fully developed one phase flow. His results

approach the Nusselt curve at greater angles than do the results of Rohsenow, Webber, and Ling, but at smaller angles than the results of this study.

Lines corresponding to different lengths of condenser are presented on Fig. 16. Average heat transfer coefficients for a two foot condenser will lie along the two foot line. The positions of the constant length lines are not significantly affected by a change in tube diameter. However, the positions of these lines do depend on temperature drop through the liquid film. Lines of constant $z'\Delta T'$ for trichloroethylene are shown in Fig. 17.

Heat transfer coefficient data from a condenser of fixed length run under various conditions should appear to depart from the Nusselt curve at a film Reynolds number less than that normally associated with the onset of turbulence in the liquid film (1800-2100). The slope of the data should be somewhat similar to the slope of the data in the turbulent film region reported by Colburn (27). However, the departure of the heat transfer data of a fixed length condenser from the Nusselt curve does not necessarily indicate turbulence or that turbulence begins at the point of departure.

Although available experimental data for a condenser of fixed length do not meet the requirement of constant temperature drop through the liquid film, they do indeed seem to exhibit this type of departure from the Nusselt curve. The data of Carpenter (39) are compared with the numerical results of this study in Fig. 18. The experimental data for water, ethanol and trichloroethylene were obtained in a 0.03825

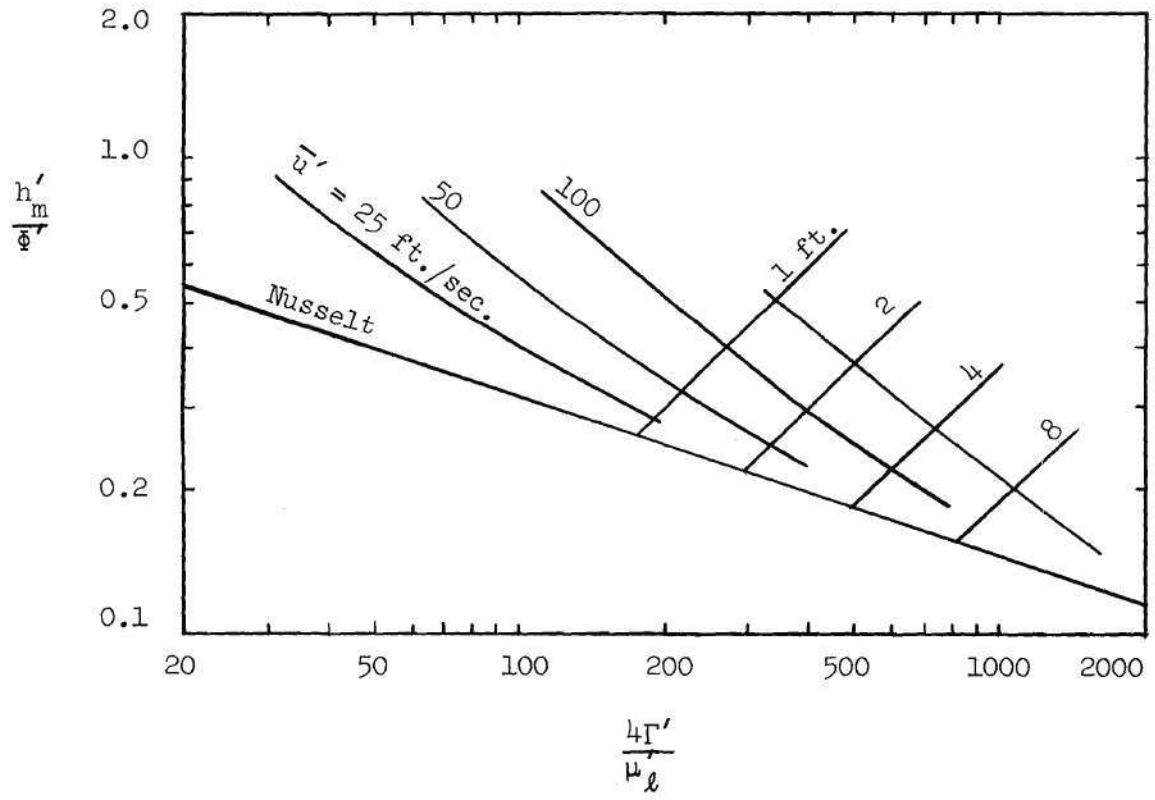

Fig. 16. Effect of Condenser Length and Entering Velocity on Heat Transfer: Water, $\Delta T' = 20^\circ$ F, $D' = 0.03825$ ft.

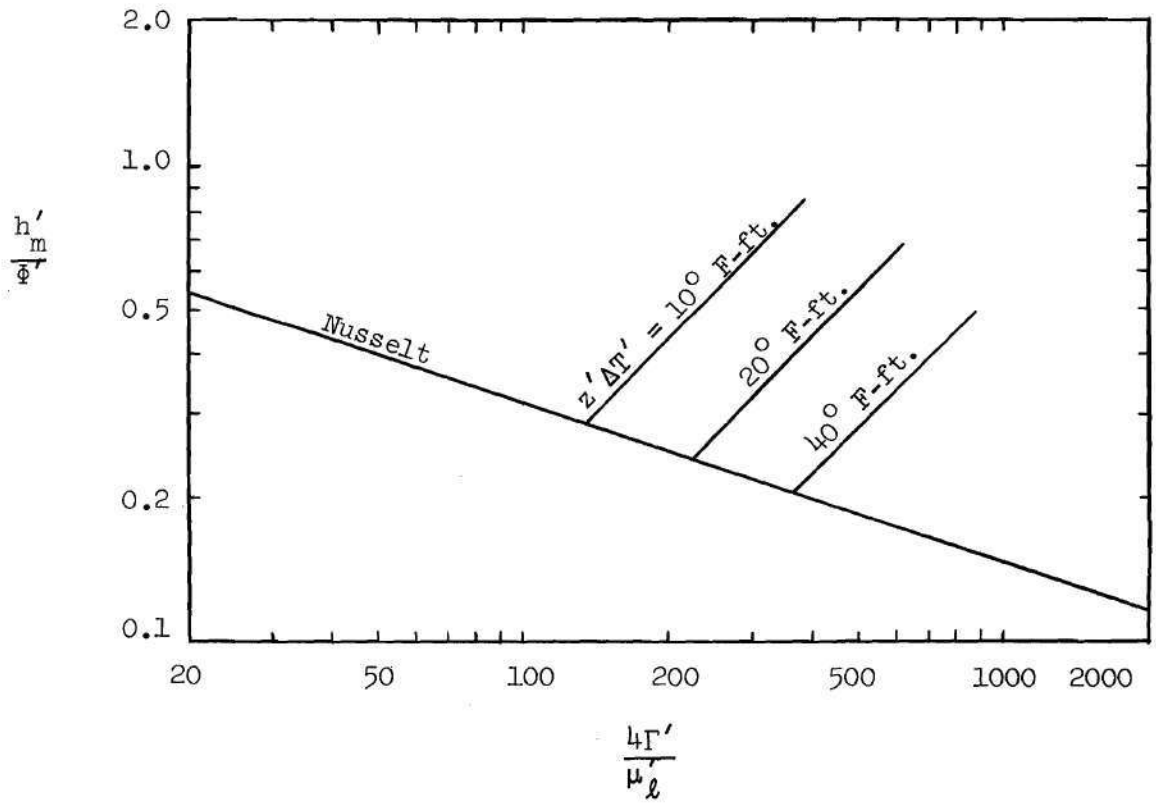

Fig. 17. Effect of $z'\Delta T'$ on Heat Transfer: Trichloroethylene

foot diameter tube which was 8.3 feet long. Entrance velocity varied from 88.5 to 572 ft./sec. The temperature drop through the liquid film varied quite a bit with length. An average temperature drop could be found for each experimental run, and these averages varied from 6.48 to 36.7° F. The heat transfer results predicted by this study for a condenser of the same size are shown in Fig. 18. The line along which the heat transfer results should lie is presented for each vapor. The temperature drop through the liquid film used in the numerical studies was constant at 20° F.

The ethanol data points in Fig. 18 would lie about an extension of the ethanol line predicted by this study. The same holds true for the water and trichloroethylene data. Apparently, turbulence is present in the liquid, or the vapor, or both. Turbulence would cause the heat transfer coefficients to be higher than those predicted by this study.

While the mathematical model does not include turbulence, the qualitative effects of certain variables, such as those illustrated in Figures 16 and 17, should remain the same if turbulence was present. The examination of the data points in more detail offers a good illustration of this hypothesis.

In Fig. 19 the average temperature drop and the entering velocity are denoted for each data point of water. The numerical solutions for temperature drops of five, ten, and twenty degrees for a condenser of identical size are presented also. The data clearly illustrate the qualitative effects of physical properties, entrance velocity, length,

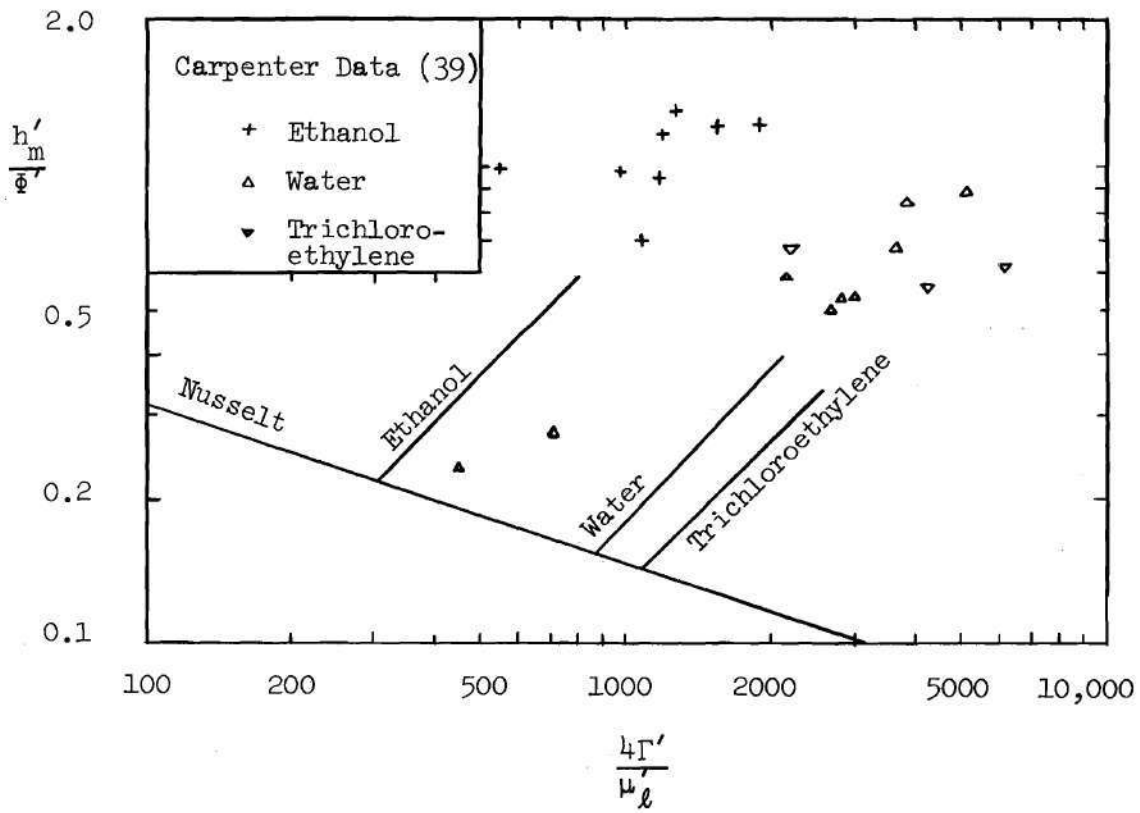

Fig. 18. Comparison of Carpenter Data with Numerical Results for a Tube 8.3 feet long and 0.03825 feet in Diameter: Numerical Results with $\Delta T' = 20^{\circ}$ F and Carpenter Data at Various Temperature Drops.

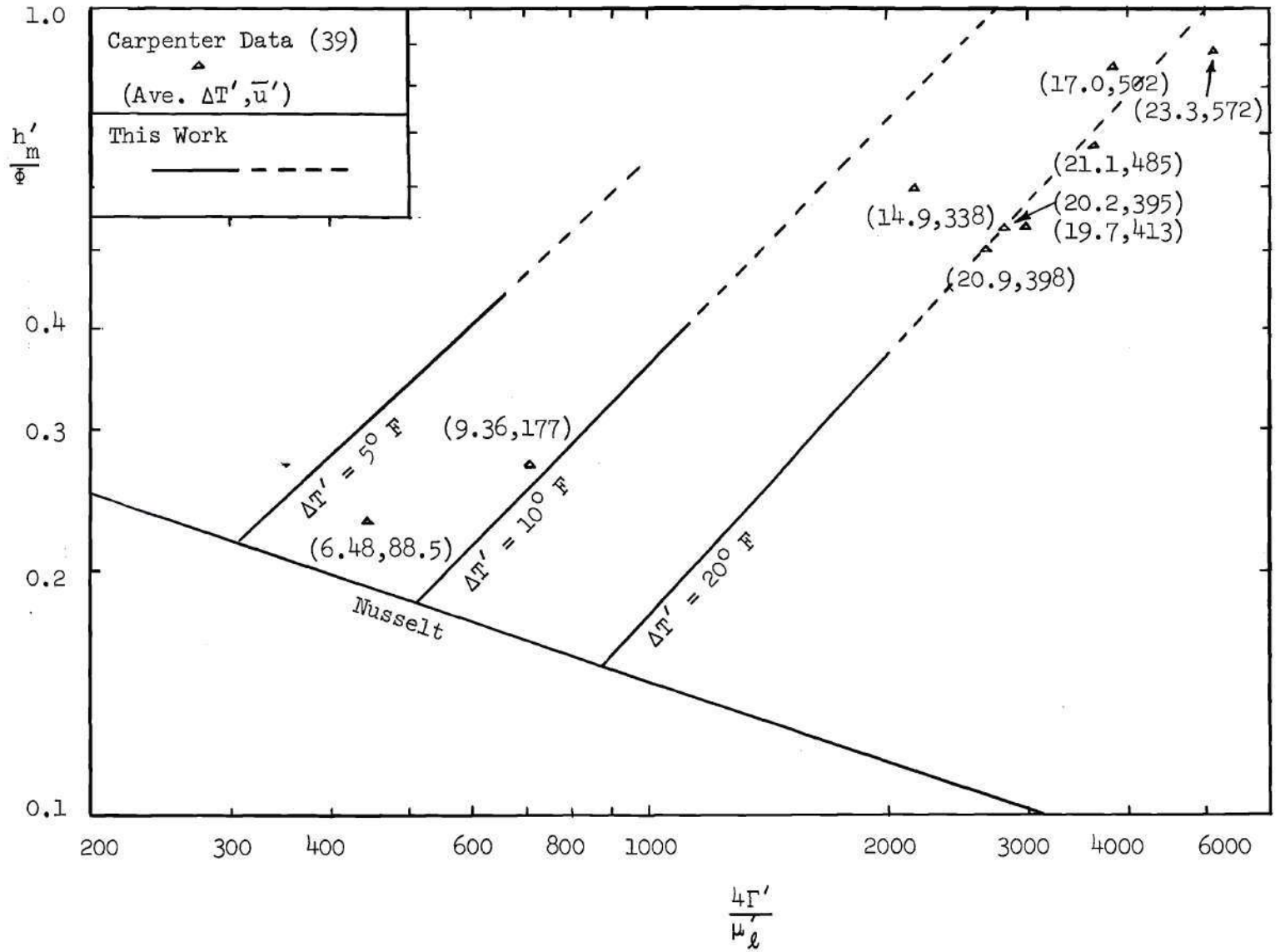

Fig. 19. Detailed Comparison of Carpenter Data with Numerical Results for a Tube 8.3 Feet Long and 0.03825 Feet in Diameter: Water

and temperature drop as shown in Figures 16 and 17. The data for ethanol and trichloroethylene also show this behavior. For instance, the average temperature drops for the three trichloroethylene points shown in Fig. 18 are 9.6, 22.1, and 29.3° F reading from left to right.

Correlation of Heat Transfer Results

The heat transfer results of this study may be expressed by an equation of the form

$$\frac{h'_m}{h'_{m_{Nu}}} = K(Fr_L)^a \left(\frac{\mu'_g}{\mu_\ell}\right)^b \left(\frac{\rho'_g}{\rho_\ell}\right)^c \left(\frac{C'_{p_\ell}\,\Delta T'}{\lambda'}\right)^d \left(\frac{z'}{D'}\right)^e (Pr_\ell)^f (Re_g)^g \qquad \text{(III-2)}$$

where $h'_{m_{Nu}}$ is the average heat transfer coefficient given by equation (I-10) of the Nusselt model. Use is made of the Nusselt model because it accurately expresses the dependence of the heat transfer coefficient on certain variables for the limiting case of no shear. The physical properties used in this equation are measured at the boiling point temperature.

The average heat transfer ratios reported in Appendix E may be fitted to equation (III-2) or various parts of it by the method of least squares. For this purpose the equation was expressed in logarithmic form and a computer program developed to find the least squares fit to the resulting linear equation. The results of a number of correlation attempts are summarized in Table 1.

No correlation was obtained which was satisfactory over the entire range of numerical results. Adequate representation was achieved by dividing the results into three main groups: those with length Froude numbers below 10, those with length Froude numbers between 10

Limitations	Unknowns in Equation (III-2)								Average % Error	Max. Pos. % Error	Max. Neg. % Error
	K	a	b	c	d	e	f	g			
$10 < Fr_L < 1000$	1.13	0.126	0.0405	0.0438	0.0008	-0.003	0.0022	0.0042	± 3.1	11.0	-14.7
$10 < Fr_L < 1000$	1.13	0.128	0.0287	0.0459					± 3.2	11.7	-14.2
$10 < Fr_L < 1000$	0.747	0.130							± 3.8	14.7	-15.0
$Fr_L > 1000$	0.475	0.328	0.0300	0.134	-0.057	0.0142	0.0564	-0.023	± 3.5	7.7	-15.3
$Fr_L > 1000$	0.166	0.316	-0.210	0.0685					± 4.7	12.6	-15.5
$Fr_L > 1000$	0.188	0.335							± 7.2	22.0	-17.7

Table 1. Correlation of Heat Transfer Results: Condensation of Pure Vapors

and 1000, and those with length Froude numbers above 1000. The length Froude number is defined as

$$Fr_L = \left(\frac{(\bar{u}')^2}{g' z'}\right) \qquad \text{(III-3)}$$

The importance of the length Froude number in correlating heat transfer results is shown in Table 1 and Fig. 20. $h'_m/h'_{m_{Nu}}$ may be correlated adequately by a constant times the length Froude number raised to a power.

When the length Froude number is less than 10 the Nusselt model can be used to estimate heat transfer coefficients. When the length Froude number is between 10 and 1000 the heat transfer coefficient can be represented by

$$\frac{h'_m}{h'_{m_{Nu}}} = 0.747\ (Fr_L)^{0.130} \qquad \text{(III-4)}$$

where $h'_{m_{Nu}}$ is given by equation (I-10). For length Froude numbers greater than 1000 the heat transfer coefficients may be represented by

$$\frac{h'_m}{h'_{m_{Nu}}} = 0.188\ (Fr_L)^{0.335} \qquad \text{(III-5)}$$

where $h'_{m_{Nu}}$ is also given by equation (I-10). The larger error reported in Table 1 for this equation is probably caused by the effect of the starting procedure used in the numerical solutions. Large Froude numbers occur near the entrance of the tube where these effects are the greatest.

The correlating equations above are based on numerical results for water, ethanol, and trichloroethylene. These equations should be

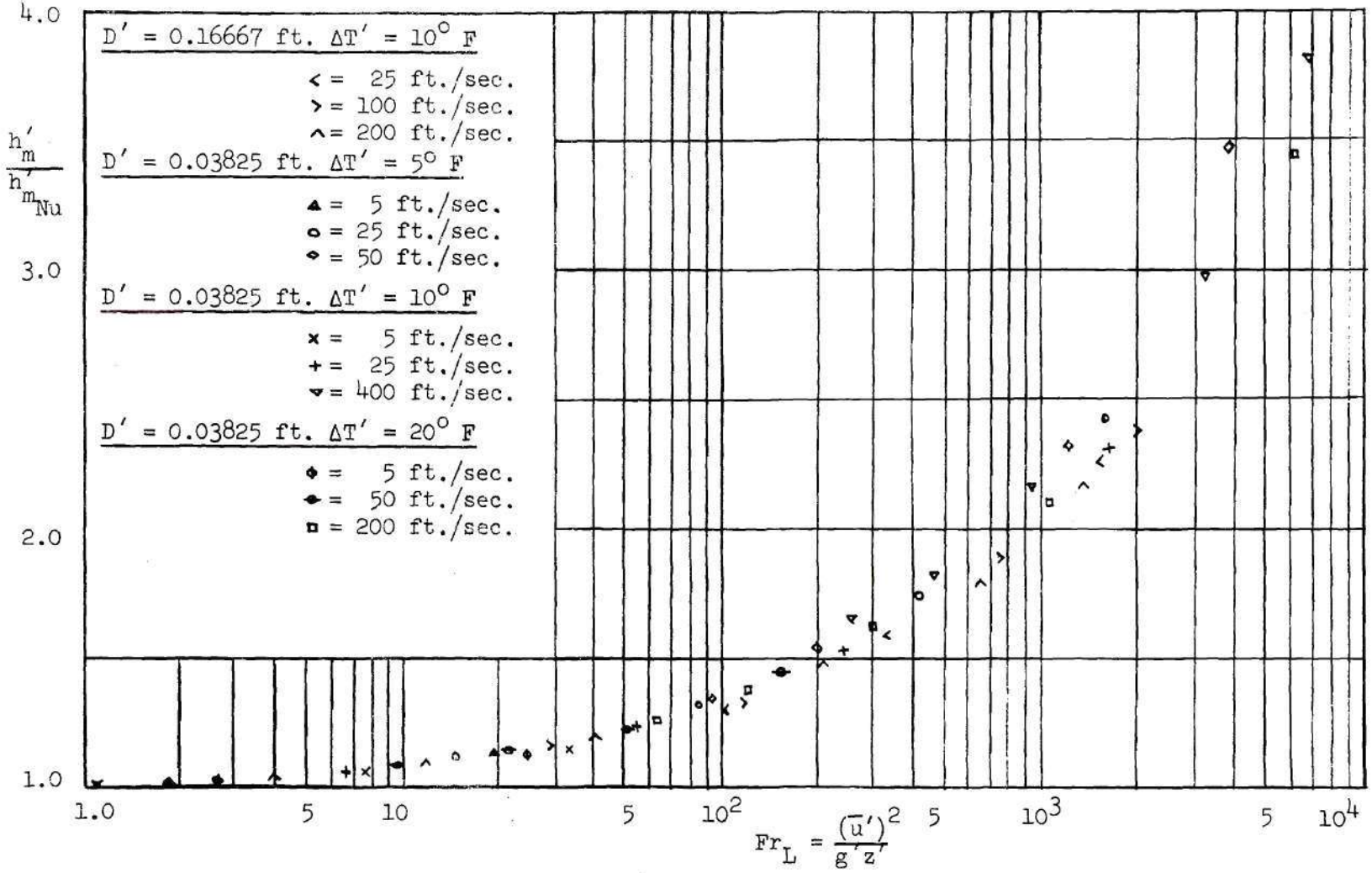

Fig. 20. Importance of Length Froude Number as a Correlating Factor: Ethanol

for a much larger range of physical properties than these three fluids encompass because the effect of physical property variation on the heat transfer coefficient has been taken into account adequately by the Nusselt model which is a part of the correlating equation.

The data of Carpenter (39) may be correlated by equation (III-2). The results are shown in Table 2. The length Froude number does not appear to be as important for correlating the experimental data as it does for correlating the numerical results of this study. The Reynolds number of the entering gas appears to be more important. However, none of the correlating equations has a distinct advantage over the others. At best they appear to correlate the data as well as the relationship suggested by Carpenter and Colburn (1):

$$h'_m = 0.065 \left(\frac{C'_{p_\ell} k'_\ell \rho'_\ell \overline{f}}{2\mu'_\ell \rho'_g} \right)^{\frac{1}{2}} G'_m \qquad \text{(III-6)}$$

Other investigators have correlated the results of their numerical studies. Hartmann (4) reports that his model may be correlated by

$$\frac{h'_m D'}{k'_\ell} = 0.36 \left(\frac{Pr_\ell}{\left(\frac{z'}{D'}\right) \frac{C'_p \Delta T'}{\lambda'}} \right)^{0.335} \left(Re_g \right)^{0.6} \left(\frac{(\mu'_g)^2 \rho'_\ell}{(\mu'_\ell)^2 \rho'_g} \right)^{1/3} \qquad \text{(III-7)}$$

over much of the range of physical properties considered. He also reports that the numerical results of Jakob (3) may be correlated by

$$\frac{h'_m D'}{k'_\ell} = 0.709 \left(\frac{(\mu'_g)^2 \rho'_\ell Pr_\ell}{(\mu'_\ell)^2 \rho'_g \left(\frac{z'}{D'}\right) \frac{C'_p \Delta T'}{\lambda'}} \right)^{1/3} \left(Re_g \right)^{0.583} \qquad \text{(III-8)}$$

Rohsenow, Webber, and Ling (4) report their results in graphical form.

Limitations	Unknowns in Equation (III-2)								Average % Error	Max. Pos. % Error	Max. Neg. % Error
	K	a	b	c	d	e	f	g			
None	0.115	0.233	0.128	0.217	-0.264	-0.485	0.467	0.465	± 12.6	49.1	-27.1
None	4.20	0.379	-0.518	0.581					± 14.6	67.9	-45.4
None	1.35	0.190							± 36.9	186	-52.4
None	0.0183	0.0459						0.450	± 20.8	79.1	-57.6
None	0.0132	0.135					0.311	0.406	± 15.5	57.5	-56.4
None	0.0123					-0.105	0.153	0.536	± 20.9	57.0	-46.0

Table 2. Correlation of Carpenter Results (39): Condensation of Pure Vapors

The results of these investigators and the results of this study are compared with the experimental data of Carpenter in Table 3. Three experimental runs at different conditions are covered in the table. Apparently, entering velocity is the most important variable in determining how well the correlating equations agree with the data.

As expected, the Nusselt model predicts heat transfer coefficients below the observed ones because the effect of interfacial shear is not included in the analysis. Jakob's results predict values which are higher than the experimental data. These results were derived for a model with constant interfacial shear with the shear being evaluated at the Reynolds number of the entering gas. Such a procedure overestimates the effect of interfacial shear on heat transfer.

The three experimental runs listed in Table 3 are outside of the range over which Hartmann's correlation is reported valid. However, the graphical results reported by Hartmann indicate that his equation may be used for these runs.

Hartmann attempted to allow for the variation of interfacial shear with length. He estimated the shear caused by decreasing vapor flow by using friction expressions for fully developed one phase flow. The liquid was always assumed to be laminar. The predictions appear low for the experimental run with the highest velocity, about right for the medium velocity run, and high for a low velocity run. The high velocity prediction may be low because it does not include entrance effects on the shear. The shear in entrance regions is higher than for fully developed flow. The low velocity prediction probably overestimates

Run Particulars \ Average Heat Transfer Coefficients in BTU/sec.-ft.^{2}-$^\circ$F	Observed by Carpenter (39)	Nusselt Equation (I-10)	This Work Equations (III-4), and (III-5)	Jakob Equation (III-8)	Hartmann Equation (III-7)	Carpenter and Colburn Equation (III-6)	Rohsenow, Webber and Ling (5)
H_2O, $\bar{u}' = 572$ ft./sec. $z' = 8.3$ ft. $D' = 0.03825$ ft. $\Delta T' = 23.3^\circ$ F, $Re_g = 96,400$	1.367	0.2334	0.428	1.65	1.01	1.28	1.3
H_2O, $\bar{u}' = 320$ ft./sec., $z' = 3.6$ ft. $D' = 0.03825$ ft. $\Delta T' = 46.1^\circ$ F, $Re_g = 54,300$	0.711	0.2426	0.438	1.237	0.752	0.725	0.69
H_2O, $\bar{u}' = 88.5$ ft./sec., $z' = 8.3$ ft. $D' = 0.03825$ ft. $\Delta T' = 6.48^\circ$ F, $Re_g = 14,980$	0.382	0.3215	0.373	0.853	0.507	0.274	0.41

Table 3. Comparison of Experimental Data with Predicted Results: Condensation of Pure Vapors

the shear and, therefore, predicts a high coefficient. It may overestimate the shear because the flow may not be fully turbulent or even turbulent at all. The Reynolds number of the entering vapor is 14,980. If there was no condensation the flow would slowly change into fully developed turbulent flow as length increases. With condensation providing a suction near the wall turbulence may not develop.

The correlating equations of this study appear to give poor results at high vapor Reynolds numbers. This was apparently caused by the fact that the flow was turbulent. The very few data available for low vapor velocities indicate that the results of this study appear good to within ten percent for vapor Reynolds numbers less than 30,000. Too few data exist to determine the exact range over which the results of this study apply.

Rohsenow, Webber, and Ling try to encompass high and low velocity runs in their model by assuming that the laminar liquid film becomes turbulent when it satisfies certain conditions. The transition from one kind of film to another is assumed to be a function of interfacial shear. The interfacial shear is assumed to be a constant in their numerical studies. In using their graphs to estimate heat transfer results, an average value of interfacial shear for the run is estimated from fully developed one phase flow friction factor expressions. Their predictions give the best overall results for the three points in Table 3. According to their results the film of the low velocity experimental run remains laminar while the films of the other runs have become turbulent.

Carpenter's data appear to have been taken over a transition region. Under certain conditions the results of this study provide adequate correlating equations. Other relationships may be necessary under other conditions. Correlation of the experimental heat transfer results with a single equation is difficult as can be seen in Table 2 and Table 3. These equations provide little insight into the real importance of the various dimensionless groups. Table 3 and a graph presented by Carpenter and Colburn seem to indicate that their correlation equation is subject to smaller error at high inlet velocities than at low inlet velocities.

Much more experimental data similar to Carpenter's should be taken. The data should cover thoroughly a large range of entrance velocities, tube lengths, temperature drops, and tube diameters. Such data would illuminate the apparent transition from one controlling mechanism to another and provide better correlations of heat transfer results.

CHAPTER IV

CONDENSATION OF A VAPOR AND NONCONDENSABLE GAS MIXTURE

Numerical solutions to equations (II-4), (II-5), (II-6), (II-10), and (II-11) and the related boundary conditions given in Chapter II are presented below. Details of the method of solution and discussion of its validity are included in Appendix A. An outline of the computer program used to solve the equations is given in Appendix B, and the complete computer program is given in Appendix C. The physical properties used in these calculations are presented in Appendix D, and the numerical results are presented in tabular form in Appendix F.

Two vapor-gas mixtures were considered: ethanol vapor and air, and water vapor and air. Entrance velocities varied from two and one-half feet per second to two hundred feet per second. The Reynolds numbers of the entering gas varied from 1843 to 360,793. Three values of the temperature of the entering mixture minus the wall temperature were considered: five, ten, and twenty degrees Fahrenheit. The concentration of air in the entering stream varied from 0.1 weight percent to 5 weight percent. Schmidt numbers of 0.5 and 0.6 were investigated in the condensation of water-air mixtures. Most numerical solutions were in a 2.0 inch diameter tube, although some results are presented for an 0.459 inch diameter tube. Tube lengths were as long as twenty feet. With the exception of density the physical properties used in the model are those of the liquid and pure vapor at the boiling point.

The density was allowed to vary as a function of concentration.

Velocity, temperature, and concentration profiles, liquid film thickness, pressure drop, interfacial shear, heat transfer results, correlation of heat transfer results, and comparison with other methods of calculation are discussed below. "Run" refers to a numerical solution unless otherwise designated.

Velocity Profiles

Typical radial and axial velocity profiles in the vapor phase are presented in Tables 41, 42, 43, 45, 46 and 47. Typical radial and axial velocity profiles in the liquid phase are presented in Tables 44 and 48.

The velocity profiles were observed to vary quite a bit with the conditions of each run. No attempt was made to generalize them. They exhibit the same general dependence on radius, length, entrance velocity, and temperature drop as the profiles presented in Chapter III for pure vapors.

The effect of noncondensable concentration on the centerline velocity is shown in Fig. 21. The greater the amount of noncondensable, the greater the length of tube necessary to condense a given amount. The presence of noncondensable gas at the interface reduces the interface temperature. Because of this, less heat is transferred and, consequently, less mass is condensed. The effect is similar to that shown in Fig. 3.

As in the pure vapor case the assumption that $v_z' >> v_r'$ does not appear to be true for low velocity runs near the interface and near

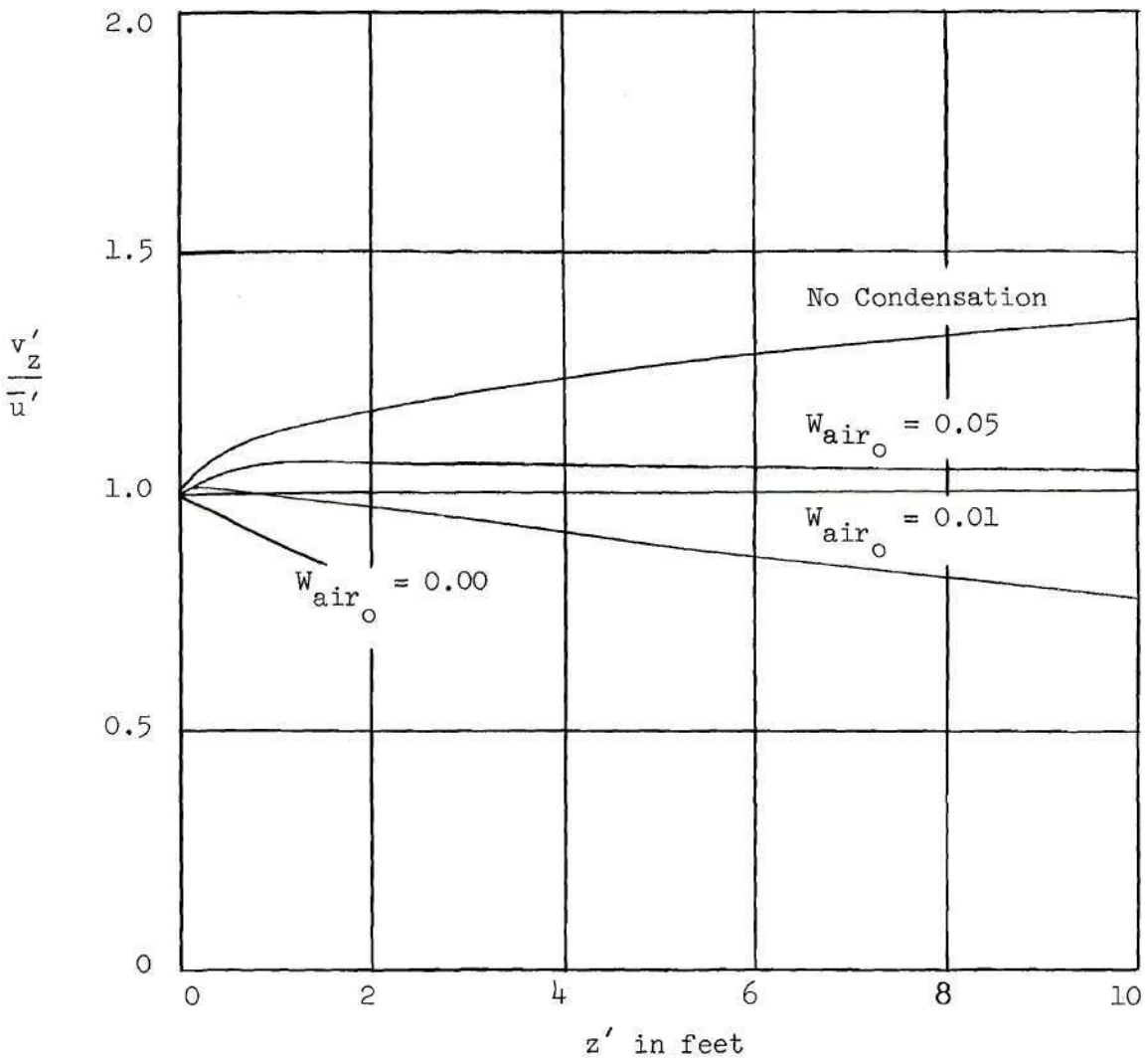

Fig. 21. Effect of Noncondensable Concentration on Centerline Velocity: Water Vapor and Air, $D' = 0.16667$ ft., $\bar{u}' = 25$ ft./sec., $Re_g = 18435$, $Sc_g = 0.500$, $T'_o = 212^\circ$ F, $T'_w = 207^\circ$ F.

the entrance. This is the case for all runs with entrance velocities of 2.5 feet per second and some with entrance velocities of 25 feet per second. Making the assumption should have only a small effect on these low velocity solutions because the region where the assumption does not hold is small.

Concentration Profiles

Concentration profiles in the vapor phase are presented in Tables 41, 42, 43, 45, 46, and 47 of Appendix F. In addition the concentration of noncondensable at the interface is presented as a function of condenser length for each case in the Summary of Results Tables in Appendix F.

The vapor phase concentration profile for a typical case is shown in Fig. 22. The concentration of the noncondensable is greater at the interface than at the center of the tube or at the entrance. This effect is predicted by the Colburn and Drew (26) analysis. As the vapor is condensed out the concentration of noncondensable gas gradually increases.

In Fig. 23 the interfacial concentration of noncondensable is shown to decrease with increasing velocity. It is less dependent on length at higher velocities. Also, the lower the entering velocity, the greater the rate at which vapor is condensed compared to the rate at which it enters the tube.

In Fig. 24 the concentration of noncondensable at the interface is shown to increase with increasing available temperature drop, $T'_o - T'_w$. This effect is predicted by the Colburn and Drew analysis.

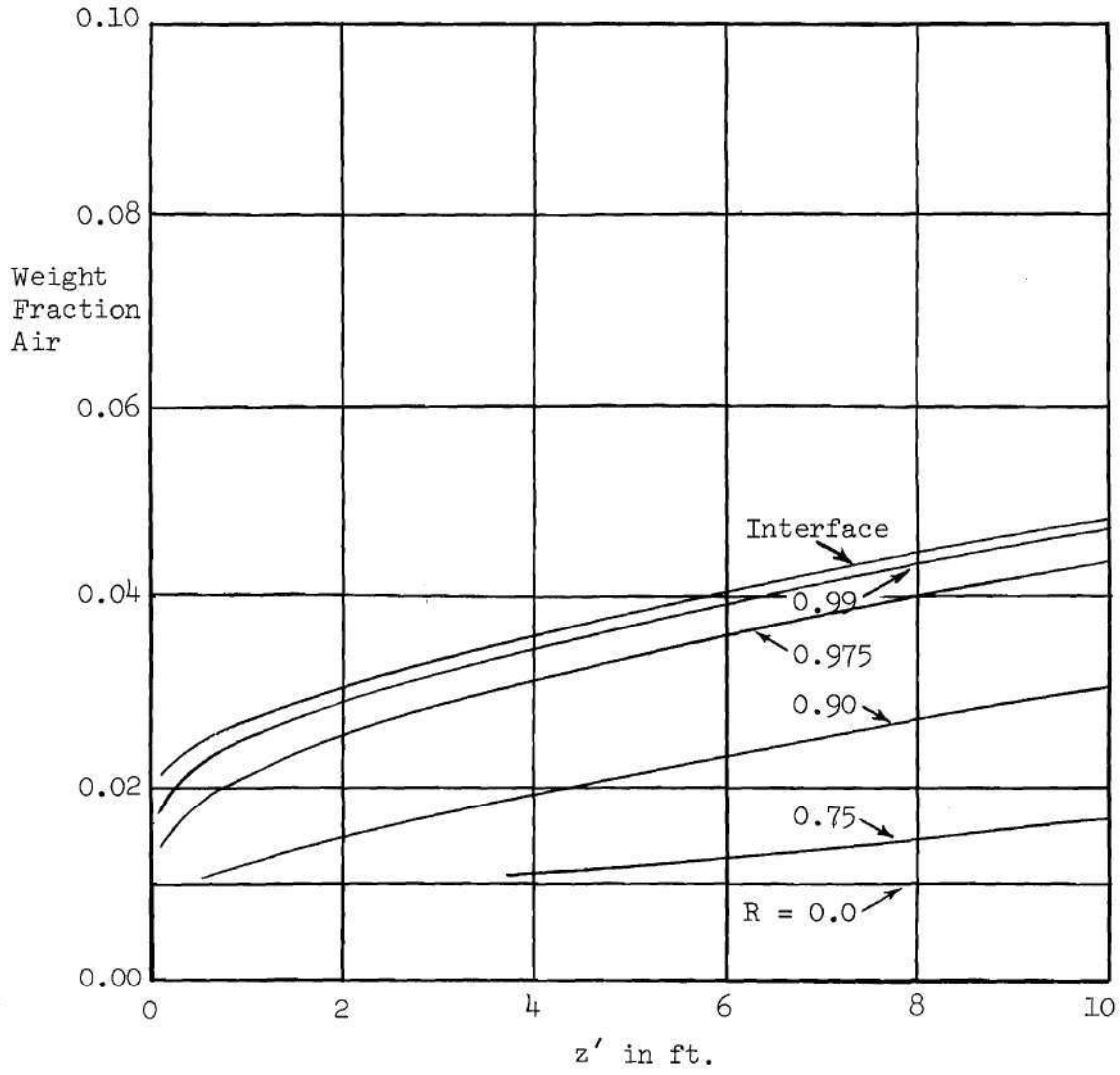

Fig. 22. Concentration Profile in the Vapor Phase: Water Vapor and Air, $D' = 0.16667$ ft., $\overline{u}' = 25$ ft./sec., $Re_g = 18435$, $Sc_g = 0.500$, $T'_o - T'_w = 5^\circ$ F, $W_{air_o} = 0.01$.

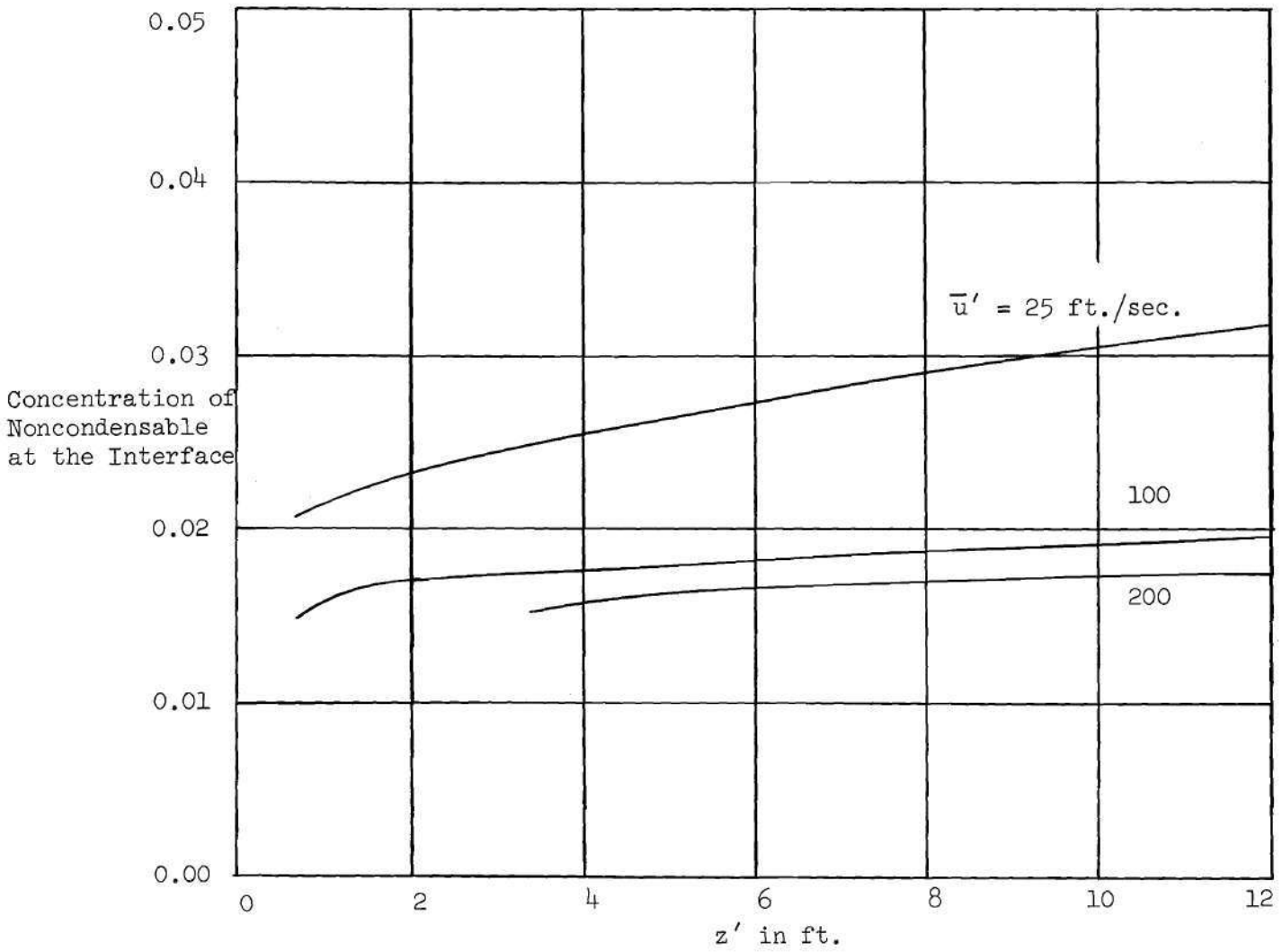

Fig. 23. Effect of Velocity on Interfacial Concentration: Ethanol Vapor and Air, $D' = 0.16667$ ft., $Sc_g = 0.537$, $W_{air_o} = 0.01$, $T'_o = 173.3^\circ$ F, $T'_w = 163.3^\circ$ F.

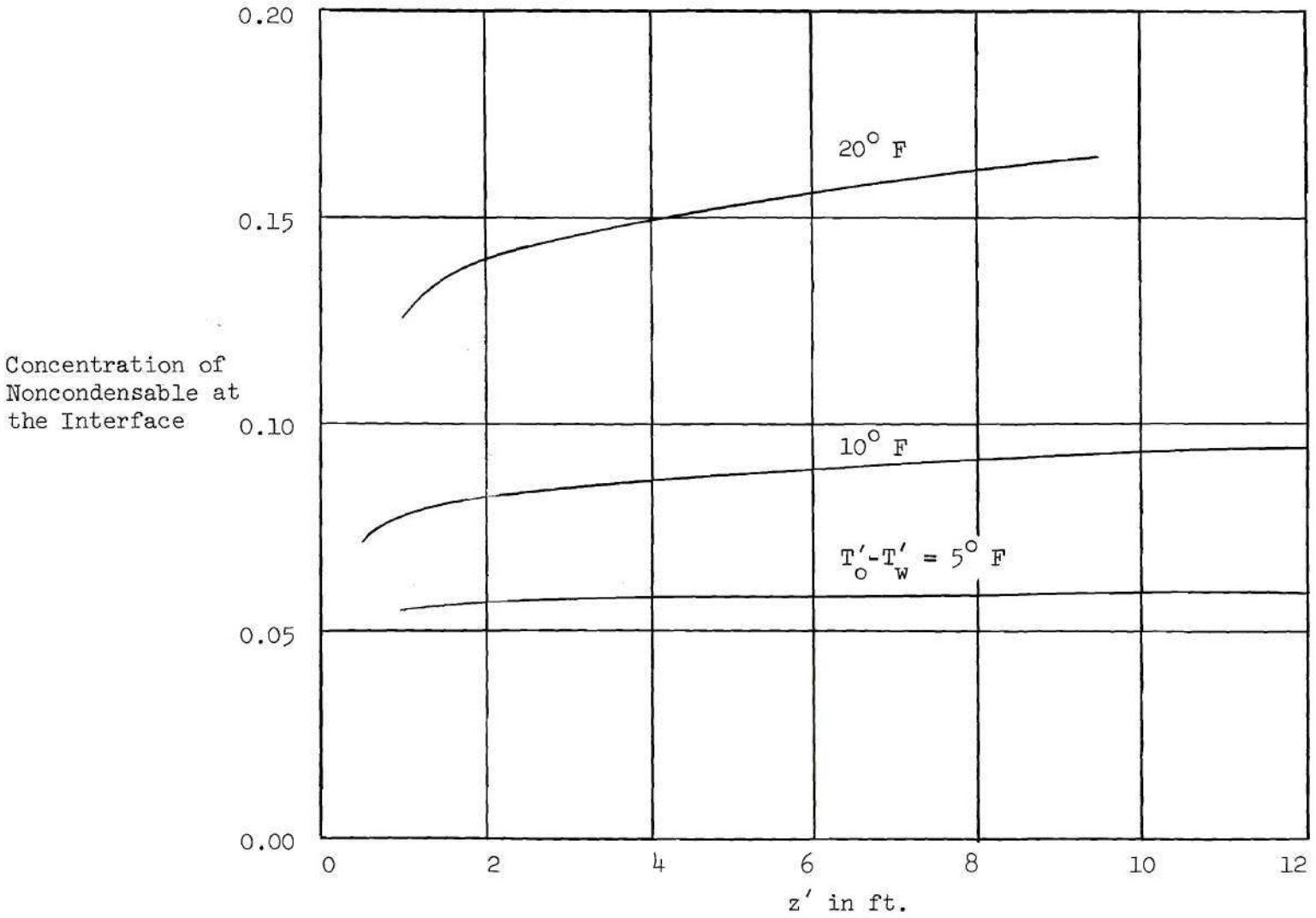

Fig. 24. Interfacial Concentration as a Function of Available Temperature Drop: Ethanol Vapor and Air, $D' = 0.16667$ ft., $\bar{u}' = 25$ ft./sec., $Re_g = 45099$, $Sc_g = 0.537$, $W_{air_o} = 0.05$, $T'_o = 173.3^\circ$ F.

Temperature Profiles

Typical temperature profiles in the vapor phase are reported in Tables 41, 42, 43, 45, 46, and 47 and in the liquid phase in Tables 44 and 48 of Appendix F. In addition, interfacial concentrations are reported for each case in the Summary of Results Tables in Appendix F. Interface temperature may be calculated from these concentrations.

Noncondensables reduce the interface temperature by reducing the partial pressure of the condensable vapor at the interface. The greater the concentration of noncondensable gas, the less the interface temperature. The smaller the interface temperature, the smaller the temperature gradient between the interface and the wall, and therefore the smaller the amount condensed.

The interface temperature decreases with increasing length as is shown in Fig. 25. In this figure less than half of the available temperature drop occurs over the liquid film. As the concentration of noncondensable in the entering mixture decreases the percentage of the temperature drop occurring over the liquid film increases.

The temperature in the liquid varies almost linearly with radius. This was also observed in Chapter III for pure vapor condensation.

Liquid Film Thickness

The effect of noncondensable concentration in the entering mixture on liquid film thickness δ' is shown in Fig. 26. Near the entrance the effect is quite small. However, as tube length increases the liquid film becomes thinner as the concentration of noncondensable increases. This is so in spite of the fact that interfacial shear

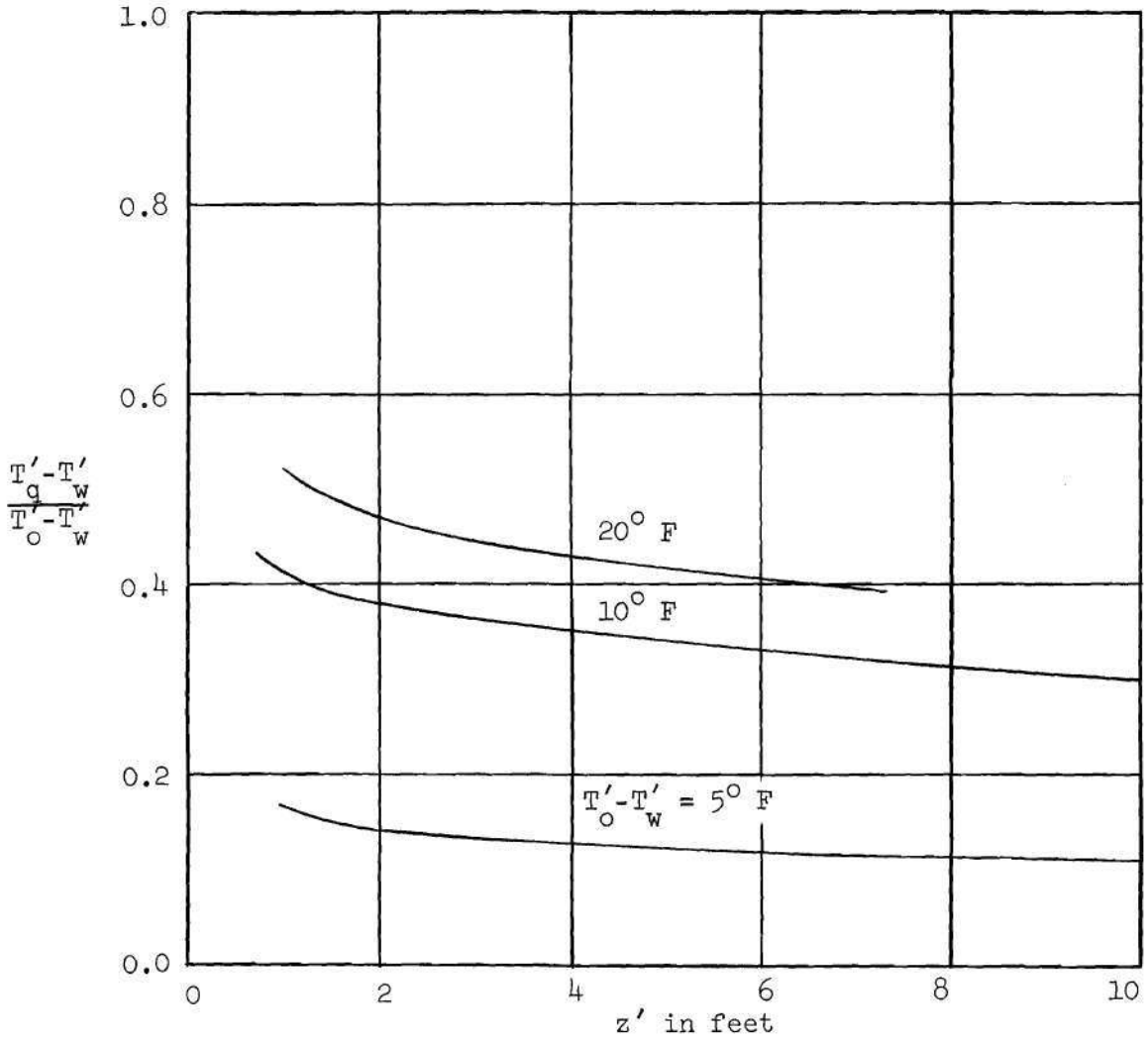

Fig. 25. Interface Temperature as a Function of Available Temperature Drop: Ethanol Vapor and Air, $D' = 0.16667$ ft., $\bar{u}' = 25$ ft./sec., $Re_g = 45099$, $Sc_g = 0.537$, $W_{air_o} = 0.05$, $T'_o = 173.3°$ F.

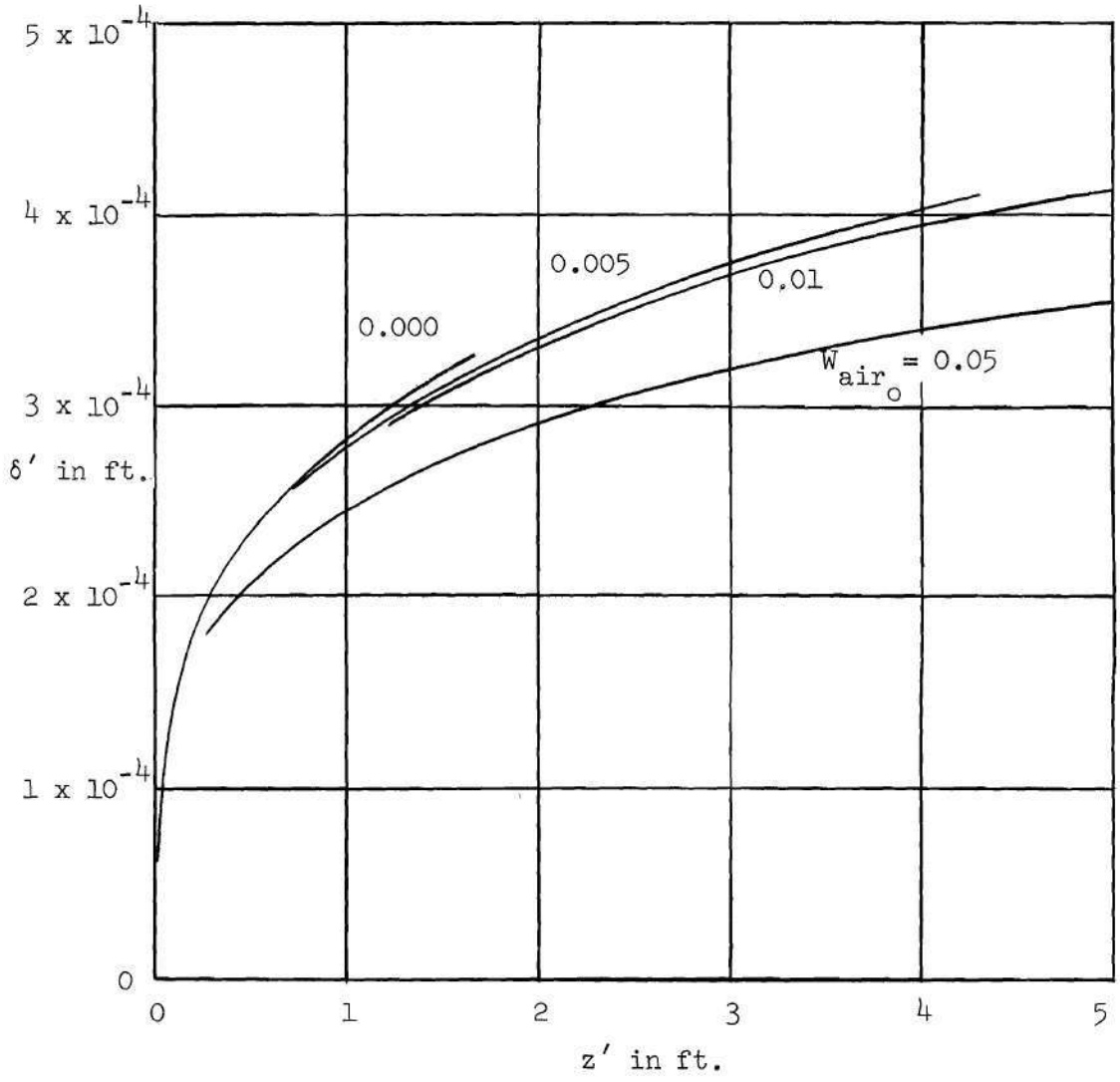

Fig. 26. Effect of Noncondensable Concentration on Liquid Film Thickness: Water Vapor and Air, $D' = 0.16667$ ft., $\bar{u}' = 25$ ft./sec., $Re_g = 18435$, $Sc_g = 0.500$, $T'_o = 212^\circ$ F, $T'_w = 202^\circ$ F.

increases with decreasing noncondensable concentration.

Pressure Drop

The pressure drop-length relationship for condensation of vapor from a vapor-air mixture is similar to that for a pure vapor. Initially, the pressure decreases with increasing length. It reaches a minimum value, and then starts increasing. It can become greater than the entrance pressure. As suggested in Chapter III this behavior is probably caused by two effects: the high pressure drop normally associated with the entrance region of tubes; and a Bernoulli effect, converting kinetic energy into pressure.

Since the presence of noncondensables reduces the amount of vapor condensed it reduces the amount of kinetic energy converted into pressure. The pressure at a given tube length is always less when there are noncondensables present than when the vapor is pure. This may be seen in Fig. 27. For this combination of condensation conditions the pressure is less than the entrance pressure only in a very small region near the inlet. The actual pressure increase when expressed in psi is quite small.

Interfacial Shear

The dimensionless interfacial shear stress for the condensation of vapor-noncondensable gas mixtures behaves in a manner similar to that exhibited by pure vapor condensation.

In the first part of the tube the interfacial shear decreases with increasing noncondensable concentration. Greater condensation

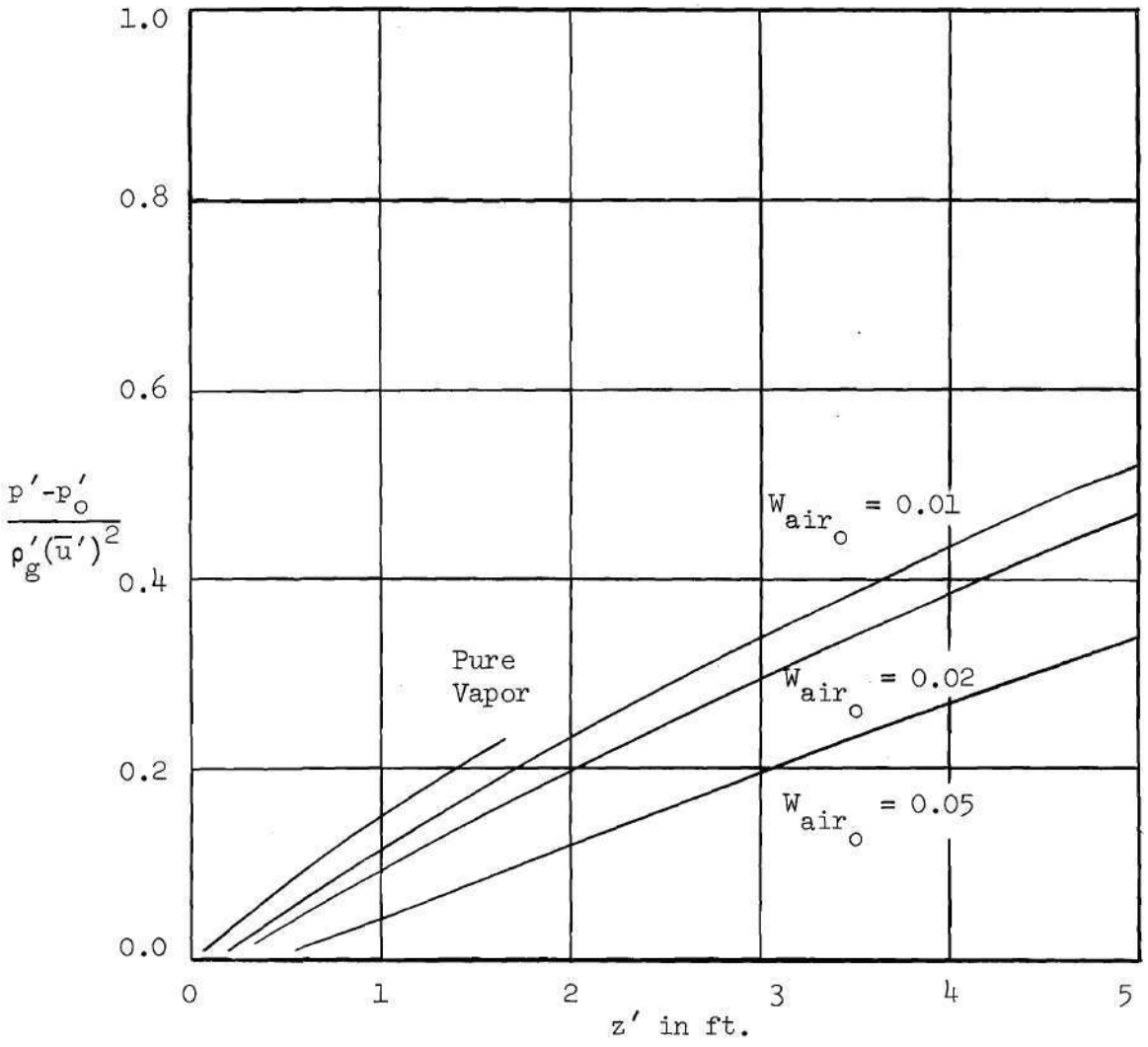

Fig. 27. Effect of Noncondensable Concentration on Pressure Drop: Water Vapor and Air, $D' = 0.16667$ ft., $\bar{u}' = 25$ ft./sec., $Re_g = 18435$, $Sc_g = 0.600$, $T'_o = 212^\circ$ F, $T'_w = 202^\circ$ F.

rates cause high speed vapor to be pulled near the interface. This causes increased shear at the interface. The same effect was achieved in pure vapor condensation by increasing the temperature drop and thereby increasing the rate of condensation. As the tube length increases, the interfacial shear decreases. It decreases at a greater rate and becomes negligible faster for lower concentrations of noncondensable.

Heat Transfer Results

Heat transfer results similar to those described in Chapter III are presented in Appendix F for vapor-noncondensable gas mixtures. These heat transfer coefficients are all based upon the available temperature drop, $T'_o - T'_w$.

The effect of noncondensable concentration on the average heat transfer coefficient is shown in Fig. 28. The coefficients are higher near the inlet where the interfacial shear is the greatest and the noncondensable concentration the lowest. In addition, h'_m decreases with increasing noncondensable concentration. The results reported in Appendix F are always less than the corresponding pure vapor case. The average coefficients can fall far below the Nusselt prediction for pure vapors.

The local heat transfer coefficients for the same cases are presented in Fig. 29. The local heat transfer coefficients exhibit the same general dependence on length and concentration as the average coefficients. The average heat transfer coefficient for a run is always greater than the local heat transfer coefficient at a given length.

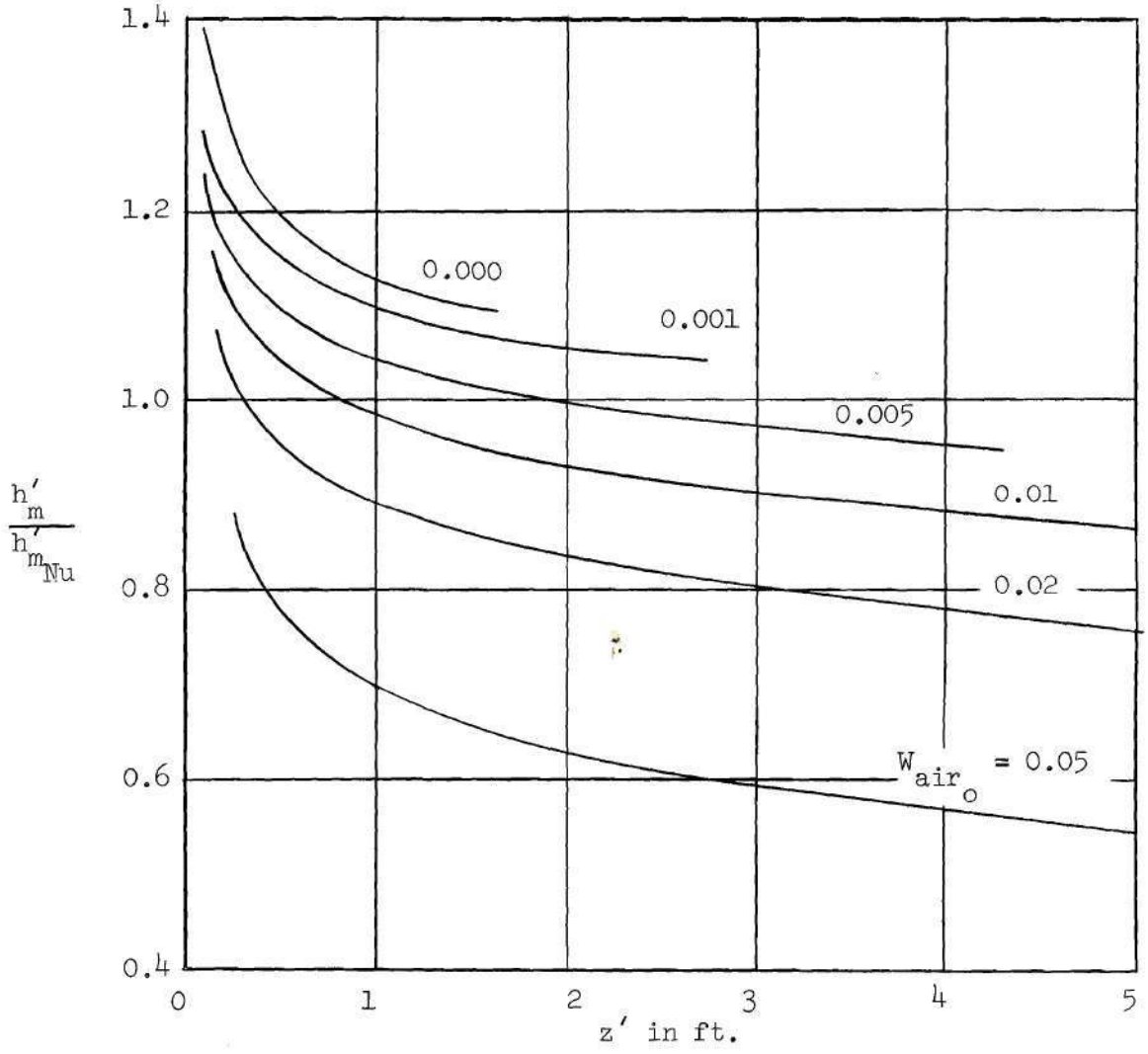

Fig. 28. Effect of Noncondensable Concentration on Average Heat Transfer Coefficients: Water Vapor and Air, $D' = 0.16667$ ft., $\bar{u}' = 25$ ft./sec., $Re_g = 18435$, $Sc_g = 0.500$, $T'_o = 212^\circ$ F, $T'_w = 202^\circ$ F.

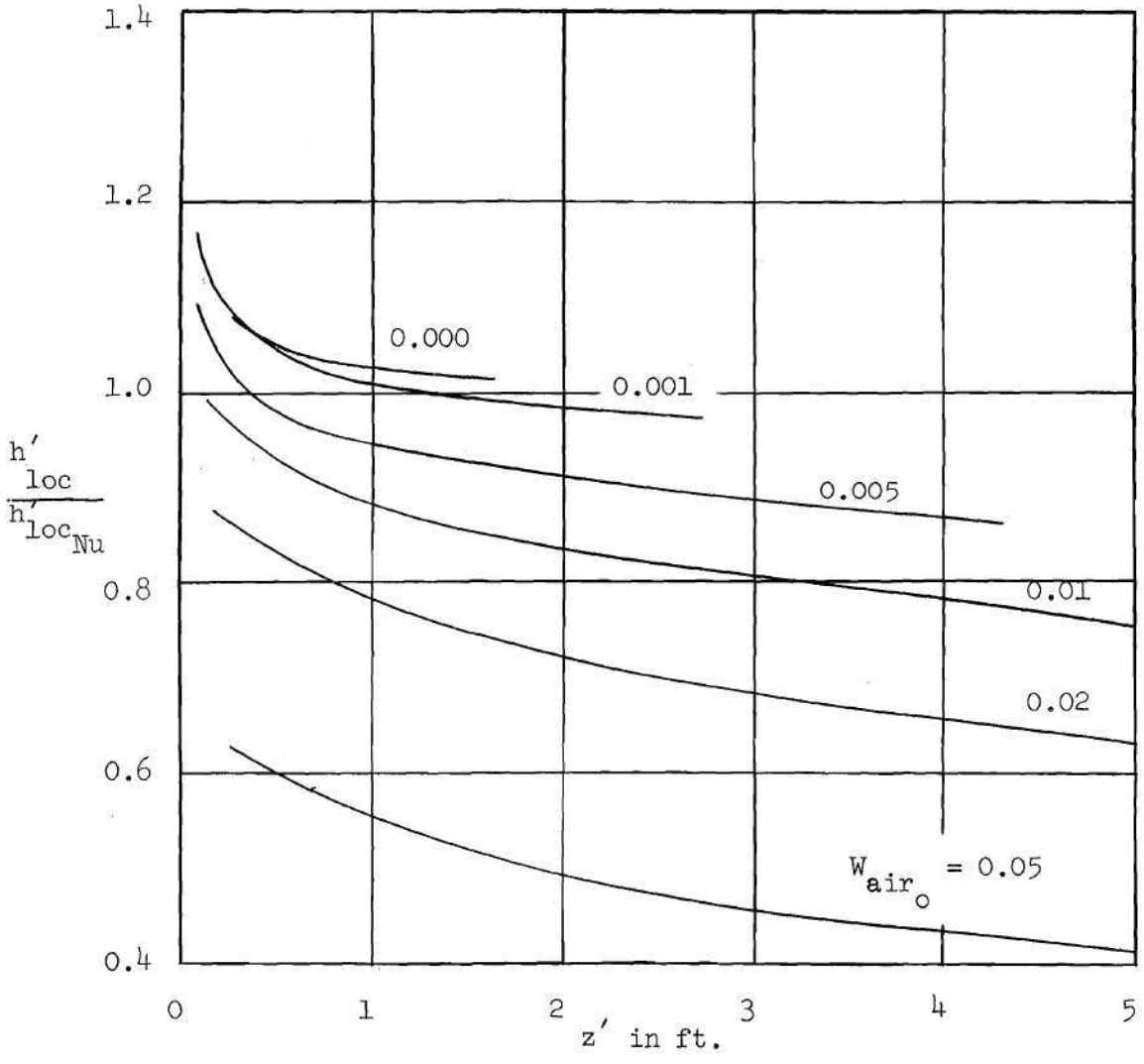

Fig. 29. Effect of Noncondensable Concentration on Local Heat Transfer Coefficients: Water Vapor and Air, $D' = 0.16667$ ft., $\bar{u}' = 25$ ft./sec., $Re_g = 18435$, $Sc_g = 0.500$, $T'_o = 212^\circ$ F, $T'_w = 202^\circ$ F.

The local heat transfer coefficient is dependent on film thickness and interface temperature. Several axial steps into the tube are necessary in numerical solutions of this type before the values of various variables, such as film thickness, smooth out. Because of this the local heat transfer coefficient may be slightly in error near the entrance. This is why the pure vapor curve intersects the 0.001 curve in Fig. 29. The latter run was started at a point much farther into the tube than the pure case.

Since diffusion of the condensable vapor to the interface is important to heat transfer the diffusion coefficient is important also. The effect of the diffusion coefficient is shown in Fig. 30. All other properties being the same the smaller the diffusion coefficient (the larger the Schmidt number), the less the heat transfer. This effect is also predicted by Sparrow and Lin (24).

The effects of entering velocity and tube length on the average heat transfer coefficient are illustrated in Fig. 31. The dependence of heat transfer on these variables is similar to that shown in Fig. 16 for pure vapor condensation. Of course, when a noncondensable gas is present the heat transfer may be less than that predicted by Nusselt (2).

The lines along which heat transfer results will lie for a constant length condenser appear independent of noncondensable concentration and tube diameter. The constant $z'\Delta T'$ lines are exactly the same as for the pure vapor case except that when noncondensables are present the lines may extend below the Nusselt prediction. The greater the

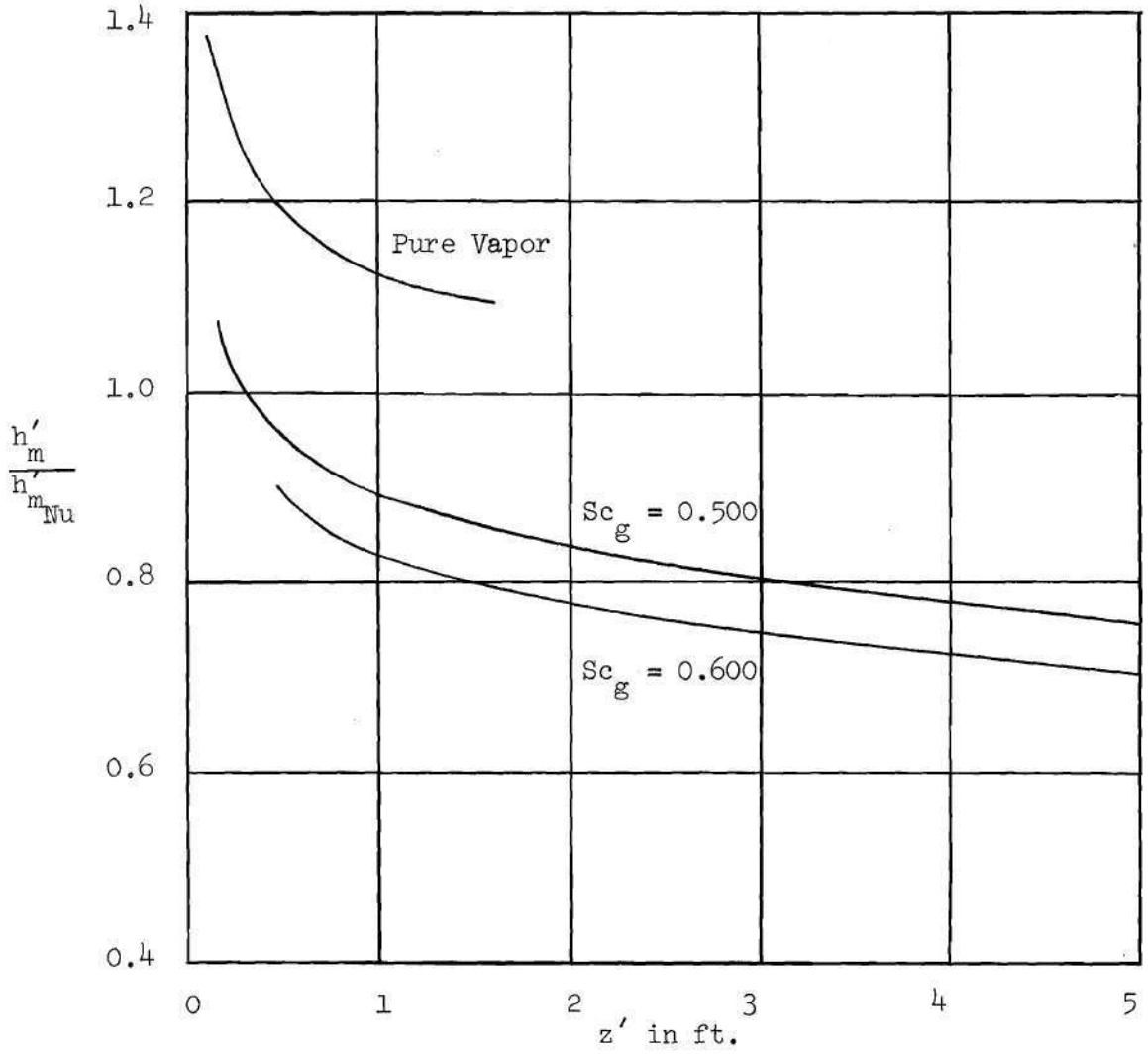

Fig. 30. Effect of Schmidt Number on Average Heat Transfer Coefficients: Water Vapor and Air, D' = 0.16667 ft., $\bar{u}'$ = 25 ft./sec., Re_g = 18435, T'_o = 212° F, T'_w = 202° F, W_{air_o} = 0.020.

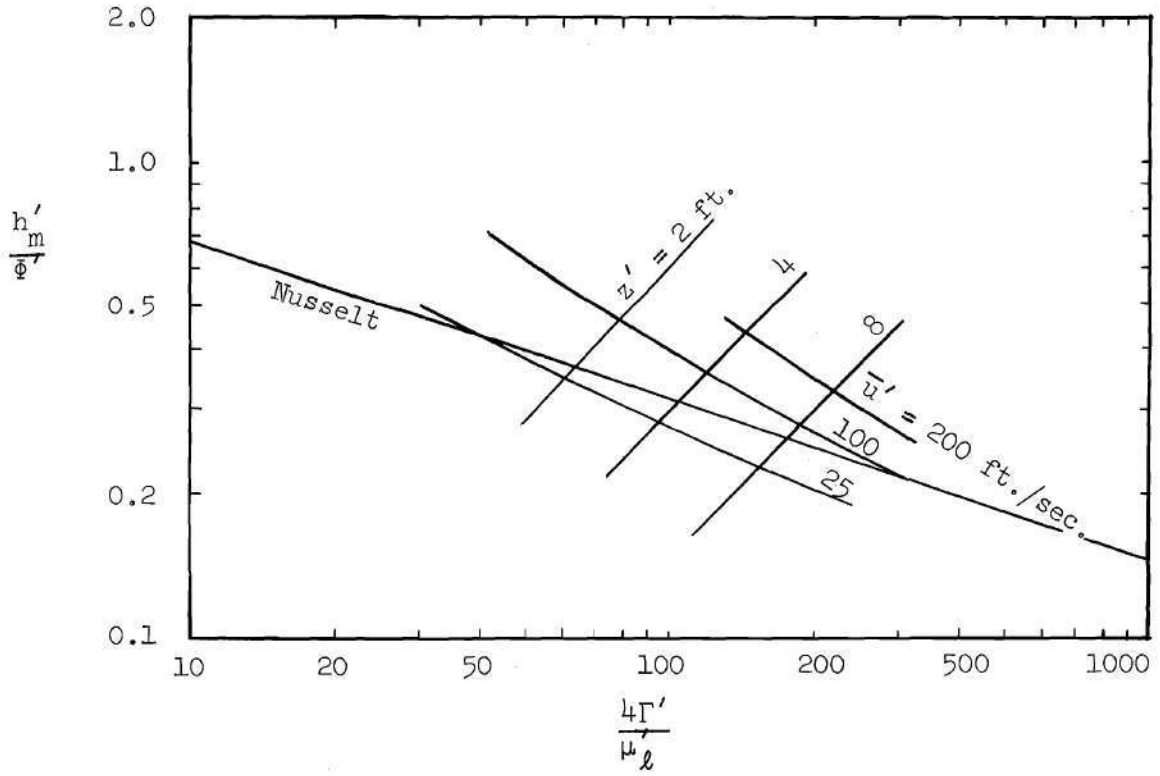

Fig. 31. Effect of Condenser Length and Entering Velocity on Heat Transfer: Ethanol Vapor and Air, $D' = 0.16667$ ft., $T'_o = 173.3^\circ$ F, $T'_w = 163.3^\circ$ F, $W_{air_o} = 0.01$.

concentration of noncondensable, the lower the heat transfer coefficient.

The temperature dependence of the constant length line is shown in Fig. 32. This dependence appears to be similar to that shown for pure vapor. In considering the temperature dependence of these lines it must be remembered that the heat transfer coefficients plotted are based on $T'_o - T'_w$, not on $T'_q - T'_w$.

There appear to be no data available on the condensation of vapor-noncondensable mixtures in tubes in the range of the results of this study. The available data are for much higher weight percentages of noncondensable, and the equipment usually had calming sections to allow the vapor to reach fully developed flow before entering the tube. Such data (17,18,19) indicate that the amount of heat transferred is significantly less than if there were no noncondensable present.

Correlation of Heat Transfer Results

The heat transfer results for water-air mixtures reported in Appendix F were correlated by the least squares procedure described in Chapter III. The data were divided into two sections: those with length Froude numbers between 0.047 and 10, and those with length Froude numbers between 10 and 532. The first section is correlated by

$$\frac{h'_m}{h'_{m_{Nu}}} = 0.882 \, (Fr_L)^{0.122} \left(1-ScW_{air_o}\right)^{20.4} \left(\frac{T'_{dp}-T'_w}{T'_o-T'_w}\right)^{0.905} \qquad \text{(IV-1)}$$

with an average error of $\pm$ 5.4 percent. For length Froude numbers greater than 10 the results may be represented by

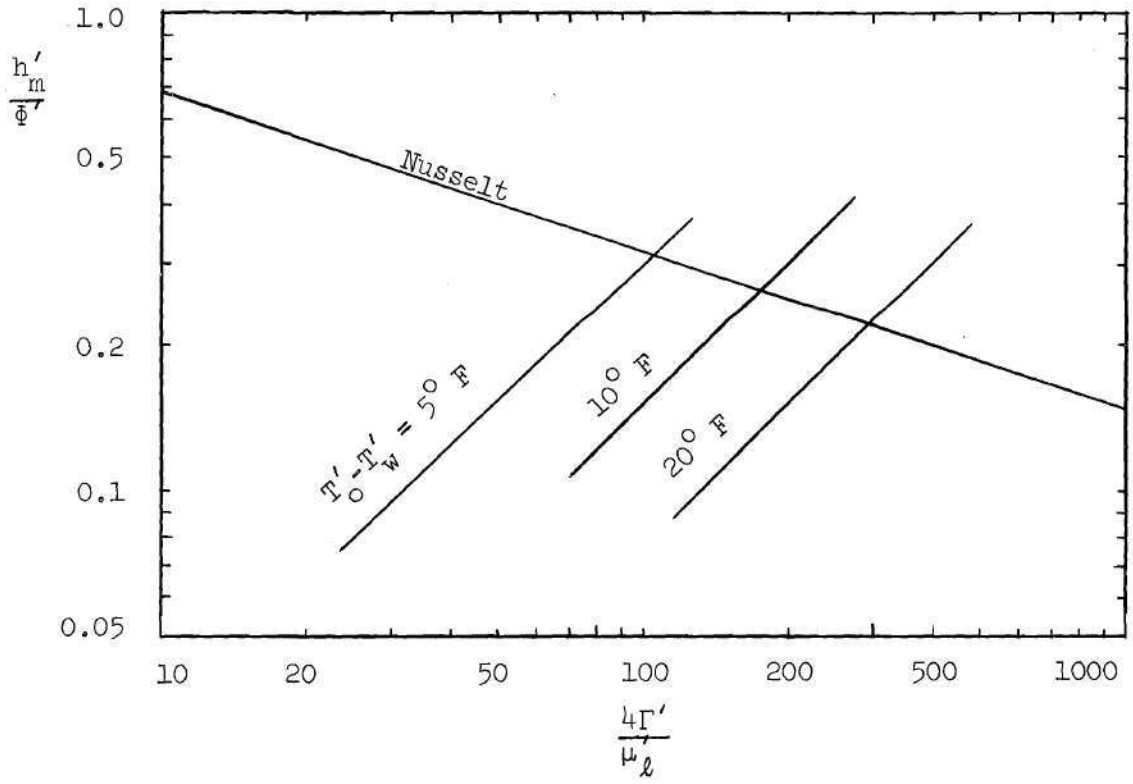

Fig. 32. Effect of Available Temperature Drop on Heat Transfer: Ethanol Vapor and Air, $D' = 0.16667$ ft., $Sc_g = 0.537$, $z' = 8$ feet.

$$\frac{h'_m}{h'_{m_{Nu}}} = 0.764\ (Fr_L)^{0.106} \left(1\text{-}Sc\ W_{air_o}\right)^{14.2} \left(\frac{T'_{dp}-T'_w}{T'_o-T'_w}\right)^{0.307} \qquad \text{(IV-2)}$$

with an average error of $\pm$ 2.7 percent.

These equations are felt to be good for predicting heat transfer only over the range of concentrations covered in Appendix F. When the entering concentration of air is zero and $T'_o = T'_{dp}$, these equations do not predict the results for pure vapor condensation very well, but they do correlate the water-air results reported in Appendix F accurately.

Comparison of Calculation Methods

In Fig. 33 four different methods of calculating condensation results for gas-vapor mixtures are compared. The differential condensation model includes no diffusional resistances or interfacial shear effects. It does take into account the gradual lowering of the interface temperature as vapor is condensed out. The Colburn and Hougen calculation method (21) does include turbulent diffusional resistances and the resulting effect on interface temperature. It does not take into account the effects of interfacial shear. The model of Sparrow and Lin (24) describes film condensation on a vertical surface immersed in a large body of vapor which contains a noncondensable gas. The laminar equations of motion (in the direction of liquid flow), diffusion, energy, and continuity are used in this study. No shear is considered at the interface.

Other investigators (17,22,23) have considered the problem of

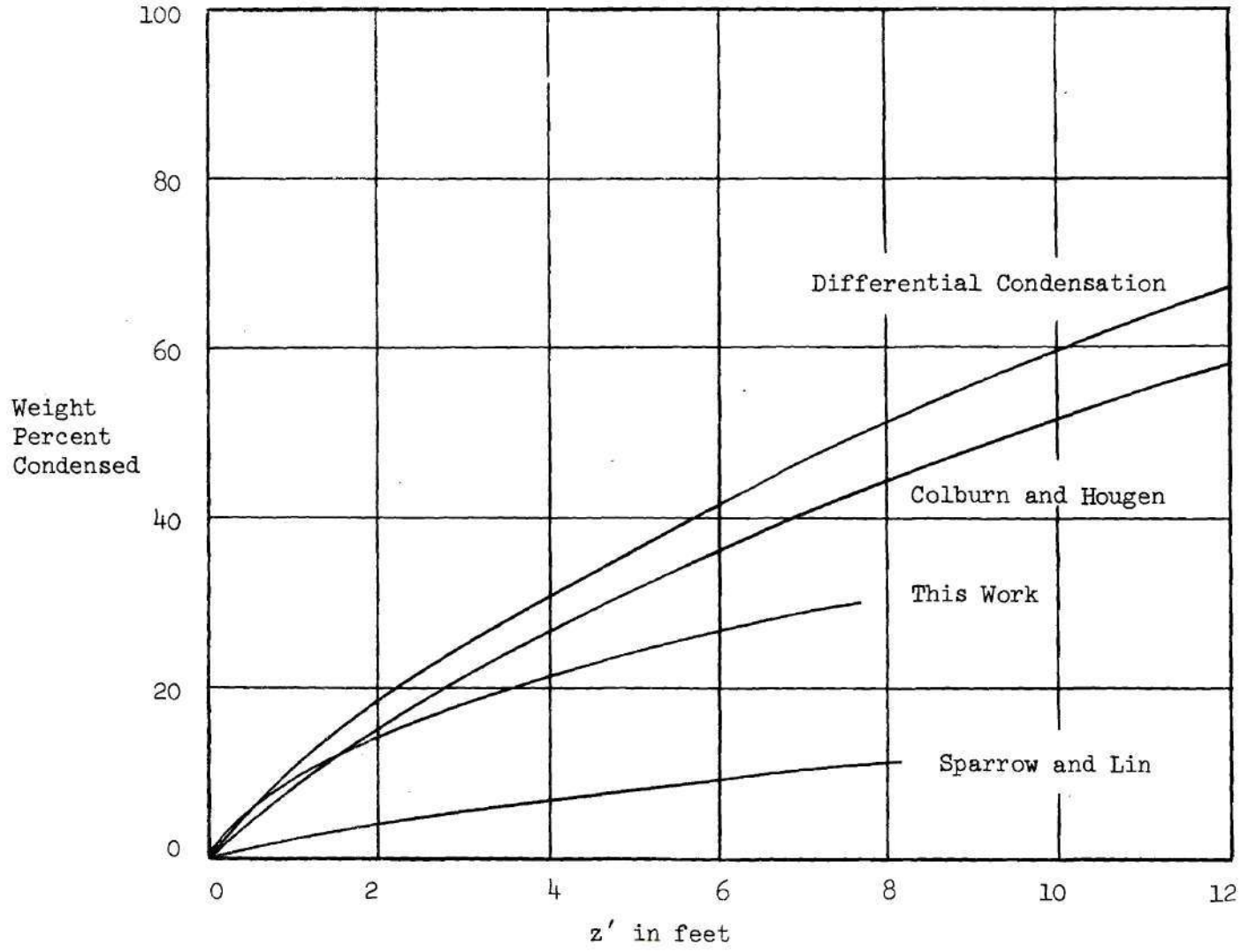

Fig. 33. Comparison of Calculation Methods: Water Vapor and Air, $\bar{u}'$ = 25 ft./sec., D' = 0.16667 ft., T_o' = 212° F, T_w' = 202° F, W_{air_o} = 0.05, Sc_g = 0.5, Re_g = 18,435.

calculating condensation from gas-vapor mixtures. These methods appear to agree with the Colburn and Hougen method and so were not included here.

As expected, the Colburn and Hougen model predicts lower rates of condensation than the differential condensation method. The difference is caused by the diffusional resistances included in the Colburn and Hougen method. In using the Colburn and Hougen method, the partial pressure of the noncondensable gas was allowed to change with length.

Near the entrance of the tube the interfacial shear is quite high. Principally for this reason the mathematical model of this work, which includes shear effects, predicts more heat transfer near the inlet than the Colburn and Hougen method which as mentioned does not include shear effects. At higher velocities it may also predict more heat transfer near the entrance than differential condensation, which does not include shear effects either. However, the interfacial shear decreases rapidly with tube length. As the shear effects become small the laminar diffusional resistances of this work cause the heat transfer to be less than either of those methods.

The laminar diffusion model of Sparrow and Lin was not intended for condensation inside a vertical tube. It does not include shear effects or allow the interfacial concentration to change with length. Because the model of this study includes these effects it predicts much greater heat transfer.

The problem of condensation inside vertical tubes with laminar gas-vapor flow was considered by Baasel and Smith (25). They assumed

parabolic entrance and exit flow of the vapor and did not consider the flow of the liquid in their model. They considered only the constant property equations of continuity and diffusion in the vapor. They did not allow the interfacial concentration to vary with length. Their mass balance varied about five percent over the length of condenser, while the results in Appendix F vary about three percent at most. One must know the correct average interfacial concentration to use their results.

Various low velocity solutions in Appendix F were compared to their work by using average values of the interfacial concentration reported in Appendix F. Their model predicted less heat transfer than shown in Appendix F, generally around half as much.

In Fig. 33 it may be seen that at a diameter Reynolds number of 18,435 and an air concentration of five weight percent, the Colburn and Hougen method predicts condenser areas which are substantially smaller than the results of this study. An extensive set of experimental data similar to that of Carpenter (39) should be taken for low concentrations of noncondensable gas to determine the exact range of applicability of these methods. Such data could also be used in the development of approximate design procedures which include the effect of interfacial shear.

CHAPTER V

CONDENSATION OF A BINARY VAPOR MIXTURE

Numerical solutions to equations (II-4), (II-5), (II-6), (II-10), and (II-11) and the boundary conditions for binary condensation given in Chapter II are presented below. Details of the method of solution and discussion of its validity are included in Appendix A. An outline of the computer program used in solving the equations is given in Appendix B, and the complete computer program is given in Appendix C. The physical properties used in these calculations are presented in Appendix D, and numerical results are presented in tabular form in Appendix G. As in the previous cases, "run" refers to a numerical solution unless otherwise designated.

Two binary vapor mixtures are considered: ethanol and water, and benzene and toluene. Ethanol-water mixtures form a minimum boiling azeotrope, and benzene-toluene mixtures approach an ideal mixture. Entrance velocity varied from two feet per second to two hundred feet per second. The Reynolds number of the entering vapor ranged from 2270 to 231,734. Values ranging from 5.0 to 34.25 degrees Fahrenheit were considered for entering mixture temperature minus the wall temperature. Concentrations of 25, 50, and 75 weight percent were investigated. Vapor entered at its dew point. Most solutions were for an 0.459 inch diameter tube, although some results are presented for a 2.0 inch diameter tube. Tube lengths as long as twenty feet are reported.

The vapor and liquid properties of binary mixtures vary strongly with concentration. Several different entering concentrations were considered and the concentrations of both phases changed with length, radius, and other variables. The physical properties should vary as a consequence of concentration changes. However, with the exception of vapor density the computer program was developed to handle constant property mixtures. Only one set of physical properties was used for ethanol-water and one for benzene-toluene. The physical properties that were used were estimated from the only mixture data available which were for the most part at much lower temperatures. They roughly correspond to a 50 weight percent solution at the average boiling point of the mixture. Some variables, such as vapor density, vapor-liquid equilibrium, and latent heat of condensation were allowed to change with concentration.

In the cases reported in Appendix G it was not possible to obtain perfect mass and component balances over the length of the condenser due to the neglect of small terms in the diffusion equation. The mass balance varied a maximum of about five percent with length and the component balances varied a maximum of about ten percent with length. Most solutions were well below these maximums.

Velocity, temperature, and concentration profiles, liquid film thickness, pressure drop, heat transfer results and comparison with other methods of calculation are discussed below.

Velocity Profiles

Typical axial and radial velocity profiles are presented in

Tables 59, 60, 61, and 62.

The velocity profiles were observed to vary quite a bit with the conditions of each run. No attempt was made to generalize them. They exhibit the same general dependence on radius, length, entrance velocity, and temperature drop as the profiles presented in Chapter III for pure vapors.

As in the pure vapor and gas-vapor cases the assumption that $v'_z >> v'_r$ does not appear to be true for low velocity runs near the interface and near the entrance. As was discussed in the previous cases, making this assumption does not cause much error because of the small region where the assumption does not hold.

Concentration Profiles

Typical concentration profiles in both phases are presented in Tables 59, 60, 61, and 62. In addition, the interface temperature as a function of length is reported in Appendix G for each run. From the temperature values the interfacial concentrations may be calculated. The concentration profiles in the vapor are presented in Fig. 34 for a typical run. The liquid concentration profiles for this run are presented in Fig. 35.

The diffusional resistance in the vapor phase causes a buildup of the more volatile component at the interface. The composition at the interface varies between the dew point and bubble point concentrations and approaches the latter with increasing length.

In the liquid the difference between the wall concentration and the interface concentration is not very large for either benzene-toluene

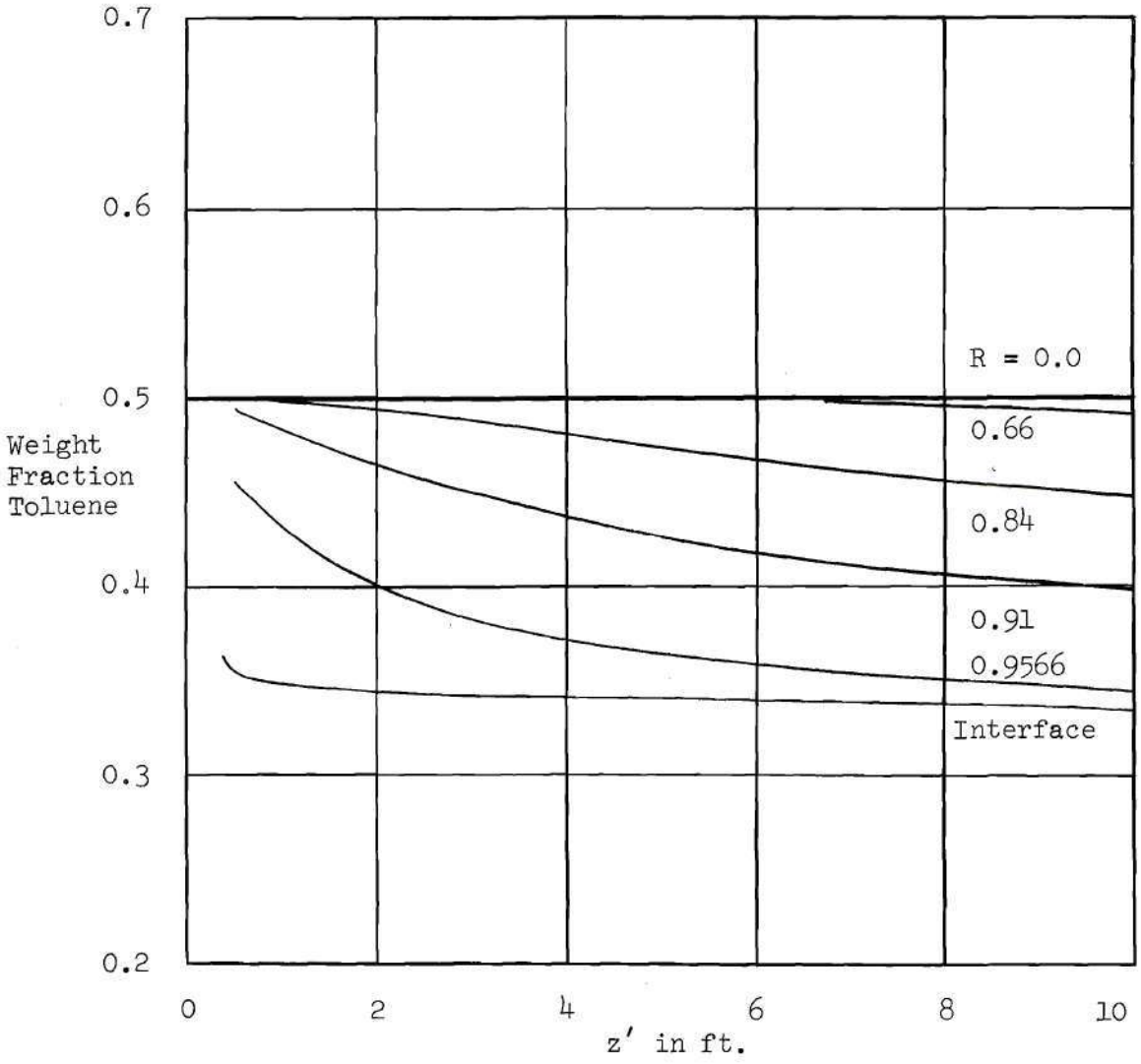

Fig. 34. Concentration Profiles in the Vapor Phase: Benzene-Toluene, $D' = 0.03825$ ft., $\bar{u}' = 100$ ft./sec., $Re_g = 115867$, $W_{tol_o} = 0.50$, $T'_o = 207.3^{\circ}$ F, $T'_w = 180^{\circ}$ F.

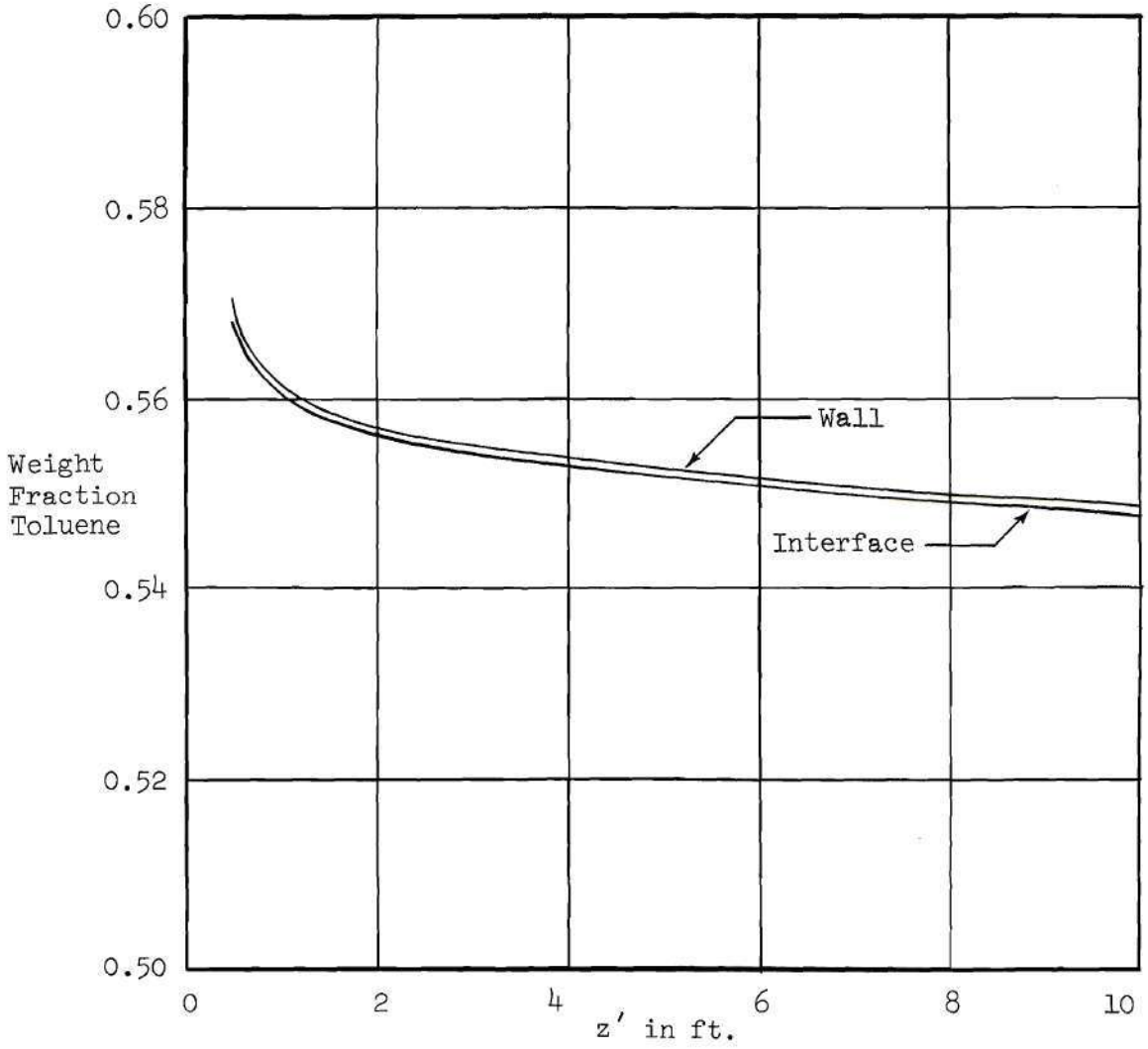

Fig. 35. Concentration Profiles in the Liquid Phase: Benzene-Toluene, $D' = 0.03825$ ft., $\overline{u}' = 100$ ft./sec., $Re_g = 115867$, $W_{Tol_o} = 0.50$, $T'_o = 207.3^\circ$ F, $T'_w = 180^\circ$ F.

or ethanol-water. The liquid phase could be adequately represented in condensation calculations by considering it to be well mixed.

Temperature Profiles

Typical temperature profiles in both phases are presented in Tables 59, 60, 61, and 62. The interface temperature is reported as a function of length for each run in the Summary of Results Tables in Appendix G.

The temperature profile in the vapor phase develops gradually with increasing length. A core whose size decreases with length remains at the entrance temperature, T'_o. The interface temperature is less than the entrance temperature and decreases with increasing length. In all cases it lies between the dew point and bubble point of the entering mixture. The temperature drop through the liquid film is almost linear with radius.

The effect of wall temperature on the interface temperature is shown in Fig. 36. The colder the wall temperature, the lower the interface temperature.

The effect of entering velocity on the interface temperature is shown in Fig. 37. The higher the entering velocity, the higher the interface temperature.

There are no actual measurements of interface temperature to compare with. The work of Pressburg and Todd (33) and Mirkovich and Missen (34) on the outside of a horizontal cylinder indicate that for total condensation the correct interface temperature is the bubble point of the entering vapor. In condensation in the entrance length of

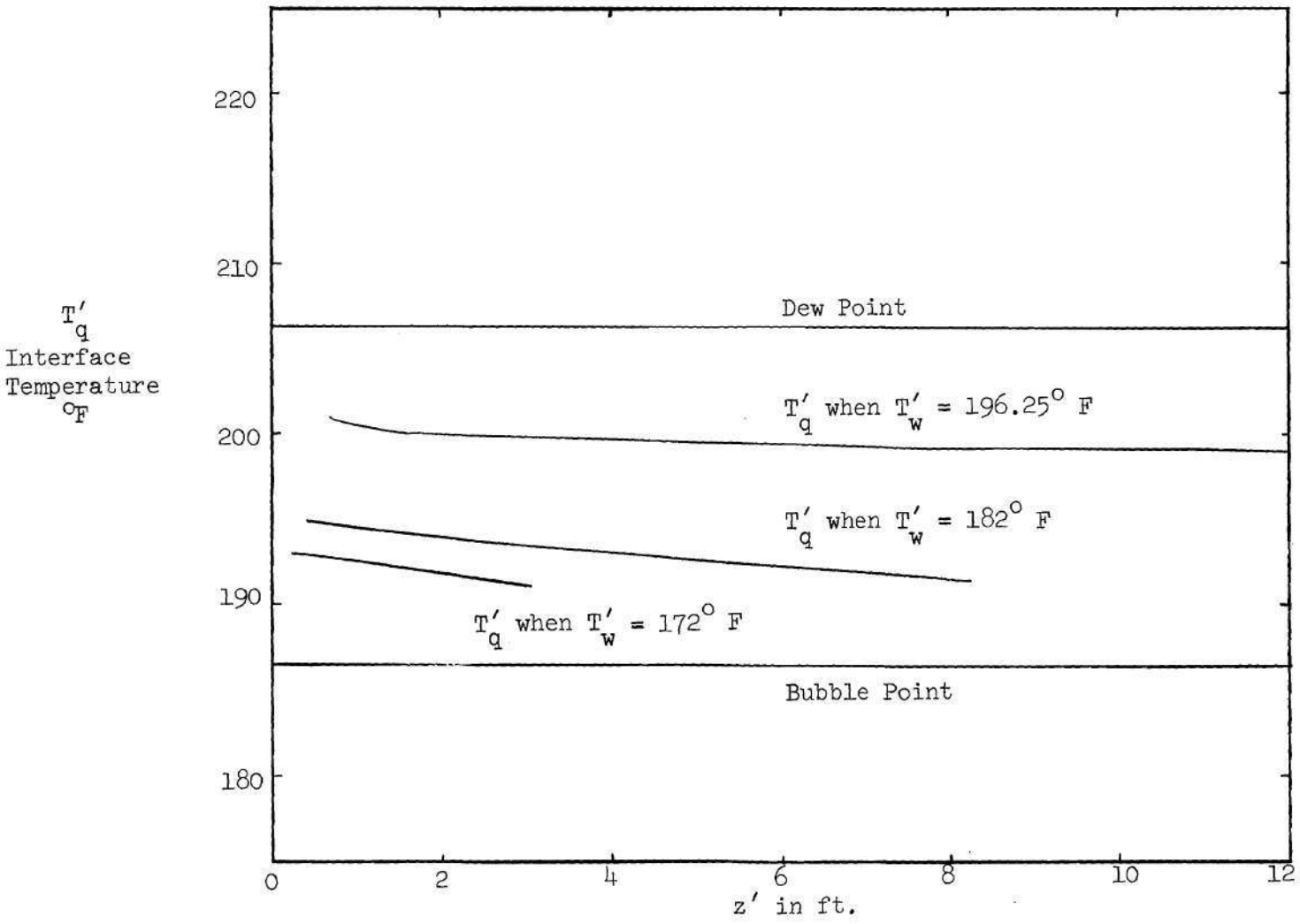

Fig. 36. Effects of Wall Temperature and Length on the Interface Temperature: Ethanol-Water, $D' = 0.03825$ ft., $\bar{u}' = 100$ ft./sec., $Re_g = 19763$, $W_{EtOH_o} = 0.25$

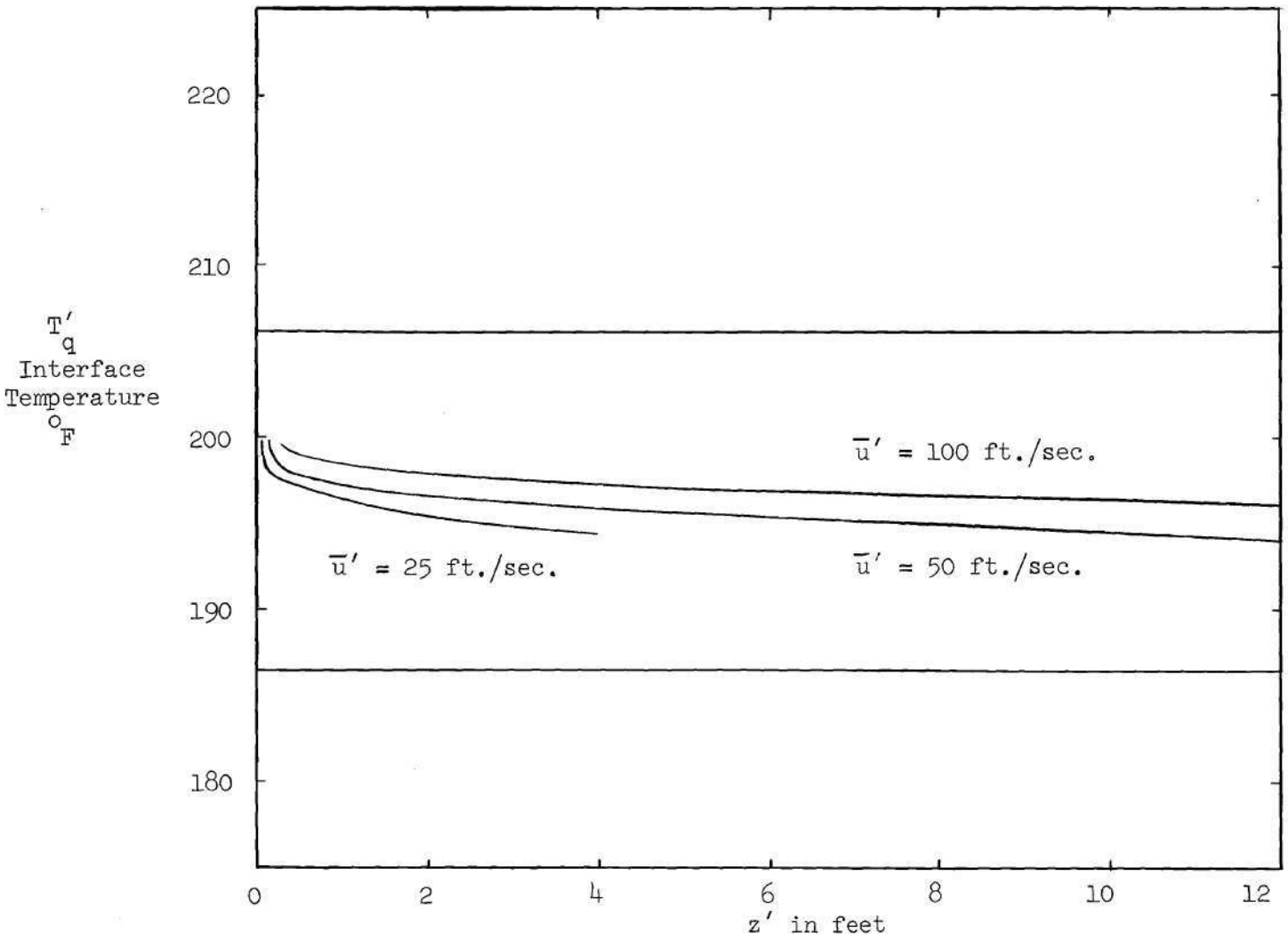

Fig. 37. Effects of Entrance Velocity and Length on the Interface Temperature: Ethanol-Water, $D' = 0.03825$ ft., $W_{EtOH_o} = 0.25$, $T'_w = 192^\circ$ F.

a vertical tube total condensation is not approached until near the end of the tube or at high temperature drops. The interface temperature in such cases does approach the bubble point temperature.

Liquid Film Thickness, Pressure Drop, and Interfacial Shear

Liquid film thickness, pressure drop, and interfacial shear show the same general dependence on condensation conditions as reported in Chapters III and IV. The film thickness is less than for either pure component at the same available temperature drop because of the lowering of the interface temperature. This causes less mass to be condensed. A similar effect was noted in Chapter IV. The effect of the lowered interface temperature on the pressure drop and the interfacial shear is similar to that discussed in Chapter IV.

Heat Transfer Results

The heat transfer coefficients reported in Appendix G are based on $T'_o - T'_w$, the entering vapor temperature minus the wall temperature. The entering vapor is always at its dew point temperature. The heat transfer coefficients may be converted to other temperature bases by multiplying by $(T'_o - T'_w)$ divided by the new temperature difference. A plot of average heat transfer coefficients based on $T'_{dp} - T'_w$ and $T'_{bp} - T'_w$ is presented in Fig. 38. The heat transfer results based on the bubble point temperature difference always lie above the Nusselt line, equation (I-11). Since the interface temperature is less than T'_{dp} the heat transfer coefficients based on $T'_{dp} - T'_w$ may cross the Nusselt line as they do in the gas-vapor case discussed in Chapter IV.

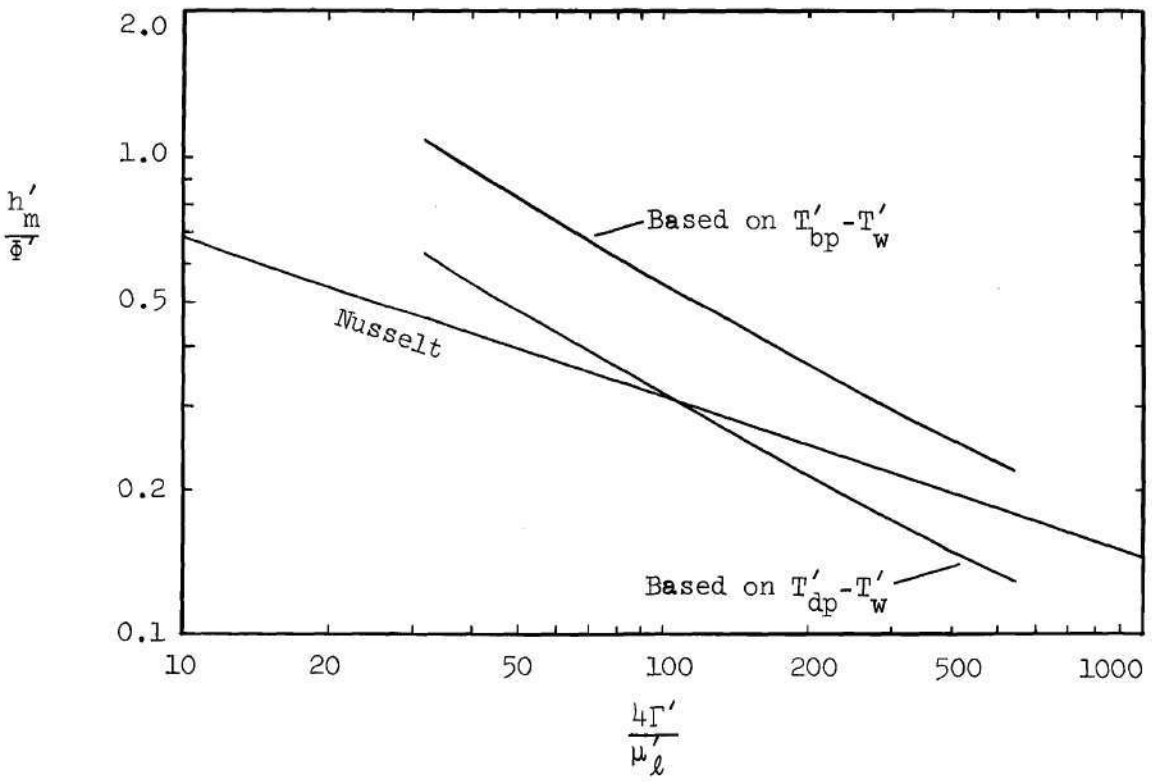

Fig. 38. Comparison of Temperature Base for Heat Transfer Coefficients: Benzene-Toluene, $D' = 0.03825$ ft., $\overline{u}' = 25$ ft./sec., $Re_g = 28967$, $W_{Tol} = 0.50$, $T'_o = T'_{dp} = 207.3^\circ$ F, $T'_{bp} = 195.8^\circ$ F, $T'_w = 180^\circ$ F.

The average and local heat transfer coefficients show the same general dependence on length and entering velocity as shown in Figures 15, 16, and 31 for the pure vapor and gas-vapor cases. In both of these cases the usefulness of the Nusselt model in predicting dependence on length, temperature drop, and physical properties was noted. For a given vapor the heat transfer results fall along lines of constant $z'\Delta T'$ as predicted by the Nusselt model.

The Nusselt model appears to be useful for binary condensation also. In Fig. 39 heat transfer coefficients based on $T'_o - T'_w$ are shown for a $z'\Delta T'$ product of 40. The results for binary mixtures fall between the extensions of the pure lines. The concentration dependence, however, appears to be opposite to that expected, and the lines for constant $z'\Delta T'$ are not straight lines. Both of these incongruities may be explained with the aid of the Nusselt model and knowledge of the physical properties used in the computer program.

The physical properties of a binary liquid may vary quite a bit with concentration. This is particularly true for an ethanol-water mixture. Because of the variations of the concentration with length and other variables, and the difficulty in estimating some of the properties, only one set of physical properties was used for ethanol-water. The only properties which were allowed to vary with concentration were the latent heat of vaporization, the vapor density and vapor-liquid equilibrium.

The Nusselt model expression for the average heat transfer coefficient is

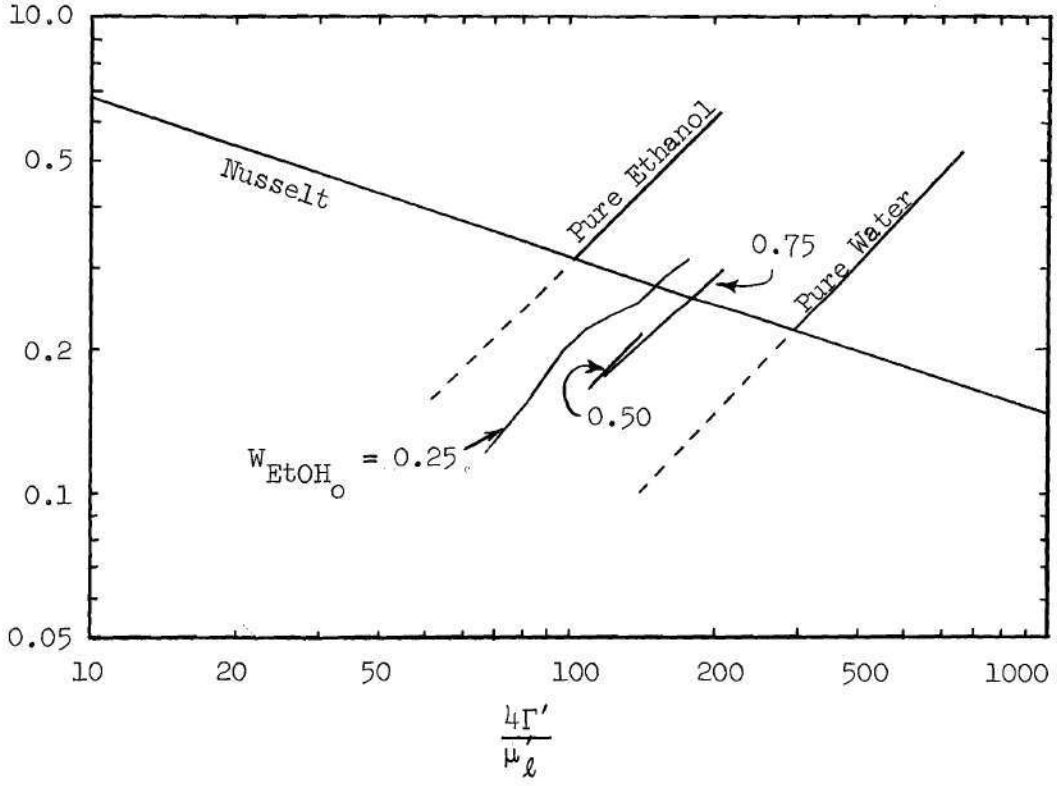

Fig. 39. Effect of Entrance Concentration on Heat Transfer Coefficients (Based on $T'_{dp}-T'_w$): Ethanol-Water, $z'\Delta T' = 40$.

$$h'_{m_{Nu}} = 0.943 \left(\frac{g' \rho_\ell'^2 k_\ell'^3 \lambda'}{\mu_\ell' z' \Delta T'} \right)^{1/4} \qquad \text{(I-10)}$$

This relation predicts heat transfer coefficients which lie along the Nusselt line in Fig. 39. Mixture properties may be used in this expression to predict where the various concentration lines will cross the Nusselt line. The latent heat of vaporization has an effect on this expression. The latent heat of vaporization changes with length, temperature drop, velocity, and diameter because the interfacial composition changes with these variables. For a given entrance concentration and a given $z'\Delta T'$ the effective average value of λ' may vary slightly depending on the condensation conditions. This is why the lines of constant $z'\Delta T'$ are not straight for binary mixtures, and, in fact, are not lines but really small bands.

The variation of the latent heat of vaporization with concentration also explains the relative position of the various concentration lines in Fig. 39. λ' decreases with increasing ethanol concentration. Equation (I-10) predicts that as the concentration of ethanol in the entering mixture increases the lines or bands of constant $z'\Delta T'$ cross the Nusselt line at lower values of the heat transfer coefficient. The positions the constant composition lines cross the Nusselt line should be proportional to the latent heat of vaporization to the one fourth power. The heat of vaporization may be estimated for each concentration line by using the average interfacial concentration for the run nearest the Nusselt line. These concentrations are then used in the heat of

vaporization expression in Appendix D to estimate average values of λ'. According to these average values the 25 weight percent line should cross the Nusselt line at a heat transfer coefficient 1.059 times higher than the 75 weight percent line and 1.041 times higher than the 50 weight percent line. In Fig. 39 these values are 1.058 and 1.041, respectively for these lines or their extensions.

It appears that equation (I-10) can be useful in determining the concentration dependence of heat transfer coefficients for binary mixtures if the variation of liquid properties with concentration is well known. When the proper physical properties are used in equation (I-10) the variation of the heat transfer coefficient with composition may or may not be linear depending on how the properties for the particular mixture vary. Pressburg and Todd (33) report approximately linear variation with molar composition for a number of systems, while Mirkovich and Missen (34) did not observe linear dependence with other systems. Cronauer (7) observed linear variation with composition for two binary systems, but not for a third.

Fig. 40 shows the type of plot used by Mirkovich and Missen and by Pressburg and Todd for determining heat transfer dependence on concentration and for determining the correct interface temperature. They discovered that only the heat transfer coefficients based on $T'_{bp}-T'_{w}$ seemed to have the proper slope (-0.25) and were between the results of the pure components. From this they concluded that the correct interface temperature was the bubble point of the condensed phase which was essentially the same composition as the entering vapor in their

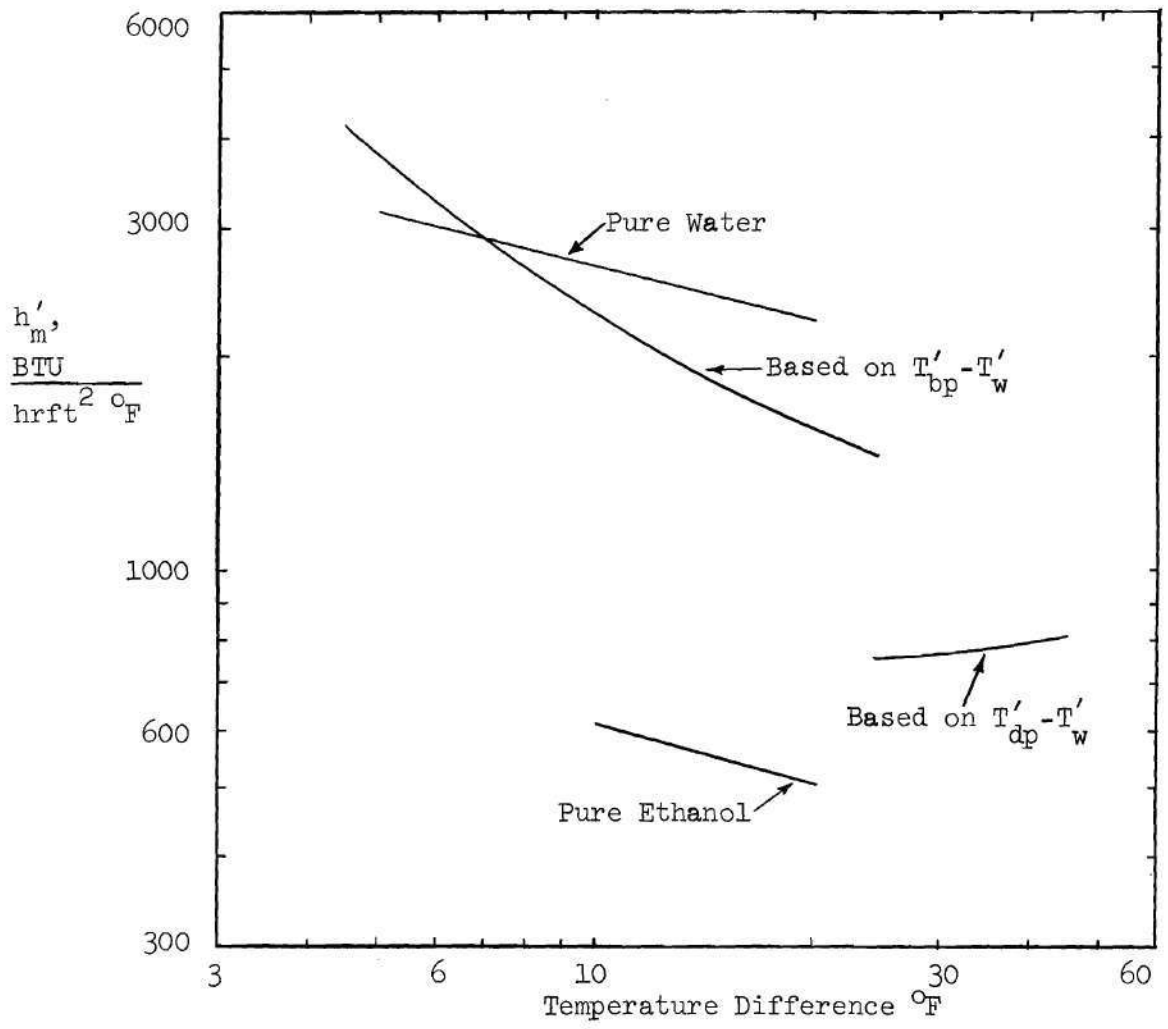

Fig. 40. Effect of Temperature Drop on Heat Transfer Coefficient: Ethanol-Water, $D' = 0.03825$ ft., $\overline{u}' = 100$ ft./sec., $Re_g = 19{,}763$, $z' = 1.0$ ft.

apparatus. In Fig. 40 the heat transfer coefficients based on $T'_{bp}-T'_{w}$ do appear to be approaching the proper slope for large temperature differences. Those coefficients based on the dew point temperature do not have the proper slope. The general position and slope of the dew point coefficients on this figure appear to agree qualitatively with those of Pressburg and Todd and Mirkovich and Missen for other systems. As the temperature difference decreases the bubble point heat transfer coefficients in Fig. 40 appear to rise because the interface temperature is rising also. Pressburg and Todd did not observe such a rise. Their bubble point temperature was calculated as the bubble point of the condensed phase. This would take into account the possible variation of interface temperature. Mirkovich and Missen did not observe such a rise for film condensation either, although they investigated values of $T'_{bp}-T'_{w}$ as low as two degrees Fahrenheit and apparently used the bubble point of the entering vapor as the bubble point temperature. However, neither of these experiments was conducted in the entrance of a vertical tube where some length is necessary for the buildup of a vapor film.

Fig. 39 is better than Fig. 40 in vertical pipe condensation for determining whether the binary results fall between those of the pure components. In Fig. 40 interface temperature effects can cause the heat transfer coefficients to fall outside of the pure component results for wall temperatures slightly below the bubble point temperature. In addition, Fig. 40 is not very useful when the wall temperature is greater than the bubble point. In Fig. 39, however, the variation of inter-

face temperature only causes the heat transfer coefficient to be a little lower; it still lies between the pure results even for wall temperatures greater than the bubble point.

Unfortunately, there appear to be no data available on the condensation of binary vapors in a vertical tube similar to those of Carpenter (39) for pure vapors.

Comparison of Calculation Methods

Two different calculation procedures will be compared to the results of this study. Kern (29) recommends using differential condensation. This approach disregards the presence of the vapor film and does not include the effect of interfacial shear on the liquid film. McAdams (30) recommends using the bubble point temperature of the entering vapor as the interface temperature. This method does not include the effect of interfacial shear on the liquid film either.

These methods are compared to the results of this study in Fig. 41. When the wall temperature is only slightly below the bubble point temperature as it is for this comparison, McAdams' method gives a conservative estimate of the amount condensed because of the unrealistic interface temperature. Near the entrance the interfacial shear is quite high and the vapor film is not fully developed. This causes the mathematical model of this study to predict condensation rates as high as the Kern method in this region. Since the interface temperature for this study is quite a bit less than that predicted by Kern, the principle reason for the high coefficients of this study is the interfacial shear. Farther into the tube the shear effects become much smaller and

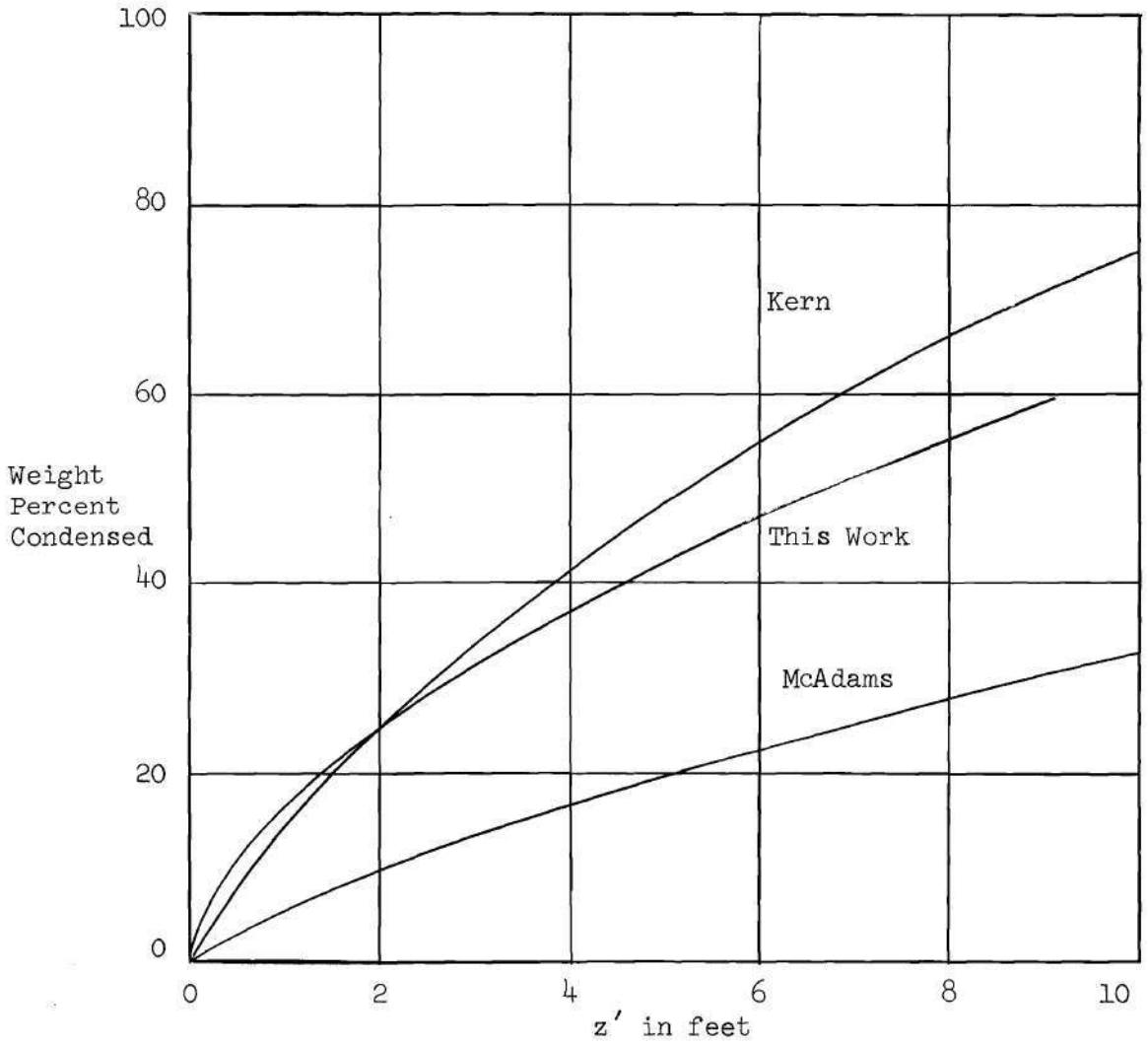

Fig. 41. Comparison of Calculation Methods: Ethanol-Water, $D' = 0.03825$ ft., $\bar{u}' = 100$ ft./sec., $Re_g = 19763$, $W_{EtOH} = 0.25$, $T'_o = T'_{dp} = 206.25^\circ$ F, $T'_{bp} = 186.5^\circ$ F, $T'_w = 182^\circ$ F.

the vapor film becomes more developed. The condensation rates of this study are then lower than the Kern method which does not include the presence of the vapor film.

The average heat transfer coefficients based on $T'_{dp}-T'_{w}$ are presented in Fig. 42. At large temperature drops the Kern and McAdams methods have been shown to agree (31). At low temperature drops they diverge quite a bit. When the wall temperature is greater than the bubble point temperature the McAdams method cannot be used. Kern's method gives results which are higher than the results of this study because of the higher interface temperature.

After a few feet into the tube the Kern method predicts condenser areas which are smaller than the results of this study for a diameter Reynolds number of 19,763. An extensive set of experimental data similar to that of Carpenter (39) should be taken for binary mixtures to determine the exact range of applicability of these methods. Such data could also be used in the development of approximate design procedures which include the effect of interfacial shear.

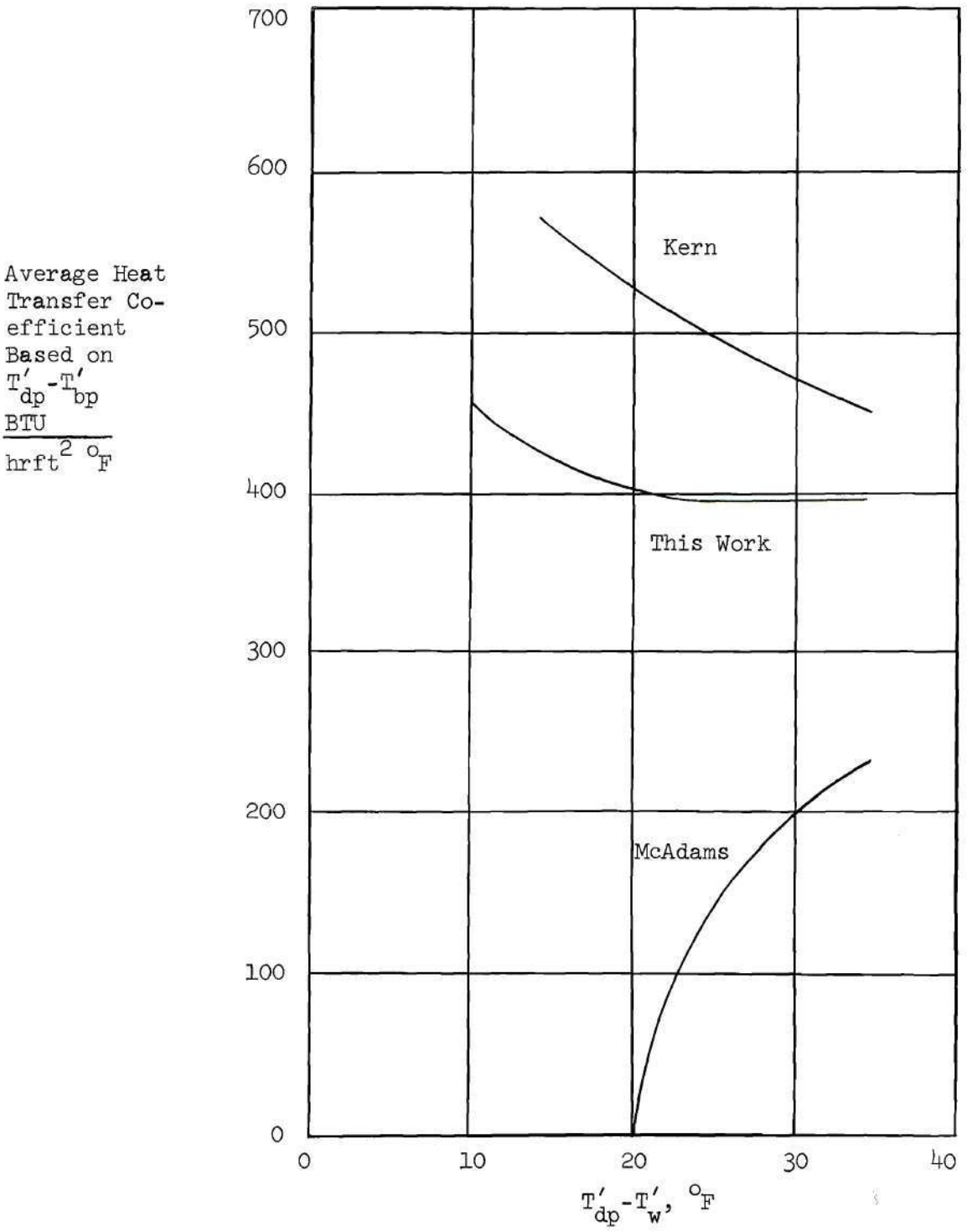

Fig. 42. Comparison of Heat Transfer Coefficient Predictions, Ethanol-Water, $D' = 0.03825$ ft., $\bar{u}' = 100$ ft./sec., $W_{EtOH_o} = 0.25$, $z' = 4$ ft., $Re_g = 19763$.

CHAPTER VI

CONCLUSIONS AND RECOMMENDATIONS

Based on the results of this work, the following conclusions are reached:

1. The computer solutions presented in this work for pure vapor condensation check with experimental data for diameter Reynolds numbers of the entering vapor less than 30,000. For entering diameter Reynolds numbers greater than 30,000 the results of this work do not check with experimental data but qualitatively predict heat transfer dependence on entrance velocity, diameter, temperature drop, length, and physical properties.

2. In the design of pure vapor condensers the method of Rohsenow, Webber and Ling (5) appears to be good for both high and low vapor velocities.

3. Entrance region interfacial shear effects are important in the design of pure vapor and binary vapor condensers and in the design of gas-vapor condensers where the concentration of noncondensable is low.

4. The design methods of Colburn and Hougen (21) for gas-vapor condensers and Kern (29) for binary vapor condensers predict areas which are smaller than the results of this work for all entering Reynolds numbers considered. No data are available to determine the range of applicability of these methods or this study.

Recommendations for extensions of this work are:

1. The use of the numerical scheme presented here for other condensation problems such as the variation of wall temperature with length, the use of parabolic entrance profiles, and the condensation of a superheated vapor.

2. Experimental studies on the condensation of pure vapors, gas-vapor mixtures, and binary vapors in the entrance region of vertical tubes similar to the study made by Carpenter and Colburn (1) for pure vapors. Such studies would determine the range of validity of these results, and shed light on the transition of one or both phases to turbulent flow, as well as extend the pure vapor data and provide data for the other cases where no data exist.

3. The development of new design procedures for gas-vapor mixtures with low noncondensable concentrations which include the effect of interfacial shear.

4. The development of new design procedures for binary vapor mixtures which include the effect of interfacial shear.

5. Experimental and semi-theoretical studies (computer simulation) on the development of turbulence in the entrance region of porous and nonporous vertical tubes for one and two phase flow.

A P P E N D I C E S

APPENDIX A

THE NUMERICAL SOLUTION OF THE MATHEMATICAL MODELS

The mathematical models in Chapter II describing the three cases of condensation in the entrance region of a vertical tube may be solved with the aid of a high speed digital computer by using finite difference approximations to the equations and boundary conditions. The approach is similar to that of Hornbeck, Rouleau, and Osterle (40) for one phase flow inthe entrance region of a porous tube. An implicit finite difference "marching" procedure is used to give point values of velocity, pressure, concentration, and temperature for succeeding axial steps.

In the condensation of a pure vapor the finite difference representations of the equations of motion and continuity are solved in matrix form to yield the pressure and point values of axial and radial velocities for the next axial step down the tube. The finite difference representation of the equation of energy using the latest values of velocity is then solved in matrix form for point values of temperature. Because of the non-linearity of the problem it is necessary to change the axial step size and repeat the above steps until the normal heat flux into the liquid at the interface is properly balanced by the normal mass flux across the interface.

The other two cases considered involve the diffusion equation in addition to the equations of motion, continuity, and energy. In both cases the representations of the equations of motion and continuity are

solved as for the pure vapor case. The finite difference representation of the diffusion equation using the latest values of velocity is then solved in matrix form to yield point values of concentration. Values of gas density may be calculated from the concentration values. The same final results are obtained with substantially less computer time if the velocity and concentration matrices for this axial step are resolved using the latest density and velocity values. The finite difference representation of the energy equation is then solved as in the pure vapor case to yield temperature values. As in the pure vapor case it is necessary to iterate the whole procedure until the normal heat flux into the liquid at the interface is properly balanced by the normal mass flux across the interface.

Detailed outlines of these procedures are given in Appendix B, and the complete computer programs are given in Appendix C.

An attempt was made to solve the equations by performing a similarity transformation like that of Dorrance (41). This approach involved transforming the equations into ordinary differential equations and solving these by Runge-Kutta methods (42) on a digital computer. The results obtained from numerical studies showed that this approach was unsatisfactory and the method was dropped.

Detailed discussions follow of the finite difference grid system, finite difference representations of partial derivatives, finite difference representations of the equations and boundary conditions, the velocity and pressure matrix, the concentration matrix, the temperature matrix, derived results, the first step into the tube, and stability and convergence considerations.

Finite Difference Grid System

The finite difference grid system used for all three cases of condensation considered is a two dimensional mesh in the r and z directions. The grid extends from the center of the tube to the wall in the radial direction and from the entrance of the tube to any desired length. There are grid points in both phases. At each step in the axial direction one of the grid points falls exactly on the gas-liquid interface. Concentration, radial velocity, and the physical properties may take two values at this point.

This grid system is shown in Fig. 43. The center of the tube is at i = 0, the tube wall at i = n+1, and the entrance of the tube at j = 0. The extra steps at the interface in the first axial step are used in a starting procedure. For binary vapor condensation four extra grid points were used; for the other cases nine extra grid points were used. Values of the various functions at the extra points and the starting procedure are discussed later.

The small thickness of the liquid film requires that the radial step sizes vary from large at the center (where values change slowly) to quite small in the liquid and adjacent vapor (where values change more rapidly). If a constant radial step size were used the number of radial steps would be prohibitive. Each time the radial interval size is changed an extra row is added to the matrix describing the equation of motion and the equation of continuity. Therefore, the radial step size was allowed to vary by stages. This kept the total number of radial steps to a minimum and kept the resulting matrix from being too

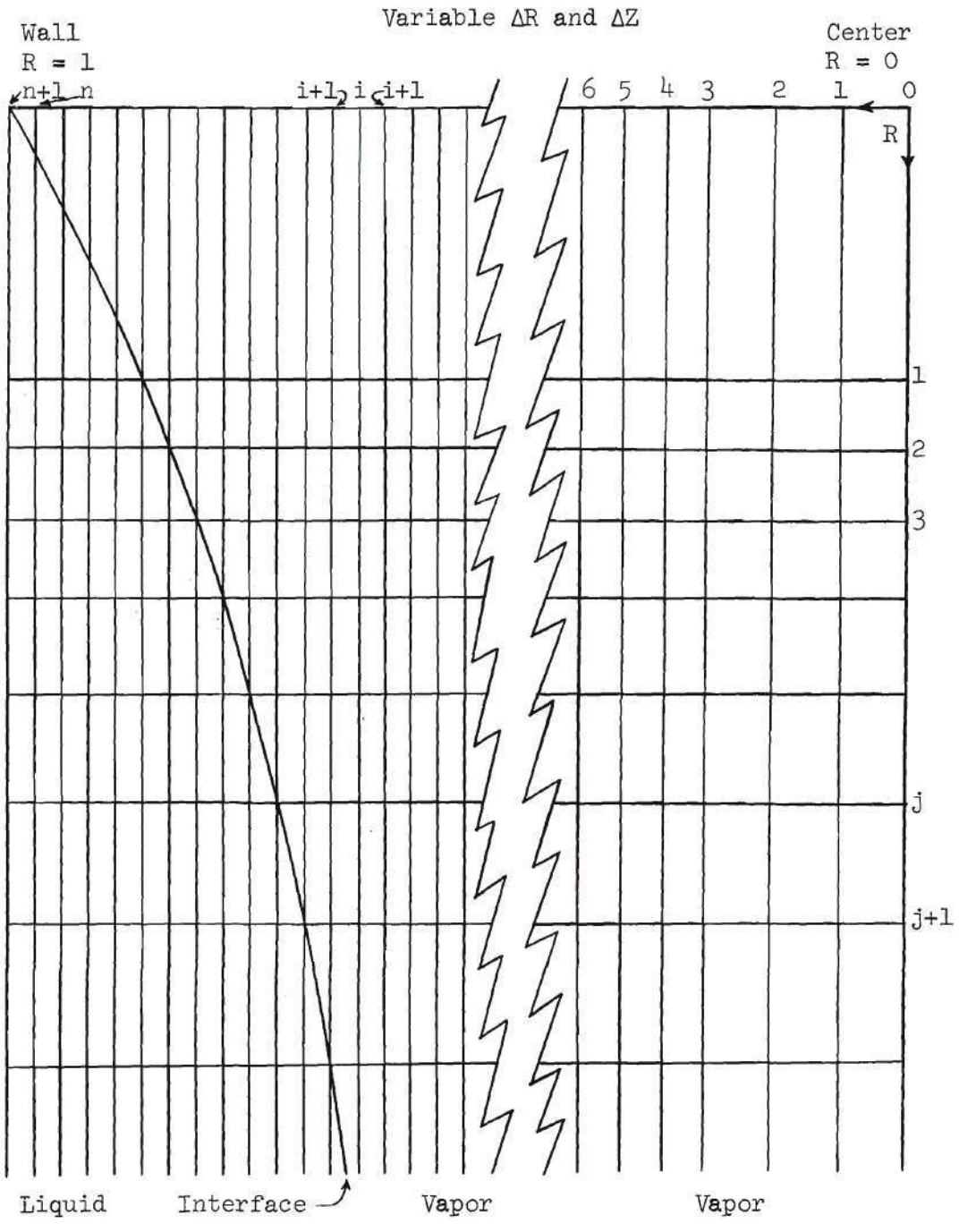

Fig. 43. Diagram of Finite Difference Grid System

unwieldy. The number of radial steps varied between 80 and 140 for the problems under consideration.

The radial grid positions near the wall were fixed by simple model estimations of film thickness discussed later. A constant value of radial step size was used in the liquid film and adjacent vapor. After a small number of steps in the axial direction this interval size was doubled in order to save computer time.

The axial step size varied, but not in stages. It was adjusted automatically until the heat being transferred at the gas-liquid interface in this axial step was matched by an equivalent amount of condensing mass. The number of axial steps used varied from about ten to forty-seven for the problems under consideration.

An implicit finite difference "marching" procedure was used to solve the equations. The velocities, temperatures, concentrations, and pressure were assumed known for any value of i at the axial position j and all axial positions upstream of j. They were unknown at the j+1 axial step.

In the equations of motion, energy, and diffusion the i-1, i, and i+1 values at the j+1 axial step were described in terms of the i^{th} value of the j axial step and the finite difference equations. This is illustrated in Fig. 44.

In the equation of continuity the i and i+1 values at the j+1 axial step were described in terms of the i and i+1 values at the j axial step and the finite difference equation. This is shown in Fig. 45.

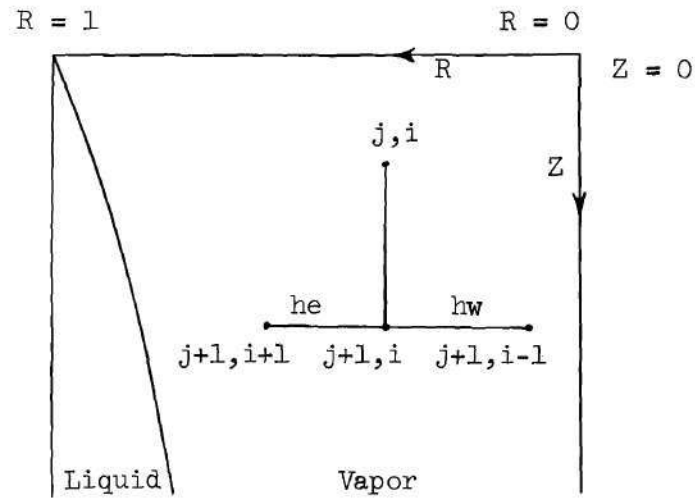

Not Drawn to Scale

Fig. 44. Difference Scheme for Motion, Energy, and Diffusion Equations.

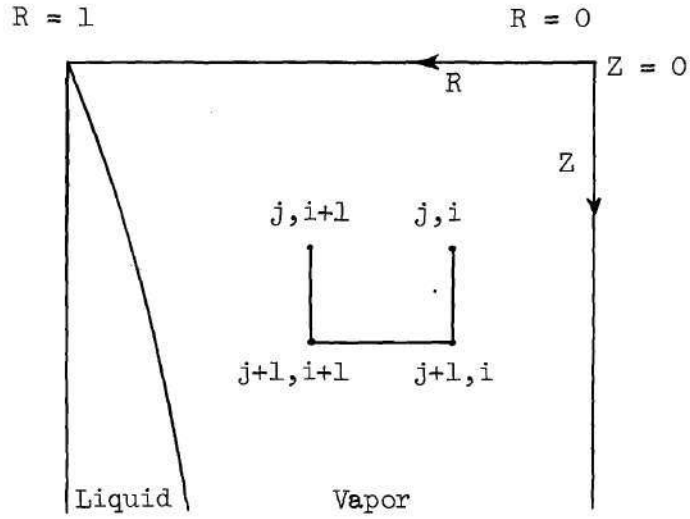

Not Drawn to Scale

Fig. 45. Difference Scheme for Continuity Equation.

A diagram of the grid system in the vicinity of the gas-liquid interface is shown in Fig. 46. The motion, energy, and diffusion equations were applied to the q-1 radial point and the q+1 radial point but not the q radial point. Values of the variables at the j+1 axial step and the q radial step were required because of the difference schemes involved. Physical properties, radial velocity, and concentration had a liquid value and a gas value at this point. The gas values were used in the equations applied to the q-1 grid point, and the liquid values were used in the equation applied to the q+1 grid point. The continuity equation was applied between the q-1 and q radial points and between the q and q+1 radial point. The gas values of radial velocity and density were used for the first step and liquid values for the second.

The implicit method described above resulted in matrices which were solved by standard methods to give all values at the j+1 axial step. One matrix solved the equation of motion and the equation of continuity to give velocities and pressure; one or two matrices solved the equation of diffusion to give the concentrations; one or two matrices solved the equation of energy to give temperatures.

Finite Difference Representations of Partial Derivatives

The finite difference representations of partial derivatives may be derived by Taylor series expansions about each grid point (37).

The forward difference first derivative of a function f(R,Z) in the axial direction is

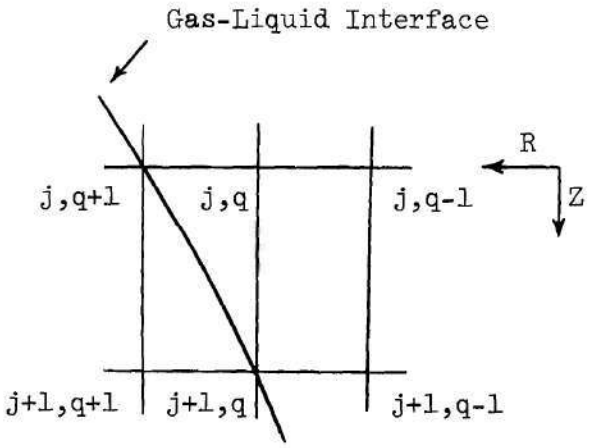

Not Drawn to Scale

Fig. 46. Diagram of Grid System Near Interface.

$$\left(\frac{\partial f}{\partial Z}\right)_{j+1,i} = \frac{f_{j+1,i} - f_{j,i}}{\Delta Z} + O(\Delta Z) \qquad \text{(A-1)}$$

where $\Delta Z = Z_{j+1} - Z_j$. The subscripts are as shown on Fig. 43. When f is replaced by pressure this expression becomes

$$\left(\frac{\partial P}{\partial Z}\right)_{j+1,i} = \frac{P_{j+1} - P_j}{\Delta Z} + O(\Delta Z) \qquad \text{(A-2)}$$

The forward difference first derivative in the radial direction is

$$\left(\frac{\partial f}{\partial R}\right)_{j+1,i} = \frac{f_{j+1,i+1} - f_{j+1,i}}{he} + O(he) \qquad \text{(A-3)}$$

where $he = R_{i+1} - R_i$. This type of first derivative in the radial direction is used exclusively in all boundary conditions except those at the center of the tube. In the equations of change the central difference first derivative in the radial direction is used. For variable radial distances this may be shown to be

$$\left(\frac{\partial f}{\partial R}\right)_{j+1,i} = \frac{hw f_{j+1,i+1}}{he(hw+he)} - \frac{(hw-he) f_{j+1,i}}{hw\ he} - \frac{he f_{j+1,i-1}}{hw(hw+he)} + O(he\ hw) \qquad \text{(A-4)}$$

where $he = R_{i+1} - R_i$ and $hw = R_i - R_{i-1}$. Obvious simplifications result if he = hw. The central difference second derivative in the radial direction is

$$\left(\frac{\partial^2 f}{\partial R^2}\right)_{j+1,i} = 2\left[\frac{f_{j+1,i+1}}{he(hw+he)} - \frac{f_{j+1,i}}{he\ hw} + \frac{f_{j+1,i-1}}{hw(hw+he)}\right] + O(he-hw) \qquad \text{(A-5)}$$

If he = hw then the truncation term is the order of he^2.

Finite Difference Representations of the Equations

In the following development the finite difference forms of each equation will have the unknown values, i.e., velocities, pressure, temperatures, concentrations, and their coefficients at the j+1 axial step on the left hand side of the equation and all known terms, i.e., velocities, pressure, temperatures, concentrations, and their coefficients at the j axial step and boundary conditions on the right hand side of the equation.

Terms involving density are found in the equation of motion, the variable density continuity equation, and various boundary conditions. In the cases where density is allowed to vary as a function of concentration it may be evaluated as

$$\rho'_{j+1,i} = \frac{\rho'_a\left(1 + \frac{W_b}{W_a}_{j+1,i}\right)}{\left(1 + \frac{\rho'_a}{\rho'_b}\frac{W_b}{W_a}_{j+1,i}\right)} \qquad \text{(A-6)}$$

where ρ'_a and ρ'_b are the densities of the pure components.

The Equation of Motion

The axial component of the equation of motion is

$$U\frac{\partial U}{\partial Z} + V\frac{\partial U}{\partial R} = -\frac{\partial P}{\partial Z} + \frac{2}{Re}\left(\frac{\partial^2 U}{\partial R^2} + \frac{1}{R}\frac{\partial U}{\partial R}\right) + \frac{1}{2Fr} \qquad \text{(II-4)}$$

Substituting the finite difference representations into this equation, making the density corrections to the pressure term mentioned in Chapter II and rearranging one obtains

$$U_{j+1,i-1}A_i + U_{j+1,i}B_i + U_{j+1,i}C_i + P_{j+1}E_i = F_i \qquad (A\text{-}7)$$

where

$$A_i = -\frac{heV_{j,i}}{hw(hw+he)} - \frac{4}{Re\ hw(hw+he)} + \frac{2\ he}{R_i\ Re\ hw(hw+he)} \qquad (A\text{-}8)$$

$$B_i = \frac{U_{j,i}}{\Delta Z} - \frac{V_{j,i}(hw-he)}{hw\ he} + \frac{4}{Re\ he\ hw} + \frac{2(hw-he)}{R_i\ Re\ hw\ he} \qquad (A\text{-}9)$$

$$C_i = \frac{hw\ V_{j,i}}{he(hw+he)} - \frac{4}{Re\ he(hw+he)} - \frac{2\ hw}{R_i\ Re\ he(hw+he)} \qquad (A\text{-}10)$$

$$E_i = \frac{\rho'_{j+1,o}}{\rho'_{j+1,i}\Delta Z}\left[1 + \frac{\rho'_{j+1,i} - \rho'_{j,i}}{\rho'_{j+1,i}}\right] \qquad (A\text{-}11)$$

and

$$F_i = \frac{1}{2\ Fr} + \frac{\rho'_{j,o}\ P_j}{\rho'_{j,i}\Delta Z} + \frac{(U_{j,i})^2}{\Delta Z} \qquad (A\text{-}12)$$

The density ratios in this equation become unity and the density difference becomes zero when density is constant in the gas. The density ratio is not unity in the liquid phase, although the density difference is zero. If the gas density is allowed to vary as a function of concentration it may be evaluated by equation (A-6).

At the center of the tube the equation of motion becomes

$$U\frac{\partial U}{\partial Z} + \frac{\partial P}{\partial Z} = \frac{4}{Re}\frac{\partial^2 U}{\partial R^2} + \frac{1}{2\ Fr} \qquad (A\text{-}13)$$

after application of L'Hôpital's rule to the necessary terms as R goes to zero and the use of the boundary condition that the radial velocity is zero at the center. Substituting the finite difference representations into this equation, making the density correction to the pressure

term mentioned in Chapter II, and using the boundary condition of no shear at the center, one obtains

$$U_{j+1,o}B_o + U_{j+1,1}C_o + P_{j+1}E_o = F_o \tag{A-14}$$

where

$$B_o = \frac{8}{Re\ he\ he} + \frac{U_{j,o}}{\Delta Z} \tag{A-15}$$

$$C_o = -\frac{8}{Re\ he\ he} \tag{A-16}$$

$$E_o = \frac{1}{\Delta Z} + \frac{\rho'_{j+1,o} - \rho'_{j,o}}{\rho_{j+1,o}\,\Delta Z} \tag{A-17}$$

and

$$F_o = \frac{1}{2\ Fr} + \frac{P_j + (U_{j,o})^2}{\Delta Z} \tag{A-18}$$

Again, the density difference becomes zero if the density is constant.

In the above equations the Reynolds number, Re, is defined as $\rho'\bar{u}'D'/\mu'$. In the liquid phase this term is $\rho'_\ell\bar{u}'D'/\mu'_\ell$. It is evaluated as $\rho'_g\bar{u}'D'/\mu'_g$ for a constant density gas and $\rho'_{g_{j+1,i}}\ \bar{u}'D'/\mu'_g$ for a variable density gas.

The Variable Density Equation of Continuity

The variable density equation of continuity is

$$\frac{\partial(\rho'RU)}{\partial Z} + \frac{\partial(\rho'RV)}{\partial R} = 0 \tag{II-10}$$

When the finite difference representations are substituted into this equation the result is

$$U_{j+1,i+1}\left[\frac{R_{i+1}\ \rho'_{j+1,i+1}}{2\Delta Z}\right] + U_{j+1,i}\left[\frac{R_i\ \rho'_{j+1,i}}{2\Delta Z}\right]$$

$$+ V_{j+1,i+1}\left[\frac{R_{i+1}\ \rho'_{j+1,i+1}}{he}\right] + V_{j+1,i}\left[\frac{R_i\ \rho'_{j+1,i}}{he}\right]$$

$$= \frac{U_{j,i+1}\ \rho'_{j,i+1}R_{i+1} + U_{j,i}\ \rho'_{j,i}R_i}{2\Delta Z} \qquad \text{(A-19)}$$

Density may be evaluated by equation (A-6). The variable density equation of continuity at the center becomes

$$\frac{\partial(\rho' U)}{\partial Z} + 2\,\frac{\partial(\rho' V)}{\partial R} = 0 \qquad \text{(A-20)}$$

when L'Hôpital's rule is applied to the necessary terms as R goes to zero. Upon substitution of the finite difference representations and the use of the condition that V = 0 at the center this becomes

$$U_{j+1,1}\left[\frac{\rho'_{j+1,1}}{2\Delta Z}\right] + U_{j+1,o}\left[\frac{\rho'_{j+1,o}}{2\Delta Z}\right] + \frac{2\ V_{j+1,1}\ \rho'_{j+1,1}}{he}$$

$$= \frac{U_{j,1}\ \rho'_{j,1} + U_{j,o}\ \rho'_{j,o}}{2\Delta Z} \qquad \text{(A-21)}$$

The radial step size varies in stages from the center to the wall. From the center to the first change in step size, step s, the following equation applies. It results from adding equation (A-21) to the summation of equation (A-19) from i = 1 to i = s-1.

$$U_{j+1,o}G_o + U_{j+1,1}G_1 + \sum_{i=2}^{s-1} U_{j+1,i}G_i + U_{j+1,s}G_s$$

$$+ V_{j+1,s}K_1 = F_{n+1} \qquad \text{(A-22)}$$

where

$$G_o = \frac{R_1 \rho'_{j+1,o}}{4\Delta Z} \tag{A-23}$$

$$G_1 = \frac{3R_1 \rho'_{j+1,1}}{4\Delta Z} \tag{A-24}$$

$$G_i = \frac{R_i \rho'_{j+1,i}}{\Delta Z} \tag{A-25}$$

$$G_s = \frac{R_s \rho'_{j+1,s}}{2\Delta Z} \tag{A-26}$$

$$K_1 = \frac{R_s \rho'_{j+1,s}}{\Delta R} \tag{A-27}$$

and

$$F_{n+1} = \frac{R_1 \rho'_{j,o} U_{j,o}}{4\Delta Z} + \frac{3R_1 \rho'_{j,1} U_{j,1}}{4\Delta Z} + \sum_{i=2}^{s-1} \frac{R_i \rho'_{j,i} U_{j,i}}{\Delta Z} + \frac{R_s \rho'_{j,s} U_{j,s}}{2\Delta Z} \tag{A-28}$$

ΔR is the radial step size in this section of the tube.

For other sections of the tube over which the radial interval size does not change, i.e., from some step, s, to some step, t, equation (A-19) may be summed from i = s to i = t-1 to yield

$$U_{j+1,s} H_s + \sum_{i=s+1}^{t-1} U_{j+1,i} H_i + U_{j+1,t} H_t + V_{j+1,s} K_{2d} + V_{j+1,t} K_{2d+1} = F_{n+d+1} \tag{A-29}$$

where

$$H_s = \frac{R_s \rho'_{j+1,s}}{2\Delta Z} \tag{A-30}$$

$$H_i = \frac{R_i \rho'_{j+1,i}}{\Delta Z} \tag{A-31}$$

$$H_t = \frac{R_t \rho'_{j+1,t}}{2\Delta Z} \tag{A-32}$$

$$K_{2d} = -\frac{R_s \rho'_{j+1,s}}{\Delta R} \tag{A-33}$$

$$K_{2d+1} = \frac{R_t \rho'_{j+1,t}}{\Delta R} \tag{A-34}$$

and

$$F_{n+d+1} = \frac{R_s \rho'_{j,s} U_{j,s}}{2\Delta Z} + \sum_{i=s+1}^{t-1} \frac{R_i \rho'_{j,i} U_{j,i}}{\Delta Z} + \frac{R_t \rho'_{j,t} U_{j,t}}{2\Delta Z} \tag{A-35}$$

ΔR is the radial step size in this region of the tube and "d" is the number of times the radial interval size has been changed between this region and the center of the tube. The value of d is increased by two if the interface is between this region and the center of the tube.

The Constant Density Equation of Continuity

The constant density equation of continuity is

$$\frac{\partial(RU)}{\partial Z} + \frac{\partial(RV)}{\partial R} = 0 \tag{II-5}$$

Upon substitution of the finite difference representations this equation becomes

$$\frac{U_{j+1,i+1} R_{i+1} + U_{j+1,i} R_i}{2\Delta Z} + \frac{V_{j+1,i+1} R_{i+1} + V_{j+1,i} R_i}{he}$$

$$= \frac{U_{j,i+1} R_{i+1} + U_{j,i} R_i}{2\Delta Z} \tag{A-36}$$

This is an obvious simplification of equation (A-19).

When L'Hôpital's rule is used on the appropriate terms at the center of the tube the constant density equation of continuity becomes

$$\frac{\partial U}{\partial Z} + 2\,\frac{\partial V}{\partial R} = 0 \tag{A-37}$$

Substituting the finite difference representations into this equation and using the condition that radial velocity is zero at the center gives

$$\frac{U_{j+1,1} + U_{j+1,o}}{2\Delta Z} + \frac{2\,V_{j+1,1}}{he} = \frac{U_{j,1} + U_{j,o}}{2\Delta Z} \tag{A-38}$$

As previously mentioned, the radial step size varies in stages from the center to the wall. From the center to the first change in step size, step s, equation (A-38) may be added to the summation of equation (A-36) from i = 1 to i = s-1 to yield

$$U_{j+1,o}G_o + U_{j+1,1}G_1 + \sum_{i=2}^{s-1} U_{j+1,i}G_i + U_{j+1,s}G_s + V_{j+1,s}K_1 = F_{n+1} \tag{A-39}$$

where

$$G_o = \frac{R_1}{4\Delta Z} \tag{A-40}$$

$$G_1 = \frac{3R_i}{4\Delta Z} \tag{A-41}$$

$$G_i = \frac{R_i}{\Delta Z} \tag{A-42}$$

$$G_s = \frac{R_s}{2\Delta Z} \tag{A-43}$$

$$K_1 = \frac{R_s}{\Delta R} \tag{A-44}$$

and

$$F_{n+1} = \frac{R_1 U_{j,o}}{4\Delta Z} + \frac{3R_1 U_{j,1}}{4\Delta Z} + \sum_{i=2}^{s-1} \frac{R_i U_{j,i}}{\Delta Z} + \frac{R_s U_{j,s}}{2\Delta Z} \qquad \text{(A-45)}$$

ΔR is the radial step size in this region of the tube.

For other sections of the tube over which the radial interval size does not change, i.e., from some step, s, to some step, t, equation (A-36) may be summed from i = s to i = t-1 to yield

$$U_{j+1,s}H_s + \sum_{i=s+1}^{t-1} U_{j+1,i}H_i + U_{j+1,t}H_t + V_{j+1,s}K_{2d}$$

$$+ V_{j+1,t}K_{2d+1} = F_{n+d+1} \qquad \text{(A-46)}$$

where

$$H_s = \frac{R_s}{2\Delta Z} \qquad \text{(A-47)}$$

$$H_i = \frac{R_i}{\Delta Z} \qquad \text{(A-48)}$$

$$H_t = \frac{R_t}{2\Delta Z} \qquad \text{(A-49)}$$

$$K_{2d} = -\frac{R_s}{\Delta R} \qquad \text{(A-50)}$$

$$K_{2d+1} = \frac{R_t}{\Delta R} \qquad \text{(A-51)}$$

and

$$F_{n+d+1} = \frac{R_s U_{j,s}}{2\Delta Z} + \sum_{i=s+1}^{t-1} \frac{R_i U_{j,i}}{\Delta Z} + \frac{R_t U_{j,t}}{2\Delta Z} \qquad \text{(A-52)}$$

ΔR is the radial step size in this region of the tube and "d" is the

number of times the radial interval size has been changed between this region and the center of the tube. The value of d is increased by two if the interface is between this region and the center of the tube.

Another representation of the constant density continuity equation is used at the interface for the first step into the liquid film in the radial direction. This representation is

$$\frac{U_{j+1,q+1}R_{q+1}}{\Delta Z} + \frac{V_{j+1,q+1}R_{q+1}}{\Delta R} - \frac{(V_{j+1,q})_{\ell}R_q}{\Delta R} = \frac{U_{j,q+1}R_{q+1}}{\Delta Z} \qquad \text{(A-53)}$$

where "q" indicates the interface position at the j+1 axial step, "ℓ" denotes a liquid value of a variable at a point which may have both a liquid and a vapor value of that variable, and $\Delta R = R_{q+1} - R_q$.

Equation (A-46) is used as the continuity equation for all other steps in the liquid film.

The Equation of Energy

The equation of energy is

$$U\frac{\partial T}{\partial Z} + V\frac{\partial T}{\partial R} = \frac{2}{Re\ Pr}\left(\frac{1}{R}\frac{\partial T}{\partial R} + \frac{\partial^2 T}{\partial R^2}\right) + \frac{2}{ReEk}\left(\frac{\partial U}{\partial R}\right)^2 \qquad \text{(II-6)}$$

When the finite difference representations are substituted into this equation and the equation rearranged the result is

$$T_{j+1,i-1}A_i + T_{j+1,i}B_i + T_{j+1,i+1}C_i = F_i \qquad \text{(A-54)}$$

where

$$A_i = -\frac{he\ V_{j+1,i}}{hw(hw+he)} + \frac{2he}{Re\ R_i\ Pr\ hw(hw+he)} - \frac{4}{Re\ Pr\ hw(hw+he)} \qquad \text{(A-55)}$$

$$B_i = -\frac{V_{j+1,i}(hw-he)}{hw\ he} + \frac{U_{j+1,i}}{\Delta Z} + \frac{2(hw-he)}{Re\ Pr\ R_i hwhe} + \frac{4}{Re\ Pr\ hw\ he} \qquad \text{(A-56)}$$

$$C_i = \frac{hw\ V_{j+1,i}}{he(hw+he)} - \frac{2\ hw}{Re\ Pr\ R_i} - \frac{4}{Re\ Pr\ he(hw+he)} \tag{A-57}$$

and

$$F_i = \frac{T_{j,i}U_{j+1,i}}{\Delta Z} + \frac{2}{Re\ Ek}\left[\frac{hw\ U_{j+1,i+1}}{he(hw+he)} - \frac{U_{j+1,i}(hw-he)}{hw\ he}\right.$$

$$\left. - \frac{U_{j+1,i-1}\,he^2}{hw(hw+he)}\right] \tag{A-58}$$

At the center of the tube the equation of energy becomes

$$U\frac{\partial T}{\partial Z} = \frac{4}{RePr}\frac{\partial^2 T}{\partial R^2} + \frac{2}{Re\ Ek}\left(\frac{\partial U}{\partial R}\right)^2 \tag{A-59}$$

with the aid of L'Hôpital's rule and the condition that radial velocity is zero at this point. With the use of the finite difference representations, the boundary condition of zero temperature gradient, and rearrangement this becomes

$$T_{j+1,o}B_o + T_{j+1,1}C_o = F_o \tag{A-60}$$

where

$$B_o = \frac{8}{Re\ Pr\ he\ he} + \frac{U_{j+1,o}}{\Delta Z} \tag{A-61}$$

$$C_o = -\frac{8}{Re\ Pr\ he\ he} \tag{A-62}$$

and

$$F_o = \frac{T_{j,o}U_{j+1,o}}{\Delta Z} \tag{A-63}$$

The Reynolds, Prandtl, and Eckert numbers above are evaluated according to the phase the equation is describing.

The Equation of Diffusion

The equation of diffusion for component a is

$$V\frac{\partial W_a}{\partial R} + U\frac{\partial W_a}{\partial Z} = \frac{2}{Sc\ Re}\left(\frac{\partial^2 W_a}{\partial R^2} + \frac{1}{R}\frac{\partial W_a}{\partial R}\right) \qquad \text{(II-11)}$$

When the finite difference representations are substituted into this equation and the equation rearranged the result is

$$W_{a_{j+1,i-1}} A_i + W_{a_{j+1,i}} B_i + W_{a_{j+1,i+1}} C_i = F_i \qquad \text{(A-64)}$$

where

$$A_i = -\frac{he\ V_{j+1,i}}{hw(hw+he)} - \frac{4}{Sc\ Re\ hw(hw+he)} + \frac{2\ he}{R_i\ Sc\ Re\ hw(hw+he)} \qquad \text{(A-65)}$$

$$B_i = -\frac{V_{j+1,i}(hw-he)}{hw\ he} + \frac{U_{j+1,i}}{\Delta Z} + \frac{4}{Sc\ Re\ hw\ he}$$

$$+ \frac{2(hw-he)}{R_i\ Sc\ Re\ hw\ he} \qquad \text{(A-66)}$$

$$C_i = \frac{hw\ V_{j+1,i}}{he(hw+he)} - \frac{4}{Sc\ Re\ he(hw+he)} - \frac{2\ hw}{R_i\ Sc\ Re\ he(hw+he)} \qquad \text{(A-67)}$$

and

$$F_i = \frac{W_{a_{j,i}} U_{j+1,i}}{\Delta Z} \qquad \text{(A-68)}$$

At the center of the tube the equation of diffusion with L'Hôpital's rule applied to the necessary terms and the use of the condition that radial velocity is zero at the center becomes

$$U\frac{\partial W_a}{\partial Z} = \frac{4}{Sc\ Re}\frac{\partial^2 W_a}{\partial R^2} \qquad \text{(A-69)}$$

Upon substitution of the finite difference representations, the boundary condition of zero concentration gradient at the center, and a slight rearrangement the equation becomes

$$W_{a_{j+1,o}} B_o + W_{a_{j+1,1}} C_o = F_o \tag{A-70}$$

where

$$B_o = \frac{8}{Sc\ Re\ he\ he} + \frac{U_{j+1,o}}{\Delta Z} \tag{A-71}$$

$$C_o = - \frac{8}{Sc\ Re\ he\ he} \tag{A-72}$$

and

$$F_o = \frac{W_{a_{j,o}} U_{j+1,o}}{\Delta Z} \tag{A-73}$$

The Schmidt and Reynolds numbers above are evaluated according to the phase the equation is describing.

The Boundary Conditions

Boundary conditions which involve a known value of a variable at a given point are easily handled. In such a case the value of this variable is known at the boundary grid point of the j+1 axial step. Terms in the above finite difference equations which involve this boundary value may be switched to the right hand sides of these equations and treated as known terms. Boundary conditions of this type will be covered further under the descriptions of the various matrices.

All boundary conditions at the center of the tube have been taken into account in the finite difference equations. Also, the

boundary conditions at the entrance of the tube are all handled as known values at the first step into the tube.

In the following discussion boundary conditions at the gas-liquid interface are considered for the three cases of condensation covered in this work. In addition, flux conditions at the wall are considered for binary condensation.

Interface Velocity

The velocity tangent to the gas-liquid interface should be a continuous function across the interface. The tangent vector is

$$\underline{t} = \frac{(\underline{i}\Delta z' - \underline{j}\Delta r')}{\Delta s'} \tag{A-74}$$

where $\Delta z' = z'_{j+1} - z'_j$, $\Delta r' = r'_{q+1} - r'_q$, and $\Delta s' = (\Delta r'^2 + \Delta z'^2)^{\frac{1}{2}}$. $\underline{i}$ and $\underline{j}$ are unit vectors in the z' and r' directions respectively. The velocity vector is

$$\underline{U}' = \underline{i}\, v_z' + \underline{j}\, v_r' \tag{A-75}$$

The tangential velocity is given by the dot product of the velocity and tangent vectors and is

$$(\underline{U}' \cdot \underline{t}) = \frac{v_z'\Delta z' - v_r'\Delta r'}{\Delta s'} \tag{A-76}$$

Equating the tangential velocity in the gas with the tangential velocity in the liquid gives

$$v_{z_g}' \Delta z' - v_{r_g}' \Delta r' = v_{z_\ell}' \Delta z' - v_{r_\ell}' \Delta r' \tag{A-77}$$

Making the boundary layer assumptions that v_z' is of the order of 1

where v_r' is of the order ϵ and that $\Delta z' >> \Delta r'$ then

$$v_{z_g}' \cong v_{z_\ell}' \tag{A-78}$$

As a result of these approximations the axial velocity at each interface grid point will have one value for both the gas and liquid phases. This relation will be applied to all three cases of condensation considered. The radial velocity will have two values at each interface grid point; one for the liquid radial velocity and one for the gas radial velocity. The relationship between the two radial velocity values is different for each of the three cases of condensation, and these relationships are discussed in the next subsection.

Interface Mass Transfer

The mass transfer normal to the gas-liquid interface is continuous across the interface. The vector normal to the interface is

$$\underline{n} = \frac{(\underline{i}\Delta r' + \underline{j}\Delta z')}{\Delta s'} \tag{A-79}$$

Pure Vapor. The mass flux vector for the condensation of a pure vapor is

$$\underline{N}' = \rho'(\underline{i}\, v_z' + \underline{j}\, v_r') \tag{A-80}$$

The dot product of the mass flux vector with the normal vector gives the normal mass flux at the interface

$$(\underline{N}' \cdot \underline{n}) = \frac{\rho'(v_z'\Delta r' + v_r'\Delta z')}{\Delta s'} \tag{A-81}$$

Equating the normal mass flux in the gas with the normal mass flux

in the liquid gives

$$\rho'_g v'_{z_g} \Delta r' + \rho'_g v'_{r_g} \Delta z' = \rho'_\ell v'_{z_\ell} \Delta r' + \rho'_\ell v'_{r_\ell} \Delta'_z \tag{A-82}$$

Expressing this in dimensionless finite difference form, using equation (A-78), and solving for the liquid radial velocity at the interface gives

$$(V_{j+1,q})_\ell = \frac{\rho'_g}{\rho'_\ell} \left[U_{j+1,q} \left(\frac{\Delta R}{\Delta Z}\right) + (V_{j+1,q})_g \right] - U_{j+1,q} \left(\frac{\Delta R}{\Delta Z}\right) \tag{A-83}$$

where q denotes the interface grid point at the j+1 axial step, $\Delta R = R_{q+1} - R_q = R_q - R_{q-1}$, and $\Delta Z = Z_{j+1} - Z_j$. Combining this expression with the equation of continuity for the first step into the liquid, equation (A-53), and rearranging gives

$$U_{j+1,q} I_q + U_{j+1,q+1} I_{q+1} + (V_{j+1,q})_g K_{2d} + V_{j+1,q+1} K_{2d+1} = F_{n+d+1} \tag{A-84}$$

where

$$I_q = - \frac{R_q}{\Delta Z} \left(\frac{\rho'_g}{\rho'_\ell} - 1\right) \tag{A-85}$$

$$I_{q+1} = \frac{R_{q+1}}{\Delta Z} \tag{A-86}$$

$$K_{2d} = - \frac{\rho'_g R_q}{\rho'_\ell \Delta R} \tag{A-87}$$

$$K_{2d+1} = \frac{R_{q+1}}{\Delta R} \tag{A-88}$$

and

$$F_{n+d+1} = \frac{U_{j,q+1} R_{q+1}}{\Delta Z} \tag{A-89}$$

In this equation "d" is the number of times plus one that the radial interval size has been changed between this region and the center of the tube.

Vapor and Noncondensable Gas. The mass flux vector for the condensable vapor is

$$\underline{N}'_{a_g} = \rho' \left(\underline{i}\, W_a v'_z + \underline{j}\, W_a v'_r - \underline{i}\, D'_{ab_g} \frac{\partial W_a}{\partial z'} - \underline{j}\, D'_{ab_g} \frac{\partial W_a}{\partial r'} \right) \tag{A-90}$$

The dot product of this vector with the normal vector gives the normal mass flux of component a at the interface

$$(\underline{N}'_{a_g} \cdot \underline{n}) = \frac{\rho'(v'_z \Delta r' + v'_r \Delta z')}{\Delta s'} - \frac{\rho' D'_{ab_g}}{\Delta s'} \left(\Delta r' \frac{\partial W_a}{\partial z'} + \Delta z' \frac{\partial W_a}{\partial r'} \right) \tag{A-91}$$

This expression will apply to the gas phase. The liquid is pure component a and equation (A-81) gives the mass flux into the liquid. Equating the two expressions gives

$$\rho'_g W_{a_g} v'_{z_g} \Delta r' + \rho'_g W_{a_g} v'_{r_g} \Delta z' - \rho'_g D'_{ab_g} \left(\frac{\partial W_a}{\partial z'} \right)_g \Delta r' - \rho'_g D'_{ab_g} \left(\frac{\partial W_a}{\partial r'} \right)_g \Delta z' = \rho'_\ell v'_{z_\ell} \Delta r' + \rho'_\ell v'_{r_\ell} \Delta z' \tag{A-92}$$

Expressing this equation in forward finite difference form, using equation (A-78), solving for the liquid radial velocity at the interface, and combining with equation (A-53) gives

$$U_{j+1,q}I_q + U_{j+1,q+1}I_{q+1} + (V_{j+1,q})_g K_{2d}$$

$$+ V_{j+1,q+1}K_{2d+1} = F_{n+d+1} \qquad \text{(A-93)}$$

where

$$I_q = -\frac{R_q}{\Delta Z}\left[\frac{(\rho'_{j+1,q})_g(1-W_{b_{j+1,q}})}{\rho'_\ell} - 1\right] \qquad \text{(A-94)}$$

$$I_{q+1} = \frac{R_{q+1}}{\Delta Z} \qquad \text{(A-95)}$$

$$K_{2d} = -\frac{(\rho'_{j+1,q})_g R_q(1-W_{b_{j+1,q}})}{\rho'_\ell \qquad \Delta R} \qquad \text{(A-96)}$$

$$K_{2d+1} = \frac{R_{q+1}}{\Delta R} \qquad \text{(A-97)}$$

$$F_{n+d+1} = \frac{2 R_q D'_{ab_g}(\rho'_{j+1,q})_g}{D'\bar{u}'\Delta R \quad \rho'_\ell}\left[\frac{(W_{b_{j+1,q}} - W_{b_{j,q}})\Delta R}{\Delta Z \Delta Z}\right.$$

$$\left. + \frac{(W_{b_{j+1,q}} - W_{b_{j+1,q-1}})}{\Delta R} + \frac{U_{j+1,q+1}R_q}{\Delta Z}\right] \qquad \text{(A-98)}$$

where $\Delta R = R_{q+1} - R_q = R_q - R_{q-1}$. In the above equation "d" is the number of times plus one that the radial interval size has been changed between this region and the center of the tube. This equation will be used in the matrix describing the equations of motion and continuity.

The condition that there be no normal mass flux of component b at the interface is used in the matrix describing the equation of diffusion of component b. The expression for no normal mass flux of b

across the interface is

$$\rho'_g W_{b_g} v'_{z_g} \Delta r' + \rho'_g W_{b_g} v'_{r_g} \Delta z' - \rho'_g D'_{ab_g} \left(\frac{\partial W_b}{\partial z'}\right)_g \Delta r'$$

$$- \rho'_g D'_{ab_g} \left(\frac{\partial W_b}{\partial r'}\right)_g \Delta z' = 0 \qquad \text{(A-99)}$$

Expressing this equation in forward finite difference form and combining with the equation of diffusion, equation (A-64), written for component b instead of component a one obtains

$$W_{b_{j+1,q-2}} A_{q-1} + W_{b_{j+1,q-1}} B_{q-1} = F_{q-1} \qquad \text{(A-100)}$$

where

$$A_{q-1} = - \frac{he\ V_{j+1,q-1}}{hw(hw+he)} - \frac{4}{Sc\ Re\ hw(hw+he)} + \frac{2\ he}{R_{q-1}\ Sc\ Re\ hw(hw+he)} \qquad \text{(A-101)}$$

$$B_{q-1} = - \frac{V_{j+1,q-1}(hw-he)}{hw\ he} + \frac{U_{j+1,q-1}}{\Delta Z} + \frac{4}{Sc\ Re\ he\ hw} + \frac{2(hw-he)}{R_{q-1}\ Sc\ Re\ hw\ he}$$

$$- \left[\frac{2D'_{ab_g}\ \Delta Z}{D'\overline{u}'he(U_{j+1,q}\,he + (V_{j+1,q})_g \Delta Z) - 2heD'_{ab_g}\left(\frac{he}{\Delta Z} + \frac{\Delta Z}{he}\right)}\right] \cdot$$

$$\left[\frac{hw\ V_{j+1,q-1}}{he(hw+he)} - \frac{4}{Sc\ Re\ he(hw+he)} - \frac{2\ hw}{R_{q-1}\ Sc\ Re\ he(hw+he)}\right] \qquad \text{(A-102)}$$

$$F_{q-1} = \left[\frac{2D'_{ab_g}\ \Delta Z}{D'\overline{u}'\Delta Z(U_{j+1,q}\,he + (V_{j+1,q})_g \Delta Z) - 2D'_{ab_g}\Delta Z\left(\frac{he}{\Delta Z} + \frac{\Delta Z}{he}\right)}\right] \cdot$$

$$\left[\frac{hw\ V_{j+1,q-1}}{he(hw+he)} - \frac{4}{Sc\ Re\ he(hw+he)} - \frac{2\ hw}{R_{q-1}\ Sc\ Re\ he(hw+he)}\right]$$

$$+ \frac{W_{b_{j,q-1}} U_{j+1,q-1}}{\Delta Z} \qquad \text{(A-103)}$$

Binary Vapor. It is required that the fluxes of the two components, a and c, be continuous across the interface. For component a this means

$$\rho'_g W_{a_g} v'_{z_g} \Delta r' + \rho'_g W_{a_g} v'_{r_g} \Delta z' - \rho'_g D'_{ac_g} \left(\frac{\partial W_a}{\partial z'}\right)_g \Delta r'$$

$$- \rho'_g D'_{ac_g} \left(\frac{\partial W_a}{\partial r'}\right)_g \Delta z'$$

$$= \rho'_\ell W_{a_\ell} v'_{z_\ell} \Delta r' + \rho'_\ell W_{a_\ell} v'_{r_\ell} \Delta z' - \rho'_\ell D'_{ac_\ell} \left(\frac{\partial W_a}{\partial z'}\right)_\ell \Delta r'$$

$$- \rho'_\ell D'_{ac_\ell} \left(\frac{\partial W_a}{\partial r'}\right)_\ell \Delta z' \qquad \text{(A-104)}$$

A similar expression may be written for component c. Adding the above expression for component a and the similar expression for component c and solving for the radial velocity in the liquid, one finds

$$v'_{r_\ell} = \frac{\rho'_g}{\rho'_\ell} \left(v'_{z_g} \frac{\Delta r'}{\Delta z'} + v'_{r_g} \right) - v'_{z_\ell} \frac{\Delta r'}{\Delta z'} \qquad \text{(A-105)}$$

Expressing this in finite difference form, using equation (A-78), and combining with the equation of continuity for the first step into the liquid gives

$$U_{j+1,q} I_q + U_{j+1,q+1} I_{q+1} + (V_{j+1,q})_g K_{2d} + V_{j+1,q+1} K_{2d+1}$$

$$= F_{n+d+1} \qquad \text{(A-106)}$$

where

$$I_q = - \frac{R_q}{\Delta Z} \left[\frac{(\rho'_{j+1,q})_g}{\rho'_\ell} - 1 \right] \qquad \text{(A-107)}$$

$$I_{q+1} = \frac{R_{q+1}}{\Delta Z} \tag{A-108}$$

$$K_{2d} = - \frac{(\rho'_{j+1,q})_g \, R_q}{\rho'_\ell \, \Delta R} \tag{A-109}$$

$$K_{2d+1} = \frac{R_{q+1}}{\Delta R} \tag{A-110}$$

$$F_{n+d+1} = \frac{U_{j,q+1} \, R_{q+1}}{\Delta Z} \tag{A-111}$$

Here $\Delta R = R_{q+1} - R_q = R_q - R_{q-1}$. In the above equation "d" is the number of times plus one that the radial interval size has been changed between this region and the center of the tube. This equation will be used in the matrix describing the equations of motion and continuity.

The condition of continuous mass flux of both components across the interface will be satisfied in the diffusion equation by a trial and error procedure. The equation of diffusion in the gas is solved using a trial value of concentration in the gas at the interface. A trial value of concentration in the liquid which is in equilibrium with the trial value in the gas is found by using the Van Laar relationships (43). This procedure also gives the interface temperature. The matrix describing the equation of diffusion in the liquid is solved using the above value of concentration in the liquid at the interface. The flux of component c from the gas is then calculated using the gas concentrations found above and

$$N'_{c_g} = \rho'_g W_{c_g} v'_{z_g} \Delta r' + \rho'_g W_{c_g} v'_{r_g} \Delta z' - \rho'_g D'_{ac_g} \left(\frac{\partial W_c}{\partial z'}\right)_g \Delta r'$$

$$- \rho'_g D'_{ac_g} \left(\frac{\partial W_c}{\partial r'}\right)_g \Delta z' \tag{A-112}$$

The flux of component c into the liquid is given by

$$N'_{c_\ell} = \rho'_\ell W_{c_\ell} v'_{z_\ell} \Delta r' + \rho'_\ell W_{c_\ell} v'_{r_\ell} \Delta z' - \rho'_\ell D'_{ac_\ell} \left(\frac{\partial W_c}{\partial z'}\right)_\ell \Delta r'$$

$$- \rho'_\ell D'_{ac_\ell} \left(\frac{\partial W_c}{\partial r'}\right)_\ell \Delta z' \qquad \text{(A-113)}$$

These two expressions will be equal only if the trial concentrations at the interface have the proper values. Newton's method (42) is used to make the difference between the two expressions go the zero by varying the trial concentrations at the interface.

The two matrices involve trial values of concentration at the interface. The terms involving these values may be treated as known terms. At the center of the tube the boundary conditions have been taken into account in the finite difference equations. At the wall the boundary conditions of no radial flux of either component reduce to

$$\left(\frac{\partial W_a}{\partial r'}\right)_\ell = \left(\frac{\partial W_c}{\partial r'}\right)_\ell = 0 \qquad \text{(A-114)}$$

Substitution of the forward finite difference representations into this equation and combination with the equation of diffusion, equation (A-64), gives

$$W_{c_{j+1,n-1}} A_n + W_{c_{j+1,n}} B_n = F_n \qquad \text{(A-115)}$$

where

$$A_n = -\frac{he\ V_{j+1,n}}{hw\ (hw+he)} - \frac{4}{Sc\ Re\ hw(hw+he)} + \frac{2\ he}{R_n\ Sc\ Re\ hw(hw+he)} \qquad \text{(A-116)}$$

$$B_n = \frac{hw\ V_{j+1,n}}{he(hw+he)} - \frac{4}{Sc\ Re\ he(hw+he)} - \frac{2\ hw}{R_n\ Sc\ Re\ he(hw+he)} - \frac{V_{j+1,n}(hw-he)}{hw\ he}$$

$$+ \frac{U_{j+1,n}}{\Delta Z} + \frac{4}{Sc\ Re\ he\ hw} + \frac{2(hw-he)}{R_n\ Sc\ Re\ hw\ he} \qquad \text{(A-117)}$$

and

$$F_n = \frac{W_{c_{j,n}}\ U_{j+1,n}}{\Delta Z} \qquad \text{(A-118)}$$

Interfacial Shear

The tangential shear stress at the gas-liquid interface should be a continuous function across the interface. The shear stress vector for constant property, Newtonian fluids is

$$\underline{\tau}' = \underline{i}\mu' \left(\frac{\partial v_z'}{\partial r'} + \frac{\partial v_r'}{\partial z'}\right) + \underline{j}\mu' \left(\frac{\partial v_z'}{\partial r'} + \frac{\partial v_r'}{\partial z'}\right) \qquad \text{(A-119)}$$

The dot product of the stress vector with the tangent vector, equation (A-74), gives the tangential shear stress.

$$(\underline{\tau}' \cdot \underline{t}) = \frac{\mu'\Delta z'\left(\frac{\partial v_z'}{\partial r'} + \frac{\partial v_r'}{\partial z'}\right) - \mu'\Delta r'\left(\frac{\partial v_z'}{\partial r'} + \frac{\partial v_r'}{\partial z'}\right)}{\Delta s'} \qquad \text{(A-120)}$$

If the boundary layer assumption that v_z' is of the order of 1 and v_r' and $\frac{\partial v_r'}{\partial z'}$ are of order ϵ and the assumption that $\Delta z' >> \Delta r'$ are made then

$$(\underline{\tau}' \cdot \underline{t}) \cong \frac{\mu'\Delta z'}{\Delta s'} \frac{\partial v_z'}{\partial r'} \qquad \text{(A-121)}$$

Equating the tangential shear in the gas phase with the tangential shear in the liquid phase gives

$$\mu'_g \left(\frac{\partial v'_z}{\partial r'}\right)_g = \mu'_\ell \left(\frac{\partial v'_z}{\partial r'}\right)_\ell \qquad \text{(A-122)}$$

Substitution of the dimensionless forward finite difference representations into this equation and the use of equation (A-78) results in

$$U_{j+1,q-1}A_q + U_{j+1,q}B_q + U_{j+1,q+1}C_q = 0 \qquad \text{(A-123)}$$

where

$$A_q = -\frac{\mu'_g}{\Delta R} \qquad \text{(A-124)}$$

$$B_q = \frac{\mu'_g}{\Delta R} + \frac{\mu'_\ell}{\Delta R} \qquad \text{(A-125)}$$

and

$$C_q = -\frac{\mu'_\ell}{\Delta R} \qquad \text{(A-126)}$$

Here $\Delta R = R_{q+1}-R_q = R_q-R_{q-1}$ and q denotes the interface grid point at the j+1 axial step. This relation will be applied at the q radial step instead of the equation of motion for each of the three cases of condensation considered.

Interface Temperature

Pure Vapor. The dimensionless temperature at the interface, $(T'_q-T'_w)/(T'_o-T'_w)$, always has the value of one. When the wall temperature is constant this means that there is a constant temperature drop through the liquid film for the entire length of condenser.

Vapor and Noncondensable Gas. The interface temperature, T'_q, is assumed to be a function of the partial pressure of the condensable

component at the interface. The dimensionless temperature at the interface is always less than one.

Binary Vapor. The conditions of equilibrium at the interface, continuity of the mass flux of each component across the interface, and heat released by the condensing mass equaling the heat transferred through the film determine the interface temperature by a procedure described previously.

Pressure and Velocity Profile

A system of simultaneous linear equations describing the equations of motion and continuity has been constructed in the previous sections of this appendix. The finite difference representations of the equation of motion and the equation of continuity in matrix form may be solved by standard Gauss elimination of the lower left hand triangle and back substitution of the remaining terms (42) to give the axial velocity profile and the pressure at the j+1 axial step. The radial velocity profile may be obtained from the axial velocity profile by use of the equation of continuity, equations (A-19) or (A-36).

A diagram of the matrix above is shown in Fig. 47. Only one radial step size change is shown (step s) instead of the six which were used in actual practice. A description of the various terms in the matrix is given for each of the three cases of condensation considered.

Pure Vapor

In the matrix shown in Fig. 47 B_o is defined by equation (A-15). C_o is defined by equation (A-16), E_o is defined by equation (A-17) and

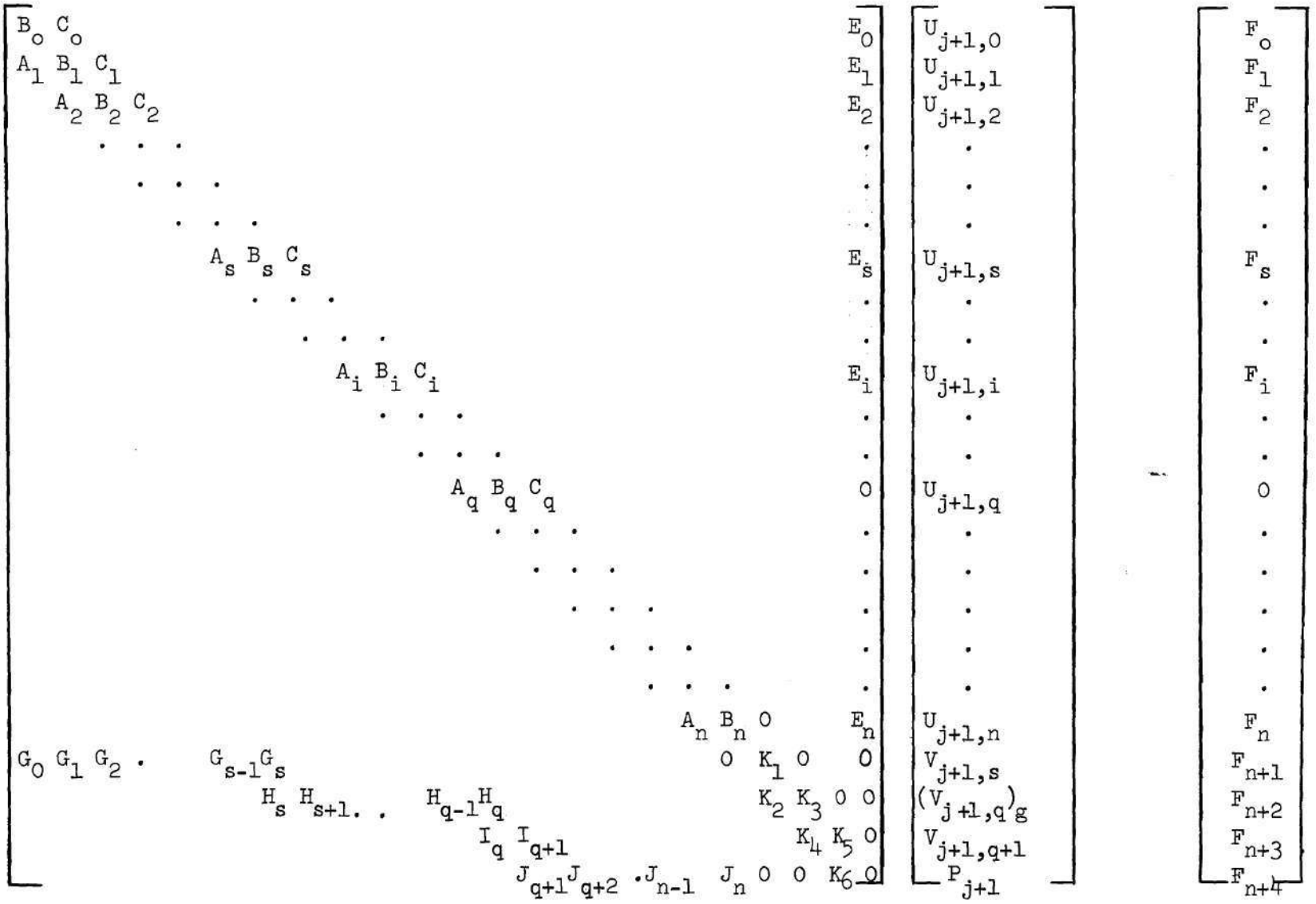

Fig. 47. Pressure and Velocity Matrix.

F_o is defined by equation (A-18). A_q is defined by equation (A-124), B_q by equation (A-125), and C_q by equation (A-126). E_q and F_q are zero. All other A_i, B_i, C_i, E_i, and F_i terms, from i = 1 to n, may be given by general formulas representing the various coefficients in equation (A-7). A_i is given by equation (A-8), B_i by equation (A-9), C_i by equation (A-10), E_i by equation (A-11), and F_i by equation (A-12).

G_o is defined by equation (A-40), G_1 by equation (A-41), G_s by equation (A-43), and all G_i terms, from i = 2 to s-1, are defined by equation (A-42). K_1 is defined by equation (A-44) and F_{n+1} by equation (A-45).

The radial step size changes at the s radial value. Here another continuity equation is used, and another line is added to the matrix. Each time the radial step size changes this is necessary. The constant density continuity equation applying between radial interval size changes is equation (A-46). H_s is defined by equation (A-47), H_q is defined by equation (A-49) with q replacing t. All H_i terms, for i = s+1 to q-1, are defined by equation (A-48). K_2 is defined by equation (A-50), K_3 by equation (A-51) with q replacing t, and F_{n+2} is defined by equation (A-52) with q replacing t.

The gas-liquid interface is at radial step q. Although radial step size is not allowed to change at the interface, it is necessary to add two extra lines to the matrix when the interface is encountered. I_q is defined by equation (A-85), I_{q+1} by equation (A-86), K_4 by equation (A-87), K_5 by equation (A-88), and F_{n+3} by equation (A-89).

The bottom line in the matrix represents equation (A-46). J_{q+1}

is defined by equation (A-47) with q+1 replacing s and J replacing H, and other J_i terms, for i = q+2 to n, are given by equation (A-48) with J replacing H. K_6 is defined by equation (A-50) with q+1 replacing s, and F_{n+4} is defined by equation (A-52) with q+1 replacing s and n+1 replacing t.

Vapor and Noncondensable Gas

All A_i, B_i, C_i, E_i, and F_i terms shown in Fig. 47 for i = 0 to n are defined exactly the same as for the condensation of a pure vapor. Also, F_{n+4}, K_6, and all J_i terms are defined as for the pure vapor case. The remaining terms are defined differently.

G_o is given by equation (A-23), G_1 by equation (A-24), G_s by equation (A-26), and all G_i terms, from i = 2 to s-1, are defined by equation (A-25). K_1 is defined by equation (A-27), and F_{n+1} is defined by equation (A-28).

The radial step size changes at the s radial value. The variable density continuity equation applying between radial interval size changes is equation (A-29). H_s is given by equation (A-30), H_q by equation (A-32) with q replacing t. All H_i terms, for i = s+1 to q-1, are defined by equation (A-31). K_2 is defined by equation (A-33), K_3 by equation (A-34) with q replacing t, and F_{n+2} by equation (A-35) with q replacing t.

The gas-liquid interface is at radial step q. I_q is defined by equation (A-94), I_{q+1} by equation (A-95), K_4 by equation (A-96), K_5 by equation (A-97), and F_{n+3} by equation (A-98).

Binary Vapor

All terms in Fig. 47 are exactly the same as for the condensation of a vapor from a vapor and noncondensable gas mixture except the I_q, I_{q-1}, K_4, K_5, and F_{n+3} terms. I_q is defined by equation (A-107), I_{q+1} by equation (A-108), K_4 by equation (A-109), K_5 by equation (A-110), and F_{n+3} by equation (A-111).

Concentration Profile

A system of simultaneous linear equations describing the equation of diffusion has been constructed in previous sections of this appendix. The finite difference representations of the equation of diffusion may be written in matrix form and the resulting tridiagonal matrix or matrices solved by Gauss elimination and back substitution (42) to give the concentration profile at the j+1 axial step.

A diagram of the tridiagonal matrix in the gas phase is shown in Fig. 48 and a diagram of the tridiagonal matrix in the liquid phase is shown in Fig. 49. A description of each of the various terms in these matrices is given below for the noncondensable and binary cases.

Vapor and Noncondensable Gas

The diffusion equation and resulting matrix apply to the gas phase only. This matrix is shown in Fig. 48.

B_o is defined by equation (A-71), C_o by equation (A-72), and F_o by equation (A-73) with component b replacing component a. A_{q-1} is given by equation (A-101), B_{q-1} by equation (A-102), and F_{q-1} by equation (A-103). All other A_i, B_i, C_i, and F_i terms, for i = 1 to q-2, are given by general formulas representing the various coeffi-

$$
\begin{bmatrix}
B_o & C_o & & & & & \\
A_1 & B_1 & C_1 & & & & \\
 & \ddots & \ddots & \ddots & & & \\
 & & A_i & B_i & C_i & & \\
 & & & \ddots & \ddots & \ddots & \\
 & & & & A_{q-2} & B_{q-2} & C_{q-2} \\
 & & & & & A_{q-1} & B_{q-1}
\end{bmatrix}
\begin{bmatrix}
Wb_{j+1,0} \\ Wb_{j+1,1} \\ \vdots \\ Wb_{j+1,i} \\ \vdots \\ Wb_{j+1,q-2} \\ Wb_{j+1,q-1}
\end{bmatrix}
=
\begin{bmatrix}
F_o \\ F_1 \\ \vdots \\ F_i \\ \vdots \\ F_{q-2} \\ F_{q-1}
\end{bmatrix}
$$

Fig. 48. Diffusion Equation for Component b in the Gas Phase

$$
\begin{bmatrix}
B_{q+1} & C_{q+1} & & & & & \\
A_{q+2} & B_{q+2} & C_{q+2} & & & & \\
 & \ddots & \ddots & \ddots & & & \\
 & & A_i & B_i & C_i & & \\
 & & & \ddots & \ddots & \ddots & \\
 & & & & A_{n-1} & B_{n-1} & C_{n-1} \\
 & & & & & & B_n
\end{bmatrix}
\begin{bmatrix}
Wc_{j+1,q+1} \\ Wc_{j+1,q+2} \\ \vdots \\ Wc_{j+1,i} \\ \vdots \\ Wc_{j+1,n-1} \\ Wc_{j+1,n}
\end{bmatrix}
=
\begin{bmatrix}
F_{q+1} \\ F_{q+2} \\ \vdots \\ F_i \\ \vdots \\ F_{n-1} \\ F_n
\end{bmatrix}
$$

Fig. 49. Diffusion Equation for Component c in the Liquid Phase.

cients in equation (A-64) written for component b. A_i is given by equation (A-65), B_i by equation (A-66), C_i by equation (A-67), and F_i by equation (A-68) with component b replacing component a.

Binary Vapor

Two tridiagonal matrices are necessary for this case. One describes the diffusion equation in the gas; the other describes the equation of diffusion in the liquid. These matrices are shown in Fig. 48 and Fig. 49.

Gas. In the matrix describing the gas, all A_i, B_i, C_i, and F_i terms, for i = 0 to q-2, are exactly the same as for the noncondensable case except that they are written for component c instead of component b. A_{q-1} and B_{q-1} are given by the general formulas for A_i and B_i, equations (A-65) and (A-66), respectively. F_{q-1} is given by equation (A-68) with component c replacing component a minus the product of $({}^{W}c_{j+1,q})_g$ with C_{q-1}, where C_{q-1} is given by equation (A-67).

Liquid. In the matrix describing the liquid all A_i, B_i, C_i, and F_i terms, for i = q+2 to n-1, are given by the various coefficients of equation (A-64) written for component c instead of component a. A_i is given by equation (A-65), B_i by equation (A-66), C_i by equation (A-67), and F_i by equation (A-68) with component c replacing component a. A_n is given by equation (A-116), B_n by equation (A-117), and F_n by equation (A-118). B_{q+1} is given by equation (A-66), C_{q+1} by equation (A-67), and F_{q+1} by equation (A-68) with component c replacing component a minus the product of $({}^{W}c_{j+1,q})_\ell$ with A_{q+1}, where A_{q+1} is defined by equation (A-65).

Temperature Profile

A system of simultaneous linear equations describing the equation of energy has been developed in previous sections of this appendix. The finite difference representations of the equation of energy may be written in tridiagonal matrix form, and the resulting matrix or matrices solved by Gauss elimination and back substitution (42) to give the temperature profile at the j+1 axial step.

Diagrams of tridiagonal matrices in the gas and liquid phases are shown in Fig. 48 and 49 with the concentration terms replaced by temperature terms. A description of each of the various terms in these matrices is given below for all three cases of condensation.

Pure Vapor

The energy equation is applied to the liquid phase only. The resulting matrix is shown in Fig. 49 with the concentration terms replaced by temperature terms.

All A_i, B_i, and C_i terms, for i = q+1 to n, may be defined by general formulas from equation (A-54). A_i is given by equation (A-55), B_i by equation (A-56), and C_i by equation (A-57). The F_i terms, for i = q+2 to n, are given by equation (A-58). F_{q+1} is given by equation (A-58) minus the product of $T_{j+1,q}$ with A_{q+1}, where A_{q+1} is defined by equation (A-55).

Vapor and Noncondensable Gas

The energy equation is applied to both phases. The resulting matrices are shown in Fig. 48 and Fig. 49 with the concentration terms replaced by temperature terms.

Gas. B_o is given by equation (A-61), C_o by equation (A-62), and F_o by equation (A-63). The A_i, B_i, and C_i terms, for i = 1 to q-1, are given by the various coefficients in equation (A-54). A_i is defined by equation (A-55), B_i by equation (A-56), and C_i by equation (A-57). The F_i terms, for i = 1 to q-2, are given by equation (A-58). F_{q-1} is given by equation (A-58) minus the product of $T_{j+1,q}$ with C_{q-1}, where C_{q-1} is defined by equation (A-57).

Liquid. The description of this matrix is exactly the same as that for the condensation of a pure vapor.

Binary Vapor

The equation of energy is applied to both phases. The descriptions of the two resulting tridiagonal matrices are exactly the same as those for the condensation of a vapor from a vapor and a noncondensable gas mixture.

Derived Results

The following results are derived from the velocity and temperature profiles obtained by numerical solution of the mathematical models.

Heat Transfer Coefficients

Pure Vapor. The local heat transfer coefficients were defined by

$$h'_{loc_{j+1}} = -\frac{k'_\ell}{(T'_o - T'_w)} \left.\frac{\partial T'}{\partial r'}\right|_{r'=wall} = \frac{k'_\ell (T'_{j+1,n} - T'_{j+1,n+1})}{(r'_{n+1} - r'_n)(T'_o - T'_w)} \qquad \text{(A-127)}$$

using notation similar to the finite difference grid system.

For the first step into the tube the average heat transfer coefficient is defined as

$$h'_{m_1} = \frac{\Gamma'_1 \lambda'}{(T'_o - T'_w)\, z'} \qquad \text{(A-128)}$$

For all other steps down the tube h'_m is defined as

$$h'_{m_{j+1}} = h'_{m_j}\left(\frac{z'_j}{z'_{j+1}}\right) + \left(\frac{h'_{loc_{j+1}} + h'_{loc_j}}{2}\right)\left(1 - \frac{z'_j}{z'_{j+1}}\right) \qquad \text{(A-129)}$$

using notation similar to the grid system. A check of the results calculated by this equation is provided by

$$h'_{m_{j+1}} = \frac{\Gamma'_{j+1} \lambda'}{(T'_o - T'_w) z'_{j+1}} \qquad \text{(A-130)}$$

This equation always agreed with equation (A-129) to within a tenth of one percent.

Vapor and Noncondensable Gas. The heat transfer coefficients are defined in the same way as the pure vapor case.

Binary Vapor. As mentioned in Chapter V two choices exist as to the correct temperature difference to use in definitions of heat transfer coefficients. Equations (A-127), (A-128), and (A-129) based on $T'_o - T'_w$ or $T'_{dp} - T'_w$ form one set of definitions, and the same equations with $T'_{bp} - T'_w$ form the second set.

Liquid Film Flow Rate

A simple numerical integration scheme was used with liquid velocity profile results at a given point down the tube to yield the flow rate of the liquid film past the given point.

Shear Stress at the Interface

The dimensionless shear stress defined by Rohsenow, Webber, and

Ling (15) may be derived from velocity profile results. It may be defined as

$$\tau^* = \frac{\mu_g'(v_{z_q}' - v_{z_{q-1}}')}{(r_q' - r_{q-1}')g'(\rho_\ell' - \rho_g')} \left(\frac{(\rho_\ell')^2 g'}{(\mu_\ell')^2}\right)^{1/3} \qquad \text{(A-131)}$$

First Step Into Tube

The first step into the tube involves the use of extra grid points on the gas-liquid interface between the entrance and the first step as shown in Fig. 43. These extra points require velocity, temperature, and concentration values. It is necessary to estimate such values from simple models.

The liquid film thickness at the first step must be estimated also. A trial first step into the tube is chosen and the thickness of the liquid film estimated from this length by simple models. Radial grid positions near the wall are then fixed, and the computer program adjusts the length of the first step until the heat transferred through the film equals the heat released by the condensing mass.

Detailed descriptions of these estimations and the effect of starting position are given below.

Liquid Film Thickness

A trial position of the first step is used to estimate the liquid film thickness in the following equation from simple Nusselt theory as modified by Rohsenow (14).

$$\delta_1' = \left(\frac{4z_1' k_\ell' (T_o' - T_w')\mu_\ell'}{g'\rho_\ell'(\rho_\ell' - \rho_g')\lambda'\left(1 + \frac{3C_p'(T_o' - T_w')}{8\lambda'}\right)}\right)^{0.25} \qquad \text{(A-132)}$$

From this thickness the grid positions near the wall are determined.

After the computer has solved the mathematical model for values of velocity, temperature, and concentration satisfying all boundary conditions at the first step into the tube the shear stress at the interface is evaluated from these results and used to make a better estimation of film thickness. A simple model (5) using constant shear stress at the interface gives

$$\delta_1' = \left(\frac{4z_1' k_\ell' (T_o' - T_w') \mu_\ell'}{g' \rho_\ell' (\rho_\ell' - \rho_g') \lambda' \left(1 + \frac{3C_p' (T_o' - T_w')}{8\lambda'}\right)} + \frac{4(v_{z_q}' - v_{z_{q-1}}') \mu_g' \delta_1'}{3(r_q' - r_{q-1}')(\rho_\ell' - \rho_g') g'} \right)^{0.25} \qquad \text{(A-133)}$$

This equation is solved by trial and error to give δ_1'. The grid positions are re-evaluated using this value, and the first step into the tube is resolved.

These equations are used for estimating film thicknesses for all three cases of condensation considered.

Effect of Starting Position

The trial first step into the tube from which film thickness is estimated has important effects on the numerical solutions. Solutions having different starting positions have slightly different numerical results. In the binary and noncondensable cases the starting position can affect the numerical solution of the equation of diffusion. In addition, under certain combinations of fluid properties,

temperature difference, entering velocity and starting position no numerical solutions were achieved. In these cases the heat transfer would not balance with the mass transfer to sufficient accuracy after 10 or 15 tries, or negative axial velocities were encountered, or z'_{j+1} was less than z'_j. Attempts at correlating the certain combinations which gave no solution proved unsuccessful. However, solutions were achieved by changing the starting position.

Typical examples of the effect of starting position on numerical results may be seen in Fig. 50 and Fig. 51. Heat transfer coefficients, interface temperature, interfacial concentration, interfacial shear, and film thickness values require several steps into the tube to smooth out. The numerical results for different starting positions agree well after several steps.

Solutions reported in Appendix E usually represent the smoothest of two or sometimes three solutions with different starting positions. The smoothest solutions were determined by plotting $h'_m/h'_{m_{Nu}}$ versus Z^* for different starting positions and temperature drops.

Trial first steps varied from $Z^* = 10^{-7}$ to 10^{-2} where Z^* is defined as $z'/D'Re$.

Velocity Values

The velocity values of the extra grid points on the interface are determined by estimating their values from the Nusselt theory as modified by Rohsenow (14). A first guess for the axial velocity values on the interface is given by

$$(U_{1,i})_{\ell} = \frac{g'(\rho'_{\ell}-\rho'_g)(\delta'_i)^2}{2\mu'_{\ell}\ \overline{u}'} \qquad \text{(A-134)}$$

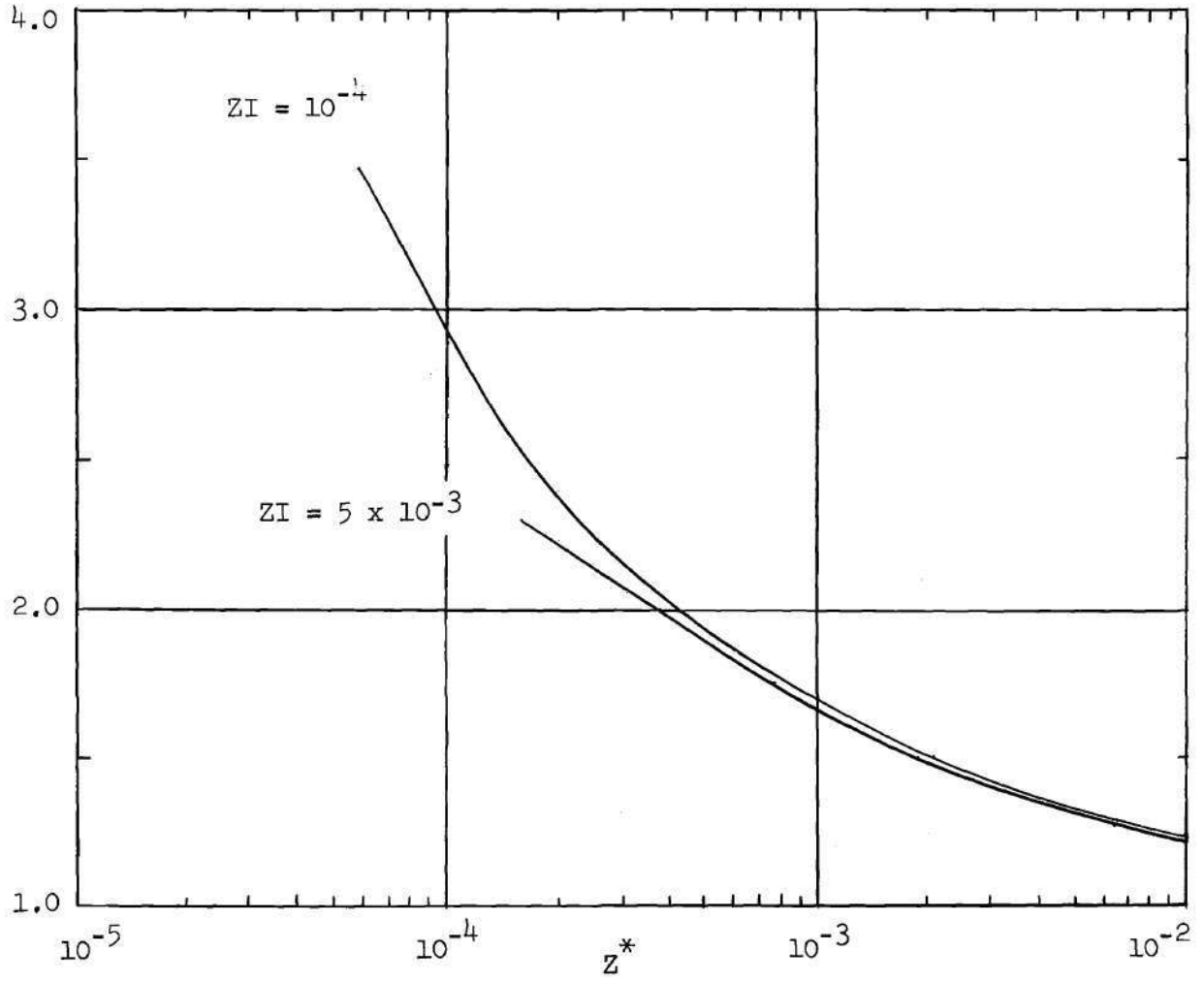

Fig. 50. Effect of Starting Position on Heat Transfer Results: Ethanol, $\Delta T' = 20^{\circ}$ F, $\bar{u}' = 200$ ft./sec., $D' = 0.019125$ ft.

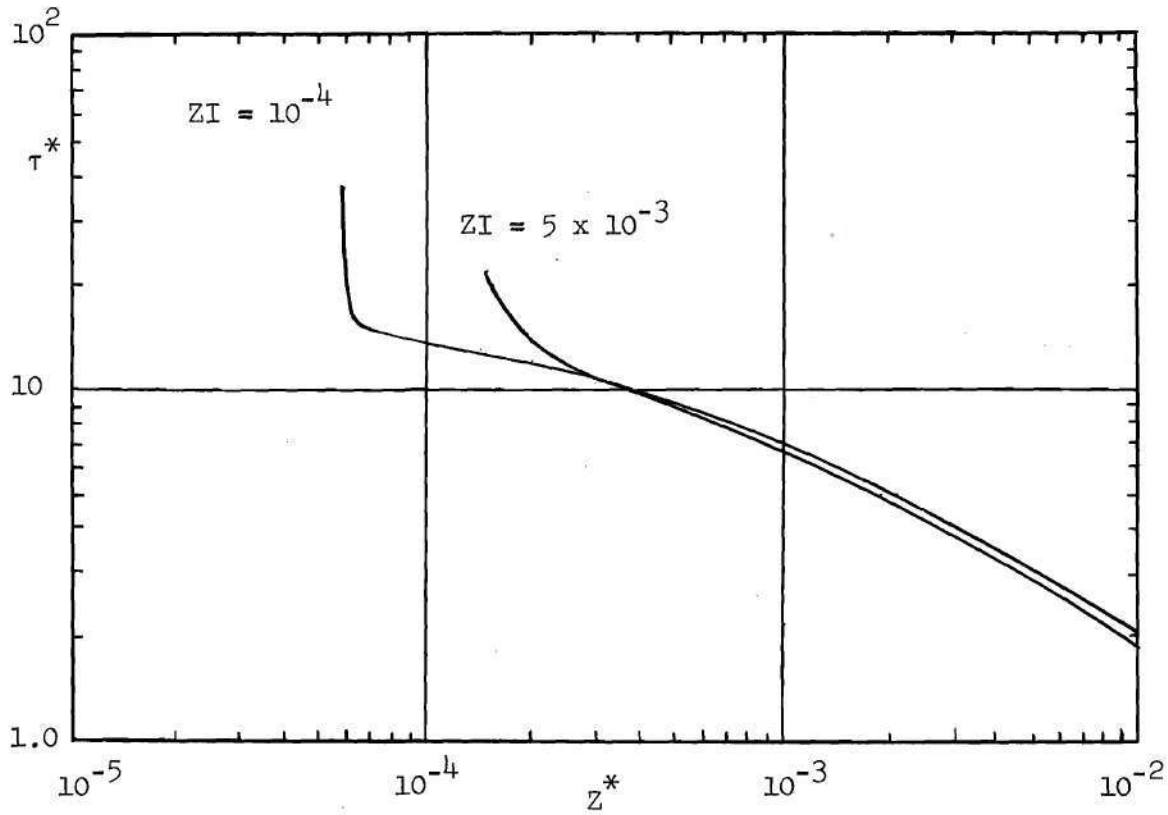

Fig. 51. Effect of Starting Position on Interfacial Shear: Ethanol, $\Delta T' = 20^{\circ}$ F, $\bar{u}' = 200$ ft./sec., $D' = 0.019125$ ft.

and the radial values are estimated by

$$(V_{1,i})_{\ell} = \frac{g'(\rho'_{\ell}-\rho'_{g})(\delta'_{i})^{2}}{4\mu'_{\ell}\,\bar{u}'} \cdot \left[\frac{4\,k'_{\ell}\,(T'_{o}-T'_{w})\,\mu'_{\ell}}{(z'_{1})^{3}g'\rho'_{\ell}(\rho'_{\ell}-\rho'_{g})\lambda'\left(1+\frac{3C'_{p}(T'_{o}-T'_{w})}{8\,\lambda'}\right)}\right]^{0.25} \qquad \text{(A-135)}$$

After the computer has solved the mathematical model for values of velocity, temperature, and concentration satisfying all boundary conditions at the first step into the tube the shear stress at the interface is evaluated from these results and used to make better estimations of the radial and axial velocities at these extra points. A simple model using constant shear stress at the interface gives

$$(U_{1,i})_{\ell} = \frac{g'(\rho'_{\ell}-\rho'_{g})(\delta'_{i})^{2}}{2\mu'_{\ell}\,\bar{u}'} - \frac{\mu'_{g}(v'_{z_q}-v'_{z_{q-1}})\,\delta'_{i}}{(r'_{q}-r'_{q-1})\mu'_{\ell}\,\bar{u}'} \qquad \text{(A-136)}$$

and

$$(V_{1,i})_{\ell} = \frac{k'_{\ell}\,(T'_{o}-T'_{w})}{\rho'_{\ell}\,\delta'_{i}\,\bar{u}'\,\lambda'\left(1+\frac{3C'_{p}(T'_{o}-T'_{w})}{8\,\lambda'}\right)} \qquad \text{(A-137)}$$

The first step into the tube is resolved using these more accurate estimations.

These equations are used for estimating the extra grid point velocities for all three cases of condensation considered.

Temperature Values

For pure vapor condensation the temperature values of the extra grid points are assumed to be T'_{o}, the entering vapor temperature.

In vapor and noncondensable gas condensation the temperature values of the extra grid points are assumed to be a linear function of distance into the tube, varying from T'_o at the entrance to $T'_{1,q}$ at the first step. For binary condensation the temperatures at the extra grid points are all assumed to be equal to $T'_{1,q}$, the equilibrium interface temperature at the first step.

Concentration Values

Concentration values of the extra grid points at the interface are not required. In the binary case the equation of diffusion in the liquid is never considered for the first step into the tube, although it is considered for all other axial steps. For the first step into the tube concentration in the liquid is assumed independent of radial position and equal to the ratio of the flux through the gas of the particular component to the total flux, as derived by Colburn and Drew (26). This and the boundary conditions at the interface determine the concentrations in the liquid phase for the first step, thus bypassing the need to know concentration values at the extra grid point.

Stability and Convergence

Systems of equations similar to those used in this work have been found to be apparently stable and convergent for a wide variety of problems in entrance flow. With these equations Bodoia (44) has investigated entrance flow between parallel plates, Hornbeck, Rouleau, and Osterle (40) investigated one phase flow in the entrance of pipes with injection or suction at the wall, Wilkins (37) investigated variable property heat transfer in the entrance of vertical tubes, and

Whatley (45) studied heat and mass transfer accompanying a reacting non-Newtonian fluid in the entrance region of a tube. All these investigators report excellent agreement with experimental data.

Wilkins (37) reviewed stability and convergence considerations for systems of equations. He found that it was quite difficult, if not impossible, to prove the stability and convergence of finite difference representations of systems of nonlinear partial differential equations with variable coefficients. However, he implied the stability of such a system by the arguments of Lax (46) and Richtmyer (47). Shohet (48) performed a similar analysis for flow in an annulus.

The equations used in this work appear to be stable and convergent over the range of study. The results agree with experimental data where available. Gas-vapor condensation results approach those of pure vapor condensation as gas concentration becomes low. Binary condensation results range between results for pure vapors. In addition, the pure vapor results approach those of the laminar, no interfacial shear model of Nusselt (2) when interfacial shear is low.

APPENDIX B

OUTLINES OF THE COMPUTER PROGRAMS

A brief outline of each of the three computer programs is given below. The program for the condensation of a pure vapor forms the major part of the program for the condensation of a vapor from a vapor and noncondensable gas mixture. The noncondensable program forms the bulk of the program for the condensation of a binary vapor mixture. Of course, there are minor differences in the similar portions of these programs resulting from slightly different equations and different boundary conditions, but all the programs follow the same general outline.

The complete program for each case is given in Appendix C.

Condensation of a Pure Vapor

The following steps form an outline of the computer program for the condensation of a pure vapor in the entrance of a vertical tube.

(1) Physical properties, most radial interval sizes, tube diameter, temperature difference, entering velocity, and starting position in the tube are read in from data cards.

(2) Various terms used throughout the program are calculated from the data of step (1).

(3) If this is the first attempt at the very first step down the tube, film thickness is estimated by the Nusselt model, equation

(A-132). All radial positions are set. Radial and axial velocities for steps at the gas-liquid interface between the entrance and the first step are calculated using equations (A-135) and(A-134).

(4) If this is the second attempt at the very first step down the tube, the shear at the gas-liquid interface is calculated from the previous attempt, and this value is used in equation (A-133) in estimating the film thickness. Radial positions are set for the rest of the program. Radial and axial velocities for steps at the gas-liquid interface between the entrance and the first step down the tube are calculated using equations (A-137) and (A-136).

(5) A trial value of axial step size is chosen.

(6) The components of the velocity and pressure matrix are calculated using the known values of velocity and pressure of the previous step and the boundary conditions. The equation of motion and equation of overall continuity are used in this matrix. The boundary conditions are those of zero shear and zero radial velocity at the center, and continuity of shear, normal mass flux, and axial velocity at the gas-liquid interface. Zero axial velocity is used at the wall. The fact that the radial velocity must be zero at the wall is used as a check of the solution of the matrix.

(7) The matrix in step (6) is solved by Gauss elimination and back substitution. Axial velocities in both phases and pressure are given for this step down the tube.

(8) Radial velocities are calculated from the overall continuity equation using the above values of axial velocity and the known values

of axial and radial velocities of the previous step.

(9) Components of the matrix describing the equation of energy in the liquid are calculated using the known temperatures of the previous step, known velocities of this step down the tube from steps (7) and (8), and the boundary conditions. The boundary conditions used are those of known temperature at the gas-liquid interface and known temperature at the wall.

(10) The energy matrix is solved by Gauss elimination and back substitution. The temperature profile in the liquid is found for this step down the tube.

(11) The mass rate of flow for the liquid film is calculated by numerical integration using the velocity profile obtained in step (7). The mass rate of flow in the liquid film at the previous step is subtracted from this. The remainder is the increase in mass during this step in the axial direction.

(12) The amount of heat transferred by conduction into the liquid film at the gas-liquid interface is evaluated from the temperature profile using Fourier's law of heat conduction. This heat, when divided by the latent heat of condensation, is equivalent to a mass flow from the vapor into the liquid film.

(13) The increase in the mass of the liquid film, calculated in step (11), is compared with the mass equivalent to the heat conducted in at the interface, as found in step (12). The difference between these two values is taken.

(14) It is desired to make the difference found in step (13)

negligible. This is accomplished by the following iterative procedure:

(A) A new trial value of axial step size is chosen.

(B) Steps (6) through (13) are then repeated.

(C) A new trial value of axial step size is estimated using the latest two values of the difference found in step (13) and Newton's method (42) to predict what axial step size will make the difference go to zero.

(D) Steps (B) and (C) are repeated until the difference is five hundredths of one percent of the mass flow found in step (12) or it is apparent that for various reasons the scheme is not converging to a value for axial step size.

If the former is the case the last values of axial and radial velocities, pressure and temperatures are assumed good. If this was the first attempt at the very first step down the tube return to step (4), take a better approximation, and run through steps (5) through (14) again, otherwise return to step (5) and go through steps (5) through (14) for the next step down the tube. Continue until the desired number of steps down the tube have been completed, then go to step (15).

If the scheme is not converging go to step (15).

(15) Print out a summary of all relevant data and results for this particular run. End of program.

Condensation of a Vapor from a Vapor and a Noncondensable Gas Mixture

The format for this program is basically that of the previous program. The following steps fit into the previous program in the marked places.

(6) The boundary conditions in step (6) are changed to zero shear and zero radial velocity at the center, and continuity of shear, normal mass flux of the condensable vapor, and the axial velocity at the gas-liquid interface. Zero axial velocity is used at the wall. The densities in the variable density gas continuity equation are calculated using the latest values of concentration.

(8a) (Follows step (8) and comes before step (9).) Components of the matrix describing the equation of diffusion of the noncondensable gas are calculated using the known values of concentration from the previous step, the latest values of velocity, and the boundary conditions of zero normal mass flux of this component at the gas-liquid interface and zero concentration gradient at the center.

(8b) The concentration matrix is solved by Gauss elimination and back substitution. A concentration profile in the gas is found for this step down the tube. If the computer gives negative values of concentration at the interface, go to step (2) and use a different starting position to start the program. This will often eliminate the problem.

(8c) If this is the first attempt at the very first step down the tube, go to step (3) and run through steps (3) to (8c) once using the latest values of concentration.

If this is the second attempt at the very first step down the

tube, return to step (4) and do the steps (4) to (8c) once using the latest values of concentration.

For all other steps down the tube return to step (5) and go through steps (5) to (8c) once using the latest values of concentration.

(8d) The temperature of the gas-liquid interface is determined from the concentration of the condensable component at the interface and the condition of equilibrium at the interface.

(8e) Components of the matrix describing the equation of energy in the gas are calculated using the known temperatures of the previous step down the tube, known velocities of this step down the tube from steps (7) and (8), and the boundary conditions. The boundary conditions used are those of zero temperature gradient at the center and known interface temperature.

(8f) The energy matrix is solved by Gauss elimination and back substitution. The temperature profile in the gas is found for this step down the tube. Now proceed to step (9).

All other steps are the same as in the previous program. In the D section of (14) if the heat crossing the interface matches the mass crossing the interface then the latest values of concentration as well as the latest values of velocity, etc., are assumed good.

Condensation of a Binary Vapor Mixture

The format for this program is basically that of the program for condensation of a vapor from a vapor and noncondensable gas mixture. The following steps fit into that program in the marked places.

(6) The boundary conditions in step (6) are changed to zero

shear and zero radial velocity at the center, and continuity of shear, normal mass flux of both vapors, and the axial velocity at the gas-liquid interface. Zero axial velocity is used at the wall.

(8a) The boundary conditions in step (8a) are changed to zero concentration gradient at the center and a trial value of vapor concentration at the gas-liquid interface.

(8b1) (Follows (8b) and comes before (8c).) The trial concentrations of the two components in the gas at the gas-liquid interface are used to find trial values of the liquid concentrations and the interface temperature using the condition of equilibrium at the interface.

(8b2) If this is the first step into the tube, then concentration in the liquid is assumed to be independent of radial position. What the liquid concentration should be according to Colburn and Drew (26) is calculated and the difference between this concentration and that found in step (8b1) is taken. This difference is made to go to zero by using Newton's method and by changing the trial value of vapor concentration. When the difference is less than five hundredths of a percent of one of the concentrations, then skip to step (8c).

If this is not the first step into the tube, then components of the matrix describing the equation of diffusion of one of the components in the liquid are calculated using the known values of concentration from the previous step, the latest values of velocity, and the boundary conditions of a trial concentration in the liquid at the gas-liquid interface and no radial mass flux of either component at the wall.

Continue to step (8b3).

(8b3) The matrix above is solved by Gauss elimination and back substitution (42). Values of liquid concentration for this step down the tube are given.

(8b4) The normal mass flux of one of the components across the gas-liquid interface is calculated two ways. First, it is calculated in the gas using values of vapor concentrations and velocities, then it is calculated in the liquid using values of liquid concentrations and velocities. These two results are compared and a difference taken.

(8b5) It is desired to make the above difference negligible. This is accomplished by the following steps:

(A) A new trial value of vapor concentration at the interface is chosen.

(B) Steps (8a) through (8b4) are repeated.

(C) A new trial value of axial step size is estimated using the latest two values of the difference found in step (8b4) and Newton's method (42) to predict what value of interface vapor concentration will make the difference go to zero.

(D) Steps (B) and (C) are repeated until the difference is five hundredths of one percent of the mass flow into the liquid as found in step (8b4). When this occurs go to step (8c).

The other steps in the binary vapor program are the same as the noncondensable gas program with one minor exception: delete step (8d)

as the value of interface temperature has been determined already in step (8b1).

APPENDIX C

COMPUTER PROGRAMS

The calculations were made on a Burroughs B-5500 Information Processing System operated by the Rich Electronic Computer Center at the Georgia Institute of Technology. The programming language was Extended Algol 60 described by Naur (49), McCracken (50), and the Burroughs Corporation (51).

Complete computer programs for the three cases of condensation considered and a general computer program nomenclature of the more important terms are included below. The positions covered in the outlines in Appendix B are marked in each program.

Computer Program Nomenclature

AA = Factor used in setting radial positions

AZ = Van Laar Constant

C[ ] = $W_{b_{j+1,i}}$ or $W_{c_{j+1,i}}$

CAQG = Van Laar prediction of $(W_{a_{j+1,q}})_g$

CLQ = $(W_{c_{j+1,q}})_\ell$

CO[ ] = $W_{b_{j,i}}$ or $W_{c_{j,i}}$

CQG = $(W_{b_{j+1,q}})_g$ or $(W_{c_{j+1,q}})_g$

CQGA[ ] = Trial interface gas concentration

D = D'

DABG = D'_{ab_g} or D'_{ac_g}

DABL = D'_{ab_ℓ} or D'_{ac_ℓ}

DELTA[ ] = $2\delta'/D'$

DT = $T'_o - T'_w$

DT_5 = $T'_{dp} - T'_w$

DT_6 = $T'_{bp} - T'_w$

DZ[ ] = $Z_{j+1} - Z_j$

E[ ] = A_i

EKG = $(\bar{u}')^2/c'_{p_g}$ $(T'_o-T'_w)$

EKL = $(\bar{u}')^2/c'_{p_\ell}$ $(T'_o-T'_w)$

EKREL = $2/Ek_\ell Re_\ell$

ENTC = Entering concentration of a or b, weight fraction

F[ ] = F_i

FR = Fr

FRE[ ] = $4\Gamma'/\mu'_\ell$

G[,] = G_i, H_i, I_i, J_i

GRAV = g'

H[ ] = B_i

HE = he

HFLUX = Heat transferred across interface

HFG = λ'

HLOC = HLOCA = h'_{loc}, Equation (A-127)

HLOC1 = HLOC1A = h_{loc}, Equation (I-9)

HLOC5 = h'_{loc} based on DT5

HLOC6 = h'_{loc} based on DT6

HM = HMA = h'_m, Equation (A-129)

HM1 = HM1A = h'_m, Equation (I-10)

HM5 = h'_m based on DT5

HM6 = h'_m based on DT6

HPHI[ ] = h'_m/Φ'

HW = hw

JT-1 = Number of extra grid points at first step

K[ ],L[ ] = Factors used in setting radial positions

LIM = Number of times first step repeated

MASSTR = Mass Transferred across interface

MEQLH = Mass equivalent to heat transferred across interface

MUG = μ'_g

MUL = μ'_ℓ

MWA = Molecular weight of compound a

MWB = Molecular weight of compound b

N = n

NBG = Mass flux of b from the gas phase

NBL = Mass flux of b into the liquid phase

NTG = Total mass flux across the interface

OT[ ] = $T_{j,i}$

P[ ] = P_i

PHI = Φ'

PRG = $\mu'_g C'_{p_g} / k'_g$

PRL = $\mu'_\ell C'_{p_\ell} / k'_\ell$

PRREL = $Pr_\ell Re_\ell$

Q = q

R[ ] = R_i

RADIUS = r'

REG = $\rho'_g \bar{u}' D' / \mu'_g$ for pure vapor condensation

$\rho'_{j+1,i} \bar{u}' D' / \mu'_g$ for other cases

REL = $\rho'_\ell \bar{u}' D' / \mu'_\ell$

REPRG = $Pr_g Re_g$

REPRL = $Pr_\ell Re_\ell$

ROG = ρ'_g

ROL = ρ'_ℓ

RON[ ] = $\rho'_{j+1,i}$

ROO[ ] = $\rho'_{j,i}$

SCREG = $Sc_g Re_g$

SCREL = $Sc_\ell Re_\ell$

SPHTG = C'_{p_g}

SPHTL = C'_{p_ℓ}

T[ ] = $T_{j+1,i}$

T1 = Boiling temperature of compound a

T2 = Boiling temperature of compound b or c

TAUV[ ] = τ^*

TC = k'_ℓ

TCG = k'_g

TS = T'_o

TW = T'_w

U[ ] = $U_{j+1,i}$

UBAR = $\bar{u}'$

UO[ ] = $U_{j,i}$

V[ ] = $V_{j+1,i}$

VO[ ] = $V_{j,i}$

VP1 = Vapor pressure of compound a

VP2 = Vapor pressure of compound b or c

VRG = $(V_{j+1,q})_g$

W[ ] = E_i

X[ ] = C_i

XO = δ'

Z[ ] = Z_i

ZI = Trial starting position

```
BEGIN REAL RADIUS,D,REG,REL,ROG,ROL,MUG,MUL,UBAR,TS,TW,TC,DT,ZL,GRAV,HFG                100
,SPHTL,TERM,XO,AA,PRL,EKL,PRG,EKG,REN,HE,HW,SUM,OLDSUM,MASSTR,HFLUX,OLDH                200
FLUX,AVEHFLUX,MEQLH,ZSTAR,SLOPE,TAG,HLOC,AVEHLOC,OLDHLOC,HTRW,HSUM,OLDHS               300
UM,HM,VZG,VRG,ZI,OHQ,HZ,HX,HY,HV,HU,HT,RET,RES,WG,SUMT,TOTT,EKREL,PRREL,               400
HS,DTA,DTB,DTDZ1,DTDZ2,LMT,NU1,NU2,NU3,NU,TCG,SPHTG,PHI,FR,FRT,PT,PTFRT,               500
MMM,MM2,OMEQLH,OMASSTR,OZ,SLOPEB,SLOPEA,MM,TERM2,TERM3,TAU,OLDXO,PCDIF,X               600
2,X3,HLOC1,HLOC2,HM1,HM2,HM3,IM,TOTAL,TOTAL1,MTR;INTEGER B,I,A,N,Q,Y,S,S               700
S,SSS,J,RT,BB,LIM,JJ,BBB,BTT,BT,JT;REAL ARRAY Z,P[0:80],M,L,K[1:10],OT,V               800
W,CO,C,V,T,U,R,UO,ZD,VO[0:200],XDZ,OLDDZ,DIF,DZ[1:20],G[0:200,0:20],ZS,H               900
MA,HM1A,HM2A,HM3A,HLOCA,HLOC1A,HLOC2A,RWLZ,FRE,NUA,NU1A,HNFPH,HMH,HMNUC,              1000
HLOCNUC,TOT,HNPHI,HRPHI,DELTA,NU2A,NU3A,HPHI,TAUV[0:80],W,F,X,E,H[-1:220              1100
];FILE OUT FL 6(2,15);FILE IN DA(2,10);LABEL FLUSH,GOD;LIST LSST(ZS[B],Z               1200
[B]×RADIUS,FRE[B],HPHI[B]/HNFPH[B],HNFPH[B],HPHI[B],UBAR×UBAR/(GRAV×Z[B]              1300
×RADIUS));FORMAT OUT FRM("RATIOS BELOW ARE BASED ON FILM RE NOT DISTANCE               1400
",//,X5,"ZSTAR",X10,"Z IN FT",X7,"FILM RE",X8,"HM/HMNF",X8,"HMNF/PHI",X7               1500
,"HM/PHI",X6,"LENGTH FR NU.",//);LIST LIS(ROG,ROL,MUG,MUL,HFG,SPHTL,TC,T              1600
```

```
S,TW,RADIUS,UBAR,L[1],K[1],L[2],K[2],L[3],K[3],L[4],K[4],AA,JT,BT,LIM,ZI                1700
);FORMAT OUT FMT9("UO[",I3,"] = ",F10 .7,X10,"VO[",I3,"] = ",F12 .10,X10               1800
,"ZD = ",E16 .7,/);LIST LST9(B,UO[B],B,VO[B],ZD[B]/RADIUS);FORMAT OUT FM               1900
F("UBAR = ",E16 .7," FT/SEC",/,"VISCOSITY GAS = ",X3,E16 .7," LBM/FT×SEC               2000
 ",/,"VISCOSITY LIQUID = ",E16 .7," LBM/FT×SEC ",//,"DENSITY GAS = ",F16               2100
 .7," LBM/FT×FT×FT",/,"DENSITY LIQUID = ",F16 .7," LBM/FT×FT×FT",//,"THE               2200
RMAL CONDUCTIVITY GAS = ",X3,E16 .7,"BTU/SEC×FT×F",/,"THERMAL CONDUCTIVI               2300
TY LIQUID = ",E16 .7,"BTU/SEC×FT×F",//,"HEAT CAPACITY GAS = ",X3,F16 .7,               2400
" BTU/LBM×F",/,"HEAT CAPACITY LIQUID = ",F16 .7," BTU/LBM×F",//,"HFG, EN               2500
THALPY, CHANGE OF PHASE = ",F16 .7," BTU/LBM",//,"TEMPERATURE DIFFERENCE               2600
 = ",F16 .7," DEG F ",//,"DIAMETER OF VERTICAL PIPE = ",F16 .9," FT  OR"               2700
,F16 .9," INCHES",/);LIST LSTF(UBAR,MUG,MUL,ROG,ROL,TCG,TC,SPHTG,SPHTL,H               2800
FG,DT,D,D×12);FORMAT OUT FMG(X7,"Z",X11,"ZSTAR",X8,"DELTA R/R",X8,"HN/PH               2900
I",X9,"HR/PHI",X11,"NU",X12,"NUN",//);FORMAT OUT FMH(7(E14 .5,X1),/);LIS               3000
T LSTH(Z[B],ZS[B],DELTA[B],HNPHI[B],HRPHI[B],NUA[B],NU1A[B]);FORMAT OUT               3100
FMTI("ROG/ROL = ",E14 .5,X10,"MUG/MUL = ",E14 .5,X10,"TCG/TCL = ",E14 .5               3200
,/,"CPG/CPL = ",E14 .5,X10,"REG/REL = ",E14 .5,X10,"REG/FR  = ",E14 .5,/               3300
/,"CPL×DT/HFG = ",E14 .5,//);LIST LSTI(ROG/ROL,MUG/MUL,TCG/TC,SPHTG/SPHT               3400
L,REG/REL,REG/FR,SPHTL×DT/HFG);FORMAT OUT FMB(X7,"Z",X16,"ZSTAR",X14,"FI               3500
```

```
LM RE",X15,"H/PHI",X15,"TAUST",X12,"R,W,L, ZST",//);FORMAT OUT FMC(6(E14      3600
 .5,X6),/);LIST LSTC(Z[B],ZS[B],FRE[B],HPHI[B],TAUV[B],RWLZ[B]);FORMAT O      3700
UT FM4(X6,"ZSTAR",X8,"ZSTAR/REG",X7,"HM/HMN",X9,"HM/HMR",X8,"HM/HMNUC",X      3800
6,"HLOC/HLOCN",X4,"HLOC/HLOCNUC",X5,"FILM RE",//);LIST LSTX(ZS[B],ZS[B]/      3900
REG,HMA[B]/HM1A[B],HMA[B]/HM2A[B],HMA[B]/HMNUC[B],HLOCA[B]/HLOC1A[B],HLO      4000
CA[B]/HLOCNUC[B],FRE[B]);FORMAT OUT FMY(X4,"Z IN FT",X9,"ZSTAR",X7,"SCRI      4100
PT P",X8,"P - GRAV",X6,"P,LBF/IN*IN",X4,"TAUST/REG",X4,"LB/SEC IN TUBE",      4200
//);LIST LSTW(Z[B]*RADIUS,ZS[B],P[B],P[B]-Z[B]*FRT,P[B]*UBAR*UBAR*ROG/(1      4300
44*GRAV)+14.696,TAUV[B]/REG,TOT[B]);LIST LST(REG,REL,PRL,EKL,FR);FORMAT      4400
OUT FMT("REG = ",F10 .3,X5,"REL = ",F12 .3,X5,"PRL = ",F10 .5,X5,"EKL =      4500
",E14 .5,X5,"FR = ",E14 .5,//);FORMAT OUT FMDA("HEAT TRANSFER COEF. BELO      4600
W ARE IN  BTU/HR*FT*FT*F.",////);FORMAT OUT FMD(X7,"Z",X11,"ZSTAR",X11,"      4700
HM",X13,"HLOC",X11,"HMN",X11,"HLOCN",X11,"HMR",X11,"HMH",//);FORMAT OUT      4800
FME(8(E14 .5,X1),/);LIST LSTE(Z[B],ZS[B],HMA[B],HLOCA[B],HM1A[B],HLOC1A[      4900
B],HM2A[B],HMH[B]);FORMAT OUT FMT1("MASS TRANSFERRED = ",E16 .7,X2,"LBS/      5000
SEC.",X5,"MASS EQUIVALENT TO HEAT = ",E16 .7,X2,"LBS/SEC.",/,"DIF[",I2,"      5100
] = ",E16 .7,X5,"TOTAL MASS TRANSFERRED = ",E16 .7,/,"P[",I2,"] = ",E16      5200
.7,X10,"Z[",I2,"] = ",E16 .7,X5,"ZSTAR = ",E16 .7,////);LIST LST1(MASSTR      5300
,MEQLH,Y,DIF[Y],SUM,I,P[I],I,Z[I],ZSTAR);FORMAT OUT FMT2(X1,"B",X11,"R",      5400
```

```
X19,"U",X19,"V",X19,"VW",X19,"T",X19,"C",//);FORMAT OUT FMT3(I3,X7,F10 .      5500
8,5(X4,F16 .10),/);LIST LST3(FOR J←0STEP 3UNTIL Q=3,Q=2STEP 1UNTIL N+1DO      5600
[J,R[J],U[J],V[J],VW[J],T[J],C[J]]);FORMAT OUT FMT4("HLOC = ",E16 .7X5,"      5700
HM = ",E16 .7,X10,"INTERFACE POSITION = ",F10 .8,X5,"Q = ",I3,/);LIST LS      5800
T4(HLOC,HM,R[Q],Q);FORMAT OUT FMT5("PROCESS TIME = ",F10 .4,//);FORMAT O      5900
UT FMT6("IN/OUT TIME = ",F10 .4,//);FORMAT OUT FMA("HM FOR VERTICAL TUBE      6000
S, BSL 13.6=4 = ",E16 .7,/);X2←TIME(2);X3←TIME(3);
                                        (1)
                                                TAG←7.0;READ(DA,/,LIS)      6100
;CLOSE(DA,RELEASE);
                                        (2)
                                                BBB←0;GOD:BB      6200
B←BBB+1;D←2×RADIUS;REG←ROG×D×UBAR/MUG;REL←ROL×D×UBAR/MUL;IM←(3.14159265)      6300
×(RADIUS*2)×ROG×UBAR;R[0]←0.0;Z[1]←ZI×REG×2;P[0]←Z[0]←0.0;FOR B←0STEP 1U      6400
NTIL 200DO BEGIN UO[B]←1.0;VO[B]←0.0;DT[B]←1.0;T[B]←1.0;END;DT←TS-TW;ZL←      6500
Z[1]×D/2;GRAV←32.174;TERM←4×TC×DT×MUL/(GRAV×ROL×(ROL-ROG)×HFG×(1+3×SPHTL      6600
×DT/(HFG×8)));FR←UBAR×UBAR/(GRAV×D);FRT←1/(2×FR);PRL←MUL×SPHTL/TC;EKL←UB      6700
AR×UBAR/(SPHTL×(TS-TW));SUMT←ROL×(3.14159265)×(RADIUS*2)×UBAR/2;TOTT←ROG      6800
×(3.14159265)×(RADIUS*2)×UBAR/2;EKREL←2/(EKL×REL);PRREL←PRL×REL;PHI←TC×(      6900
```

```
(ROL×ROL×GRAV/(MUL×MUL))*0.33333);JJ←0;RT←0;I←0;FOR BB←1STEP 1UNTIL BT D      7000
O BEGIN REAL QQQQQ;LABEL HELL,SLEEP;I←I+1;IF RT<LIM THEN I←1;
```

(3) AND (4)

```
                                                        IF RT=0THEN          7100
      X0←SQRT(SQRT(TERM×ZL));                    IF RT<LIM AND RT>0THEN BEGIN 7200
 TERM2←4×TAU/(3×(ROL-ROG)×GRAV);FOR A←1STEP 1UNTIL 200O BEGIN OLDX0←X0;I     7300
F TERM×ZL+TERM2×(X0*3)≤0THEN X0←X0/2.0ELSE X0←SQRT(SQRT(TERM×ZL+TERM2×(X     7400
0*3)));PCDIF←(X0-OLDX0)×100/X0;END;END;J←JT;IF I=1THEN BEGIN IF 1-4×AA×X     7500
0/(RADIUS×J)≤2×K[1]THEN GO TO FLUSH;IF L[4]≥1-4×AA×X0/(RADIUS×J)THEN BEG     7600
IN FOR B←1STEP 1UNTIL 396DO IF L[4]≥1-4×AA×X0/(RADIUS×J)THEN L[4]←L[4]-K     7700
[4]ELSE B←397;END;IF L[3]≥L[4]THEN BEGIN FOR B←1STEP 1UNTIL 80DO IF L[3]     7800
≥L[4]THEN L[3]←L[3]-K[3]ELSE B←81;K[4]←L[4]-L[3];END;IF L[2]≥L[3]THEN BE     7900
GIN FOR B←1STEP 1UNTIL 80DO IF L[2]≥L[3]THEN L[2]←L[2]-K[2]ELSE B←81;K[3     8000
]←L[3]-L[2];END;IF L[1]≥L[2]THEN BEGIN FOR B←1STEP 1UNTIL 80DO IF L[1]≥L     8100
[2]THEN L[1]←L[1]-K[1]ELSE B←81;K[2]←L[2]-L[1];END;L[5]←1-4×AA×X0/(RADIU     8200
S×J);K[5]←L[5]-L[4];L[6]←1-AA×X0/(RADIUS×J);K[6]←2×X0/(RADIUS×J);L[7]←1.     8300
001;K[7]←X0/(RADIUS×J);A←1;FOR B←1STEP 1UNTIL 200DO BEGIN IF R[B-1]>(0.9     8400
999)×L[A]THEN BEGIN R[B]←R[B-1]+K[A+1];M[A]←B-1;A←A+1;END ELSE R[B]←R[B-     8500
1]+K[A];IF R[B]>0.999999THEN BEGIN N←B-1;U[B]←U0[B]←0.0;GO TO SLEEP;END;     8600
```

```
END;SLEEP;END;IF I=J THEN DHQ←(DT[Q+1]-DT[Q])/(R[Q+1]-R[Q]);IF I=J THEN      8700
BEGIN A←(1+N-M[6])/2;FOR B←0STEP 1UNTIL A DO BEGIN R[M[6]+B]←R[M[6]+2×B]      8800
;UO[M[6]+B]←UO[M[6]+2×B];VO[M[6]+B]←VO[M[6]+2×B];DT[M[6]+B]←DT[M[6]+2×B]      8900
;END;U[M[6]+A]←0.0;N←M[6]+(N-M[6]-1)/2;JJ←J/2+(I-2)/2;END;Q←N-I-J+2+JJ;I      9000
F I≠J THEN DHQ←(DT[Q+2]-DT[Q+1])/(R[Q+2]-R[Q+1]);IF RT=0THEN BEGIN FOR B      9100
←Q+1STEP 1UNTIL N DO BEGIN UO[B]←GRAV×(ROL-ROG)×(((1-R[B])×RADIUS)*2)/(2      9200
×MUL×UBAR);ZD[B]←(((1-R[B])×RADIUS)*4)/TERM;VO[B]←(GRAV×(ROL-ROG)×(((1-R      9300
[B])×RADIUS)*2)/(4×MUL))×(SQRT(SQRT(TERM/(ZD[B]*3))))/UBAR;WRITE(FL,FMT9      9400
,LST9);END;END;IF RT<LIM AND RT>0THEN BEGIN TERM3←ROL×TAU×HFG×(1+3×SPHTL      9500
×DT/(HFG×8))/(3×MUL×TC×DT);FOR B←Q+1STEP 1UNTIL N DO BEGIN UO[B]←GRAV×(R      9600
OL-ROG)×(((1-R[B])×RADIUS)*2)/(2×MUL×UBAR)-TAU×(1-R[B])×RADIUS/(MUL×UBAR      9700
);ZD[B]←(((1-R[B])×RADIUS)*4)/TERM-(((1-R[B])×RADIUS)*3)×TERM3;VO[B]←TC×      9800
DT/(ROL×(1-R[B])×RADIUS×HFG×(1+3×SPHTL×DT/(HFG×8))×UBAR);WRITE(FL,FMT9,L      9900
ST9);END;END;
```

(5)

```
        Y←0;IF I=1THEN Z[0]←ZI×REG×2;IF RT>0AND RT<LIM THEN Z[0]←(1      10000
.2)×ZD[Q+1]/RADIUS;MM←2.5;IF I=2THEN MM←0.04;IF I=3THEN MM←0.05;IF I=4TH      10100
EN MM←0.10;IF I=1OR I=2THEN MMM←(1+MM/J)ELSE MMM←Z[I-1]/Z[I-2];FOR Z[I]←      10200
MMM×Z[I-1],MM2×Z[I-1]DO BEGIN
```

```
                                HELL;Y←Y+1;IF I=1THEN Z[0]←0.0;DZ[Y]←Z[I]-    10300
Z[I-1];ZSTAR←Z[I]/(2×REG);HE←R[1]-R[0];H[0]←8/(REG×HE×HE)+UO[0]/DZ[Y];X[    10400
1]←-8/(REG×HE×HE);WG←1/DZ[Y];FOR B←0STEP 1UNTIL Q DO BEGIN W[B]←WG;F[B]←    10500
(UO[B]*2+P[I-1])/DZ[Y]+FRT;END;WG←(ROG/ROL)/DZ[Y];PT←ROG×P[I-1]/(ROL×DZ[    10600
Y]);PTFRT←PT+FRT;FOR B←Q+1STEP 1UNTIL N DO BEGIN IF I=1THEN XDZ[Y]←Z[I]-    10700
ZD[B]/RADIUS;IF I>1THEN XDZ[Y]←DZ[Y];W[B]←WG;F[B]←(UO[B]*2)/XDZ[Y]+PTFRT    10800
;END;W[Q]←F[Q]←0.0;FOR B←0STEP 1UNTIL N DO FOR J←0STEP 1UNTIL 12DO G[B,J    10900
]←0.0;FOR J←N+1STEP 1UNTIL N+13DO BEGIN W[J]←F[J]←X[J]←0.0;END;E[N]←0.0;    11000
G[0,0]←R[1]/(4×DZ[Y]);G[1,0]←3×R[1]/(4×DZ[Y]);OLDDZ[Y]←DZ[Y];S←SS←0;REN←    11100
REG;HE←R[1]-R[0];HZ←2/(REG×HE×HE);HX←1/(REG×HE×R[B]);HY←1/(2×HE);A←1;FOR    11200
 B←1STEP 1UNTIL N-1DO BEGIN REAL QQQ;LABEL GIRL,SCHOOL;IF B=Q THEN REN←R    11300
EL;IF I=1AND B≥Q THEN DZ[Y]←Z[I]-ZD[B]/RADIUS;IF B=Q OR B=M[A]THEN BEGIN    11400
 HE←R[B+1]-R[B];HW←R[B]-R[B-1];A←A+1;HV←HW×(HW+HE);HU←HE×(HW+HE);HT←(HW-    11500
HE)/(HW×HE);RET←4/REN;RES←2/(REN×R[B]);E[B-1]←(-VO[B]×HE-RET+HE×RES)/HV;    11600
H[B]←UO[B]/DZ[Y]-VO[B]×HT+RET/(HW×HE)+RES×HT;X[B+1]←(VO[B]×HW-RET-RES×HW    11700
)/HU;HZ←2/(REN×HE×HE);HY←1/(2×HE);HX←1/(REN×HE);END ELSE BEGIN HS←VO[B]×    11800
HY-HX/R[B];E[B-1]←-HS-HZ;H[B]←UO[B]/DZ[Y]+2×HZ;X[B+1]←HS-HZ;END;IF Q≤M[6    11900
]THEN M[6]←0;IF B>1THEN BEGIN FOR J←1STEP 1UNTIL TAG DO IF B=M[J]THEN BE    12000
```

```
GIN S←S+1;GO TO GIRL;END;IF B=Q THEN BEGIN SS←1;GO TO GIRL;END;IF B=Q+1T    12100
HEN BEGIN SS←2;GO TO GIRL;END;G[B,SS+S]←R[B]/DZ[Y];F[N+S+1+SS]←F[N+S+1+S    12200
S]+R[B]×UO[B]/DZ[Y];GO TO SCHOOL;GIRL:G[B,S-1+SS]←R[B]/(2×DZ[Y]);G[B,S+S    12300
S]←G[B,S-1+SS];F[N+S+SS]←R[B]×UO[B]/(2×DZ[Y])+F[N+S+SS];F[N+S+1+SS]←R[B]    12400
×UO[B]/(2×DZ[Y]);IF S=1THEN F[N+S]←F[N+S]+UO[1]×3×R[1]/(4×DZ[Y])+UO[0]×R    12500
[1]/(4×DZ[Y]);H[N+S+SS]←R[B]/(R[B]-R[B-1]);E[N+S+SS]←-R[B]/(R[B+1]-R[B])    12600
;IF SS=1THEN BEGIN IF I=1THEN DZ[Y]←Z[I]-ZD[Q+1]/RADIUS;F[N+S+SS+1]←0.0;    12700
E[N+S+SS]←-(R[Q]/HE)×ROG/ROL;G[B,S+SS]←-(R[Q]/HE)×(ROG/ROL-1)×(HE/DZ[Y])    12800
;END;IF SS=2THEN BEGIN F[N+S+SS]←R[Q+1]×UO[Q+1]/DZ[Y];G[B,S+SS-1]←R[Q+1]    12900
/DZ[Y];H[N+S+SS]←R[Q+1]/HE;END;SCHOOL:END;END;IF I=1THEN DZ[Y]←Z[I]-ZD[N    13000
]/RADIUS;E[N-1]←-VO[N]×HE/(HW×(HW+HE))-4/(REN×HW×(HE+HW))+2×HE/(REN×R[N]    13100
×HW×(HW+HE));H[N]←UO[N]/DZ[Y]-VO[N]×(HW-HE)/(HW×HE)+4/(REN×HW×HE)+2×(HW-    13200
HE)/(REN×R[N]×HW×HE);E[Q-1]←-MUG/(R[Q]-R[Q-1]);H[Q]←MUG/(R[Q]-R[Q-1])+MU    13300
L/(R[Q+1]-R[Q]);X[Q+1]←-MUL/(R[Q+1]-R[Q]);G[N,S+SS]←R[N]/DZ[Y];F[N+S+1+S    13400
S]←F[N+S+1+SS]+R[N]×UO[B]/DZ[Y];
```

(7)

```
                                DZ[Y]←OLDDZ[Y];S←0;SSS←0;FOR B←0STEP 1UN    13500
TIL N-1DO BEGIN F[B]←F[B]/H[B];W[B]←W[B]/H[B];X[B+1]←X[B+1]/H[B];F[B+1]←    13600
F[B+1]-F[B]×E[B];W[B+1]←W[B+1]-W[B]×E[B];H[B+1]←H[B+1]-X[B+1]×E[B];IF AB    13700
```

```
S(G[B,S+1])>0THEN BEGIN S←S+1;SSS←SSS+1;END;FOR J←0STEP 1UNTIL SSS DO BE    13800
GIN F[N+1+J]←F[N+1+J]-F[B]×G[B,J];W[N+1+J]←W[N+1+J]-W[B]×G[B,J];G[B+1,J]    13900
←G[B+1,J]-X[B+1]×G[B,J];END;END;F[N]←F[N]/H[N];W[N]←W[N]/H[N];FOR S←0STE    14000
P 1UNTIL SSS DO BEGIN F[N+1+S]←F[N+1+S]-F[N]×G[N,S];W[N+1+S]←W[N+1+S]-W[    14100
N]×G[N,S];END;FOR B←N+1STEP 1UNTIL SSS+N DO BEGIN F[B]←F[B]/H[B];W[B]←W[    14200
B]/H[B];F[B+1]←F[B+1]-F[B]×E[B];W[B+1]←W[B+1]-W[B]×E[B];END;P[I]←F[N+1+S    14300
SS]/W[N+1+SSS];U[N]←F[N]-W[N]×P[I];FOR B←N-1STEP-1UNTIL ODD U[B]←F[B]-W[    14400
B]×P[I]-X[B+1]×U[B+1];VZG←U[Q];
```

(8)

```
                                DZ[Y]←Z[I]-Z[I-1];HE←R[1]-R[0];V[1]←-HE×(    14500
U[1]+U[0]-UO[1]-UO[0])/(4×DZ[Y]);FOR B←2STEP 1UNTIL N+1DO BEGIN REAL XXX    14600
;IF B≤Q THEN V[B]←(V[B-1]×R[B-1]/(R[B]-R[B-1])-(R[B-1]×(U[B-1]-UO[B-1])+    14700
R[B]×(U[B]-UO[B]))/(2×DZ[Y]))×(R[B]-R[B-1])/R[B];IF B=Q+1THEN BEGIN XDZ[    14800
Y]←DZ[Y];IF I=1THEN DZ[Y]←Z[I]-ZD[B]/RADIUS;VRG←V[Q];V[Q]←U[Q]×(ROG/ROL-    14900
1)×(R[Q+1]-R[Q])/DZ[Y]+V[Q]×ROG/ROL;V[Q+1]←(R[Q+1]×UO[Q+1]/DZ[Y]-U[Q+1]×    15000
R[Q+1]/DZ[Y]+V[Q]×R[Q]/(R[Q+1]-R[Q]))×(R[Q+1]-R[Q])/R[Q+1];END;IF B>Q+1T    15100
HEN BEGIN XDZ[Y]←DZ[Y];IF I=1THEN DZ[Y]←Z[I]-ZD[B]/RADIUS;V[B]←(V[B-1]×R    15200
[B-1]/(R[B]-R[B-1])-R[B-1]×(U[B-1]-UO[B-1])/(2×XDZ[Y])-R[B]×(U[B]-UO[B])    15300
/(2×DZ[Y]))×(R[B]-R[B-1])/R[B];END;END;
```

(9)

```
                                        DZ[Y]←OLDDZ[Y];HE←R[Q+2]-R[Q+1];H    15400
W←R[Q+1]-R[Q];DT[N+1]←0.0;T[N+1]←0.0;IF I=1THEN DZ[Y]←Z[I]-ZD[Q+1]/RADIU    15500
S;H[Q+1]←-V[Q+1]×(HW-HE)/(HW×HE)+U[Q+1]/DZ[Y]+2×(HW-HE)/(PRL×REL×HW×HE×R    15600
[Q+1])+4/(REL×PRL×HE×HW);X[Q+2]←V[Q+1]×HW/(HE×(HW+HE))-2×HW/(REL×PRL×R[Q    15700
+1]×HE×(HW+HE))-4/(REL×PRL×HE×(HW+HE));F[Q+1]←U[Q+1]×DT[Q+1]/DZ[Y]+(2/(R    15800
EL×EKL))×((HW×U[Q+2]/(HE×(HW+HE))-(HW-HE)×U[Q+1]/(HW×HE)-HE×U[Q]/(HW×(HW    15900
+HE)))*2)-(-V[Q+1]×HE/(HW×(HW+HE))+2×HE/(REL×PRL×R[Q+1]×HW×(HW+HE))-4/(R    16000
EL×PRL×HW×(HW+HE)));FOR B←Q+2STEP 1UNTIL N DO BEGIN IF I=1THEN DZ[Y]←Z[I    16100
]-ZD[B]/RADIUS;H[B]←U[B]/DZ[Y]+4/(PRREL×HW×HE);X[B+1]←V[B]×HY-1/(PRREL×R    16200
[B]×HE)-4/(PRREL×HU);E[B-1]←-V[B]×HY+1/(PRREL×R[B]×HE)-4/(PRREL×HV);F[B]    16300
←U[B]×DT[B]/DZ[Y]+EKREL×((U[B+1]×HY-U[B-1]×HY)*2);END;
```

(10)

```
                                                FOR B←Q+1STEP 1UNT    16400
IL N-1DO BEGIN F[B]←F[B]/H[B];X[B+1]←X[B+1]/H[B];F[B+1]←F[B+1]-F[B]×E[B]    16500
;H[B+1]←H[B+1]-X[B+1]×E[B];END;T[N]←F[N]/H[N];FOR B←N-1STEP-1UNTIL Q+1DO    16600
 T[B]←F[B]-X[B+1]×T[B+1];DZ[Y]←OLDDZ[Y];
```

(11)

```
                                   IF I=1THEN OLDSUM←0.0;SUM←0.0;FO    16700
```

```
R B←N STEP-1UNTIL Q DO SUM←SUM+SUMT×(R[B+1]*2-R[B]*2)×(U[B+1]+U[B]);MASS   16800
TR←SUM-OLDSUM;
```

(12)

```
            IF I=1THEN BEGIN HFLUX←(-TC)×DT×(3.14159265)×((R[N+1]*2-R[   16900
N]*2)×(RADIUS*2)×(T[N]-OT[N])/(((Z[I]-ZD[N]/RADIUS+DZ[Y])×RADIUS/2)+(ZD[N   17000
]/RADIUS)×(RADIUS*2)×(R[N]+R[N+1])×(-1)/((2-R[N+1]-R[N])×RADIUS/2));FOR   17100
B←N-1STEP-1UNTIL Q+1DO HFLUX←HFLUX+(-TC)×DT×(3.14159265)×((R[B+1]*2-R[B]   17200
*2)×(RADIUS*2)×(((T[B]-OT[B])/((Z[I]-ZD[B]/RADIUS)×2×RADIUS)+(T[B+1]-OT[B   17300
+1])/((Z[I]-ZD[B+1]/RADIUS)×2×RADIUS))+(ZD[B]/RADIUS-ZD[B+1]/RADIUS)×(RA   17400
DIUS*2)×(R[B]+R[B+1])×(-1)/((2-R[B+1]-R[B])×RADIUS/2));HFLUX←HFLUX+(-TC)   17500
×DT×(3.14159265)×((R[Q+1]*2-R[Q]*2)×(RADIUS*2)×(T[Q+1]-OT[Q+1])/((Z[I]-Z   17600
D[Q+1]/RADIUS)×RADIUS)+(Z[I]-ZD[Q+1]/RADIUS)×(RADIUS*2)×(R[Q]+R[Q+1])×(T   17700
[Q+1]-T[Q])/((R[Q+1]-R[Q])×RADIUS));END;IF I>1THEN HFLUX←(3.14159265)×RA   17800
DIUS×(-TC)×DT×((R[Q+1]+R[Q])×DZ[Y]×((T[Q+1]-T[Q])/(R[Q+1]-R[Q])+OHQ)×(1/   17900
2)+(R[Q+1]*2-R[Q]*2)×(T[Q+1]-OT[Q+1])/DZ[Y]);MEQLH←HFLUX/HFG;IF I=1THEN   18000
MEQLH←MEQLH/(1+3×SPHTL×DT/(8×HFG));
```

(13)

```
                                    DIF[Y]←MASSTR-MEQLH;TAU←MUG×(U[Q]-U[Q   18100
-1])×UBAR/((R[Q]-R[Q-1])×RADIUS);IF Y=2THEN BEGIN SLOPEB←(MEQLH-OMEQLH)/   18200
```

```
(Z[I]-OZ);SLOPEA←(MASSTR-OMASSTR)/(Z[I]-OZ);END;OMEQLH←MEQLH;OMASSTR←MAS   18300
STR;OZ←Z[I];
```

(14)

```
          IF Y=1AND I≥3THEN MM2←(Z[I]+DIF[1]/(SLOPEB-SLOPEA))/Z[I-1];I   18400
F Y=1AND I≤2THEN MM2←(1+(0.80)×MM/JT);IF Y≥2THEN BEGIN REAL XXXX;IF Y=15   18500
OR ABS(DIF[Y]/MEQLH)<0.0005THEN BEGIN TOTAL←0.0;FOR B←1STEP 1UNTIL Q DO   18600
TOTAL←TOTAL+TOTT×(R[B]*2-R[B-1]*2)×(U[B]+U[B-1]);TOTAL1←TOTAL+SUM;MTR←SU   18700
MT×(R[Q+1]*2-R[Q]*2)×(U[Q]+UO[Q+1])+TOTT×(R[Q]+R[Q+1])×DZ[Y]×(V[Q]+VO[Q+   18800
1]);HLOC1←SQRT(SQRT((TC*4)/(TERM×Z[I]×RADIUS)));HM1←(0.943)×(SQRT(SQRT((   18900
TC*4)×4/(TERM×Z[I]×RADIUS))));HLOC←TC×T[N]/((R[N+1]-R[N])×RADIUS);IF I=1   19000
THEN BEGIN OLDHLOC←HLOC;OLDHSUM←0.0;END;AVEHLOC←(OLDHLOC+HLOC)/2;HMH[I←   19100
SUM×HFG×(1+3×SPHTL×DT/(8×HFG))×3600/((3.14159265)×D×Z[I]×RADIUS×DT);IF I   19200
=1THEN AVEHLOC←HMH[1]/3600;HTRW←AVEHLOC×(Z[I]-Z[I-1])×RADIUS;HSUM←OLDHSU   19300
M+HTRW;HM←HSUM/(Z[I]×RADIUS);IF I MOD 3=1THEN BEGIN WRITE(FL[PAGE]);WRIT   19400
E(FL,FMA,HM1);WRITE(FL,FMT4,LST4);WRITE(FL,FMT1,LST1);WRITE(FL,FMT2);WRI   19500
TE(FL,FMT3,LST3);END;FOR B←0STEP 1UNTIL N DO BEGIN UO[B]←U[B];VO[B]←V[B]   19600
;END;FOR B←Q+1STEP 1UNTIL N DO OT[B]←T[B];OLDHSUM←HSUM;OLDHLOC←HLOC;OLDS   19700
UM←SUM;RT←RT+1;IF RT<LIM THEN BEGIN ZL←Z[I]×D/2.0;FOR B←0STEP 1UNTIL 200   19800
DO BEGIN T[B]←UO[B]←OT[B]←1.0;VO[B]←0.0;END;END;HM2←HM1×SQRT(SQRT((1+(0.   19900
```

```
68)×SPHTL×DT/HFG)/(1+3×SPHTL×DT/(8×HFG))));HPHI[I]←HM/PHI;HNPHI[I]←HM1/P   20000
HI;HRPHI[I]←HM2/PHI;RWLZ[I]←4×Z[I]×RADIUS×DT×SPHTL×((GRAV×ROL×ROL/(MUL×M   20100
UL))*0.33333)/(PRL×HFG×(1+3×SPHTL×DT/(8×HFG))×(1-ROG/ROL));DELTA[I]←1-R[   20200
Q];NUA[I]←HM×RADIUS×Z[I]/TC;NU1A[I]←HM1×RADIUS×Z[I]/TC;HM2A[I]←HM2×3600;   20300
HMA[I]←HM×3600;HLOCA[I]←HLOC×3600;HM1A[I]←HM1×3600;HLOC1A[I]←HLOC1×3600;   20400
ZS[I]←ZSTAR;FRE[I]←4×SUM/(MUL×(3.14159265)×D);HNFPH[I]←1.46×((FRE[I])*(-   20500
0.333333));TAUV[I]←-TAU/(GRAV×(ROL-ROG)×((MUL×MUL/(ROL×ROL×GRAV))*0.3333   20600
3));TOT[I]←TOTAL1;HLOCNUC[I]←HLOC1A[I]×(SQRT(SQRT(8×HFG/(8×HFG+3×SPHTL×D   20700
T))));HMNUC[I]←HM1A[I]×(SQRT(SQRT(8×HFG/(8×HFG+3×SPHTL×DT))));IF Y=15THE   20800
N GO TO FLUSH;Y←15;BTT←I;IF U[0]<0.0THEN GO TO FLUSH;IF Z[I]<Z[I-1]THEN   20900
GO TO FLUSH;IF ABS(U[0])>10.0THEN GO TO FLUSH;IF(TIME(2)-X2)/60>860.0THE   21000
N GO TO FLUSH;END;IF Y<15THEN BEGIN SLOPE←(DIF[Y]-DIF[Y-1])/(DZ[Y]-DZ[Y-   21100
1]);DZ[Y+1]←-DIF[Y]/SLOPE+DZ[Y];Z[I]←Z[I-1]+DZ[Y+1];GO TO HELL;END;END;I   21200
F I=1THEN Z[0]←ZI×REG×2;IF RT>0AND RT<LIM THEN Z[0]←(1.2)×ZD[Q+1]/RADIUS   21300
;J←JT;END;END;
```

(15)

```
FLUSH:WRITE(FL[PAGE]);WRITE(FL,FMT,LST);WRITE(FL,FMF,LSTF)   21400
;WRITE(FL,FMTI,LSTI);WRITE(FL[PAGE]);WRITE(FL,FMG);FOR B←1STEP 1UNTIL BT   21500
T DO WRITE(FL,FMH,LSTH);WRITE(FL[PAGE]);WRITE(FL,FMB);FOR B←1STEP 1UNTIL   21600
```

```
 BTT DO WRITE(FL,FMC,LSTC);WRITE(FL[PAGE]);WRITE(FL,FMDA);WRITE(FL,FMD);    21700
FOR B←1STEP 1UNTIL BTT DO WRITE(FL,FME,LSTE);WRITE(FL[PAGE]);WRITE(FL,FM    21800
Y);FOR B←1STEP 1UNTIL BTT DO WRITE(FL,FMH,LSTW);WRITE(FL[PAGE]);WRITE(FL    21900
,FMZ);FOR B←1STEP 1UNTIL BTT DO WRITE(FL,FME,LSTX);WRITE(FL[PAGE]);WRITE    22000
(FL,FRM);FOR B←1STEP 1UNTIL BTT DO WRITE(FL,FMH,LSST);WRITE(FL,FMT5,(TIM    22100
E(2)-X2)/60);WRITE(FL,FMT6,(TIME(3)-X3)/60);IF BBB≤3THEN BEGIN IF(TIME(2    22200
)-X2)/60<300OR(TIME(2)-X2)/60<600THEN BEGIN WRITE(FL[PAGE]);WRITE(FL[PAG    22300
E]);UBAR←2×UBAR;GO TO GOD;END;END ELSE BBB←BBB;END.                         22400
```

Data Read Into the Pure Vapor Program

A typical set of data in the order it is read into the pure vapor program is given below.

0.03731 ROG, 59.802 ROL, 0.00000843̄4 MUG, 0.0001907 MUL, 970.3 HFG, 1.007 SPHTL, 0.0001073 TC, 212 TS, 202 TW, 0.083333 RADIUS, 25 UBAR, 0.6 L[1], 0.03 K[1], 0.75 L[2], 0.015 K[2], 0.95 L[3], 0.01 K[3], 0.995 L[4], 0.0025 K[4], 24 AA, 10 JT, 48 BT, 2 LIM, 0.00001 ZI,

```
BEGIN REAL RADIUS,D,REG,REL,ROG,ROL,MUG,MUL,UBAR,TS,TW,TC,DT,ZL,GRAV,HFG                100
,SPHTL,TERM,X0,AA,PRL,EKL,PRG,EKG,REN,HE,HW,SUM,OLDSUM,MASSTR,HFLUX,OLDH                200
FLUX,AVEHFLUX,MEQLH,ZSTAR,SLOPE,TAG,HLOC,AVEHLOC,OLDHLOC,HTRW,HSUM,OLDHS               300
UM,HM,VZG,VRG,ZI,OHQ,HZ,HX,HY,HV,HU,HT,RET,RES,WG,SUMT,TOTT,EKREL,PRREL,               400
HS,NU1,NU2,NU3,NU,TCG,SPHTG,PHI,ENTC,REPRG,REPRL,FR,FRT,PT,PTFRT,SCREG,D                500
ABG,CTERM,ROGA,ROGB,PRES,BC,CC,DC,MWA,MWB,TEMP,MMM,MM2,OMEQLH,OMASSTR,OZ                600
,SLOPEB,SLOPEA,MM,TERM2,TERM3,TAU,OLDX0,PCDIF,X2,X3,HLOC1,HLOC2,HM1,HM2,               700
HM3,IM,TOTAL,TOTAL1,MTR;INTEGER B,I,A,N,Q,Y,S,SS,SSS,J,RT,BB,LIM,JJ,YY,B                800
TT,ZQZ,BBB,BT,JT;REAL ARRAY Z,P[0:80],M,L,K[1:10],DT,VW,CO,C,V,T,U,R,UO,                900
ZD,ROO,VO[0:200],XDZ,OLDDZ,DIF,DZ[1:20],G[0:200,0:20],RON[0:200],TM[1:5,               1000
1:4],TI[0:80],ZS,HMA,HM1A,HM2A,HM3A,HLOCA,HLOC1A,HLOC2A,RWLZ,FRE,NUA,NU1              1100
A,HNFPH,ICG,AMB,HMH,HMNUC,HLOCNUC,TOT,HNPHI,HRPHI,DELTA,NU2A,NU3A,HPHI,T              1200
AUV[0:80],ABP[0:50],W,F,X,E,H[-1:220];FILE OUT FL 6(2,15);FILE IN DA(2,1               1300
0);LABEL FLUSH,GOO,TECH;FORMAT FTB("TRY NO. ",I2,X10," ZI = ",E15 .6,//)               1400
;FORMAT OUT FM62("PRES = ",F10 .5,X10,"TEMP = ",F10 .4,/);LIST LST62(PRE                1500
S,TEMP);LIST LSST(ZS[B],Z[B]×RADIUS,FRE[B],HPHI[B]/HNFPH[B],HNFPH[B],HPH               1600
```

```
I[B],UBAR×UBAR/(GRAV×Z[B]×RADIUS));FORMAT OUT FRM("RATIOS BELOW ARE BASE      1700
D ON FILM RE NOT DISTANCE",//,X5,"ZSTAR",X10,"Z IN FT",X7,"FILM RE",X8,"      1800
HM/HMNF",X8,"HMNF/PHI",X7,"HM/PHI",X6,"LENGTH FR NO.",//);LIST LIS(ROG,R      1900
OL,MUG,MUL,HFG,SPHTL,TC,TS,TW,ENTC,DABG,RADIUS,UBAR,L[1],K[1],L[2],K[2],      2000
L[3],K[3],L[4],K[4],AA,JT,BT,LIM,ZI);FORMAT OUT FMT9("UO[",I3,"] = ",F10      2100
 .7,X10,"VO[",I3,"] = ",F12 .10,X10,"ZO = ",E16 .7,/);LIST LST9(B,UO[B],      2200
B,VO[B],ZO[B]/RADIUS);FORMAT OUT FMF("UBAR = ",E16 .7," FT/SEC",/,"VISCO      2300
SITY GAS = ",X3,E16 .7," LBM/FT×SEC ",/,"VISCOSITY LIQUID = ",E16 .7," L      2400
BM/FT×SEC ",//,"DENSITY GAS = ",F16 .7," LBM/FT×FT×FT",/,"DENSITY LIQUID      2500
 = ",F16 .7," LBM/FT×FT×FT",//,"THERMAL CONDUCTIVITY GAS = ",X3,E16 .7,"      2600
BTU/SEC×FT×F",/,"THERMAL CONDUCTIVITY LIQUID = ",E16 .7,"BTU/SEC×FT×F",/      2700
/,"HEAT CAPACITY GAS = ",X3,F16 .7," BTU/LBM×F",/,"HEAT CAPACITY LIQUID      2800
= ",F16 .7," BTU/LBM×F",//,"INITIAL CONCENTRATION OF NON-CONDENSABLE = "      2900
,E16 .7," W, WT CONC",//,"SCHMIDT NUMBER OF GAS = ",E14 .5,/"DAB GAS = "      3000
,E16 .7," FT×FT/SEC ",//,"HFG, ENTHALPY, CHANGE OF PHASE = ",F16 .7," BT      3100
U/LBM",//,"TEMPERATURE DIFFERENCE = ",F16 .7," DEG F ",//,"DIAMETER OF V      3200
ERTICAL PIPE = ",F16 .9," FT  OR",F16 .9," INCHES",/);LIST LSTF(UBAR,MUG      3300
,MUL,ROG,ROL,TCG,TC,SPHTG,SPHTL,ENTC,MUG/(ROG×DABG),DABG,HFG,DT,D,D×12);      3400
FORMAT OUT FMG(X7,"Z",X11,"ZSTAR",X8,"DELTA R/R",X8,"HN/PHI",X9,"HR/PHI"      3500
```

```
,X11,"NU",X12,"NUN",//);FORMAT FM35(X3,"FR LENGTH",X5,"Z IN FT",X6,"HM R      3600
ATIO",X6,"HM/PHI",X4,"HLOC RATIO",X4,"2×DELTA/D",X6,"FILM RE",X6,"TAUSTA      3700
R",X10,"P",//),FM36(9(E13 .5),X3));LIST LST36(UBAR×UBAR/(GRAV×Z[B]×RADIUS      3800
),Z[B]×RADIUS,HMA[B]/HM1A[B],HPHI[B],HLOCA[B]/HLOC1A[B],DELTA[B],FRE[B],      3900
TAUV[B],P[B]));FORMAT FMH(7(E14 .5,X1),X15);FORMAT FFZ(X7,"Z IN FT",X14,"      4000
ZSTAR",X8,"INTERFACE CONC",X6,"INTERFACE TEMP",X8,"AMOUNT OF B",X15,"HMD      4100
/K",//);LIST LLZ(RADIUS×Z[B],ZS[B],ICG[B],TI[B],AMB[B],NU3A[B]);LIST LST      4200
H(Z[B],ZS[B],DELTA[B],HNPHI[B],HRPHI[B],NUA[B],NU1A[B]);FORMAT OUT FMTI(      4300
"ROG/ROL = ",E14 .5,X10,"MUG/MUL = ",E14 .5,X10,"TCG/TCL = ",E14 .5,/,"C      4400
PG/CPL = ",E14 .5,X10,"REG/REL = ",E14 .5,X10,"REG/FR  = ",E14 .5,//,"CP      4500
L×DT/HFG = ",E14 .5,//);LIST LSTI(ROG/ROL,MUG/MUL,TCG/TC,SPHTG/SPHTL,REG      4600
/REL,REG/FR,SPHTL×DT/HFG);FORMAT OUT FMB(X7,"Z",X16,"ZSTAR",X14,"FILM RE      4700
",X15,"H/PHI",X15,"TAUST",X12,"R,W,L, ZST",//);FORMAT FMC(6(E14 .5,X6));      4800
LIST LSTC(Z[B],ZS[B],FRE[B],HPHI[B],TAUV[B],RWLZ[B]);FORMAT OUT FMZ(X6,"      4900
ZSTAR",X8,"ZSTAR/REG",X7,"HM/HMN",X9,"HM/HMR",X8,"HM/HMNUC",X6,"HLOC/HLO      5000
CN",X4,"HLOC/HLOCNUC",X5,"FILM RE",//);LIST LSTX(ZS[B],ZS[B]/REG,HMA[B]/      5100
HM1A[B],HMA[B]/HM2A[B],HMA[B]/HMNUC[B],HLOCA[B]/HLOC1A[B],HLOCA[B]/HLOCN      5200
UC[B],FRE[B]);FORMAT OUT FMY(X4,"Z IN FT",X9,"ZSTAR",X7,"SCRIPT P",X8,"P      5300
 - GRAV",X6,"P,LBF/IN×IN",X4,"TAUST/REG",X4,"LB/SEC IN TUBE",//);LIST LS      5400
```

```
TW(Z[B]×RADIUS,ZS[B],P[B],P[B]-Z[B]×FRT,ABP[B],TAUV[B]/REG,TOT[B]);LIST      5500
LST(REG,REL,PRL,EKL,FR);FORMAT OUT FMT("REG = ",F10 .3,X5,"REL = ",F12 .    5600
3,X5,"PRL = ",F10 .5,X5,"EKL = ",E14 .5,X5,"FR = ",E14 .5,//);FORMAT OUT    5700
 FMDA("HEAT TRANSFER COEF. BELOW ARE IN  BTU/HR×FT×FT×F.",////);FORMAT O    5800
UT FMD(X7,"Z",X11,"ZSTAR",X11,"HM",X13,"HLOC",X11,"HMN",X11,"HLOCN",X11,    5900
"HMR",X11,"HMH",//);FORMAT FME(8(E14 .5,X1));LIST LSTE(Z[B],ZS[B],HMA[B]    6000
,HLOCA[B],HM1A[B],HLOC1A[B],HM2A[B],HMH[B]);FORMAT OUT FMT1("MASS TRANSF    6100
ERRED = ",E16 .7,X2,"LBS/SEC.",X5,"MASS EQUIVALENT TO HEAT = ",E16 .7,X2    6200
,"LBS/SEC.",/,"DIF[",I2,"] = ",E16 .7,X5,"TOTAL MASS TRANSFERRED = ",E16    6300
 .7,/,"P[",I2,"] = ",E16 .7,X10,"Z[",I2,"] = ",E16 .7,X5,"ZSTAR = ",E16    6400
 .7,////);LIST LST1(MASSTR,MEQLH,Y,DIF[Y],SUM,I,P[I],I,Z[I],ZSTAR);FORMAT    6500
 OUT FMT2(X1,"B",X11,"R",X19,"U",X19,"V",X19,"VW",X19,"T",X19,"C",//);FO    6600
RMAT FMT3(I3,X7,F10 .8,5(X4,F16 .10));LIST LST3(FOR J←0STEP 3UNTIL M[4]-    6700
2,M[4]STEP 6UNTIL Q=2,Q-1,Q,Q+1,Q+2STEP 4UNTIL N=1,N,N+1DO[J,R[J],U[J],V    6800
[J],VW[J],T[J],C[J]]);FORMAT OUT FMT4("HLOC = ",E16 .7X5,"HM = ",E16 .7,    6900
X10,"INTERFACE POSITION = ",F10 .8,X5,"Q = ",I3,/);LIST LST4(HLOC,HM,R[Q    7000
],Q);FORMAT OUT FMT5("PROCESS TIME = ",F10 .4,//);FORMAT OUT FMT6("IN/OU    7100
T TIME = ",F10 .4,//);FORMAT OUT FMA("HM FOR VERTICAL TUBES, BSL 13.6-4    7200
= ",E16 .7,/);X2←TIME(2);X3←TIME(3);
```

(1)

```
                                    TAG←7.0;READ(DA,/,LIS);CLOSE(DA,RELE    7300
ASE);
```

(2)

```
     BBB←0;GOD:BBB←BBB+1;ZQZ←0;TECH:D←2×RADIUS;REG←ROG×D×UBAR/MUG;REL←RO    7400
L×D×UBAR/MUL;TCG←0.00000407;SPHTG←0.454;ROGA←0.037313;ROGB←0.0590;ROG←RO    7500
GA;MWA←18.02;MWB←28.97;IM←(3.14159265)×(RADIUS*2)×ROG×UBAR;R[0]←0.0;Z[1]    7600
←ZI×REG×2;P[0]←Z[0]←0.0;FOR B←0STEP 1UNTIL 2000 BEGIN U0[B]←1.0;V0[B]←0    7700
.0;0T[B]←1.0;T[B]←1.0;C0[B]←C[B]←ENTC;END;RON[0]←(1/(1+ROGA×C[0]/(ROGB×(    7800
1-C[0])))×ROGA×(1+C[0]/(1-C[0]));FOR B←0STEP 1UNTIL 2000 RON[B]←ROO[B]    7900
←RON[0];DT←TS-TW;ZL←Z[1]×D/2;GRAV←32.174;TERM←4×TC×DT×MUL/(GRAV×ROL×(ROL    8000
-ROG)×HFG×(1+3×SPHTL×DT/(HFG×8)));FR←UBAR×UBAR/(GRAV×D);FRT←1/(2×FR);PRL    8100
←MUL×SPHTL/TC;EKL←UBAR×UBAR/(SPHTL×(TS-TW));SUMT←ROL×(3.14159265)×(RADIU    8200
S*2)×UBAR/2;TOTT←ROG×(3.14159265)×(RADIUS*2)×UBAR/2;EKREL←2/(EKL×REL);PR    8300
REL←PRL×REL;PHI←TC×((ROL×ROL×GRAV/(MUL×MUL))*0.33333);SCREG←UBAR×D/DABG;    8400
PRG←MUG×SPHTG/TCG;EKG←UBAR×UBAR/(SPHTG×DT);JJ←0;RT←0;I←0;FOR BB←1STEP 1U    8500
NTIL BT DO BEGIN REAL QQQQQ;LABEL HELL,SLEEP,TOWN;I←I+1;IF RT<LIM THEN I    8600
←1;
```

(3) AND (4)

```
IF RT=0THEN X0←SQRT(SQRT(TERM×ZL));IF RT<LIM AND RT>0THEN BEGIN TERM2
←4×TAU/(3×(ROL-ROG)×GRAV);FOR A←1STEP 1UNTIL 20DO BEGIN OLDX0←X0;IF TERM
×ZL+TERM2×(X0*3)≤0THEN X0←X0/2.0ELSE X0←SQRT(SQRT(TERM×ZL+TERM2×(X0*3)))
;PCDIF←(X0-OLDX0)×100/X0;END;END;J←JT;IF I=1THEN BEGIN IF 1-4×AA×X0/(RAD
IUS×J)≤2×K[1]THEN GO TO FLUSH;IF L[4]≥1-4×AA×X0/(RADIUS×J)THEN BEGIN FOR
 B←1STEP 1UNTIL 396DO IF L[4]≥1-4×AA×X0/(RADIUS×J)THEN L[4]←L[4]-K[4]ELS
E B←397;END;IF L[3]≥L[4]THEN BEGIN FOR B←1STEP 1UNTIL 80DO IF L[3]≥L[4]T
HEN L[3]←L[3]-K[3]ELSE B←81;K[4]←L[4]-L[3];END;IF L[2]≥L[3]THEN BEGIN FO
R B←1STEP 1UNTIL 80DO IF L[2]≥L[3]THEN L[2]←L[2]-K[2]ELSE B←81;K[3]←L[3]
-L[2];END;IF L[1]≥L[2]THEN BEGIN FOR B←1STEP 1UNTIL 80DO IF L[1]≥L[2]THE
N L[1]←L[1]-K[1]ELSE B←81;K[2]←L[2]-L[1];END;L[5]←1-4×AA×X0/(RADIUS×J);K
[5]←L[5]-L[4];L[6]←1-AA×X0/(RADIUS×J);K[6]←2×X0/(RADIUS×J);L[7]←1.001;K[
7]←X0/(RADIUS×J);A←1;FOR B←1STEP 1UNTIL 200DO BEGIN IF R[B-1]>(0.9999)×L
[A]THEN BEGIN R[B]←R[B-1]+K[A+1];M[A]←B-1;A←A+1;END ELSE R[B]←R[B-1]+K[A
];IF R[B]>0.999999THEN BEGIN N←B-1;U[B]←U0[B]←0.0;GO TO SLEEP;END;END;SL
EEP:END;IF I=J THEN OHQ←(OT[Q+1]-OT[Q])/(R[Q+1]-R[Q]);IF I=J THEN BEGIN
A←(1+N-M[6])/2;FOR B←0STEP 1UNTIL A DO BEGIN R[M[6]+B]←R[M[6]+2×B];U0[M[
6]+B]←U0[M[6]+2×B];V0[M[6]+B]←V0[M[6]+2×B];OT[M[6]+B]←OT[M[6]+2×B];C0[M[
6]+B]←C0[M[6]+2×B];END;U[M[6]+A]←0.0;N←M[6]+(N-M[6]-1)/2;JJ←J/2+(I-2)/2;
```

```
END;Q←N←I-J+2+JJ;FOR B←Q+1STEP 1UNTIL N+1DO CO[B]←C[B]←0.0;IF I≠J THEN O   10600
HQ←(OT[Q+2]-OT[Q+1])/(R[Q+2]-R[Q+1]);IF RT=OTHEN BEGIN FOR B←Q+1STEP 1UN   10700
TIL N DO BEGIN UO[B]←GRAV×(ROL-ROG)×(((1-R[B])×RADIUS)*2)/(2×MUL×UBAR);Z   10800
D[B]←(((1-R[B])×RADIUS)*4)/TERM;VO[B]←(GRAV×(ROL-ROG)×(((1-R[B])×RADIUS)   10900
*2)/(4×MUL))×(SQRT(SQRT(TERM/(ZD[B]*3))))/UBAR;END;END;IF RT<LIM AND RT>   11000
OTHEN BEGIN TERM3←ROL×TAU×HFG×(1+3×SPHTL×DT/(HFG×8))/(3×MUL×TC×DT);FOR B   11100
←Q+1STEP 1UNTIL N DO BEGIN UO[B]←GRAV×(ROL-ROG)×(((1-R[B])×RADIUS)*2)/(2   11200
×MUL×UBAR)-TAU×(1-R[B])×RADIUS/(MUL×UBAR);ZD[B]←(((1-R[B])×RADIUS)*4)/TE   11300
RM-(((1-R[B])×RADIUS)*3)×TERM3;VO[B]←TC×DT/(ROL×(1-R[B])×RADIUS×HFG×(1+3   11400
×SPHTL×DT/(HFG×8))×UBAR);END;END;
```

(5)

```
                                        Y←0;IF I=1THEN Z[0]←ZI×REG×2;IF RT>0AND   11500
 RT<LIM THEN Z[0]←(1.2)×ZD[Q+1]/RADIUS;MM←14.6;IF I=1OR I=2THEN MMM←(1+M   11600
M/J)ELSE MMM←Z[I-1]/Z[I-2];FOR Z[I]←MMM×Z[I-1],MM2×Z[I-1]DO BEGIN
```

(6)

```
                                                              HELL;Y   11700
←Y+1;IF I=1THEN Z[0]←0.0;YY←0;TOWN;YY←YY+1;DZ[Y]←Z[I]-Z[I-1];ZSTAR←Z[I]/   11800
(2×REG);HE←R[1]-R[0];FOR B←0STEP 1UNTIL Q DO RON[B]←(1/(1+ROGA×C[B]/(ROG   11900
B×(1-C[B]))))×ROGA×(1+C[B]/(1-C[B]));FOR B←Q+1STEP 1UNTIL N DO ROO[B]←RO   12000
```

```
N[B]←ROL;REN←RON[0]×UBAR×D/MUG;H[0]←8/(REN×HE×HE)+UO[0]/DZ[Y];X[1]←-8/(R   12100
EN×HE×HE);WG←1/DZ[Y];FOR B←0STEP 1UNTIL Q DO BEGIN W[B]←(RON[0]/RON[B])×   12200
(1+(RON[B]-ROO[B])/RON[B])/DZ[Y];F[B]←((UO[B]*2)+(ROO[0]/ROO[B])×P[I-1])   12300
/DZ[Y]+FRT;END;WG←(ROG/ROL)/DZ[Y];PT←ROG×P[I-1]/(ROL×DZ[Y]);PTFRT←PT+FRT   12400
;FOR B←Q+1STEP 1UNTIL N DO BEGIN IF I=1THEN XDZ[Y]←Z[I]-ZD[B]/RADIUS;IF   12500
I>1THEN XDZ[Y]←DZ[Y];W[B]←(RON[0]/ROL)/DZ[Y];F[B]←(UO[B]*2)/XDZ[Y]+(ROO[   12600
0]/ROL)×P[I-1]/DZ[Y]+FRT;END;W[Q]←F[Q]←0.0;FOR B←0STEP 1UNTIL N DO FOR J   12700
←0STEP 1UNTIL 12DO G[B,J]←0.0;FOR J←N+1STEP 1UNTIL N+13DO BEGIN W[J]←F[J   12800
]←X[J]←0.0;END;E[N]←0.0;G[0,0]←R[1]×RON[0]/(4×DZ[Y]);G[1,0]←3×R[1]×RON[1   12900
]/(4×DZ[Y]);OLDDZ[Y]←DZ[Y];S←SS←0;HE←R[1]-R[0];HW←HE;HV←HE×HE×(2.0);HU←H   13000
V;HT←0.0;HZ←HE/HV;HY←HZ;A←1;BEGIN REAL QQQ;FOR B←1STEP 1UNTIL N-1DO BEGI   13100
N LABEL GIRL,SCHOOL;IF B<Q THEN REN←RON[B]×D×UBAR/MUG;IF B=Q THEN REN←RE   13200
L;IF I=1AND B>Q THEN DZ[Y]←Z[I]-ZD[B]/RADIUS;IF B=Q OR B=M[A]THEN BEGIN   13300
A←A+1;HE←R[B+1]-R[B];HW←R[B]-R[B-1];HV←HW×(HW+HE);HU←HE×(HW+HE);HT←(HW-H   13400
E)/(HW×HE);HZ←HE/HV;HY←HW/HU;E[B-1]←-HZ×VO[B]-4/(REN×HV)+2×HZ/(REN×R[B])   13500
;H[B]←UO[B]/DZ[Y]-HT×VO[B]+4/(REN×HW×HE)+2×HT/(REN×R[B]);X[B+1]←HY×VO[B]   13600
-4/(REN×HU)-2×HY/(REN×R[B]);HW←HE;HV←HU←2×HE×HE;HZ←HY←1/(2×HE);END ELSE   13700
BEGIN E[B-1]←-HZ×VO[B]-4/(REN×HV)+2×HZ/(REN×R[B]);H[B]←UO[B]/DZ[Y]+8/(RE   13800
N×HV);X[B+1]←HY×VO[B]-4/(REN×HV)-2×HY/(REN×R[B]);END;IF Q≤M[6]THEN M[6]←   13900
```

```
O;IF B>1THEN BEGIN FOR J←1STEP 1UNTIL TAG DO IF B=M[J]THEN BEGIN S←S+1;G    14000
O TO GIRL;END;IF B=Q THEN BEGIN SS←1;GO TO GIRL;END;IF B=Q+1THEN BEGIN S    14100
S←2;GO TO GIRL;END;G[B,SS+S]←R[B]×RON[B]/DZ[Y];F[N+S+1+SS]←F[N+S+1+SS]+R    14200
[B]×UO[B]×ROO[B]/DZ[Y];GO TO SCHOOL;GIRL:G[B,S-1+SS]←R[B]×RON[B]/(2×DZ[Y    14300
]);G[B,S+SS]←G[B,S-1+SS];F[N+S+SS]←R[B]×ROO[B]×UO[B]/(2×DZ[Y])+F[N+S+SS]    14400
;F[N+S+1+SS]←R[B]×ROO[B]×UO[B]/(2×DZ[Y]);IF S=1THEN F[N+S]←F[N+S]+UO[1]×    14500
ROO[1]×3×R[1]/(4×DZ[Y])+UO[0]×R[1]×ROO[0]/(4×DZ[Y]);H[N+S+SS]←RON[B]×R[B    14600
]/(R[B]-R[B-1]);E[N+S+SS]←-RON[B]×R[B]/(R[B+1]-R[B]);IF SS=1THEN BEGIN I    14700
F I=1THEN DZ[Y]←Z[I]-ZD[Q+1]/RADIUS;F[N+S+SS+1]←0.0;E[N+S+SS]←-(R[Q]/HE)    14800
×(RON[Q]/ROL)×(1-C[Q]);G[B,S+SS]←-(R[Q]/HE)×(((RON[Q]/ROL)×(1-C[Q])-1)×H    14900
E/DZ[Y]);END;IF SS=2THEN BEGIN F[N+S+SS]←R[Q+1]×UO[Q+1]/DZ[Y]+(R[Q]/HE)×    15000
(DABG×(RON[Q]/ROL)×((C[Q]-CO[Q])×HE/(DZ[Y]*2)+(C[Q]-C[Q-1])/HE))×(1/(UBA    15100
R×RADIUS));G[B,S+SS-1]←R[Q+1]/DZ[Y];H[N+S+SS]←R[Q+1]/HE;END;SCHOOL:END;E    15200
ND;END;BEGIN REAL XXX;IF I=1THEN DZ[Y]←Z[I]-ZD[N]/RADIUS;E[N-1]←-VO[N]×H    15300
E/(HW×(HW+HE))-4/(REN×HW×(HE+HW))+2×HE/(REN×R[N]×HW×(HW+HE));H[N]←UO[N]/    15400
DZ[Y]-VO[N]×(HW-HE)/(HW×HE)+4/(REN×HW×HE)+2×(HW-HE)/(REN×R[N]×HW×HE);E[Q    15500
-1]←-MUG/(R[Q]-R[Q-1]);H[Q]←MUG/(R[Q]-R[Q-1])+MUL/(R[Q+1]-R[Q]);X[Q+1]←-    15600
MUL/(R[Q+1]-R[Q]);G[N,S+SS]←R[N]×RON[N]/DZ[Y];F[N+S+1+SS]←F[N+S+1+SS]+R[    15700
N]×UO[N]×ROO[N]/DZ[Y];
```

(7)

```
                    DZ[Y]←OLDDZ[Y];S←0;SSS←0;FOR B←0STEP 1UNTIL N-1DO    15800
BEGIN F[B]←F[B]/H[B];W[B]←W[B]/H[B];X[B+1]←X[B+1]/H[B];F[B+1]←F[B+1]-F[B    15900
]×E[B];W[B+1]←W[B+1]-W[B]×E[B];H[B+1]←H[B+1]-X[B+1]×E[B];IF ABS(G[B,S+1]    16000
)>0THEN BEGIN S←S+1;SSS←SSS+1;END;FOR J←0STEP 1UNTIL SSS DO BEGIN F[N+1+    16100
J]←F[N+1+J]-F[B]×G[B,J];W[N+1+J]←W[N+1+J]-W[B]×G[B,J];G[B+1,J]←G[B+1,J]-    16200
X[B+1]×G[B,J];END;END;F[N]←F[N]/H[N];W[N]←W[N]/H[N];FOR S←0STEP 1UNTIL S    16300
SS DO BEGIN F[N+1+S]←F[N+1+S]-F[N]×G[N,S];W[N+1+S]←W[N+1+S]-W[N]×G[N,S];    16400
END;FOR B←N+1STEP 1UNTIL SSS+N DO BEGIN F[B]←F[B]/H[B];W[B]←W[B]/H[B];F[    16500
B+1]←F[B+1]-F[B]×E[B];W[B+1]←W[B+1]-W[B]×E[B];END;P[I]←F[N+1+SSS]/W[N+1+    16600
SSS];U[N]←F[N]-W[N]×P[I];FOR B←N-1STEP-1UNTIL 0DO U[B]←F[B]-W[B]×P[I]-X[    16700
B+1]×U[B+1];VZG←U[Q];
```

(8)

```
                    DZ[Y]←Z[I]-Z[I-1];HE←R[1]-R[0];V[1]←-HE×(RON[1]×U[1    16800
]+RON[0]×U[0]-ROO[1]×UO[1]-ROO[0]×UO[0])/(4×DZ[Y]×RON[1]);FOR B←2STEP 1U    16900
NTIL N+1DO BEGIN IF B≤Q THEN V[B]←((-R[B]×(RON[B]×U[B]-ROO[B]×UO[B])-R[B    17000
-1]×(RON[B-1]×U[B-1]-ROO[B-1]×UO[B-1]))/(2×DZ[Y])+RON[B-1]×V[B-1]×R[B-1]    17100
/(R[B]-R[B-1]))×(R[B]-R[B-1])/(RON[B]×R[B]);IF B=Q+1THEN BEGIN XDZ[Y]←DZ    17200
[Y];IF I=1THEN DZ[Y]←Z[I]-ZD[B]/RADIUS;VRG←V[Q];V[Q]←(RON[Q]/ROL)×((1-C[    17300
```

```
Q])×U[Q]×(R[Q+1]-R[Q])/DZ[Y]+(1-C[Q])×V[Q]+DABG×(C[Q]-CO[Q])×(R[Q+1]-R[Q   17400
])/(UBAR×RADIUS×DZ[Y]×DZ[Y])+DABG×(C[Q]-C[Q-1])/((R[Q+1]-R[Q])×UBAR×RADI   17500
US))-U[Q]×(R[Q+1]-R[Q])/DZ[Y];V[Q+1]←(R[Q+1]×UO[Q+1]/DZ[Y]-U[Q+1]×R[Q+1]   17600
/DZ[Y]+V[Q]×R[Q]/(R[Q+1]-R[Q]))×(R[Q+1]-R[Q])/R[Q+1];END;IF B>Q+1THEN BE   17700
GIN XDZ[Y]←DZ[Y];IF I=1THEN DZ[Y]←Z[I]-ZD[B]/RADIUS;V[B]←(V[B-1]×R[B-1]/   17800
(R[B]-R[B-1])-R[B-1]×(U[B-1]-UO[B-1])/(2×XDZ[Y])-R[B]×(U[B]-UO[B])/(2×DZ   17900
[Y]))×(R[B]-R[B-1])/R[B];END;END;END;
```

(8A)

```
                                        BEGIN REAL XXXXX;DZ[Y]←OLDDZ[Y];HE←   18000
R[1]-R[0];HW←HE;HV←HE×HE×(2.0);HU←HV;HT←0.0;HZ←HE/HV;HY←HZ;A←1;H[0]←-8/(   18100
SCREG×HE×HE)-U[0]/DZ[Y];X[1]←8/(SCREG×HE×HE);F[0]←-U[0]×CO[0]/DZ[Y];CTER   18200
M←RADIUS×UBAR×(VZG×(R[Q+1]-R[Q])+VRG×DZ[Y])-DABG×((R[Q+1]-R[Q])/DZ[Y]+DZ   18300
[Y]/(R[Q+1]-R[Q]));FOR B←1STEP 1UNTIL Q-1DO BEGIN IF B=Q OR B=M[A]THEN B   18400
EGIN A←A+1;HE←R[B+1]-R[B];HW←R[B]-R[B-1];HV←HW×(HW+HE);HU←HE×(HW+HE);HT←   18500
(HW-HE)/(HW×HE);HZ←HE/HV;HY←HW/HU;E[B-1]←-HZ×V[B]-4/(SCREG×HV)+2×HZ/(SCR   18600
EG×R[B]);H[B]←U[B]/DZ[Y]-HT×V[B]+4/(SCREG×HE×HW)+2×HT/(SCREG×R[B]);X[B+1   18700
]←HY×V[B]-4/(SCREG×HU)-2×HY/(SCREG×R[B]);HW←HE;HV←HU←2×HE×HE;HZ←HY←1/(2×   18800
HE);END ELSE BEGIN E[B-1]←-HZ×V[B]-4/(SCREG×HV)+2×HZ/(SCREG×R[B]);H[B]←U   18900
[B]/DZ[Y]+8/(SCREG×HV);X[B+1]←HY×V[B]-4/(SCREG×HU)-2×HY/(SCREG×R[B]);END   19000
```

```
;F[B]←CO[B]×U[B]/DZ[Y];END;F[Q-1]←F[Q-1]-X[Q]×(-DABG×CO[Q]×(R[Q+1]-R[Q])    19100
/(CTERM×DZ[Y]));H[Q-1]←H[Q-1]+X[Q]×(-DABG×DZ[Y]/((R[Q+1]-R[Q])×CTERM));
```

(8B)

```
                                                                F    19200
OR B←0STEP 1UNTIL Q=200 BEGIN F[B]←F[B]/H[B];X[B+1]←X[B+1]/H[B];F[B+1]←F    19300
[B+1]-F[B]×E[B];H[B+1]←H[B+1]-X[B+1]×E[B];END;C[Q-1]←F[Q-1]/H[Q-1];FOR B    19400
←Q-2STEP-1UNTIL 0DO C[B]←F[B]-X[B+1]×C[B+1];C[Q]←-DABG×CO[Q]×(R[Q+1]-R[Q    19500
])/(CTERM×DZ[Y])-DABG×C[Q-1]×DZ[Y]/((R[Q+1]-R[Q])×CTERM);END;IF C[Q]<0.0    19600
THEN BEGIN ZQZ←ZQZ+1;ZI←ZI×3;IF ZQZ<10THEN BEGIN WRITE(FL,FTB,ZQZ,ZI);IF    19700
 I<5THEN GO TO TECH;END ELSE GO TO FLUSH;END;
```

(8C)

```
                                        IF YY<2THEN BEGIN GO TO TOW    19800
N;END;
```

(8D)

```
      BEGIN REAL QQQ;PRES←((1-C[Q])/MWA)×14.696/((1-C[Q])/MWA+C[Q]/MWB);    19900
TI[I]←1/((1/(TS+460))+LN(14.696/PRES)/(HFG×MWA/1.986));TI[I]←(TI[I]-460-    20000
TW)/DT;T[Q]←TI[I];
```

(8E)

```
                HE←R[I]-R[0];HW←HE;HV←2×HE×HE;HU←HV;HT←0.0;HZ←HY←HE/HV    20100
```

```
;A←1;REN←RON[0]×D×UBAR/MUG;H[0]←8/(REN×PRG×HE×HE)+U[0]/DZ[Y];X[1]←-8/(RE    20200
N×PRG×HE×HE);F[0]←U[0]×OT[0]/DZ[Y];OT[N+1]←0.0;T[N+1]←0.0;FOR B←1STEP 1U    20300
NTIL Q-1DO BEGIN REN←RON[B]×D×UBAR/MUG;REPRG←REN×PRG;IF B=Q OR B=M[A]THE    20400
N BEGIN A←A+1;HE←R[B+1]-R[B];HW←R[B]-R[B-1];HV←HW×(HW+HE);HU←HE×(HW+HE);    20500
HT←(HW-HE)/(HW×HE);HZ←HE/HV;HY←HW/HU;E[B-1]←-HZ×V[B]+2×HZ/(REPRG×R[B])-4    20600
/(REPRG×HV);H[B]←U[B]/DZ[Y]-HT×V[B]+2×HT/(REPRG×R[B])+4/(REPRG×HE×HW);X[    20700
B+1]←HY×V[B]-2×HY/(REPRG×R[B])-4/(REPRG×HU);F[B]←U[B]×OT[B]/DZ[Y]+(2/(RE    20800
N×EKG))×((HY×U[B+1]-HT×U[B]-HZ×U[B-1])*2);HW←HE;HV←HU←2×HE×HE;HZ←HY←1/(2    20900
×HE);END ELSE BEGIN E[B-1]←-HZ×V[B]+2×HZ/(REPRG×R[B])-4/(REPRG×HV);H[B]←    21000
U[B]/DZ[Y]+8/(REPRG×HV);X[B+1]←HY×V[B]-2×HY/(REPRG×R[B])-4/(REPRG×HU);F[    21100
B]←U[B]×OT[B]/DZ[Y]+(2/(REN×EKG))×((HY×U[B+1]-HZ×U[B-1])*2);END;END;F[Q-    21200
1]←F[Q-1]-X[Q]×T[Q];
```

(8F)

```
                    FOR B←0STEP 1UNTIL Q-2DO BEGIN F[B]←F[B]/H[B];X[B+1]    21300
←X[B+1]/H[B];F[B+1]←F[B+1]-F[B]×E[B];H[B+1]←H[B+1]-X[B+1]×E[B];END;T[Q-1    21400
]←F[Q-1]/H[Q-1];FOR B←Q-2STEP-1UNTIL 0DO T[B]←F[B]-X[B+1]×T[B+1];
```

(9)

```
                                                        IF I=1T    21500
HEN BEGIN FOR B←Q+1STEP 1UNTIL N DO OT[B]←1-(ZD[B]/RADIUS)×(1-T[Q])/DZ[Y    21600
```

```
];END;END;DZ[Y]←OLDDZ[Y];HE←R[Q+2]-R[Q+1];HW←R[Q+1]-R[Q];HU←HV←2×HE×HE;H    21700
Z←HY←HE/HV;REPRL←REL×PRL;HT←2/(REL×EKL);DT[N+1]←0.0;T[N+1]←0.0;FOR B←Q+1    21800
STEP 1UNTIL N DO BEGIN IF I=1THEN DZ[Y]←Z[I]-ZD[B]/RADIUS;E[B-1]←-HZ×V[B    21900
]+2×HZ/(REPRL×R[B])-4/(REPRL×HV);H[B]←U[B]/DZ[Y]+8/(REPRL×HV);X[B+1]←HY×    22000
V[B]-2×HY/(REPRL×R[B])-4/(REPRL×HU);F[B]←U[B]×DT[B]/DZ[Y]+HT×((HY×U[B+1]    22100
-HZ×U[B-1])*2);END;F[Q+1]←F[Q+1]-E[Q]×T[Q];
                                        (10)
                                                FOR B←Q+1STEP 1UNTIL N-1DO BE    22200
GIN F[B]←F[B]/H[B];X[B+1]←X[B+1]/H[B];F[B+1]←F[B+1]-F[B]×E[B];H[B+1]←H[B    22300
+1]-X[B+1]×E[B];END;T[N]←F[N]/H[N];FOR B←N-1STEP-1UNTIL Q+1DO T[B]←F[B]-    22400
X[B+1]×T[B+1];BEGIN REAL XXXX;DZ[Y]←OLDDZ[Y];
                                        (11)
                                                IF I=1THEN OLDSUM←0.0;SUM←0    22500
.0;FOR B←N STEP-1UNTIL Q DO SUM←SUM+SUMT×(R[B+1]*2-R[B]*2)×(U[B+1]+U[B])    22600
;MASSTR←SUM-OLDSUM;
                                        (12)
                        IF I=1THEN BEGIN HFLUX←(-TC)×DT×(3.14159265)×((R[N+1]    22700
*2-R[N]*2)×(RADIUS*2)×(T[N]-DT[N])/((Z[I]-ZD[N]/RADIUS+DZ[Y])×RADIUS/2)+    22800
(ZD[N]/RADIUS)×(RADIUS*2)×(R[N]+R[N+1])×(-DT[N])/((2-R[N+1]-R[N])×RADIUS    22900
```

```
/2))+TCG×DT×(3.14159265)×((R[N+1]*2-R[N]*2)×(RADIUS*2)×(OT[N]-1)/(ZD[N]/    23000
2)+(ZD[N]/RADIUS)×(RADIUS*2)×(R[N]+R[N+1])×((ZD[N]/RADIUS)/DZ[Y])×(T[Q]-    23100
T[Q-1])/((R[Q]-R[Q-1])×RADIUS))⍝FOR B←N-1STEP-1UNTIL Q+1DO HFLUX←HFLUX+(    23200
-TC)×DT×(3.14159265)×((R[B+1]*2-R[B]*2)×(RADIUS*2)×((T[B]-OT[B])/((Z[I]-    23300
ZD[B]/RADIUS)×2×RADIUS)+(T[B+1]-OT[B+1])/((Z[I]-ZD[B+1]/RADIUS)×2×RADIUS    23400
))+(ZD[B]/RADIUS-ZD[B+1]/RADIUS)×(RADIUS*2)×(R[B]+R[B+1])×((-OT[B]-OT[B+    23500
1])/2)/((2-R[B+1]-R[B])×RADIUS/2))+TCG×DT×(3.14159265)×((R[B+1]*2-R[B]*2    23600
)×(RADIUS*2)×((OT[B+1]+OT[B]-2)/2)/((ZD[B+1]+ZD[B])/2)+(ZD[B]-ZD[B+1])×R    23700
ADIUS×(R[B+1]+R[B])×(ZD[B]/(RADIUS×DZ[Y]))×(T[Q]-T[Q-1])/((R[Q]-R[Q-1])×    23800
RADIUS))⍝HFLUX←HFLUX+(-TC)×DT×(3.14159265)×((R[Q+1]*2-R[Q]*2)×(RADIUS*2)    23900
×(T[Q+1]-OT[Q+1])/((Z[I]-ZD[Q+1]/RADIUS)×RADIUS)+(Z[I]-ZD[Q+1]/RADIUS)×(    24000
RADIUS*2)×(R[Q]+R[Q+1])×(T[Q+1]-T[Q])/((R[Q+1]-R[Q])×RADIUS))+TCG×DT×(3.    24100
14159265)×((R[Q+1]*2-R[Q]*2)×(RADIUS*2)×((OT[Q+1]+T[Q]-2)/2)/(((ZD[Q+1]/    24200
RADIUS+DZ[Y])/2)×RADIUS)+(DZ[Y]-ZD[Q+1]/RADIUS)×(RADIUS*2)×(R[Q]+R[Q+1])    24300
×(((ZD[Q+1]/RADIUS)/DZ[Y]+1)/2)×(T[Q]-T[Q-1])/((R[Q]-R[Q-1])×RADIUS))⍝EN    24400
D⍝IF I>1THEN HFLUX←(3.14159265)×RADIUS×(-TC)×DT×((R[Q+1]+R[Q])×DZ[Y]×((T    24500
[Q+1]-T[Q])/(R[Q+1]-R[Q])+DHQ)×(1/2)+(R[Q+1]*2-R[Q]*2)×(T[Q+1]-OT[Q+1])/    24600
DZ[Y])+TCG×DT×(3.14159265)×((R[Q+1]*2-R[Q]*2)×(RADIUS*2)×(T[Q]-OT[Q])/(D    24700
Z[Y]×RADIUS)+DZ[Y]×(RADIUS*2)×(R[Q]+R[Q+1])×((T[Q]-T[Q-1]+OT[Q+1]-OT[Q])    24800
```

```
/2)/((R[Q]-R[Q-1])×RADIUS));MEQLH←HFLUX/HFG;IF I=1THEN MEQLH←MEQLH/(1+3×   24900
SPHTL×DT/(8×HFG));
```

(13)

```
                DIF[Y]←MASSTR-MEQLH;TAU←MUG×(U[Q]-U[Q-1])×UBAR/((R[Q]-   25000
R[Q-1])×RADIUS);END;IF Y=2THEN BEGIN SLOPEB←(MEQLH-OMEQLH)/(Z[I]-OZ);SLO   25100
PEA←(MASSTR-OMASSTR)/(Z[I]-OZ);END;OMEQLH←MEQLH;OMASSTR←MASSTR;OZ←Z[I];
```

(14)

```
                                                                  I   25200
F Y=1AND I≥3THEN MM2←(Z[I]+DIF[1]/(SLOPEB-SLOPEA))/Z[I-1];IF Y=1AND I≤2T   25300
HEN MM2←(1+(0.80)×MM/JT);IF Y≥2THEN BEGIN REAL XXXX;IF Y=15OR ABS(DIF[Y]   25400
/MEQLH)<0.0005THEN BEGIN TOTAL←0.0;FOR B←1STEP 1UNTIL Q DO TOTAL←TOTAL+T   25500
OTT×(R[B]*2-R[B-1]*2)×(U[B]+U[B-1]);TOTAL1←TOTAL+SUM;MTR←SUMT×(R[Q+1]*2-   25600
R[Q]*2)×(U[Q]+UO[Q+1])+TOTT×(R[Q]+R[Q+1])×DZ[Y]×(V[Q]+VO[Q+1]);HLOC1←SQR   25700
T(SQRT((TC*4)/(TERM×Z[I]×RADIUS)));HM1←(0.943)×(SQRT(SQRT((TC*4)×4/(TERM   25800
×Z[I]×RADIUS))));HLOC←TC×T[N]/((R[N+1]-R[N])×RADIUS);IF I=1THEN BEGIN OL   25900
DHLOC←HLOC;OLDHSUM←0.0;END;AVEHLOC←(OLDHLOC+HLOC)/2;HMH[I]←SUM×HFG×(1+3×   26000
SPHTL×DT/(8×HFG))×3600/((3.14159265)×D×Z[I]×RADIUS×DT);IF I=1THEN AVEHLO   26100
C←HMH[1]/3600;HTRW←AVEHLOC×(Z[I]-Z[I-1])×RADIUS;HSUM←OLDHSUM+HTRW;HM←HSU   26200
M/(Z[I]×RADIUS);NU3A[I]←HM×D/TC;IF I MOD 4=1THEN BEGIN WRITE(FL[PAGE]);W   26300
```

```
RITE(FL,FMA,HM1);WRITE(FL,FMT4,LST4);WRITE(FL,FMT1,LST1);WRITE(FL,FMT2);    26400
WRITE(FL,FMT3,LST3);END;FOR B←0STEP 1UNTIL N DO BEGIN UO[B]←U[B];VO[B]←V    26500
[B];OT[B]←T[B];CO[B]←C[B];ROO[B]←RON[B];END;OLDHSUM←HSUM;OLDHLOC←HLOC;OL    26600
DSUM←SUM;RT←RT+1;IF RT<LIM THEN BEGIN ZL←Z[I]×D/2.0;FOR B←0STEP 1UNTIL 2    26700
000 BEGIN T[B]←UO[B]←OT[B]←1.0;CO[B]←ENTC;VO[B]←0.0;END;END;HM2←HM1×SQR    26800
T(SQRT((1+(0.68)×SPHTL×DT/HFG)/(1+3×SPHTL×DT/(8×HFG))));HPHI[I]←HM/PHI;H    26900
NPHI[I]←HM1/PHI;HRPHI[I]←HM2/PHI;ABP[I]←P[I]×UBAR×UBAR×RON[0]/(144×GRAV)    27000
+14.696;RWLZ[I]←4×Z[I]×RADIUS×DT×SPHTL×((GRAV×ROL×ROL/(MUL×MUL))*0.33333    27100
)/(PRL×HFG×(1+3×SPHTL×DT/(8×HFG))×(1-ROG/ROL));DELTA[I]←1-R[Q];NUA[I]←HM    27200
×RADIUS×Z[I]/TC;NU1A[I]←HM1×RADIUS×Z[I]/TC;HM2A[I]←HM2×3600;HMA[I]←HM×36    27300
00;HLOCA[I]←HLOC×3600;HM1A[I]←HM1×3600;HLOC1A[I]←HLOC1×3600;ICG[I]←C[Q];    27400
AMB[I]←0.0;FOR B←1STEP 1UNTIL Q DO AMB[I]←(3.14159265)×RADIUS×RADIUS×(R[    27500
B]*2-R[B-1]*2)×(RON[B]+RON[B-1])×(1/8)×(C[B]+C[B-1])×(U[B]+U[B-1])×UBAR+    27600
AMB[I];ZS[I]←ZSTAR;FRE[I]←4×SUM/(MUL×(3.14159265)×D);HNFPH[I]←1.46×((FRE    27700
[I])*(-0.333333));TAUV[I]←-TAU/(GRAV×(ROL-ROG)×((MUL×MUL/(ROL×ROL×GRAV))    27800
*0.33333));TOT[I]←TOTAL1;HLOCNUC[I]←HLOC1A[I]×(SQRT(SQRT(8×HFG/(8×HFG+3×    27900
SPHTL×DT))));HMNUC[I]←HM1A[I]×(SQRT(SQRT(8×HFG/(8×HFG+3×SPHTL×DT))));IF    28000
Y=15THEN GO TO FLUSH;Y←15;BTT←I;IF U[0]<0.0THEN GO TO FLUSH;IF Z[I]<Z[I-    28100
1]THEN GO TO FLUSH;IF ABS(U[0])>10.0THEN GO TO FLUSH;IF(TIME(2)-X2)/60>8    28200
```

```
00.0THEN GO TO FLUSH;END;IF Y<15THEN BEGIN SLOPE←(DIF[Y]-DIF[Y-1])/(DZ[Y   28300
]-DZ[Y-1]);DZ[Y+1]←-DIF[Y]/SLOPE+DZ[Y];Z[I]←Z[I-1]+DZ[Y+1];GO TO HELL;EN   28400
D;END;IF I=1THEN Z[0]←ZI×REG×2;IF RT>0AND RT<LIM THEN Z[0]←(1.2)×ZD[Q+1]   28500
/RADIUS;J←JT;END;END;
```

(15)

```
                    FLUSH:WRITE(FL,FMG);FOR B←1STEP 1UNTIL BTT DO WRITE   28600
(FL,FMH,LSTH);WRITE(FL,FMB);FOR B←1STEP 1UNTIL BTT DO WRITE(FL,FMC,LSTC)   28700
;WRITE(FL,FMDA);WRITE(FL,FMD);FOR B←1STEP 1UNTIL BTT DO WRITE(FL,FME,LST   28800
E);WRITE(FL,FMZ);FOR B←1STEP 1UNTIL BTT DO WRITE(FL,FME,LSTX);WRITE(FL,F   28900
MY);FOR B←1STEP 1UNTIL BTT DO WRITE(FL,FMH,LSTW);WRITE(FL,FFZ);FOR B←1ST   29000
EP 1UNTIL BTT DO WRITE(FL,FMC,LLZ);WRITE(FL,FRM);FOR B←1STEP 1UNTIL BTT    29100
DO WRITE(FL,FMH,LSST);WRITE(FL,FM35);FOR B←1STEP 1UNTIL BTT DO WRITE(FL,   29200
FM36,LST36);WRITE(FL[PAGE]);WRITE(FL,FMT,LST);WRITE(FL,FMF,LSTF);WRITE(F   29300
L,FMTI,LSTI);WRITE(FL,FMT5,(TIME(2)-X2)/60);WRITE(FL,FMT6,(TIME(3)-X3)/6   29400
0);IF BBB≤5THEN BEGIN IF I=7000THEN BEGIN WRITE(FL[PAGE]);WRITE(FL[PAGE]   29500
);UBAR←2×UBAR;GO TO GOD;END;END ELSE BBB←BBB;END.                          29600
```

Data Read Into the Gas-Vapor Program

A typical set of data in the order it is read into the gas-vapor program is given below.

0.03731 ROG, 59.802 ROL, 0.00000843 MUG, 0.0001907 MUL, 970.3 HFG, 1.007 SPHTL, 0.0001073 TC, 212 TS, 207 TW, 0.05 ENTC, 0.000452 DABG, 0.019125 RADIUS, 25 UBAR, 0.6 L [1], 0.03 K [1], 0.75 L [2], 0.015 K [2], 0.95 L [3], 0.01 K [3], 0.995 L [4], 0.0025 K [4], 24 AA, 10 JT, 48 BT, 2 LIM, 0.000001 ZI,

```
BEGIN REAL RADIUS,D,REG,REL,ROG,ROL,MUG,MUL,UBAR,TS,TW,TC,DT,ZL,GRAV,HFG                100
,SPHTL,TERM,XO,AA,PRL,EKL,PRG,EKG,REN,HE,HW,SUM,OLDSUM,MASSTR,HFLUX,OLDH                200
FLUX,AVEHFLUX,MEQLH,ZSTAR,SLOPE,TAG,HLOC,AVEHLOC,OLDHLOC,HTRW,HSUM,OLDHS               300
UM,HM,VZG,VRG,ZI,OHQ,HZ,HX,HY,HV,HU,HT,RET,RES,WG,SUMT,NBG,NBL,SCREL,SCL               400
,YB,YA,VP1,P1,T1,P2,T2,HFG1,RS2,DABL,MMMX,CCC,BPTEM,DPTEM,CLQ,NTG,HFG2,V               500
P2,OVRG,DT5,DT6,OLDHSUM5,OLDHSUM6,HSUM5,HSUM6,AVEHLOC5,AVEHLOC6,HTRW5,HT               600
RW6,OLDHLOC5,OLDHLOC6,HM5,HM6,HM55,HM66,HLOC5,HLOC6,HLOC55,HLOC66,CQG,LS               700
2,XA,XB,AZ,BZ,CAQG,SL,TOTT,EKREL,PRREL,HS,NU1,NU2,NU3,NU,TCG,SPHTG,PHI,E               800
NTC,REPRG,REPRL,FR,FRT,PT,PTFRT,SCREG,DABG,CTERM,ROGA,ROGB,PRES,BC,CC,DC               900
,MWA,MWB,TEMP,MMM,MM2,OMEQLH,OMASSTR,OZ,SLOPEB,SLOPEA,MM,TERM2,TERM3,TAU             1000
,OLDXO,PCDIF,X2,X3,HLOC1,HLOC2,HM1,HM2,HM3,IM,TOTAL,TOTAL1,MTR;INTEGER B             1100
,I,A,N,Q,Y,S,SS,SSS,J,RT,BB,LIM,JJ,YY,BTT,YYY,YYB,YYA,ZQZ,BBB,BT,JT;REAL             1200
 ARRAY Z,P[0:80],M,L,K[1:10],DT,VW,CO,C,V,T,U,R,UO,ZD,ROO,VO[0:200],XDZ,              1300
OLDDZ,DIF,DZ[1:20],G[0:200,0:20],AVGLB,AVGGB,PCCON,ABP[0:50],CQGA,TEM,XX              1400
B,DLR,DFCAB,DFLUX[0:20],HM6A,HM5A,HPHI5,HPHI6,HRAT5,HRAT6,HLRAT5,HLRAT6[             1500
0:50],RON[0:200],TM[1:5,1:4],TI[0:80],ZS,HMA,HM1A,HM2A,HM3A,HLOCA,HLOC1A             1600
```

```
,HLOC2A,RWLZ,FRE,NUA,NU1A,HNFPH,ICG,AMB,HMH,HMNUC,HLOCNUC,TOT,HNPHI,HRPH      1700
I,DELTA,NU2A,NU3A,HPHI,TAUV[0:80],W,F,X,E,H[-1:220];FILE OUT FL 6(2,15);     1800
FILE IN DA(2,10);LABEL FLUSH,GOD,TECH;FORMAT FTB("TRY NO. ",I2,X10," Z=      1900
= ",E15.6,//);FORMAT OUT FM62("PRES = ",F10.5,X10,"TEMP = ",F10.4,/);LIS     2000
T LST62(PRES,TEMP);LIST LSST(ZS[B],Z[B]×RADIUS,FRE[B],HPHI[B]/HNFPH[B],H     2100
NFPH[B],HPHI[B],UBAR×UBAR/(GRAV×Z[B]×RADIUS));FORMAT OUT FRM("RATIOS BEL     2200
OW ARE BASED ON FILM RE NOT DISTANCE",//,X5,"ZSTAR",X10,"Z IN FT",X7,"FI     2300
LM RE",X8,"HM/HMNF",X8,"HMNF/PHI",X7,"HM/PHI",X6,"LENGTH FR NO.",//);LIS     2400
T LIS(ROG,ROL,MUG,MUL,HFG,SPHTL,TC,TS,TW,RADIUS,UBAR,L[1],K[1],L[2],K[2]     2500
,L[3],K[3],L[4],K[4],AA,JT,BT,LIM,ZI,DABG,DABL,AZ,BZ,TCG,SPHTG,P1,T1,P2,     2600
T2,CCC,BPTEM,DPTEM,HFG2,ROGA,ROGB,MWA,MWB,ENTC);FORMAT OUT FMT9("UO[",I3      2700
,"] = ",F10.7,X10,"VO[",I3,"] = ",F12.10,X10,"ZO = ",E16.7,/);LIST LST9(     2800
B,UO[B],B,VO[B],ZO[B]/RADIUS);FORMAT OUT FMF("UBAR = ",E16.7," FT/SEC",/     2900
,/,"DABG = ",X3,E14 .5," FT-FT/SEC ",X10,"DABL = ",X3,E14 .5,"FT×FT/SEC"     3000
,//,"VAN LAAR A = ",F7 .4,X10,"VAN LAAR B = ",F7 .4,//,"SCHMIDT NO. GAS      3100
= ",X3,E14 .5,X10,"SCHMIDT NO. LIQ = ",X3,E14 .5,//,"VISCOSITY GAS = ",X     3200
3,E16.7," LBM/FT×SEC ",/,"VISCOSITY LIQUID = ",E16.7," LBM/FT×SEC ",//,"     3300
DENSITY GAS = ",F16.7," LBM/FT×FT×FT",/,"DENSITY LIQUID = ",F16.7," LBM/     3400
FT×FT×FT",//,"THERMAL CONDUCTIVITY GAS = ",X3,E16.7,"BTU/SEC×FT×F",/,"TH     3500
```

```
ERMAL CONDUCTIVITY LIQUID = ",E16.7,"BTU/SEC×FT×F",//,"HEAT CAPACITY GAS      3600
 = ",X3,F16.7," BTU/LBM×F",/,"HEAT CAPACITY LIQUID = ",F16.7," BTU/LBM×F     3700
",//,"INITIAL CONCENTRATION OF B COMPONENT = ",E14 .5," W, WT CONC",//,"      3800
HFG, ENTHALPY, CHANGE OF PHASE = ",F16.7," BTU/LBM",//,"TEMPERATURE DIFF     3900
ERENCE = ",F16.7," DEG F ",//,"DIAMETER OF VERTICAL PIPE = ",F16.9," FT      4000
 OR",F16.9," INCHES",/);LIST LSTF(UBAR,DABG,DABL,AZ,BZ,MUG/(ROG×DABG),MU     4100
L/(ROL×DABL),MUG,MUL,ROG,ROL,TCG,TC,SPHTG,SPHTL,ENTC,HFG,DT,D,D×12);FORM     4200
AT OUT FMG(X7,"Z",X11,"ZSTAR",X8,"DELTA R/R",X8,"HN/PHI",X9,"HR/PHI",X11     4300
,"NU",X12,"NUN",//);FORMAT FM82("YYY = ",I3,X5,"YYA = ",I3,X5,"YYB = ",I     4400
3,X5,"CQG = ",E14 .5,//);LIST LS90(DFCAB[YYB],DLR[YYA],TEM[YYB],C[Q],CAQ     4500
G,VP1,VP2,SL);LIST LS82(YYY,YYA,YYB,CQG);FORMAT FMH(7(E14 .5,X1),X15);FO     4600
RMAT FFZ(X7,"Z IN FT",X14,"ZSTAR",X8,"INTERFACE CONC",X6,"INTERFACE TEMP     4700
",X8,"AMOUNT OF B",X15,"HMD/K",//);LIST LLZ(RADIUS×Z[B],ZS[B],ICG[B],TI[     4800
B],AMB[B],NU3A[B]);LIST LSTH(Z[B],ZS[B],DELTA[B],HNPHI[B],HRPHI[B],NUA[B     4900
],NU1A[B]);FORMAT OUT FMTI("ROG/ROL = ",E14.5,X10,"MUG/MUL = ",E14.5,X10     5000
,"TCG/TCL = ",E14.5,/,"CPG/CPL = ",E14.5,X10,"REG/REL = ",E14.5,X10,"REG     5100
/FR  = ",E14.5,//,"CPL×DT/HFG = ",E14.5,//);LIST LSTI(ROG/ROL,MUG/MUL,TC     5200
G/TC,SPHTG/SPHTL,REG/REL,REG/FR,SPHTL×DT/HFG);FORMAT FMB(/,X5,"Z IN FT",     5300
X11,"WT % COND",X9,"AV WT % B GAS",X7,"AV WT % B LIQ",X12,"TAUST",X12,"R     5400
```

```
,W,L ZST",/);FORMAT FMC(6(E14 .5,X6));LIST LSTC(Z[B]×RADIUS,PCCON[B],AVG      5500
GB[B],AVGLB[B],TAUV[B],RWLZ[B]);FORMAT OUT FMZ(X6,"ZSTAR",X8,"ZSTAR/REG"      5600
,X7,"HM/HMN",X9,"HM/HMR",X8,"HM/HMNUC",X6,"HLOC/HLOCN",X4,"HLOC/HLOCNUC"      5700
,X5,"FILM RE",//);LIST LSTX(ZS[B],ZS[B]/REG,HMA[B]/HM1A[B],HMA[B]/HM2A[B      5800
],HMA[B]/HMNUC[B],HLOCA[B]/HLOC1A[B],HLOCA[B]/HLOCNUC[B],FRE[B]);FORMAT       5900
OUT FMY(X4,"Z IN FT",X9,"ZSTAR",X7,"SCRIPT P",X8,"P - GRAV",X6,"P,LBF/IN      6000
×IN",X4,"TAUST/REG",X4,"LB/SEC IN TUBE",//);FORMAT FM35(X3,"FR LENGTH",X      6100
5,"Z IN FT",X6,"HM RATIO",X6,"HM/PHI",X4,"HLOC RATIO",X4,"2×DELTA/D",X6,      6200
"FILM RE",X6,"TAUSTAR",X10,"P",//),FM38(//,"     Z IN FT",X3,"DP HM/PHI"      6300
,X5,"BP HM/PHI",X3,"DP HM/HMN",X4,"BP HM/HMN",X4,"DP HLOC RAT",X2,"BP HL      6400
OC RAT",X3,"FILM RE",X5,"INT TEMP F",/),FM36(9(E13 .5),X3));LIST LST38(Z[      6500
B]×RADIUS,HPHI5[B],HPHI6[B],HRAT5[B],HRAT6[B],HLRAT5[B],HLRAT6[B],FRE[B]      6600
,TI[B]×DT+TW);LIST LST36(UBAR×UBAR/(GRAV×Z[B]×RADIUS),Z[B]×RADIUS,HMA[B]      6700
/HM1A[B],HPHI[B],HLOCA[B]/HLOC1A[B],DELTA[B],FRE[B],TAUV[B],P[B]);LIST L      6800
STW(Z[B]×RADIUS,ZS[B],P[B],P[B]-Z[B]×FRT,ABP[B],TAUV[B]/REG,TOT[B]);LIST      6900
 LST(REG,REL,PRL,EKL,FR);FORMAT OUT FMT("REG = ",F10.3,X5,"REL = ",F12.3      7000
,X5,"PRL = ",F10.5,X5,"EKL = ",E14.5,X5,"FR = ",E14.5,//);FORMAT OUT FMD      7100
A("HEAT TRANSFER COEF. BELOW ARE IN  BTU/HR×FT×FT×F.",////);FORMAT OUT F      7200
MD(X7,"Z",X11,"ZSTAR",X11,"HM",X13,"HLOC",X11,"HMN",X11,"HLOCN",X11,"HMR      7300
```

```
",X11,"HMH",//);FORMAT FME(8(E14 .5,X1));LIST LSTE(Z[B],ZS[B],HMA[B],HLO                    7400
CA[B],HM1A[B],HLOC1A[B],HM2A[B],HMH[B]);FORMAT OUT FMT1("MASS TRANSFERRE                    7500
D = ",E16.7,X2,"LBS/SEC.",X5,"MASS EQUIVALENT TO HEAT = ",E16.7,X2,"LBS/                    7600
SEC.",/,"DIF[",I2,"] = ",E16.7,X5,"TOTAL MASS TRANSFERRED = ",E16.7,/,"P                    7700
[",I2,"] = ",E16.7,X10,"Z[",I2,"] = ",E16.7,X5,"ZSTAR = ",E16.7,////);LI                    7800
ST LST1(MASSTR,MEQLH,Y,DIF[Y],SUM,I,P[I],I,Z[I],ZSTAR);FORMAT OUT FMT2(X                    7900
1,"B",X11,"R",X19,"U",X19,"V",X19,"VW",X19,"T",X19,"C",//);FORMAT FMT3(I                    8000
3,X7,F10 .8,5(X4,F16 .10));LIST LST3(FOR J←0STEP 3UNTIL M[4]-2,M[4]STEP                    8100
6UNTIL Q-2,Q-1,Q STEP 1UNTIL N+1DO[J,R[J],U[J],V[J],VW[J],T[J],C[J]]);FO                    8200
RMAT OUT FMT4("HLOC = ",E16.7X5,"HM = ",E16.7,X10,"INTERFACE POSITION =                    8300
",F10.8,X5,"Q = ",I3,/);LIST LST4(HLOC,HM,R[Q],Q);FORMAT OUT FMT5("PROCE                    8400
SS TIME = ",F10.4,//);FORMAT OUT FMT6("IN/OUT TIME = ",F10.4,//);FORMAT                    8500
OUT FMA("HM FOR VERTICAL TUBES, BSL 13.6-4 = ",E16.7,/);X2←TIME(2);X3←TI                    8600
ME(3);
                                        (1)
    TAG←7.0;READ(DA,/,LIS);CLOSE(DA,RELEASE);
                                        (2)
                                                BBB←0;GOD:BBB←BBB+1;ZQZ←0                    8700
;TECH:D←2×RADIUS;REL←ROL×D×UBAR/MUL;DT5←DPTEM-TW;DT6←BPTEM-TW;CQG←ENTC;I                    8800
```

```
M←(3.14159265)×(RADIUS*2)×ROG×UBAR;R[0]←0.0;P[0]←Z[0]←0.0;FOR B←0STEP 1U    8900
NTIL 2000 BEGIN U0[B]←1.0;V0[B]←0.0;0T[B]←1.0;T[B]←1.0;C0[B]←C[B]←ENTC;    9000
END;RON[0]←(1/(1+ROGA×C[0]/(ROGB×(1-C[0]))))×ROGA×(1+C[0]/(1-C[0]));FOR    9100
B←0STEP 1UNTIL 2000 RON[B]←ROO[B]←RON[0];ROG←ROO[0];REG←ROG×D×UBAR/MUG;    9200
Z[1]←ZI×REG×2;DT←TS-TW;ZL←Z[1]×D/2;GRAV←32.174;TERM←4×TC×DT×MUL/(GRAV×RO    9300
L×(ROL-ROG)×HFG×(1+3×SPHTL×DT/(HFG×8)));FR←UBAR×UBAR/(GRAV×D);FRT←1/(2×F    9400
R);PRL←MUL×SPHTL/TC;EKL←UBAR×UBAR/(SPHTL×(TS-TW));SUMT←ROL×(3.14159265)×    9500
(RADIUS*2)×UBAR/2;TOTT←ROG×(3.14159265)×(RADIUS*2)×UBAR/2;EKREL←2/(EKL×R    9600
EL);PRREL←PRL×REL;PHI←TC×((ROL×ROL×GRAV/(MUL×MUL))*0.33333);SCREG←UBAR×D    9700
/DABG;SCREL←UBAR×D/DABL;PRG←MUG×SPHTG/TCG;EKG←UBAR×UBAR/(SPHTG×DT);JJ←0;    9800
RT←0;I←0;FOR BB←1STEP 1UNTIL BT DO BEGIN REAL QQQQQ;LABEL BURNS,ESSO,TEX    9900
AS,HELL,SLEEP,TOWN;I←I+1;IF RT<LIM THEN I←1;
```

(3) AND (4)

```
                                        IF RT=0THEN X0←SQRT(SQRT(TER   10000
M×ZL));IF RT<LIM AND RT>0THEN BEGIN TERM2←4×TAU/(3×(ROL-ROG)×GRAV);FOR A   10100
←1STEP 1UNTIL 2000 BEGIN OLDX0←X0;IF TERM×ZL+TERM2×(X0*3)≤0THEN X0←X0/2.   10200
0ELSE X0←SQRT(SQRT(TERM×ZL+TERM2×(X0*3)));PCDIF←(X0-OLDX0)×100/X0;END;EN   10300
D;J←JT;IF I=1THEN BEGIN IF 1-4×AA×X0/(RADIUS×J)≤2×K[1]THEN GO TO FLUSH;B   10400
EGIN REAL XXXXX;IF L[4]≥1-4×AA×X0/(RADIUS×J)THEN BEGIN FOR B←1STEP 1UNTI   10500
```

```
L 3960 IF L[4]≥1-4×AA×XO/(RADIUS×J)THEN L[4]←L[4]-K[4]ELSE B←397;END;IF   10600
 L[3]≥L[4]THEN BEGIN FOR B←1STEP 1UNTIL 800 IF L[3]≥L[4]THEN L[3]←L[3]-   10700
K[3]ELSE B←81;K[4]←L[4]-L[3];END;IF L[2]≥L[3]THEN BEGIN FOR B←1STEP 1UNT   10800
IL 800 IF L[2]≥L[3]THEN L[2]←L[2]-K[2]ELSE B←81;K[3]←L[3]-L[2];END;IF L   10900
[1]≥L[2]THEN BEGIN FOR B←1STEP 1UNTIL 800 IF L[1]≥L[2]THEN L[1]←L[1]-K[   11000
1]ELSE B←81;K[2]←L[2]-L[1];END;L[5]←1-4×AA×XO/(RADIUS×J);K[5]←L[5]-L[4];   11100
L[6]←1-AA×XO/(RADIUS×J);K[6]←2×XO/(RADIUS×J);L[7]←1.001;K[7]←XO/(RADIUS×   11200
J);A←1;END;FOR B←1STEP 1UNTIL 2000 BEGIN IF R[B-1]>(0.9999)×L[A]THEN BE   11300
GIN R[B]←R[B-1]+K[A+1];M[A]←B-1;A←A+1;END ELSE R[B]←R[B-1]+K[A];IF R[B]>   11400
0.999999THEN BEGIN N←B-1;U[B]←UO[B]←0.0;GO TO SLEEP;END;END;SLEEP:END;BE   11500
GIN REAL XXXXX;IF I=J THEN OHQ←(OT[Q+1]-OT[Q])/(R[Q+1]-R[Q]);IF I=J THEN   11600
 BEGIN A←(1+N-M[6])/2;FOR B←0STEP 1UNTIL A DO BEGIN R[M[6]+B]←R[M[6]+2×B   11700
];UO[M[6]+B]←UO[M[6]+2×B];VO[M[6]+B]←VO[M[6]+2×B];OT[M[6]+B]←OT[M[6]+2×B   11800
];CO[M[6]+B]←CO[M[6]+2×B];END;U[M[6]+A]←0.0;N←M[6]+(N-M[6]-1)/2;JJ←J/2+(   11900
I-2)/2;END;Q←N-I-J+2+JJ;IF I≠J THEN OHQ←(OT[Q+2]-OT[Q+1])/(R[Q+2]-R[Q+1]   12000
);IF RT=0THEN BEGIN FOR B←Q+1STEP 1UNTIL N DO BEGIN UO[B]←GRAV×(ROL-ROG)   12100
×(((1-R[B])×RADIUS)*2)/(2×MUL×UBAR);ZD[B]←(((1-R[B])×RADIUS)*4)/TERM;VO[   12200
B]←(GRAV×(ROL-ROG)×(((1-R[B])×RADIUS)*2)/(4×MUL))×(SQRT(SQRT(TERM/(ZD[B]   12300
*3))))/UBAR;END;END;IF RT<LIM AND RT>0THEN BEGIN TERM3←ROL×TAU×HFG×(1+3×   12400
```

```
SPHTL×DT/(HFG×8))/(3×MUL×TC×DT);FOR B←Q+1STEP 1UNTIL N DO BEGIN UO[B]←GR    12500
AV×(ROL-ROG)×(((1-R[B])×RADIUS)*2)/(2×MUL×UBAR)-TAU×(1-R[B])×RADIUS/(MUL    12600
×UBAR);ZD[B]←(((1-R[B])×RADIUS)*4)/TERM-(((1-R[B])×RADIUS)*3)×TERM3;VO[B    12700
]←TC×DT/(ROL×(1-R[B])×RADIUS×HFG×(1+3×SPHTL×DT/(HFG×8))×UBAR);END;END;EN    12800
D;IF I=1THEN OVRG←VO[Q+1];
```

(5)

```
                    Y←0;IF I=1THEN Z[0]←ZI×REG×2;IF RT>0AND RT<LIM    12900
 THEN Z[0]←(1.2)×ZD[Q+1]/RADIUS;MM←60.0;IF I=2THEN MM←6.0;IF I=1OR I=2TH    13000
EN MMM←(1+MM/J)ELSE MMM←Z[I-1]/Z[I-2];FOR Z[I]←MMM×Z[I-1],MM2×Z[I-1]DO B    13100
EGIN
```

(6)

```
    HELL;Y←Y+1;IF I=1THEN Z[0]←0.0;YY←0;TOWN;YY←YY+1;YYY←0;DZ[Y]←Z[I]-Z    13200
[I-1];ZSTAR←Z[I]/(2×REG);HE←R[1]-R[0];FOR B←0STEP 1UNTIL Q DO RON[B]←(1/    13300
(1+ROGA×C[B]/(ROGB×(1-C[B]))))×ROGA×(1+C[B]/(1-C[B]));RON[Q]←(1/(1+ROGA×    13400
CQG/(ROGB×(1-CQG))))×ROGA×(1+CQG/(1-CQG));FOR B←Q+1STEP 1UNTIL N DO ROO[    13500
B]←RON[B]←ROL;REN←RON[0]×UBAR×D/MUG;H[0]←8/(REN×HE×HE)+UO[0]/DZ[Y];X[1]←    13600
-8/(REN×HE×HE);WG←1/DZ[Y];FOR B←0STEP 1UNTIL Q DO BEGIN W[B]←(RON[0]/RON    13700
[B])×(1+(RON[B]-ROO[B])/RON[B])/DZ[Y];F[B]←((UO[B]*2)+(ROO[0]/ROO[B])×P[    13800
I-1])/DZ[Y]+FRT;END;WG←(ROG/ROL)/DZ[Y];PT←ROG×P[I-1]/(ROL×DZ[Y]);PTFRT←P    13900
```

```
T←FRT;FOR B←Q+1STEP 1UNTIL N DO BEGIN IF I=1THEN XDZ[Y]←Z[I]-ZD[B]/RADIU    14000
S;IF I>1THEN XDZ[Y]←DZ[Y];W[B]←(RON[0]/ROL)/DZ[Y];F[B]←(UO[B]*2)/XDZ[Y]+    14100
(ROO[0]/ROL)×P[I-1]/DZ[Y]←FRT;END;W[Q]←F[Q]←0.0;FOR B←0STEP 1UNTIL N DO    14200
FOR J←0STEP 1UNTIL 12DO G[B,J]←0.0;FOR J←N+1STEP 1UNTIL N+13DO BEGIN W[J    14300
]←F[J]←X[J]←0.0;END;E[N]←0.0;G[0,0]←R[1]×RON[0]/(4×DZ[Y]);G[1,0]←3×R[1]×    14400
RON[1]/(4×DZ[Y]);OLDDZ[Y]←DZ[Y];S←SS←0;HE←R[1]-R[0];HW←HE;HV←HE×HE×(2.0)    14500
;HU←HV;HT←0.0;HZ←HE/HV;HY←HZ;A←1;BEGIN REAL QQQ;FOR B←1STEP 1UNTIL N-1DO    14600
 BEGIN LABEL GIRL,SCHOOL;IF B<Q THEN REN←RON[B]×D×UBAR/MUG;IF B=Q THEN R    14700
EN←REL;IF I=1AND B>Q THEN DZ[Y]←Z[I]-ZD[B]/RADIUS;IF B=Q OR B=M[A]THEN B    14800
EGIN A←A+1;HE←R[B+1]-R[B];HW←R[B]-R[B-1];HV←HW×(HW+HE);HU←HE×(HW+HE);HT←    14900
(HW-HE)/(HW×HE);HZ←HE/HV;HY←HW/HU;E[B-1]←-HZ×VO[B]-4/(REN×HV)+2×HZ/(REN×    15000
R[B]);H[B]←UO[B]/DZ[Y]-HT×VO[B]+4/(REN×HW×HE)+2×HT/(REN×R[B]);X[B+1]←HY×    15100
VO[B]-4/(REN×HU)-2×HY/(REN×R[B]);HW←HE;HV←HU←2×HE×HE;HZ←HY←1/(2×HE);END    15200
ELSE BEGIN E[B-1]←-HZ×VO[B]-4/(REN×HV)+2×HZ/(REN×R[B]);H[B]←UO[B]/DZ[Y]+    15300
8/(REN×HV);X[B+1]←HY×VO[B]-4/(REN×HV)-2×HY/(REN×R[B]);END;IF Q≤M[6]THEN    15400
M[6]←0;IF B>1THEN BEGIN FOR J←1STEP 1UNTIL TAG DO IF B=M[J]THEN BEGIN S←    15500
S+1;GO TO GIRL;END;IF B=Q THEN BEGIN SS←1;GO TO GIRL;END;IF B=Q+1THEN BE    15600
GIN SS←2;GO TO GIRL;END;G[B,SS+S]←R[B]×RON[B]/DZ[Y];F[N+S+1+SS]←F[N+S+1+    15700
SS]+R[B]×UO[B]×ROO[B]/DZ[Y];GO TO SCHOOL;GIRL;G[B,S-1+SS]←R[B]×RON[B]/(2    15800
```

```
xDZ[Y]);G[B,S+SS]←G[B,S-1+SS]);F[N+S+SS]←R[B]×ROO[B]×UO[B]/(2×DZ[Y])+F[N+    15900
S+SS]);F[N+S+1+SS]←R[B]×ROO[B]×UO[B]/(2×DZ[Y]);IF S=1THEN F[N+S]←F[N+S]+U    16000
O[1]×ROO[1]×3×R[1]/(4×DZ[Y])+UO[0]×R[1]×ROO[0]/(4×DZ[Y]);H[N+S+SS]←RON[B    16100
]×R[B]/(R[B]-R[B-1]);E[N+S+SS]←-RON[B]×R[B]/(R[B+1]-R[B]);IF SS=1THEN BE    16200
GIN IF I=1THEN DZ[Y]←Z[I]-ZD[Q+1]/RADIUS;F[N+S+SS+1]←0.0;E[N+S+SS]←-(RON    16300
[Q]/ROL)×R[Q]/(R[Q+1]-R[Q]);G[B,S+SS]←-(((RON[Q]/ROL)-1)×R[Q]/DZ[Y]);END    16400
;IF SS=2THEN BEGIN F[N+S+SS]←UO[Q+1]×R[Q+1]/DZ[Y];G[B,S+SS-1]←R[Q+1]/DZ[    16500
Y];H[N+S+SS]←R[Q+1]/HE;END;SCHOOL;END;END;END;BEGIN REAL XXX;IF I=1THEN     16600
DZ[Y]←Z[I]-ZD[N]/RADIUS;E[N-1]←-VO[N]×HE/(HW×(HW+HE))-4/(REN×HW×(HE+HW))    16700
+2×HE/(REN×R[N]×HW×(HW+HE));H[N]←UO[N]/DZ[Y]-VO[N]×(HW-HE)/(HW×HE)+4/(RE    16800
N×HW×HE)+2×(HW-HE)/(REN×R[N]×HW×HE);E[Q-1]←-MUG/(R[Q]-R[Q-1]);H[Q]←MUG/(    16900
R[Q]-R[Q-1])+MUL/(R[Q+1]-R[Q]);X[Q+1]←-MUL/(R[Q+1]-R[Q]);G[N,S+SS]←R[N]×    17000
RON[N]/DZ[Y];F[N+S+1+SS]←F[N+S+1+SS]+R[N]×UO[N]×ROO[N]/DZ[Y];
```

(7)

```
                                                          DZ[Y]←OLDDZ    17100
[Y];S←0;SSS←0;FOR B←0STEP 1UNTIL N-1DO BEGIN F[B]←F[B]/H[B];W[B]←W[B]/H[    17200
B];X[B+1]←X[B+1]/H[B];F[B+1]←F[B+1]-F[B]×E[B];W[B+1]←W[B+1]-W[B]×E[B];H[    17300
B+1]←H[B+1]-X[B+1]×E[B];IF ABS(G[B,S+1])>0THEN BEGIN S←S+1;SSS←SSS+1;END    17400
;FOR J←0STEP 1UNTIL SSS DO BEGIN F[N+1+J]←F[N+1+J]-F[B]×G[B,J];W[N+1+J]←    17500
```

```
W[N+1+J]-W[B]×G[B,J]};G[B+1,J]←G[B+1,J]-X[B+1]×G[B,J]};END};END};F[N]←F[N]/H   17600
[N]};W[N]←W[N]/H[N]};FOR S←OSTEP 1UNTIL SSS DO BEGIN F[N+1+S]←F[N+1+S]-F[N   17700
]×G[N,S]};W[N+1+S]←W[N+1+S]-W[N]×G[N,S]};END};FOR B←N+1STEP 1UNTIL SSS+N DO   17800
 BEGIN F[B]←F[B]/H[B]};W[B]←W[B]/H[B]};F[B+1]←F[B+1]-F[B]×E[B]};W[B+1]←W[B+   17900
1]-W[B]×E[B]};END};P[I]←F[N+1+SSS]/W[N+1+SSS]};U[N]←F[N]-W[N]×P[I]};FOR B←N-   18000
1STEP-1UNTIL ODO U[B]←F[B]-W[B]×P[I]-X[B+1]×U[B+1]};VZG←U[Q]};
```



```
                                                        DZ[Y]←Z[I]-Z   18100
[I-1]};HE←R[1]-R[0]};V[1]←-HE×(RON[1]×U[1]+RON[0]×U[0]-ROO[1]×UO[1]-ROO[0]   18200
×UO[0])/(4×DZ[Y]×RON[1])};FOR B←2STEP 1UNTIL N+1DO BEGIN IF B≤Q THEN V[B]   18300
←((-R[B]×(RON[B]×U[B]-ROO[B]×UO[B])-R[B-1]×(RON[B-1]×U[B-1]-ROO[B-1]×UO[   18400
B-1]))/(2×DZ[Y])+RON[B-1]×V[B-1]×R[B-1]/(R[B]-R[B-1]))×(R[B]-R[B-1])/(RO   18500
N[B]×R[B])};IF B=Q+1THEN BEGIN XDZ[Y]←DZ[Y]};IF I=1THEN DZ[Y]←Z[I]-ZD[B]/R   18600
ADIUS};VRG←V[Q]};V[Q]←(U[Q]×(R[Q+1]-R[Q])/DZ[Y])×((RON[Q]/ROL)-1)+VRG×(RON   18700
[Q]/ROL)};V[Q+1]←(R[Q+1]×UO[Q+1]/DZ[Y]-U[Q+1]×R[Q+1]/DZ[Y]+V[Q]×R[Q]/(R[Q   18800
+1]-R[Q]))×(R[Q+1]-R[Q])/R[Q+1]};END};IF B>Q+1THEN BEGIN XDZ[Y]←DZ[Y]};IF I   18900
=1THEN DZ[Y]←Z[I]-ZD[B]/RADIUS};V[B]←(V[B-1]×R[B-1]/(R[B]-R[B-1])-R[B-1]×   19000
(U[B-1]-UO[B-1])/(2×XDZ[Y])-R[B]×(U[B]-UO[B])/(2×DZ[Y]))×(R[B]-R[B-1])/R   19100
[B]};END};END};END};
```

(8A)

```
IF I=1THEN MMMX←CCC×ENTC;IF I>1THEN MMMX←CQG;BURNS;YYY←Y                    19200
YY+1;IF YYY=1THEN CQGA[1]←MMMX;IF YYY=2THEN CQGA[2]←1.1×MMMX;C[Q]←CQG←CQ    19300
GA[YYY];DZ[Y]←OLDDZ[Y];HE←R[1]-R[0];HW←HE;HV←HE×HE×(2.0);HU←HV;HT←0.0;HZ     19400
←HE/HV;HY←HZ;A←1;H[0]←-8/(SCREG×HE×HE)-U[0]/DZ[Y];X[1]←8/(SCREG×HE×HE);F    19500
[0]←-U[0]×CO[0]/DZ[Y];FOR B←1STEP 1UNTIL Q-1DO BEGIN IF B=Q OR B=M[A]THE     19600
N BEGIN A←A+1;HE←R[B+1]-R[B];HW←R[B]-R[B-1];HV←HW×(HW+HE);HU←HE×(HW+HE);     19700
HT←(HW-HE)/(HW×HE);HZ←HE/HV;HY←HW/HU;E[B-1]←-HZ×V[B]-4/(SCREG×HV)+2×HZ/(     19800
SCREG×R[B]);H[B]←U[B]/DZ[Y]-HT×V[B]+4/(SCREG×HE×HW)+2×HT/(SCREG×R[B]);X[     19900
B+1]←HY×V[B]-4/(SCREG×HU)-2×HY/(SCREG×R[B]);HW←HE;HV←HU←2×HE×HE;HZ←HY←1/     20000
(2×HE);END ELSE BEGIN E[B-1]←-HZ×V[B]-4/(SCREG×HV)+2×HZ/(SCREG×R[B]);H[B     20100
]←U[B]/DZ[Y]+8/(SCREG×HV);X[B+1]←HY×V[B]-4/(SCREG×HU)-2×HY/(SCREG×R[B]);     20200
END;F[B]←CO[B]×U[B]/DZ[Y];END;F[Q-1]←F[Q-1]-C[Q]×X[Q];
```

(8B)

```
                                                    FOR B←0STEP 1UNTIL      20300
 Q-2DO BEGIN F[B]←F[B]/H[B];X[B+1]←X[B+1]/H[B];F[B+1]←F[B+1]-F[B]×E[B];H     20400
[B+1]←H[B+1]-X[B+1]×E[B];END;C[Q-1]←F[Q-1]/H[Q-1];FOR B←Q-2STEP-1UNTIL 0    20500
DO C[B]←F[B]-X[B+1]×C[B+1];
```

(8B1)

```
                                YB←(CQG/MWB)/(CQG/MWB+(1-CQG)/MWA)⍝YA←1-YB⍝YY   20600
B←0⍝FOR TEM[YYB+1]←TS⍵TS-DT/3DO BEGIN TEXAS⍝YYB←YYB+1⍝VP1←P1×((2.71828)*   20700
((-HFG×MWA/(1.986))×(1/(TEM[YYB]+459.69)-1/T1)))⍝VP2←P2×((2.71828)*((-HF   20800
G2×MWB/(1.986))×(1/(TEM[YYB]+459.69)-1/T2)))⍝RS2←(14.696)×YB/VP2⍝YYA←0⍝F   20900
OR C[Q]←ENTC⍵(0.9)×ENTC DO BEGIN ESSO⍝YYA←YYA+1⍝XXB[YYA]←XB←(C[Q]/MWB)/(   21000
C[Q]/MWB+(1-C[Q])/MWA)⍝XA←1-XB⍝LS2←XB×((10.0)*(AZ×XA×XA/((AZ×XB/BZ+XA)*2   21100
)))⍝DLR[YYA]←LS2-RS2⍝IF YYA≥2THEN IF ABS(DLR[YYA]/RS2)>0.0005AND YYA<20T   21200
HEN BEGIN SL←(DLR[YYA]-DLR[YYA-1])/(XXB[YYA]-XXB[YYA-1])⍝XXB[YYA+1]←-DLR   21300
[YYA]/SL+XXB[YYA]⍝C[Q]←XXB[YYA+1]×MWB/(XXB[YYA+1]×MWB+(1-XXB[YYA+1])×MWA   21400
)⍝GO TO ESSO⍝END⍝END⍝CAQG←(10.0)*(BZ×XB×XB/((XB+BZ×XA/AZ)*2))⍝CAQG←CAQG×   21500
VP1×XA/14.696⍝CAQG←(CAQG×MWA)/(CAQG×MWA+(1-CAQG)×MWB)⍝DFCAB[YYB]←CAQG-1+   21600
CQG⍝IF YYB≥2THEN IF ABS(DFCAB[YYB]/CQG)>0.0005AND YYB<10THEN BEGIN SL←(D   21700
FCAB[YYB]-DFCAB[YYB-1])/(TEM[YYB]-TEM[YYB-1])⍝TEM[YYB+1]←-DFCAB[YYB]/SL+   21800
TEM[YYB]⍝GO TO TEXAS⍝END⍝END⍝
```

(8B2), (8B3), AND (8B4)

```
                  IF I=1THEN FOR B←Q+1STEP 1UNTIL N DO CO[B]←   21900
C[Q]⍝CLQ←C[Q]⍝IF I>1THEN BEGIN HE←R[Q+1]-R[Q]⍝FOR B←Q+1STEP 1UNTIL N DO   22000
BEGIN IF I=1THEN DZ[Y]←Z[I]-ZD[B]/RADIUS⍝E[B-1]←-V[B]/(2×HE)-4/(SCREL×(2   22100
.0)×HE×HE)+1/(SCREL×R[B]×HE)⍝H[B]←U[B]/DZ[Y]+4/(SCREL×HE×HE)⍝X[B+1]←+V[B   22200
```

```
]/(2×HE)-4/(SCREL×(2.0)×HE×HE)-1/(SCREL×R[B]×HE)};F[B]←CO[B]×U[B]/DZ[Y]};E   22300
ND};F[Q+1]←F[Q+1]-C[Q]×E[Q]};H[N]←H[N]+X[N+1]};FOR B←Q+1STEP 1UNTIL N-1DO B   22400
EGIN F[B]←F[B]/H[B]};X[B+1]←X[B+1]/H[B]};F[B+1]←F[B+1]-F[B]×E[B]};H[B+1]←H[   22500
B+1]-X[B+1]×E[B]};END};C[N]←F[N]/H[N]};FOR B←N-1STEP-1UNTIL Q+1DO C[B]←F[B]   22600
-X[B+1]×C[B+1]};C[N+1]←C[N]};END};BEGIN REAL XXXXXXX};NTG←RON[Q]×(3.14159265   22700
)×RADIUS×RADIUS×UBAR×(U[Q]×(R[Q+1]↑2-R[Q]*2)+VRG×(R[Q+1]+R[Q])×DZ[Y])};IF   22800
 I=1THEN DZ[Y]←Z[I]-ZD[Q+1]/RADIUS};NBG←RON[Q]×(3.14159265)×((R[Q+1])*2-(   22900
R[Q])*2)×CQG×U[Q]×RADIUS×UBAR×RADIUS+RON[Q]×(3.14159265)×(R[Q+1]+R[Q])×D   23000
Z[Y]×CQG×VRG×RADIUS×RADIUS×UBAR-RON[Q]×(3.14159265)×RADIUS×((R[Q+1])*2-(   23100
R[Q])*2)×(CQG-CO[Q])×DABG/OLDDZ[Y]-RON[Q]×(3.14159265)×RADIUS×(R[Q+1]+R[   23200
Q])×DZ[Y]×(CQG-C[Q-1])×DABG/(R[Q+1]-R[Q])};NBL←ROL×(3.14159265)×((R[Q+1])   23300
*2-(R[Q])*2)×C[Q]×U[Q]×RADIUS×RADIUS×UBAR+ROL×(3.14159265)×(R[Q+1]+R[Q])   23400
×DZ[Y]×C[Q]×V[Q]×RADIUS×RADIUS×UBAR-ROL×(3.14159265)×((R[Q+1])*2-(R[Q])*   23500
2)×RADIUS×(C[Q+1]-CO[Q+1])×DABL/DZ[Y]-ROL×(3.14159265)×RADIUS×(R[Q+1]+R[   23600
Q])×DZ[Y]×(C[Q+1]-C[Q])×DABL/(R[Q+1]-R[Q])};DZ[Y]←OLDDZ[Y]};END};IF I=1THEN   23700
 BEGIN C[Q]←NBG/NTG};FOR B←Q+1STEP 1UNTIL N+1DO C[B]←C[Q]};DFLUX[YYY]←C[Q]   23800
-CLQ};IF YYY=1THEN GO TO BURNS};NBL←CLQ};END ELSE
```

(8B5)

```
                                        BEGIN DFLUX[YYY]←NBG-NBL};   23900
```

```
IF YYY=1THEN GO TO BURNS;END;IF YYY=12THEN BEGIN WRITE(FL,FMT2);WRITE(FL    24000
,FMT3,LST3);ZQZ←ZQZ+1;ZI←ZI×3;IF ZQZ<5AND I<4THEN BEGIN WRITE(FL,FTB,ZQZ    24100
,ZI);GO TO TECH;END ELSE GO TO FLUSH;END;IF ABS(DFLUX[YYY]/NBL)>0.0005AN    24200
D YYY<15THEN BEGIN SL←(DFLUX[YYY]-DFLUX[YYY-1])/(CQGA[YYY]-CQGA[YYY-1]);    24300
CQGA[YYY+1]←-DFLUX[YYY]/SL+CQGA[YYY];IF CQGA[YYY+1]<0.0THEN CQGA[YYY+1]←    24400
CQGA[YYY]/3;IF CQGA[YYY+1]>1.0THEN CQGA[YYY+1]←CQGA[YYY]+(1-CQGA[YYY])/2    24500
;GO TO BURNS;END;IF C[N+1]<0.0THEN BEGIN ZQZ←ZQZ+1;ZI←ZI×3;IF ZQZ<5AND I    24600
<4THEN BEGIN WRITE(FL,FTB,ZQZ,ZI);WRITE(FL,FMT2);WRITE(FL,FMT3,LST3);GO    24700
TO TECH;END ELSE GO TO FLUSH;END;
```

(8C)

```
IF YY<2THEN BEGIN GO TO TOWN;END;
```

(8E)

```
                                                          BEGIN    24800
REAL QQQ;T[Q]←TI[I]←(TEM[YYB]-TW)/DT;HE←R[I]-R[0];HW←HE;HV←2×HE×HE;HU←HV    24900
;HT←0.0;HZ←HY←HE/HV;A←1;REN←RON[0]×D×UBAR/MUG;H[0]←8/(REN×PRG×HE×HE)+U[0    25000
]/DZ[Y];X[1]←-8/(REN×PRG×HE×HE);F[0]←U[0]×DT[0]/DZ[Y];DT[N+1]←0.0;T[N+1]    25100
←0.0;FOR B←1STEP 1UNTIL Q-1DO BEGIN REN←RON[B]×D×UBAR/MUG;REPRG←REN×PRG;    25200
IF B=Q OR B=M[A]THEN BEGIN A←A+1;HE←R[B+1]-R[B];HW←R[B]-R[B-1];HV←HW×(HW    25300
+HE);HU←HE×(HW+HE);HT←(HW-HE)/(HW×HE);HZ←HE/HV;HY←HW/HU;E[B-1]←-HZ×V[B]+    25400
```

```
2×HZ/(REPRG×R[B])-4/(REPRG×HV)}H[B]←U[B]/DZ[Y]-HT×V[B]+2×HT/(REPRG×R[B])   25500
+4/(REPRG×HE×HW)}X[B+1]←HY×V[B]-2×HY/(REPRG×R[B])-4/(REPRG×HU)}F[B]←U[B]   25600
×OT[B]/DZ[Y]+(2/(REN×EKG))×((HY×U[B+1]-HT×U[B]-HZ×U[B-1])*2)}HW←HE}HV←HU   25700
←2×HE×HE}HZ←HY←1/(2×HE)}END ELSE BEGIN E[B-1]←-HZ×V[B]+2×HZ/(REPRG×R[B])   25800
-4/(REPRG×HV)}H[B]←U[B]/DZ[Y]+8/(REPRG×HV)}X[B+1]←HY×V[B]-2×HY/(REPRG×R[   25900
B])-4/(REPRG×HU)}F[B]←U[B]×OT[B]/DZ[Y]+(2/(REN×EKG))×((HY×U[B+1]-HZ×U[B-   26000
1])*2)}END}END}F[Q-1]←F[Q-1]-X[Q]×T[Q]}
```

(8F)

```
                                        FOR B←0STEP 1UNTIL Q-2DO BEGIN F[   26100
B]←F[B]/H[B]}X[B+1]←X[B+1]/H[B]}F[B+1]←F[B+1]-F[B]×E[B]}H[B+1]←H[B+1]-X[   26200
B+1]×E[B]}END}T[Q-1]←F[Q-1]/H[Q-1]}FOR B←Q-2STEP-1UNTIL 0DO T[B]←F[B]-X[   26300
B+1]×T[B+1]}END}
```

(9)

```
                IF I=1THEN FOR B←Q+1STEP 1UNTIL N DO OT[B]←TI[I]}DZ[Y]←O   26400
LDDZ[Y]}HE←R[Q+2]-R[Q+1]}HW←R[Q+1]-R[Q]}HU←HV←2×HE×HE}HZ←HY←HE/HV}REPRL←   26500
REL×PRL}HT←2/(REL×EKL)}OT[N+1]←0.0}T[N+1]←0.0}FOR B←Q+1STEP 1UNTIL N DO   26600
BEGIN IF I=1THEN DZ[Y]←Z[I]-ZD[B]/RADIUS}E[B-1]←-HZ×V[B]+2×HZ/(REPRL×R[B   26700
])-4/(REPRL×HV)}H[B]←U[B]/DZ[Y]+8/(REPRL×HV)}X[B+1]←HY×V[B]-2×HY/(REPRL×   26800
R[B])-4/(REPRL×HU)}F[B]←U[B]×OT[B]/DZ[Y]+HT×((HY×U[B+1]-HZ×U[B-1])*2)}EN   26900
```

```
D;F[Q+1]←F[Q+1]-E[Q]×T[Q];
                                    (10)
                          FOR B←Q+1STEP 1UNTIL N-1DO BEGIN F[B]←F[B]/H[B   27000
];X[B+1]←X[B+1]/H[B];F[B+1]←F[B+1]-F[B]×E[B];H[B+1]←H[B+1]-X[B+1]×E[B];E   27100
ND;T[N]←F[N]/H[N];FOR B←N-1STEP-1UNTIL Q+1DO T[B]←F[B]-X[B+1]×T[B+1];BEG   27200
IN REAL XXXX;DZ[Y]←OLDDZ[Y];
                                    (11)
                            IF I=1THEN OLDSUM←0.0;SUM←0.0;FOR B←N STEP-1    27300
UNTIL Q DO SUM←SUM+SUMT×(R[B+1]*2-R[B]*2)×(U[B+1]+U[B]);MASSTR←SUM-OLDSU   27400
M;
                                    (12)
  IF I=1THEN BEGIN HFLUX←(-TC)×DT×(3.14159265)×((R[N+1]*2-R[N]*2)×(RADIU   27500
S*2)×(T[N]-OT[N])/((Z[I]-ZD[N]/RADIUS+DZ[Y])×RADIUS/2)+(ZD[N]/RADIUS)×(R   27600
ADIUS*2)×(R[N]+R[N+1])×(-OT[N])/((2-R[N+1]-R[N])×RADIUS/2))+TC_G×DT×(3.14   27700
159265)×((R[N+1]*2-R[N]*2)×(RADIUS*2)×(OT[N]-1)/(ZD[N]/2)+(ZD[N]/RADIUS)   27800
×(RADIUS*2)×(R[N]+R[N+1])×((ZD[N]/RADIUS)/DZ[Y])×(T[Q]-T[Q-1])/((R[Q]-R[   27900
Q-1])×RADIUS));FOR B←N-1STEP-1UNTIL Q+1DO HFLUX←HFLUX+(-TC)×DT×(3.141592   28000
65)×((R[B+1]*2-R[B]*2)×(RADIUS*2)×((T[B]-OT[B])/((Z[I]-ZD[B]/RADIUS)×2×R   28100
ADIUS)+(T[B+1]-OT[B+1])/((Z[I]-ZD[B+1]/RADIUS)×2×RADIUS))+(ZD[B]/RADIUS-   28200
```

```
ZD[B+1]/RADIUS)×(RADIUS*2)×(R[B]+R[B+1])×((-OT[B]-OT[B+1])/2)/((2-R[B+1]   28300
-R[B])×RADIUS/2))+TCG×DT×(3.14159265)×((R[B+1]*2-R[B]*2)×(RADIUS*2)×((OT   28400
[B+1]+OT[B]-2)/2)/((ZD[B+1]+ZD[B])/2)+(ZD[B]-ZD[B+1])×RADIUS×(R[B+1]+R[B   28500
])×(ZD[B]/(RADIUS×DZ[Y]))×(T[Q]-T[Q-1])/((R[Q]-R[Q-1])×RADIUS));HFLUX←HF   28600
LUX+(-TC)×DT×(3.14159265)×((R[Q+1]*2-R[Q]*2)×(RADIUS*2)×(T[Q+1]-OT[Q+1])   28700
/((Z[I]-ZD[Q+1]/RADIUS)×RADIUS)+(Z[I]-ZD[Q+1]/RADIUS)×(RADIUS*2)×(R[Q]+R   28800
[Q+1])×(T[Q+1]-T[Q])/((R[Q+1]-R[Q])×RADIUS))+TCG×DT×(3.14159265)×((R[Q+1   28900
]*2-R[Q]*2)×(RADIUS*2)×((OT[Q+1]+T[Q]-2)/2)/(((ZD[Q+1]/RADIUS+DZ[Y])/2)×   29000
RADIUS)+(DZ[Y]-ZD[Q+1]/RADIUS)×(RADIUS*2)×(R[Q]+R[Q+1])×(((ZD[Q+1]/RADIU   29100
S)/DZ[Y]+1)/2)×(T[Q]-T[Q-1])/((R[Q]-R[Q-1])×RADIUS));END;IF I>1THEN HFLU   29200
X←(3.14159265)×RADIUS×(-TC)×DT×((R[Q+1]+R[Q])×DZ[Y]×((T[Q+1]-T[Q])/(R[Q+   29300
1]-R[Q])+OHQ)×(1/2)+(R[Q+1]*2-R[Q]*2)×(T[Q+1]-OT[Q+1])/DZ[Y])+TCG×DT×(3.   29400
14159265)×((R[Q+1]*2-R[Q]*2)×(RADIUS*2)×(T[Q]-OT[Q])/(DZ[Y]×RADIUS)+DZ[Y   29500
]×(RADIUS*2)×(R[Q]+R[Q+1])×((T[Q]-T[Q-1]+OT[Q+1]-OT[Q])/2)/((R[Q]-R[Q-1]   29600
)×RADIUS));MEQLH←HFLUX/(985-690×CQG+85.0×C[Q]);IF I=1THEN MEQLH←MEQLH/(1   29700
+3×SPHTL×DT/(8×HFG));
```



```
DIF[Y]←MASSTR-MEQLH;TAU←MUG×(U[Q]-U[Q-1])×UBAR/((R[   29800
Q]-R[Q-1])×RADIUS);END;IF Y=2THEN BEGIN SLOPEB←(MEQLH-OMEQLH)/(Z[I]-OZ);   29900
```

```
SLOPEA←(MASSTR-OMASSTR)/(Z[I]-OZ);END;OMEQLH←MEQLH;OMASSTR←MASSTR;OZ←Z[I    30000
];
```



```
  IF Y=1AND I≥3THEN MM2←(Z[I]+DIF[1]/(SLOPEB-SLOPEA))/Z[I-1];IF Y=1AND I    30100
≤2THEN MM2←(1+(0.80)×MM/JT);IF Y≥2THEN BEGIN REAL XXXX;IF I=1THEN CTERM←    30200
0.002ELSE CTERM←0.0005;IF Y=2OR ABS(DIF[Y]/MEQLH)<CTERM THEN BEGIN TOTA    30300
L←0.0;FOR B←1STEP 1UNTIL Q DO TOTAL←TOTAL+RADIUS×RADIUS×UBAR×(3.14159265    30400
)×(R[B]*2-R[B-1]*2)×(RON[B]×U[B]+RON[B-1]×U[B-1])/2;TOTAL1←TOTAL+SUM;PCC    30500
ON[I]←100×SUM/TOTAL1;MTR←SUMT×(R[Q+1]*2-R[Q]*2)×(U[Q]+UO[Q+1])+TOTT×(R[Q    30600
]+R[Q+1])×DZ[Y]×(V[Q]+VO[Q+1]);HLOC1←SQRT(SQRT((TC*4)/(TERM×Z[I]×RADIUS)    30700
));HM1←(0.943)×(SQRT(SQRT((TC*4)×4/(TERM×Z[I]×RADIUS))));HLOC←TC×T[N]/((    30800
R[N+1]-R[N])×RADIUS);HLOC5←DT×TC×T[N]/((R[N+1]-R[N])×RADIUS×DT5);HLOC6←D    30900
T×TC×T[N]/((R[N+1]-R[N])×RADIUS×DT6);IF I=1THEN BEGIN OLDHLOC←HLOC;OLDHS    31000
UM←0.0;OLDHSUM5←OLDHSUM6←0.0;OLDHLOC5←HLOC5;OLDHLOC6←HLOC6;END;AVEHLOC←(    31100
OLDHLOC+HLOC)/2;AVEHLOC5←(OLDHLOC5+HLOC5)/2;AVEHLOC6←(OLDHLOC6+HLOC6)/2;    31200
HMH[I]←SUM×HFG×(1+3×SPHTL×DT/(8×HFG))×3600/((3.14159265)×D×Z[I]×RADIUS×D    31300
T);IF I=1THEN AVEHLOC←HMH[1]/3600;IF I=1THEN AVEHLOC5←HMH[1]×DT/(DT5×360    31400
0);IF I=1THEN AVEHLOC6←HMH[1]×DT/(DT6×3600);HTRW←AVEHLOC×(Z[I]-Z[I-1])×R    31500
ADIUS;HTRW5←AVEHLOC5×(Z[I]-Z[I-1])×RADIUS;HTRW6←AVEHLOC6×(Z[I]-Z[I-1])×R    31600
```

```
ADIUS;HSUM←OLDHSUM+HTRW;HSUM5←OLDHSUM5+HTRW5;HSUM6←OLDHSUM6+HTRW6;HM←HSU   31700
M/(Z[I]×RADIUS);HM5←HSUM5/(Z[I]×RADIUS);HM6←HSUM6/(Z[I]×RADIUS);NU3A[I]←   31800
HM×D/TC;WRITE(FL,FME,LS90);WRITE(FL,FM82,LS82);WRITE(FL,FMT1,LST1);WRITE   31900
(FL,FMT2);WRITE(FL,FMT3,LST3);FOR B←0STEP 1UNTIL N DO BEGIN UO[B]←U[B];V   32000
O[B]←V[B];OT[B]←T[B];CO[B]←C[B];ROO[B]←RON[B];END;OLDHSUM←HSUM;OLDHLOC←H   32100
LOC;OLDSUM←SUM;OLDHLOC5←HLOC5;OLDHLOC6←HLOC6;OLDHSUM5←HSUM5;OLDHSUM6←HSU   32200
M6;RT←RT+1;IF RT<LIM THEN BEGIN ZL←Z[I]×D/2.0;FOR B←0STEP 1UNTIL 200DO B   32300
EGIN T[B]←UO[B]←OT[B]←1.0;VO[B]←0.0;CO[B]←ENTC;END;END;HM2←HM1×SQRT(SQRT   32400
((1+(0.68)×SPHTL×DT/HFG)/(1+3×SPHTL×DT/(8×HFG))));HPHI[I]←HM/PHI;HPHI5[I   32500
]←HM5/PHI;HPHI6[I]←HM6/PHI;HRAT5[I]←HM5/(HM1×((DT/DT5)*0.25));HRAT6[I]←H   32600
M6/(HM1×((DT/DT6)*0.25));HLRAT5[I]←HLOC5/(HLOC1×((DT/DT5)*0.25));HLRAT6[   32700
I]←HLOC6/(HLOC1×((DT/DT6)*0.25));HNPHI[I]←HM1/PHI;HRPHI[I]←HM2/PHI;RWLZ[   32800
I]←4×Z[I]×RADIUS×DT×SPHTL×((GRAV×ROL×ROL/(MUL×MUL))*0.33333)/(PRL×HFG×(1   32900
+3×SPHTL×DT/(8×HFG))×(1-ROG/ROL));ABP[I]←P[I]×UBAR×UBAR×RON[0]/(144×GRAV   33000
)+14.696;DELTA[I]←1-R[Q];NUA[I]←HM×RADIUS×Z[I]/TC;NU1A[I]←HM1×RADIUS×Z[I   33100
]/TC;HM2A[I]←HM2×3600;HMA[I]←HM×3600;HLOCA[I]←HLOC×3600;HM1A[I]←HM1×3600   33200
;OVRG←VRG;HLOC1A[I]←HLOC1×3600;ICG[I]←C[Q];AMB[I]←0.0;FOR B←1STEP 1UNTIL   33300
 Q DO AMB[I]←(3.14159265)×RADIUS×RADIUS×(R[B]*2-R[B-1]*2)×(RON[B]+RON[B-   33400
1])×(1/8)×(C[B]+C[B-1])×(U[B]+U[B-1])×UBAR+AMB[I];AVGGB[I]←AMB[I]/TOTAL;   33500
```

```
MTR←AMB[I];FOR B←Q+1STEP 1UNTIL N+1DO AMB[I]←(3.14159265)×RADIUS×RADIUS×   33600
(R[B]*2-R[B-1]*2)×ROL×(1/4)×(C[B]+C[B-1])×(U[B]+U[B-1])×UBAR+AMB[I];AVGL   33700
B[I]←(AMB[I]-MTR)/SUM;ZS[I]←ZSTAR;FRE[I]←4×SUM/(MUL×(3.14159265)×D);HNFP   33800
H[I]←1.46×((FRE[I])*(-0.333333));TAUV[I]←-TAU/(GRAV×(ROL-ROG)×((MUL×MUL/   33900
(ROL×ROL×GRAV))*0.33333));TOT[I]←TOTAL1;HLOCNUC[I]←HLOC1A[I]×(SQRT(SQRT(   34000
8×HFG/(8×HFG+3×SPHTL×DT))));HMNUC[I]←HM1A[I]×(SQRT(SQRT(8×HFG/(8×HFG+3×S   34100
PHTL×DT))));IF Y=20THEN GO TO FLUSH;Y←20;IF U[0]<0.0THEN GO TO FLUSH;IF   34200
Z[I]<Z[I-1]THEN GO TO FLUSH;IF ABS(U[0])>10.0THEN GO TO FLUSH;BTT←I;IF(T   34300
IME(2)-X2)/60>860.0THEN GO TO FLUSH;IF Z[I]×RADIUS>20.0THEN GO TO FLUSH;   34400
END;IF Y<20THEN BEGIN SLOPE←(DIF[Y]-DIF[Y-1])/(DZ[Y]-DZ[Y-1]);DZ[Y+1]←-D   34500
IF[Y]/SLOPE+DZ[Y];Z[I]←Z[I-1]+DZ[Y+1];GO TO HELL;END;END;IF I=1THEN Z[0]   34600
←ZI×REG×2;IF RT>0AND RT<LIM THEN Z[0]←(1.2)×ZD[Q+1]/RADIUS;J←JT;END;END;   34700
```

(15)

```
FLUSH:WRITE(FL[PAGE]);WRITE(FL,FMG);FOR B←1STEP 1UNTIL BTT DO WRITE(FL,F   34800
MH,LSTH);WRITE(FL,FMB);FOR B←1STEP 1UNTIL BTT DO WRITE(FL,FMC,LSTC);WRIT   34900
E(FL,FMDA);WRITE(FL,FMD);FOR B←1STEP 1UNTIL BTT DO WRITE(FL,FME,LSTE);WR   35000
ITE(FL,FMZ);FOR B←1STEP 1UNTIL BTT DO WRITE(FL,FME,LSTX);WRITE(FL,FMY);F   35100
OR B←1STEP 1UNTIL BTT DO WRITE(FL,FMH,LSTW);WRITE(FL,FFZ);FOR B←1STEP 1U   35200
NTIL BTT DO WRITE(FL,FMC,LLZ);WRITE(FL,FRM);FOR B←1STEP 1UNTIL BTT DO WR   35300
```

```
ITE(FL,FMH,LSST);WRITE(FL,FM38);FOR B←1STEP 1UNTIL BTT DO WRITE(FL,FM36,    35400
LST38);WRITE(FL,FM35);FOR B←1STEP 1UNTIL BTT DO WRITE(FL,FM36,LST36);WRI    35500
TE(FL[PAGE]);WRITE(FL,FMT,LST);WRITE(FL,FMF,LSTF);WRITE(FL,FMTI,LSTI);WR    35600
ITE(FL,FMT5,(TIME(2)-X2)/60);WRITE(FL,FMT6,(TIME(3)-X3)/60);IF BBB≤5THEN    35700
 BEGIN IF I=7000THEN BEGIN WRITE(FL[PAGE]);WRITE(FL[PAGE]);UBAR←2×UBAR;G    35800
O TO GOD;END;END ELSE BBB←BBB;END.                                          35900
```

Data Read Into the Binary Vapor Program

A typical set of data in the order it is read into the binary vapor program is given below.

0.0544 ROG, 53.6 ROL, 0.00000851 MUG, 0.000268 MUL, 970.3 HFG, 0.932 SPHTL, 0.0000599 TC, 206.25 TS, 177 TW, 0.019125 RADIUS, 100 UBAR, 0.6 L [1], 0.03 K [1], 0.75 L[2], 0.015 K [2], 0.95 L [3], 0.01 K [3], 0.995 L [4], 0.0025 K [4], 12 AA, 5 JT, 24 BT, 2 LIM, 0.00001 ZI, 0.0002087 DABG, 0.00000001814 DABL, 0.74 AZ, 0.3795 BZ, 0.000003608 TCG, 0.454 SPHTG, 14.696 P1, 671.69 T1, 14.696 P2, 632.63 T2, 2.5 CCC (Use 1.2 for 50 and 1.05 for 75 weight percent), 186.5 BPTEM, 206.25 DPTEM, 368 HFG2, 0.03731 ROGA, 0.0946 ROGB, 18.02 MWA, 46.07 MWB, 0.25 ENTC,

APPENDIX D

PHYSICAL PROPERTIES

The physical properties of the various materials investigated were taken or extrapolated principally from data in the International Critical Tables (52), the Chemical Engineers' Handbook (53), and the Handbook of Chemistry and Physics (54). When it was necessary to estimate a property the estimation techniques described in Properties of Gases and Liquids (55) were used. Other sources are noted where used.

The integrated form of the Clausius-Clapeyron equation was used in binary and gas-vapor mixtures for determining the temperature dependence of vapor pressure.

The Van Laar model fits ethanol-water data to within five percent.

The equation for the vapor-liquid enthalpy difference for ethanol-water is (56).

$$e'_g - e'_\ell = 985 - 690\, W_{EtOH_g} + 85\, W_{EtOH_\ell}$$

For benzene-toluene the expression is (57)

$$e'_g - e'_\ell = 174.0 - 25\, W_{Tol_\ell}$$

Table 4. Physical Properties of Pure Vapors and Air-Vapor Mixtures

Property	Units	Water	Ethanol	Trichloro-ethylene
ρ'_g	lb./cu.ft.	0.03731	0.0946	0.262
ρ'_ℓ	lb./cu.ft.	59.802	47.0	84.05(39)
μ'_g	lb./ft.-sec.	0.00000843 4	0.00000874	0.0000082
μ'_ℓ	lb./ft.-sec.	0.0001907	0.000306	0.000234
k'_g	BTU/sec.-ft.-^{o}F	0.00000407	0.00000315	---
k'_ℓ	BTU/sec.-ft.-^{o}F	0.0001073	0.0000259	0.00001745
C'_{p_g}	BTU/lb.-^{o}F	0.454	0.454	---
C'_{p_ℓ}	BTU/lb.-^{o}F	1.007	0.680	0.243
λ'	BTU/lb.	970.3	368	103.1
D'_{ab} for air-vapor	ft.^{2}/sec.	0.000452 and 0.0003768	0.0001721	---
M_{vapor}	molecular weight	18.02	46.07	---
M_{air}	molecular weight	28.97	28.97	---
Boil. Pt.	^{o}F	212	173.3	194(39)

Table 5. Physical Properties of Binary Vapor Mixtures

Property	Units	Ethanol-Water	Benzene-Toluene
ρ'_g	lb./cu.ft.	varies with conc.	varies with conc.
ρ'_ℓ	lb./cu.ft.	53.6	49.45
μ'_g	lb./ft.-sec.	0.00000851	0.000005955
μ'_ℓ	lb./ft.-sec.	0.000268	0.00020
k'_g	BTU/sec.-ft.-$^\circ$F	0.000003608	0.00000254
k'_ℓ	BTU/sec.-ft.-$^\circ$F	0.0000599	0.00002296
C'_{p_g}	BTU/lb.-$^\circ$F	0.454	0.352
C'_{p_ℓ}	BTU/lb.-$^\circ$F	0.932	0.472
Boil. Pts.	$^\circ$F	E = 173.3, W = 212	B = 176.2, T = 231.1
M_{vapor}	Molecular weight	E = 46.07, W = 18.02	B = 78.11, T = 92.13
Van Laar	Dimensionless	0.74, 0.3795	-----
D'_{ab_g}	ft.^{2}/sec.	0.0002087	0.0000532
D'_{ab_ℓ}	ft.^{2}/sec.	0.00000001814	0.00000046
λ'	BTU/lb.	E = 368, W = 970.3	B = 169.8, T = 155.8

APPENDIX E

PURE VAPOR CONDENSATION RESULTS

This appendix contains the numerical results described in Chapter III for the condensation of pure vapors.

Table 6. Condensation of Water Vapor
Summary of Results: $D' = 0.03825$ Ft., $\Delta T' = 5^{\circ}$ F, $Pr_{\ell} = 1.79$, $C'_p \Delta T'/\lambda' = 0.00519$

$\bar{u}'$ ft./sec.	Re_g	Fr_L	z' ft	h'_m ratio	$\frac{h'_m}{\Phi'}$	h'_{loc} ratio	$\frac{2\delta'}{D'}$	Film Re	τ^*	P
5	846	66.13	0.0117	1.208	1.356	1.059	0.00399	2.7	0.370	+0.0093
		21.72	0.0358	1.109	0.942	1.016	0.00549	5.7	0.220	+0.0845
		8.87	0.0876	1.059	0.719	0.998	0.00699	10.7	0.128	+0.2445
		4.23	0.184	1.031	0.581	0.989	0.00849	18.1	0.061	+0.5121
		2.04	0.380	1.012	0.476	0.983	0.01024	30.7	0.001	+0.9508
10	1692	28.25	0.110	1.127	0.723	1.018	0.00725	13.5	0.333	+0.0663
		13.80	0.225	1.078	0.578	1.000	0.00883	22.1	0.211	+0.1782
		8.38	0.371	1.052	0.498	0.990	0.0101	31.4	0.134	+0.3120
		4.83	0.644	1.030	0.425	0.982	0.0117	46.4	0.054	+0.5340
		3.25	0.957	1.017	0.380	0.978	0.0129	61.7	0.001	+0.7411
25	4231	176.87	0.110	1.375	0.882	1.116	0.00661	16.5	1.213	-0.0310
		71.33	0.273	1.228	0.628	1.050	0.00882	29.0	0.789	-0.0063
		36.84	0.527	1.151	0.499	1.019	0.0107	44.7	0.546	+0.0446
		18.93	1.026	1.094	0.402	0.997	0.0129	70.0	0.332	+0.1497
		11.48	1.693	1.062	0.344	0.984	0.0148	98.8	0.184	+0.2831
50	8462	2576.4	0.0302	2.256	2.000	1.590	0.00337	10.2	5.132	-0.0350
		242.6	0.320	1.448	0.711	1.145	0.00842	38.7	1.979	-0.0482
		69.8	1.113	1.224	0.440	1.040	0.0126	83.2	1.058	-0.0129
		31.4	2.477	1.131	0.333	1.001	0.0160	140.0	0.606	+0.0771
		14.7	5.275	1.068	0.260	0.976	0.0198	233.2	0.233	+0.2608
100	16923	1553.9	0.200	2.047	1.131	1.505	0.00570	38.4	6.505	-0.0434
		743.3	0.418	1.772	0.814	1.321	0.00780	57.8	4.651	-0.0543
		438.6	0.709	1.607	0.647	1.223	0.00961	77.9	3.656	-0.0610
		275.4	1.128	1.483	0.532	1.156	0.0114	101.9	2.942	-0.0641
		158.8	1.957	1.361	0.425	1.095	0.0138	141.3	2.239	-0.0603
200	33846	2482.5	0.501	2.224	0.976	1.656	0.00652	83.1	11.27	-0.0644
		836.5	1.486	1.806	0.604	1.356	0.0104	152.5	7.17	-0.0840
		299.0	4.159	1.504	0.389	1.166	0.0156	274.6	4.45	-0.0980
		133.2	9.333	1.324	0.280	1.068	0.0209	443.4	2.85	-0.0861
		67.7	18.358	1.209	0.216	1.009	0.0261	672.3	1.72	-0.0333

Table 7. Condensation of Water Vapor
Summary of Results: $D' = 0.03825$ Ft., $\Delta T' = 10^{\circ}$ F, $Pr_{\ell} = 1.79$, $C'_p \Delta T'/\lambda' = 0.0104$

$\bar{u}'$ ft./sec	Re_g	Fr_L	z' ft	h'_m ratio	$\frac{h'_m}{\Phi'}$	h'_{loc} ratio	$\frac{2\delta'}{D'}$	Film Re	τ^*	P
5	846	68.51	0.0113	1.237	1.178	1.072	0.00465	4.5	0.511	+0.0787
		32.75	0.0237	1.157	0.916	1.031	0.00581	7.4	0.351	+0.1534
		14.89	0.0522	1.094	0.711	1.004	0.00726	12.6	0.210	+0.2984
		8.63	0.0900	1.062	0.602	0.991	0.00843	18.4	0.124	+0.4553
		5.32	0.1460	1.039	0.522	0.983	0.00959	25.8	0.050	+0.6367
10	1692	286.4	0.0109	1.462	1.407	1.221	0.00404	5.2	1.327	+0.0226
		83.5	0.0372	1.262	0.892	1.074	0.00624	11.3	0.739	+0.0852
		26.7	0.116	1.131	0.602	1.011	0.00881	23.8	0.371	+0.2362
		12.0	0.259	1.071	0.467	0.986	0.0110	40.9	0.162	+0.4407
		6.1	0.509	1.034	0.380	0.972	0.0132	65.6	0.001	+0.6688
25	4231	931.0	0.0209	1.731	1.418	1.452	0.00399	10.0	3.285	-0.0001
		285.5	0.0680	1.478	0.901	1.200	0.00648	20.6	2.004	+0.0340
		62.7	0.310	1.214	0.507	1.033	0.0110	52.8	0.847	+0.1589
		28.0	0.693	1.121	0.383	0.991	0.0140	89.2	0.414	+0.3161
		14.1	1.378	1.064	0.306	0.968	0.0170	141.7	0.088	+0.5134
50	8462	1261.0	0.0616	1.844	1.150	1.517	0.00501	24.0	5.223	-0.0040
		404.2	0.192	1.562	0.733	1.239	0.00815	47.8	3.190	+0.0296
		148.9	0.522	1.343	0.491	1.086	0.0119	86.8	1.818	+0.0919
		45.0	1.727	1.156	0.313	0.991	0.0175	183.3	0.674	+0.2803
		23.6	3.290	1.085	0.249	0.961	0.0213	282.4	0.152	+0.4579
100	16923	1975.6	0.157	2.014	0.994	1.632	0.00589	53	8.744	-0.0123
		678.8	0.458	1.708	0.645	1.330	0.00942	100	5.610	+0.0179
		221.0	1.406	1.416	0.404	1.109	0.0149	193	2.934	+0.0802
		101.6	3.058	1.258	0.296	1.021	0.0196	306	1.627	+0.1779
		38.5	8.077	1.114	0.205	0.954	0.0267	562	0.289	+0.4020
200	33846	451.1	2.756	1.535	0.370	1.221	0.0160	346	5.964	+0.0381
		251.8	4.938	1.401	0.292	1.107	0.0204	489	4.077	+0.0905
		151.7	8.193	1.296	0.238	1.033	0.0248	661	2.657	+0.1595
		96.2	12.922	1.212	0.199	0.981	0.0292	869	1.519	+0.2487
		63.3	19.633	1.145	0.169	0.945	0.0335	1123	0.565	+0.3537

Table 8. Condensation of Water Vapor
Summary of Results: $D' = 0.03825$ Ft., $\Delta T' = 20^{\circ}$ F,
$Pr_{\ell} = 1.79$, $C'_p \Delta T'/\lambda' = 0.0208$

$\bar{u}'$ ft/sec	Re_g	Fr_L	z' ft	h'_m ratio	$\frac{h'_m}{\Phi'}$	h'_{loc} ratio	$\frac{2\delta'}{D'}$	Film Re	τ^*	P
5	846	70.80	0.0110	1.291	1.044	1.087	0.00541	7.7	0.728	+0.1724
		41.71	0.0186	1.217	0.862	1.044	0.00642	10.8	0.530	+0.2475
		22.27	0.0349	1.145	0.693	1.009	0.00778	16.3	0.325	+0.3722
		12.81	0.0607	1.095	0.577	0.987	0.00913	23.6	0.160	+0.5136
		7.83	0.0992	1.059	0.493	0.972	0.01048	33.0	0.018	+0.6426
10	1692	219.8	0.0141	1.484	1.125	1.222	0.00512	10.8	1.725	+0.1051
		87.7	0.0354	1.313	0.792	1.084	0.00726	18.9	1.012	+0.1970
		39.9	0.0778	1.194	0.591	1.019	0.00939	31.1	0.570	+0.3287
		23.0	0.135	1.130	0.488	0.988	0.0111	44.4	0.304	+0.4531
		12.6	0.248	1.073	0.398	0.964	0.0132	66.5	0.029	+0.5938
25	4231	518.1	0.0375	1.742	1.036	1.342	0.00595	26.2	3.697	+0.0884
		197.2	0.0985	1.472	0.687	1.138	0.00893	45.7	2.089	+0.1660
		79.6	0.244	1.276	0.475	1.032	0.0123	78.2	1.087	+0.2966
		40.5	0.479	1.168	0.367	0.982	0.0153	118.8	0.486	+0.4365
		22.4	0.868	1.095	0.297	0.953	0.0183	173.9	0.015	+0.5550
50	8462	698.0	0.111	1.833	0.830	1.381	0.00759	62.4	5.635	+0.0987
		248.8	0.312	1.509	0.528	1.135	0.0119	111.3	2.923	+0.1897
		131.3	0.592	1.347	0.402	1.045	0.0152	160.5	1.776	+0.2827
		68.4	1.136	1.216	0.308	0.982	0.0190	236.3	0.814	+0.4109
		38.3	2.030	1.126	0.247	0.944	0.0228	338.0	0.075	+0.5265
100	16923	1001.8	0.310	1.959	0.686	1.439	0.0094	143.9	8.855	+0.1064
		423.6	0.734	1.641	0.464	1.187	0.0141	229.8	4.990	+0.1800
		210.7	1.475	1.426	0.338	1.058	0.0188	337.1	2.839	+0.2750
		115.2	2.697	1.276	0.260	0.982	0.0235	474.3	1.359	+0.3878
		62.1	5.002	1.156	0.202	0.930	0.0289	682.7	0.088	+0.5091
200	33846	1380.9	0.900	1.983	0.532	1.537	0.0115	324	13.94	+0.1115
		629.7	1.974	1.709	0.377	1.243	0.0172	503	8.05	+0.1830
		302.1	4.116	1.468	0.270	1.064	0.0241	749	4.19	+0.2838
		161.9	7.681	1.296	0.204	0.964	0.0310	1055	1.69	+0.4017
		100.7	12.344	1.188	0.166	0.912	0.0367	1380	0.11	+0.4948

Table 9. Condensation of Water Vapor,
Summary of Results: $D' = 0.16667$ Ft., $\Delta T' = 5^{\circ}$ F,
$Pr_{\ell} = 1.79$, $C_p'\Delta T'/\lambda' = 0.00519$

$\bar{u}'$ ft./sec	Re_g	Fr_L	z' ft	h_m' ratio	$\frac{h_m'}{\Phi'}$	h_{loc}' ratio	$\frac{2\delta'}{D'}$	Film Re	τ^*	P
2.5	1843	18.56	0.0105	1.078	1.245	1.025	0.00092	2.2	0.165	+0.0607
		6.73	0.0289	1.046	0.937	1.010	0.00121	4.6	0.120	+0.1802
		1.82	0.107	1.017	0.657	0.993	0.00170	11.9	0.076	+0.6630
		0.75	0.258	1.006	0.521	0.994	0.00213	22.8	0.045	+1.5618
		0.36	0.535	1.003	0.433	0.999	0.00255	39.1	0.021	+3.1326
25	18435	1920.0	0.0101	2.030	2.365	1.463	0.00064	4	2.821	-0.0068
		242.6	0.0801	1.427	0.991	1.155	0.00136	13	1.382	-0.0047
		62.8	0.309	1.214	0.601	1.058	0.00208	32	0.802	+0.0125
		19.6	0.991	1.110	0.411	1.022	0.00288	69	0.500	+0.0725
		7.18	2.706	1.058	0.305	1.006	0.00376	140	0.312	+0.2224
50	36869	3113.8	0.0250	2.289	2.127	1.649	0.00071	9	5.386	-0.0062
		559.8	0.139	1.637	0.990	1.266	0.00142	23	2.765	-0.0097
		90.5	0.859	1.262	0.484	1.075	0.00264	71	1.302	+0.0021
		29.2	2.658	1.139	0.329	1.029	0.00366	149	0.811	+0.0469
		10.9	7.131	1.075	0.243	1.008	0.00478	294	0.504	+0.1625
100	73739	3365.4	0.0923	2.388	1.600	1.603	0.00102	25	7.337	-0.0097
		464.0	0.670	1.596	0.652	1.232	0.00217	74	3.615	-0.0143
		110.6	2.810	1.293	0.369	1.085	0.00352	176	1.988	-0.0056
		44.8	6.939	1.177	0.268	1.039	0.00460	316	1.344	+0.0234
		16.3	19.108	1.095	0.193	1.011	0.00609	628	0.814	+0.1182

Table 10. Condensation of Water Vapor, Summary of Results: $D' = 0.16667$ Ft., $\Delta T' = 10^{\circ}$ F, $Pr_{\ell} = 1.79$, $C_p'\Delta T'/\lambda' = 0.0104$

$\frac{\bar{u}'}{\frac{\text{ft.}}{\text{sec}}}$	Re_g	Fr_L	z' ft	h_m' ratio	$\frac{h_m'}{\Phi'}$	h_{loc}' ratio	$\frac{2\delta'}{D'}$	Film Re	τ^*	P
25	18435	1463.1	0.0133	1.973	1.806	1.592	0.00075	8	4.268	+0.0004
		324.5	0.0599	1.561	0.906	1.228	0.00141	20	2.234	+0.0094
		73.6	0.264	1.271	0.551	1.080	0.00233	49	1.206	+0.0433
		28.3	0.687	1.160	0.396	1.037	0.00308	92	0.812	+0.1061
		11.6	1.638	1.095	0.301	1.014	0.00391	167	0.537	+0.2297
100	73739	382.0	0.814	1.558	0.510	1.269	0.00263	141	4.842	+0.0128
		126.7	2.452	1.341	0.333	1.114	0.00394	277	2.929	+0.0431
		58.5	5.313	1.227	0.251	1.057	0.00503	452	2.049	+0.0908
		30.0	10.365	1.153	0.200	1.026	0.00613	701	1.445	+0.1658
		16.7	18.591	1.104	0.165	1.007	0.00722	1041	0.991	+0.2723

Table 11. Condensation of Water Vapor, Summary of Results: $D' = 0.16667$ Ft., $\Delta T' = 20^{\circ}$ F, $Pr_{\ell} = 1.79$, $C'_p \Delta T'/\lambda' = 0.0208$

$\bar{u}'$ ft./sec	Re_g	Fr_L	z' ft	h'_m ratio	$\frac{h'_m}{\Phi'}$	h'_{loc} ratio	$\frac{2\delta'}{D'}$	Film Re	τ^*	P
25	18435	182.5	0.106	1.486	0.681	1.234	0.00193	49	2.913	+0.0498
		46.5	0.417	1.256	0.409	1.074	0.00312	115	1.526	+0.1346
		13.9	1.398	1.126	0.271	1.017	0.00446	256	0.790	+0.3237
		6.52	2.977	1.074	0.214	0.995	0.00550	430	0.398	+0.5413
		3.75	5.185	1.045	0.181	0.983	0.00639	634	0.116	+0.7551
50	36869	394.5	0.197	1.659	0.651	1.348	0.00206	87	5.277	+0.0376
		109.3	0.711	1.387	0.395	1.135	0.00337	190	2.970	+0.0958
		30.7	2.528	1.195	0.248	1.038	0.00506	423	1.557	+0.2361
		11.4	6.842	1.100	0.178	0.998	0.00675	822	0.704	+0.4580
		6.0	13.002	1.057	0.146	0.980	0.00806	1278	0.188	+0.6552
100	73739	825.6	0.376	1.861	0.621	1.540	0.00212	158	10.08	+0.0307
		215.3	1.444	1.525	0.364	1.212	0.00377	355	5.45	+0.0802
		89.0	3.491	1.340	0.256	1.098	0.00519	605	3.49	+0.1480
		33.5	9.275	1.192	0.179	1.027	0.00707	1119	1.94	+0.2877
		16.4	18.923	1.116	0.140	0.994	0.00872	1789	0.98	+0.4486

Table 12. Condensation of Ethanol Vapor,
Summary of Results: $D' = 0.03825$ Ft., $\Delta T' = 5^{\circ}$ F,
$Pr_{\ell} = 8.03$, $C_p'\Delta T'/\lambda' = 0.00924$

$\bar{u}'$ ft./sec	Re_g	Fr_L	z' ft	h_m' ratio	$\frac{h_m'}{\Phi'}$	h_{loc}' ratio	$\frac{2\delta'}{D'}$	Film Re	τ^*	P
5	2070	73.15	0.0106	1.276	2.083	1.070	0.00437	0.93	0.316	-0.0469
		18.85	0.0412	1.125	1.309	1.022	0.00641	2.26	0.188	-0.0426
		5.84	0.133	1.059	0.919	1.004	0.00875	5.11	0.118	+0.0430
		2.33	0.333	1.029	0.710	0.996	0.0111	9.88	0.077	+0.2906
		1.01	0.766	1.012	0.567	0.991	0.0137	18.15	0.046	+0.8855
25	10350	1571.0	0.0124	2.395	3.764	1.667	0.00292	1.95	3.393	-0.0250
		277.9	0.0699	1.609	1.641	1.198	0.00625	4.79	1.335	-0.0743
		38.2	0.508	1.212	0.752	1.051	0.0117	15.98	0.634	-0.1442
		14.1	1.377	1.117	0.540	1.019	0.0154	31.11	0.434	-0.1692
		5.77	3.362	1.064	0.412	1.000	0.0196	57.86	0.296	-0.1334
50	20701	6249.8	0.0124	4.291	6.737	1.638	0.00297	3.50	6.143	-0.0364
		1055.1	0.0736	2.233	2.247	1.404	0.00540	6.91	3.292	-0.0681
		339.4	0.229	1.704	1.291	1.241	0.0081	12.36	2.184	-0.1030
		170.3	0.456	1.499	0.956	1.163	0.0103	18.25	1.693	-0.1334
		88.1	0.882	1.356	0.733	1.107	0.0127	27.04	1.332	-0.1697

Table 13. Condensation of Ethanol Vapor, Summary of Results: $D' = 0.03825$ Ft., $\Delta T' = 10^{\circ}$ F, $Pr_{\ell} = 8.03$, $C'_p \Delta T'/\lambda' = 0.0185$

$\bar{u}'$ ft./sec	Re_g	Fr_L	z' ft	h'_m ratio	$\frac{h'_m}{\Phi'}$	h'_{loc} ratio	$\frac{2\delta'}{D'}$	Film Re	τ^*	P
5	2070	25.9	0.0299	1.135	1.204	1.028	0.00701	3.00	0.245	-0.0089
		12.1	0.0642	1.084	0.950	1.010	0.00863	5.08	0.179	+0.0388
		5.42	0.143	1.047	0.751	0.987	0.0108	8.96	0.127	+0.1726
		1.93	0.403	1.015	0.562	0.983	0.0140	18.82	0.067	+0.6300
		0.85	0.915	1.001	0.451	0.981	0.0173	34.27	0.020	+1.4896
25	10350	1784.4	0.0109	2.294	3.134	1.663	0.00337	2.84	3.701	-0.0211
		249.8	0.0778	1.536	1.283	1.187	0.00769	8.31	1.472	-0.0582
		55.6	0.350	1.245	0.714	1.061	0.0125	20.80	0.806	-0.0800
		17.9	1.088	1.124	0.485	1.016	0.0173	43.99	0.492	-0.0570
		6.68	2.910	1.060	0.358	0.992	0.0226	86.78	0.281	+0.0738
50	20701	2154.2	0.0361	2.448	2.478	1.729	0.00437	7.4	5.841	-0.0274
		372.7	0.208	1.669	1.090	1.249	0.00936	18.9	2.544	-0.0724
		73.1	1.063	1.294	0.562	1.079	0.0162	49.8	1.332	-0.1161
		22.1	3.510	1.144	0.369	1.018	0.0231	107.8	0.787	-0.1167
		9.35	8.308	1.077	0.280	0.991	0.0293	193.6	0.475	-0.0348
100	41401	4349.5	0.0715	3.257	2.779	1.848	0.00484	16.5	9.939	-0.0690
		1041.6	0.298	2.111	1.260	1.420	0.00900	31.3	5.409	-0.1244
		165.7	1.876	1.474	0.556	1.165	0.0173	86.8	2.889	-0.1874
		54.1	5.747	1.264	0.360	1.066	0.0249	172.4	1.849	-0.2382
		22.2	13.993	1.153	0.263	1.016	0.0325	306.6	1.216	-0.2518
200	82802	5428.6	0.229	3.516	2.242	1.957	0.00612	42.8	16.82	-0.0726
		1595.4	0.779	2.401	1.127	1.548	0.0105	73.2	9.84	-0.1260
		409.7	3.034	1.763	0.589	1.300	0.0175	149.0	6.15	-0.1834
		132.1	9.412	1.445	0.364	1.145	0.0262	285.3	4.01	-0.2580
		64.6	19.235	1.305	0.275	1.077	0.0332	440.3	3.00	-0.3115
400	165604	6884.0	0.722	3.804	1.820	2.085	0.00765	110	27.78	-0.0942
		3289.0	1.512	2.977	1.185	1.754	0.0109	149	19.39	-0.1387
		946.1	5.256	2.145	0.625	1.492	0.0175	274	12.91	-0.1949
		469.1	10.602	1.846	0.451	1.351	0.0229	399	10.06	-0.2436
		266.1	18.688	1.656	0.351	1.254	0.0284	547	8.18	-0.2941

Table 14. Condensation of Ethanol Vapor,
Summary of Results: $D' = 0.03825$ Ft., $\Delta T' = 20^{\circ}$ F
$Pr_{\ell} = 8.03$, $C_p'\Delta T'/\lambda' = 0.0370$

$\bar{u}'$ ft./sec	Re_g	Fr_L	z' ft	h_m' ratio	$\frac{h_m'}{\Phi'}$	h_{loc}' ratio	$\frac{2\delta'}{D'}$	Film Re	τ^*	P
5	2070	25.5	0.0304	1.118	0.995	1.038	0.00829	5.00	0.306	+0.0463
		12.1	0.0643	1.079	0.797	1.017	0.0102	8.46	0.227	+0.1341
		5.52	0.141	1.048	0.636	0.990	0.0127	14.75	0.150	+0.3202
		2.72	0.285	1.024	0.521	0.986	0.0153	24.45	0.086	+0.6477
		1.50	0.520	1.011	0.443	0.986	0.0178	37.74	0.027	+1.1089
50	20701	778.5	0.0998	1.883	1.245	1.413	0.00818	20.6	4.213	-0.0328
		163.7	0.475	1.440	0.645	1.144	0.0149	50.6	2.168	-0.0393
		52.4	1.484	1.235	0.416	1.046	0.0216	102.1	1.268	-0.0087
		23.0	3.374	1.137	0.312	1.003	0.0275	173.9	0.777	+0.0749
		9.83	7.901	1.066	0.236	0.974	0.0350	308.6	0.331	+0.2809
100	41401	946.1	0.329	1.916	0.940	1.470	0.0106	51.1	6.410	-0.0453
		272.2	1.142	1.552	0.558	1.215	0.0174	105.4	3.909	-0.0558
		75.2	4.135	1.284	0.335	1.062	0.0274	228.8	2.124	-0.0392
		31.0	10.037	1.159	0.242	1.001	0.0361	401.4	1.219	+0.0404
		16.3	19.050	1.092	0.194	0.970	0.0436	611.5	0.637	+0.1760
200	82802	6295.4	0.197	3.417	1.905	1.923	0.00713	62.3	16.34	-0.0897
		1080.2	1.151	2.080	0.746	1.490	0.0143	142.2	10.13	-0.1358
		302.0	4.116	1.627	0.425	1.241	0.0234	289.2	6.26	-0.1524
		123.4	10.074	1.401	0.292	1.111	0.0326	487.2	4.14	-0.1556
		64.2	19.368	1.274	0.226	1.042	0.0407	722.8	2.89	-0.1313

Table 15. Condensation of Ethanol Vapor, Summary of Results: $D' = 0.16667$ Ft., $\Delta T' = 5^{\circ}$ F, $Pr_{\ell} = 8.03$, $C'_p \Delta T'/\lambda' = 0.00924$

$\frac{\bar{u}'}{\frac{\text{ft.}}{\text{sec}}}$	Re_g	Fr_L	z' ft	h'_m ratio	$\frac{h'_m}{\Phi'}$	h'_{loc} ratio	$\frac{2\delta'}{D'}$	Film Re	τ^*	P
25	45099	110.07	0.176	1.334	1.079	1.085	0.00200	8	0.774	-0.0181
		17.15	1.133	1.113	0.566	1.020	0.00338	27	0.378	+0.0081
		4.62	4.202	1.048	0.384	1.004	0.00477	67	0.225	+0.1493
		2.08	9.319	1.027	0.308	0.999	0.00585	120	0.161	+0.4118
		0.98	19.804	1.014	0.252	0.995	0.00708	209	0.111	+0.9711
100	180397	1319.4	0.236	2.292	1.725	1.287	0.00181	17	3.611	-0.0326
		188.9	1.645	1.453	0.673	1.141	0.00332	46	2.017	-0.0477
		77.4	4.013	1.284	0.476	1.081	0.00438	80	1.460	-0.0564
		33.5	9.267	1.179	0.354	1.044	0.00559	137	1.060	-0.0604
		16.5	18.831	1.119	0.281	1.024	0.00679	222	0.806	-0.0509

Table 16. Condensation of Ethanol Vapor, Summary of Results: $D' = 0.16667$ Ft., $\Delta T' = 10^{\circ}$ F, $Pr_{\ell} = 8.03$, $C'_p \Delta T'/\lambda' = 0.0185$

$\bar{u}'$ ft./sec	Re_g	Fr_L	z' ft	h'_m ratio	$\frac{h'_m}{\Phi'}$	h'_{loc} ratio	$\frac{2\delta'}{D'}$	Film Re	τ^*	P
25	45099	981.16	0.0198	2.005	2.359	1.318	0.00113	3.9	2.069	-0.0100
		461.22	0.0421	1.685	1.641	1.237	0.00146	5.8	1.636	-0.0108
		230.77	0.0842	1.489	1.219	1.168	0.00184	8.6	1.296	-0.0109
		140.67	0.138	1.382	1.000	1.124	0.00216	11.5	1.071	-0.0104
		84.26	0.231	1.293	0.823	1.087	0.00254	15.8	0.871	-0.0083
100	180397	1830.0	0.170	2.325	1.598	1.582	0.00162	23	6.677	-0.0104
		498.2	0.624	1.726	0.857	1.262	0.00280	45	3.596	-0.0210
		105.6	2.943	1.335	0.450	1.099	0.00474	110	1.956	-0.0285
		37.3	8.342	1.189	0.309	1.045	0.00646	215	1.293	-0.0215
		15.9	19.572	1.114	0.234	1.020	0.00819	381	0.910	+0.0123
200	360793	1225.5	1.014	2.070	0.910	1.494	0.00267	77	7.977	-0.0181
		645.0	1.928	1.808	0.677	1.316	0.00356	109	5.764	-0.0273
		255.7	4.862	1.524	0.453	1.183	0.00499	183	4.022	-0.0366
		120.3	10.331	1.359	0.335	1.110	0.00641	288	2.989	-0.0433
		62.9	19.759	1.254	0.262	1.068	0.00784	432	2.309	-0.0456

Table 17. Condensation of Ethanol Vapor,
Summary of Results: $D' = 0.16667$ Ft., $\Delta T' = 20^{\circ}$ F,
$Pr_{\ell} = 8.03$, $C'_p \Delta T'/\lambda' = 0.0370$

$\bar{u}'$ ft./sec	Re_g	Fr_L	z' ft	h'_m ratio	$\frac{h'_m}{\Phi'}$	h'_{loc} ratio	$\frac{2\delta'}{D'}$	Film Re	τ^*	P
25	45099	240.64	0.0807	1.461	1.019	1.209	0.00209	14	1.736	-0.0035
		32.28	0.602	1.179	0.498	1.050	0.00397	50	0.812	+0.0322
		6.88	2.822	1.073	0.308	1.011	0.00606	144	0.432	+0.1959
		2.71	7.178	1.039	0.236	1.000	0.00773	280	0.268	+0.5042
		1.07	18.236	1.017	0.183	0.994	0.00982	552	0.127	+1.2341
100	180397	2011.3	0.155	2.247	1.332	1.612	0.00184	34	7.798	-0.0078
		345.5	0.900	1.613	0.615	1.251	0.00368	92	4.111	-0.0107
		88.5	3.513	1.318	0.358	1.098	0.00589	208	2.343	-0.0021
		37.9	8.210	1.201	0.264	1.050	0.00761	358	1.655	+0.0228
		16.8	18.532	1.125	0.201	1.022	0.00957	618	1.157	+0.0833

Table 18. Condensation of Trichloroethylene Vapor, Summary of Results: $D' = 0.03825$ Ft., $\Delta T' = 5^{\circ}$ F, $Pr_{\ell} = 3.26$, $C'_p \Delta T'/\lambda' = 0.0118$

$\bar{u}'$ ft./sec	Re_g	Fr_L	z' ft	h'_m ratio	$\frac{h'_m}{\Phi'}$	h'_{loc} ratio	$\frac{2\delta'}{D'}$	Film Re	τ^*	P
25	30553	1182.9	0.0164	2.188	2.089	1.704	0.00267	7.9	5.318	-0.0123
		218.0	0.0891	1.566	0.979	1.206	0.00575	20.1	2.144	-0.0333
		41.7	0.466	1.242	0.513	1.062	0.0099	55.4	1.106	-0.0354
		11.0	1.763	1.108	0.329	1.013	0.0144	134.0	0.623	+0.0336
		3.7	5.317	1.047	0.236	0.991	0.0193	289.8	0.333	+0.2826
50	61107	1376.9	0.0564	2.313	1.621	1.675	0.00369	21.2	7.397	-0.0189
		421.4	0.184	1.789	0.933	1.312	0.00633	39.8	4.067	-0.0395
		86.6	0.897	1.367	0.480	1.111	0.0111	99.6	2.160	-0.0597
		19.3	4.026	1.156	0.279	1.025	0.0174	259.7	1.148	-0.0388
		5.3	14.606	1.061	0.186	0.990	0.0248	626.7	0.560	+0.1510
100	122213	1870.4	0.166	2.503	1.340	1.798	0.00450	51.5	12.36	-0.0234
		487.6	0.637	1.859	0.711	1.353	0.0083	104.9	6.36	-0.0529
		133.0	2.337	1.468	0.406	1.156	0.0135	219.3	3.77	-0.0807
		49.3	6.308	1.277	0.275	1.070	0.0187	401.7	2.51	-0.0960
		16.6	18.728	1.143	0.188	1.015	0.0257	813.0	1.53	-0.0693
200	244427	8240.3	0.151	4.367	2.362	2.221	0.00356	82.5	30.17	-0.0367
		1863.4	0.667	2.571	0.972	1.609	0.0071	150.1	14.36	-0.0781
		432.5	2.875	1.832	0.481	1.349	0.0122	319.8	9.05	-0.1062
		144.3	8.618	1.504	0.300	1.179	0.0183	598.0	5.94	-0.1418
		65.6	18.964	1.338	0.219	1.097	0.0239	961.0	4.32	-0.1686
400	488854	12076	0.412	4.676	1.994	2.469	0.00412	190	53.41	-0.0400
		3277	1.517	2.992	0.921	1.840	0.00764	326	27.92	-0.0794
		1072	4.639	2.257	0.525	1.578	0.01176	564	19.40	-0.1038
		465	10.701	1.890	0.357	1.386	0.01646	884	14.17	-0.1338
		262	19.014	1.692	0.277	1.277	0.02058	1218	11.35	-0.1606

Table 19. Condensation of Trichloroethylene Vapor, Summary of Results: $D' = 0.03825$ Ft., $\Delta T' = 10^{\circ}$ F, $Pr_{\ell} = 3.26$, $C'_p \Delta T'/\lambda' = 0.0236$

$\bar{u}'$ ft./sec	Re_g	Fr_L	z' ft	h'_m ratio	$\frac{h'_m}{\Phi'}$	h'_{loc} ratio	$\frac{2\delta'}{D'}$	Film Re	τ^*	P
25	30553	1682.5	0.0115	2.284	2.005	1.225	0.00404	10.7	2.644	-0.0883
		337.6	0.0575	1.514	0.889	1.189	0.00621	23.6	2.067	-0.0748
		93.1	0.208	1.296	0.514	1.130	0.00901	53.0	1.720	-0.0455
		42.3	0.459	1.209	0.422	1.077	0.01149	89.3	1.344	-0.0137
		18.9	1.025	1.138	0.325	1.035	0.01460	153.7	0.962	+0.0517
50	61107	5315.8	0.0146	3.511	2.904	1.912	0.00277	19.6	10.72	-0.0247
		955.0	0.0814	1.990	1.072	1.368	0.00589	40.2	5.08	-0.0586
		247.2	0.314	1.559	0.599	1.249	0.00903	86.8	3.93	-0.0476
		73.5	1.058	1.323	0.375	1.109	0.0137	183.9	2.48	-0.0289
		28.7	2.705	1.194	0.268	1.042	0.0185	333.8	1.62	+0.0220
100	122213	6927.7	0.0449	3.837	2.398	2.174	0.00319	49.6	20.53	-0.0297
		2022.5	0.153	2.465	1.132	1.476	0.00640	80.2	9.24	-0.0710
		300.5	1.034	1.643	0.469	1.284	0.0118	223.4	6.28	-0.0618
		106.2	2.926	1.402	0.308	1.139	0.0172	415.7	4.15	-0.0523
		43.5	7.139	1.250	0.220	1.057	0.0231	723.3	2.73	-0.0169
200	244427	11920	0.104	4.450	2.252	2.309	0.00372	108	31.23	-0.0364
		3060	0.406	2.705	0.975	1.617	0.00744	183	16.23	-0.0831
		586	2.122	1.870	0.446	1.422	0.0127	436	11.90	-0.0776
		207	6.003	1.565	0.288	1.226	0.0191	796	7.97	-0.0785
		100	12.461	1.398	0.214	1.124	0.0249	1228	5.75	-0.0701
400	488854	14320	0.347	4.794	1.796	2.140	0.00540	287	37.53	-0.0745
		4469	1.113	3.059	0.857	1.636	0.00945	439	24.32	-0.1409
		1264	3.934	2.172	0.444	1.567	0.0135	804	21.25	-0.1340
		507	9.800	1.830	0.297	1.403	0.0189	1343	16.65	-0.1320
		250	19.883	1.622	0.221	1.263	0.0250	2024	12.73	-0.1335

Table 20. Condensation of Trichloroethylene Vapor, Summary of Results: $D' = 0.03825$ Ft., $\Delta T' = 20^{\circ}$ F, $Pr_{\ell} = 3.26$, $C'_p \Delta T'/\lambda' = 0.0471$

$\bar{u}'$ ft./sec	Re_g	Fr_L	z' ft	h'_m ratio	$\frac{h'_m}{\Phi'}$	h'_{loc} ratio	$\frac{2\delta'}{D'}$	Film Re	τ^*	P
50	61107	7300.9	0.0106	3.613	2.727	1.971	0.00294	26.5	9.694	-0.0271
		1391.4	0.0558	2.031	1.013	1.295	0.00673	51.7	4.885	-0.0911
		200.6	0.387	1.465	0.450	1.242	0.0114	159.3	4.449	-0.0238
		87.3	0.890	1.336	0.334	1.145	0.0151	271.3	3.409	+0.0257
		39.5	1.967	1.231	0.252	1.067	0.0198	452.6	2.357	+0.1048
100	122213	9455.7	0.0329	3.935	2.240	2.095	0.00368	67.3	15.49	-0.0349
		2687.0	0.116	2.482	1.032	1.422	0.0074	109.1	9.49	-0.1024
		341.0	0.916	1.624	0.403	1.330	0.0131	335.6	8.01	-0.0390
		137.9	2.253	1.440	0.285	1.188	0.0184	586.8	5.84	+0.0080
		60.7	5.120	1.296	0.209	1.083	0.0247	977.2	3.89	+0.0813
200	244427	12716	0.0978	4.282	1.856	2.258	0.00448	166	25.36	-0.0451
		2669	0.466	2.487	0.729	1.541	0.00960	311	16.51	-0.1075
		402	3.091	1.723	0.315	1.368	0.0173	890	12.89	-0.0412
		183	6.800	1.526	0.229	1.212	0.0237	1424	9.27	-0.0234
		98	12.698	1.388	0.178	1.112	0.0301	2067	6.67	+0.0517

Table 21. Condensation of Trichloroethylene Vapor, Summary of Results: $D' = 0.16667$ Ft., $\Delta T' = 10^{\circ}$ F, $Pr_{\ell} = 2.26$, $C'_p \Delta T'/\lambda' = 0.0236$

$\bar{u}'$ ft/sec	Re_g	Fr_L	z' ft	h'_m ratio	$\frac{h'_m}{\Phi'}$	h'_{loc} ratio	$\frac{2\delta'}{D'}$	Film Re	τ^*	P
25	133130	1541.8	0.0126	2.267	1.946	1.627	0.00071	11.3	5.576	-0.00194
		220.5	0.0881	1.588	0.838	1.240	0.00152	34.0	2.809	+0.00064
		46.5	0.418	1.276	0.457	1.083	0.00257	87.8	1.497	+0.01991
		15.6	1.242	1.153	0.314	1.038	0.0035	179.8	0.988	+0.07291
		6.47	3.002	1.092	0.239	1.018	0.0045	329.9	0.702	+0.18641

Table 22. Radial and Axial Velocity Profiles in the Vapor Phase: Trichloroethylene, $D' = 0.03825$ ft., $\Delta T' = 10^{\circ}$ F., $\bar{u}' =$ 100 ft./sec., $Re_g = 122213$, $Pr_\ell = 3.26$, $C_p'\Delta T'/\lambda' = 0.0236$.

z' in ft.	R = 0.0		R = 0.45		R = 0.75		R = 0.90		R = 0.96	
	U	V	U	V	U	V	U	V	U	V
0.0453	1.031	0.00000	1.031	-0.01634	1.031	-0.02723	1.031	-0.03268	1.028	-0.03474
0.201	1.069	0.00000	1.069	0.00005	1.069	0.00009	1.056	0.00012	0.743	0.00030
0.547	1.064	0.00000	1.064	0.00003	1.064	0.00005	1.035	0.00008	0.666	0.00024
0.923	1.064	0.00000	1.064	0.00000	1.064	0.00000	1.010	0.00004	0.579	0.00021
1.894	1.063	0.00000	1.063	0.00001	1.063	0.00001	0.929	0.00007	0.430	0.00019
3.174	1.059	0.00000	1.059	0.00001	1.057	0.00003	0.831	0.00010	0.326	0.00018
5.027	1.051	0.00000	1.051	0.00002	1.040	0.00004	0.722	0.00012	0.244	0.00016
6.668	1.042	0.00000	1.042	0.00002	1.018	0.00005	0.650	0.00012	0.199	0.00015

Table 23. Velocity and Temperature Profiles in the Liquid Phase: Trichloroethylene, $D' = 0.03825$ Ft., $\Delta T' = 10^{\circ}$ F., $\bar{u}' = 100$ ft./sec., $Re_g = 122213$, $Pr_\ell = 3.26$, $C_p'\Delta T'/\lambda' = 0.0236$

	$z' = 0.0453$ Ft.			$z' = 0.201$ Ft.			$z' = 0.547$ Ft.			$z' = 0.923$ Ft.		
R	$Ux10^5$	$Vx10^9$	T	$Ux10^5$	$Vx10^9$	T	$Ux10^5$	$Vx10^9$	T	$Ux10^5$	$Vx10^9$	T
1,000000	0	0	0.000	0	0	0.000	0	0	0.000	0	0	0.000
0.999508	161	-2453	0.143	73	-1	0.071	69	-1	0.053	66	0	0.043
0.999016	317	-9855	0.286	145	-6	0.143	138	-2	0.105	131	-1	0.087
0.998524	468	-22238	0.429	216	-12	0.214	205	-5	0.158	195	-3	0.130
0.998032	612	-39543	0.572	286	-22	0.286	272	-9	0.210	258	-6	0.174
0.997540	750	-61576	0.715	355	-34	0.357	337	-14	0.263	320	-9	0.217
0.997047	879	-87961	0.857	423	-48	0.429	402	-20	0.315	381	-13	0.260
0.996555	998	-117712	1.000	491	-65	0.500	466	-27	0.368	440	-18	0.304
0.996063	---	-------	-----	557	-85	0.572	528	-35	0.420	500	-23	0.347
0.995571	---	-------	-----	622	-107	0.643	590	-45	0.473	558	-29	0.391
0.995079	---	-------	-----	686	-131	0.715	650	-56	0.526	615	-36	0.434
0.994587	---	-------	-----	749	-158	0.786	710	-67	0.578	671	-43	0.477
0.994095	---	-------	-----	812	-187	0.857	769	-80	0.632	726	-52	0.521
0.993603	---	-------	-----	873	-218	0.929	826	-94	0.684	780	-61	0.565
0.993111	---	-------	-----	933	-250	1.000	883	-110	0.737	833	-71	0.608
0.992619	---	-------	-----	---	----	-----	939	-126	0.790	886	-81	0.652
0.992127	---	-------	-----	---	----	-----	993	-144	0.842	937	-92	0.696
0.991634	---	-------	-----	---	----	-----	1047	-162	0.895	987	-104	0.739
0.991142	---	-------	-----	---	----	-----	1100	-182	0.947	1036	-117	0.783
0.990650	---	-------	-----	---	----	-----	1152	-203	1.000	1084	-130	0.826
0.990158	---	-------	-----	---	----	-----	----	----	-----	1131	-144	0.870
0.989666	---	-------	-----	---	----	-----	----	----	-----	1177	-159	0.913
0.989174	---	-------	-----	---	----	-----	----	----	-----	1222	-175	0.957
0.988682	---	-------	-----	---	----	-----	----	----	-----	1266	-191	1.000

(continued)

Table (concluded)

R	z′ = 1.894 Ft.			z′ = 3.174 Ft.			z′ = 5.027 Ft.			z′ = 6.668 Ft.		
	$Ux10^5$	$Vx10^9$	T	$Ux10^5$	$Vx10^9$	T	$Ux10^5$	$Vx10^9$	T	$Ux10^5$	$Vx10^9$	T
1.000000	0	0	0.000	0	0	0.000	0	0	0.000	0	0	0.000
0.999016	12	-0	0.066	12	0	0.055	12	0	0.047	13	0	0.043
0.998032	24	-1	0.133	24	0	0.110	24	1	0.095	25	1	0.086
0.997047	36	-3	0.199	36	0	0.166	36	1	0.142	37	1	0.129
0.996063	47	-5	0.266	47	0	0.221	47	2	0.189	48	2	0.173
0.995079	58	-8	0.332	57	0	0.277	58	3	0.237	59	3	0.216
0.994095	68	-12	0.399	68	0	0.332	69	4	0.284	70	5	0.259
0.993111	78	-16	0.466	78	1	0.388	79	6	0.332	80	7	0.303
0.992127	88	-21	0.533	87	1	0.443	88	8	0.379	90	9	0.346
0.991142	97	-27	0.599	96	1	0.499	98	10	0.427	100	11	0.389
0.990158	106	-33	0.666	105	1	0.554	107	12	0.475	109	14	0.433
0.989174	115	-40	0.733	113	1	0.610	115	14	0.522	118	17	0.476
0.988189	123	-47	0.799	121	2	0.666	123	17	0.570	126	20	0.520
0.987206	130	-55	0.866	129	2	0.721	131	20	0.618	134	23	0.564
0.986221	137	-64	0.933	136	2	0.777	138	23	0.665	141	27	0.607
0.985237	144	-74	1.000	142	2	0.833	145	27	0.713	148	31	0.651
0.984253	---	---	-----	149	3	0.889	151	30	0.761	155	35	0.694
0.983269	---	---	-----	155	3	0.944	158	34	0.809	161	40	0.738
0.982285	---	---	-----	160	4	1.000	163	39	0.857	167	45	0.782
0.981300	---	---	-----	---	-	-----	169	43	0.904	173	50	0.825
0.980316	---	---	-----	----	-	-----	173	48	0.952	178	55	0.869
0.979332	---	---	-----	---	-	-----	178	53	1.000	183	61	0.913
0.978348	---	---	-----	---	-	-----	---	--	-----	187	67	0.956
0.977364	---	---	-----	---	-	-----	---	--	-----	191	73	1.000

Table 24. Radial and Axial Velocity Profiles in the Vapor Phase: Water, $D' = 0.03825$ Ft., $\Delta T' = 5^{\circ}$ F., $\bar{u}' = 10$ ft./sec., $Re_g = 1692$, $Pr_\ell = 1.79$, $C_p'\Delta T'/\lambda' = 0.00519$

z' in ft.	R = 0.0		R = 0.45		R = 0.75		R = 0.90		R = 0.96	
	U	V	U	V	U	V	U	V	U	V
0.00599	1.026	0.00000	1.026	-0.00066	1.026	-0.00111	1.021	-0.00089	0.810	0.01198
0.0212	1.022	0.00000	1.022	0.00143	1.021	0.00239	0.960	0.00545	0.588	0.01445
0.0674	0.997	0.00000	0.997	0.00265	0.990	0.00462	0.765	0.00923	0.375	0.01241
0.128	0.957	0.00000	0.956	0.00293	0.921	0.00552	0.612	0.00932	0.275	0.01072
0.291	0.843	0.00000	0.839	0.00308	0.716	0.00623	0.392	0.00838	0.163	0.00872
0.466	0.719	0.00000	0.700	0.00323	0.523	0.00635	0.257	0.00766	0.106	0.00771
0.713	0.539	0.00000	0.487	0.00353	0.298	0.00630	0.132	0.00700	0.060	0.00690
0.957	0.339	0.00000	0.264	0.00391	0.117	0.00625	0.047	0.00657	0.032	0.00639

Table 25. Velocity and Temperature Profiles in the Liquid Phase: Water, $D' = 0.03825$ Ft., $\Delta T' = 5^{\circ}$ F., $\bar{u}' = 10$ ft./sec., $Re_g = 1692$, $Pr_\ell = 1.79$, $C_p'\Delta T'/\lambda' = 0.00519$

	$z' = 0.00599$ Ft.			$z' = 0.0212$ Ft.			$z' = 0.0674$ Ft.			$z' = 0.128$ Ft.		
R	$Ux10^5$	$Vx10^9$	T	$Ux10^5$	$Vx10^9$	T	$Ux10^5$	$Vx10^9$	T	$Ux10^5$	$Vx10^9$	T
1.000000	0	0	0.000	0	0	0.000	0	0	0.000	0	0	0.000
0.999685	78	-30	0.111	77	5	0.071	87	6	0.050	96	4	0.042
0.999369	152	-122	0.222	151	19	0.143	170	23	0.100	189	17	0.083
0.999054	223	-273	0.333	221	43	0.214	250	52	0.150	278	37	0.125
0.998739	290	-485	0.444	288	77	0.285	326	92	0.200	364	67	0.166
0.998423	353	-757	0.555	351	120	0.357	399	145	0.250	446	104	0.208
0.998108	413	-1089	0.667	410	173	0.428	467	208	0.300	524	150	0.249
0.997793	469	-1481	0.778	466	236	0.500	533	283	0.349	599	204	0.291
0.997477	522	-1933	0.889	518	308	0.571	594	370	0.399	670	266	0.333
0.997162	570	-2436	1.000	566	390	0.643	652	469	0.449	737	337	0.374
0.996847	---	----	-----	611	482	0.714	706	579	0.499	801	416	0.416
0.996531	---	----	-----	652	583	0.786	757	700	0.549	861	504	0.458
0.996216	---	----	-----	689	694	0.857	804	834	0.600	917	599	0.499
0.995901	---	----	-----	723	815	0.929	847	979	0.650	970	704	0.541
0.995585	---	----	-----	753	941	1.000	887	1135	0.700	1019	816	0.583
0.995270	---	----	-----	---	---	-----	923	1303	0.750	1065	937	0.624
0.994955	---	----	-----	---	---	-----	955	1483	0.800	1107	1066	0.666
0.994639	---	----	-----	---	---	-----	984	1675	0.850	1145	1204	0.708
0.994324	---	----	-----	---	---	-----	1009	1878	0.900	1179	1350	0.750
0.994009	---	----	-----	---	---	-----	1030	2093	0.950	1210	1505	0.791
0.993694	---	----	-----	---	---	-----	1048	2314	1.000	1238	1668	0.833
0.993378	---	----	-----	---	---	-----	----	----	-----	1261	1839	0.875
0.993063	---	----	-----	---	---	-----	----	----	-----	1281	2019	0.916
0.992748	---	----	-----	---	---	-----	----	----	-----	1297	2207	0.958
0.992432	---	----	-----	---	---	-----	----	----	-----	1310	2399	1.000

(continued)

Table (concluded)

R	z′ = 0.291 Ft.			z′ = 0.466 Ft.			z′ = 0.713 Ft.			z′ = 0.957 Ft.		
	$Ux10^5$	$Vx10^9$	T	$Ux10^5$	$Vx10^9$	T	$Ux10^5$	$Vx10^9$	T	$Ux10^5$	$Vx10^9$	T
1.00000	0	0	0.000	0	0	0.000	0	0	0.000	0	0	0.000
0.999369	221	10	0.066	245	7	0.059	269	5	0.052	288	4	0.049
0.998739	429	39	0.133	476	29	0.117	524	21	0.105	561	17	0.097
0.998108	622	89	0.199	692	64	0.176	764	48	0.157	820	39	0.146
0.997477	800	158	0.266	893	114	0.234	989	85	0.210	1064	69	0.194
0.996847	964	247	0.332	1078	179	0.293	1200	133	0.262	1293	108	0.243
0.996216	1113	356	0.399	1252	257	0.352	1397	191	0.315	1509	156	0.292
0.995585	1247	484	0.466	1410	350	0.411	1579	260	0.367	1709	212	0.340
0.994955	1367	633	0.532	1554	458	0.469	1746	340	0.420	1895	277	0.389
0.994324	1473	801	0.599	1682	579	0.528	1899	430	0.472	2067	351	0.438
0.993694	1563	989	0.666	1796	715	0.587	2038	531	0.525	2224	433	0.486
0.993063	1640	1197	0.733	1896	866	0.646	2162	643	0.578	2367	524	0.535
0.992432	1701	1425	0.799	1981	1031	0.705	2271	766	0.630	2494	624	0.584
0.991802	1748	1674	0.866	2051	1210	0.764	2365	899	0.683	2608	733	0.633
0.991171	1781	1942	0.933	2107	1404	0.823	2445	1042	0.736	2706	850	0.682
0.990540	1799	2227	1.000	2148	1613	0.882	2511	1198	0.789	2791	976	0.731
0.989910	----	----	-----	2175	1836	0.941	2562	1363	0.841	2860	1111	0.780
0.989279	----	----	-----	2187	2071	1.000	2598	1539	0.894	2915	1255	0.829
0.988648	----	----	-----	----	----	-----	2620	1726	0.947	2955	1407	0.878
0.988018	----	----	-----	----	----	-----	2626	1923	1.000	2981	1568	0.926
0.987387	----	----	-----	----	----	-----	----	----	-----	2992	1738	0.975
0.987072	----	----	-----	----	----	-----	----	----	-----	2992	1826	1.000

Table 26. Radial and Axial Velocity Profiles in the Vapor Phase: Water, $D' = 0.16667$ Ft., $\Delta T' = 5^{\circ}$ F., $\bar{u}' = 100$ ft./sec., $Re_g = 73{,}739$, $Pr_\ell = 1.79$, $C_p'\Delta T'/\lambda' = 0.00519$

z' in ft.	R = 0.0		R = 0.45		R = 0.75		R = 0.90		R = 0.96	
	U	V	U	V	U	V	U	V	U	V
0.105	1.012	0.00000	1.012	-0.00264	1.012	-0.00440	1.012	-0.00528	1.010	-0.00561
0.390	1.015	0.00000	1.015	-0.00010	1.015	-0.00016	1.015	-0.00019	0.978	-0.00008
1.080	1.017	0.00000	1.017	-0.00002	1.017	-0.00004	1.016	-0.00004	0.858	0.00023
2.478	1.015	0.00000	1.015	0.00004	1.015	0.00007	0.998	0.00011	0.700	0.00037
5.041	1.007	0.00000	1.007	0.00007	1.007	0.00012	0.934	0.00021	0.559	0.00037
9.361	0.988	0.00000	0.988	0.00009	0.987	0.00014	0.831	0.00025	0.444	0.00034
16.153	0.956	0.00000	0.956	0.00009	0.946	0.00016	0.711	0.00026	0.350	0.00031

Table 27. Radial and Axial Velocity Profiles in the Vapor Phase: Water, $D' = 0.03825$ Ft., $\Delta T' = 5^{\circ}$ F., $\bar{u}' = 100$ ft./sec., $Re_g = 16{,}923$, $Pr_\ell = 1.79$, $C_p'\Delta T'/\lambda' = 0.00519$

z′ in ft.	R = 0.0		R = 0.45		R = 0.75		R = 0.90		R = 0.96	
	U	V	U	V	U	V	U	V	U	V
0.200	1.043	0.00000	1.043	-0.00033	1.043	-0.00055	0.965	-0.00028	0.544	0.00087
0.280	1.048	0.00000	1.048	-0.00025	1.048	-0.00041	0.917	0.00001	0.472	0.00088
0.380	1.053	0.00000	1.053	-0.00018	1.051	-0.00029	0.861	0.00021	0.412	0.00086
0.503	1.057	0.00000	1.057	-0.00013	1.053	-0.00020	0.803	0.00034	0.362	0.00082
0.652	1.060	0.00000	1.060	-0.00009	1.049	-0.00011	0.744	0.00042	0.319	0.00077
0.832	1.063	0.00000	1.063	-0.00006	1.040	-0.00003	0.688	0.00047	0.281	0.00073
1.304	1.066	0.00000	1.066	-0.00001	1.002	0.00010	0.583	0.00051	0.220	0.00064
1.957	1.065	0.00000	1.064	0.00002	0.936	0.00021	0.491	0.00050	0.173	0.00057

Table 28. Radial and Axial Velocity Profiles in the Vapor Phase: Ethanol, $D' = 0.03825$ Ft., $\Delta T' = 10^{\circ}$ F., $\bar{u}' = 200$ ft./sec., $Re_g = 82{,}802$, $Pr_\ell = 8.02$, $C_p'\Delta T'/\lambda' = 0.0185$

z' in ft.	R = 0.0		R = 0.45		R = 0.75		R = 0.90		R = 0.96	
	U	V	U	V	U	V	U	V	U	V
0.277	1.091	0.00000	1.091	-0.00134	1.091	-0.00224	1.069	-0.00256	0.980	-0.00215
0.968	1.127	0.00000	1.127	-0.00014	1.127	-0.00024	0.951	-0.00014	0.749	-0.00002
2.646	1.166	0.00000	1.166	-0.00008	1.150	-0.00012	0.759	0.00001	0.541	0.00006
5.585	1.206	0.00000	1.206	-0.00005	1.120	-0.00005	0.593	0.00005	0.394	0.00007
10.366	1.246	0.00000	1.243	-0.00003	1.034	0.00000	0.463	0.00006	0.290	0.00007
17.706	1.282	0.00000	1.262	-0.00001	0.917	0.00003	0.361	0.00006	0.213	0.00006

APPENDIX F

GAS-VAPOR CONDENSATION RESULTS

This appendix contains the numerical results described in Chapter IV for the condensation of vapors from gas-vapor mixtures.

Table 29. Condensation of Water Vapor From a Water Vapor and Air Mixture, Summary of Results: $D' = 0.16667$ ft., $\overline{u}' = 100$ ft./sec., $Re_g = 73739$, $Pr_\ell = 1.79$, $Sc_g = 0.500$

W_{air_o}	$\Delta T'$ °F	Fr_L	z' ft	h'_m ratio	$\frac{h'_m}{\Phi'}$	h'_{loc} ratio	$\frac{2\delta'}{D'}$	Film Re	τ^*	W_{air_q}
0.001	10	63.69	4.880	1.148	0.240	1.057	0.00481	397	2.082	0.00722
		39.66	7.836	1.117	0.208	1.030	0.00555	551	1.726	0.00738
		31.99	9.717	1.104	0.194	1.019	0.00592	640	1.548	0.00757
		26.05	11.932	1.091	0.182	1.008	0.00629	738	1.379	0.00785
		21.39	14.528	1.079	0.172	0.999	0.00666	846	1.220	0.00823
0.010	5	72.39	4.293	1.085	0.279	0.910	0.00389	203	1.522	0.02535
		41.65	7.463	1.021	0.228	0.882	0.00454	289	1.207	0.02730
		25.25	12.310	0.975	0.192	0.862	0.00519	402	0.981	0.02911
		20.05	15.502	0.956	0.178	0.852	0.00552	468	0.883	0.03015
		16.10	19.304	0.940	0.166	0.841	0.00584	543	0.792	0.03131
0.010	10	69.26	4.488	1.054	0.225	0.920	0.00462	342	1.880	0.05072
		39.85	7.799	1.005	0.187	0.896	0.00539	494	1.582	0.05322
		24.79	12.537	0.968	0.160	0.869	0.00616	679	1.263	0.05689
		19.91	15.608	0.952	0.149	0.854	0.00654	787	1.112	0.05949
		16.14	19.258	0.937	0.139	0.838	0.00693	907	0.969	0.06270

Table 30. Condensation of Water Vapor From a Water Vapor and Air Mixture, Summary of Results: $D' = 0.16667$ ft., $\bar{u}' = 25$ ft./sec., $Re_g = 18435$, $Pr_\ell = 1.79$, $Sc_g = 0.500$

W_{air_o}	$\Delta T'_o$ F	Fr_L	z' ft	h'_m ratio	$\frac{h'_m}{\Phi'}$	h'_{loc} ratio	$\frac{2\delta'}{D'}$	Film Re	τ^*	W_{air_q}
0.001	10	203.18	0.0956	1.285	0.718	1.168	0.00164	23	1.634	0.00503
		96.00	0.202	1.219	0.565	1.106	0.00209	39	1.355	0.00512
		51.81	0.375	1.169	0.464	1.062	0.00254	59	1.087	0.00526
		16.07	1.209	1.085	0.322	1.003	0.00359	132	0.702	0.00665
		7.10	2.737	1.042	0.252	0.976	0.00448	233	0.434	0.00899
0.005	10	184.82	0.105	1.237	0.675	1.094	0.00169	24	1.518	0.02235
		85.43	0.227	1.160	0.522	1.038	0.00216	40	1.240	0.02340
		26.67	0.728	1.066	0.359	0.960	0.00308	89	0.814	0.02687
		10.11	1.922	1.001	0.264	0.916	0.00401	172	0.532	0.03397
		4.54	4.282	0.951	0.205	0.863	0.00493	298	0.299	0.04762
0.010	10	131.18	0.148	1.158	0.580	0.992	0.00190	29	1.261	0.04100
		48.42	0.401	1.058	0.413	0.944	0.00254	56	0.977	0.04400
		15.97	1.217	0.971	0.287	0.871	0.00348	118	0.647	0.05359
		6.31	3.078	0.905	0.212	0.806	0.00443	221	0.382	0.06911
		3.65	5.322	0.862	0.176	0.744	0.00506	318	0.243	0.08650
0.020	10	112.81	0.172	1.074	0.518	0.876	0.00197	30	1.100	0.07034
		39.20	0.496	0.952	0.353	0.829	0.00263	59	0.830	0.07720
		12.19	1.594	0.853	0.236	0.741	0.00362	127	0.529	0.09411
		4.52	4.295	0.770	0.166	0.646	0.00460	242	0.287	0.11895
		2.47	7.873	0.708	0.131	0.548	0.00526	350	0.165	0.14452
0.050	10	75.05	0.259	0.881	0.384	0.627	0.00215	34	0.796	0.13221
		22.10	0.879	0.708	0.227	0.567	0.00287	68	0.534	0.14766
		8.92	2.178	0.621	0.159	0.484	0.00359	117	0.363	0.16586
		3.77	5.150	0.539	0.111	0.408	0.00430	193	0.231	0.18420
		1.70	11.455	0.458	0.077	0.308	0.00502	299	0.125	0.20625

Table 31. Condensation of Water Vapor From a Water Vapor and Air Mixture, Summary of Results: $D' = 0.16667$ ft., $\bar{u}' = 25$ ft./sec., $Re_g = 18435$, $Pr_\ell = 1.79$, $Sc_g = 0.500$

W_{air_o}	$\Delta T'$ °F	Fr_L	z' ft	h'_m ratio	$\frac{h'_m}{\Phi'}$	h'_{loc} ratio	$\frac{2\delta'}{D'}$	Film Re	τ^*	W_{air_q}
0.010	5	532.03	0.0365	1.406	1.188	1.112	0.00101	7	1.617	0.0196
		26.04	0.746	0.993	0.395	0.889	0.00257	50	0.538	0.0259
		6.72	2.892	0.905	0.256	0.826	0.00365	126	0.286	0.0331
		2.61	7.447	0.848	0.190	0.760	0.00459	240	0.156	0.0431
		1.44	13.526	0.803	0.155	0.685	0.00527	355	0.089	0.0547
0.050	5	58.61	0.331	0.805	0.392	0.512	0.00191	22	0.561	0.0835
		15.34	1.266	0.594	0.207	0.446	0.00255	44	0.312	0.0937
		5.68	3.417	0.502	0.136	0.381	0.00319	79	0.213	0.1021
		2.29	8.472	0.429	0.093	0.324	0.00382	133	0.143	0.1098
		1.02	19.079	0.366	0.065	0.257	0.00446	209	0.091	0.1179

Table 32. Condensation of Water Vapor From a Water Vapor and Air Mixture, Summary of Results: $D' = 0.16667$ ft., $\overline{u}' = 2.5$ ft./sec., $Re_g = 1843$, $Pr_\ell = 1.79$, $Sc_g = 0.500$

W_{air_o}	$\Delta T'$ °F	Fr_L	z' ft	h'_m ratio	$\frac{h'_m}{\Phi'}$	h'_{loc} ratio	$\frac{2\delta'}{D'}$	Film Re	τ^*	W_{air_q}
0.010	5	17.686	0.0110	0.953	1.087	0.864	0.00090	2.0	0.148	0.0292
		3.643	0.0533	0.866	0.666	0.800	0.00135	6.0	0.088	0.0371
		1.091	0.1780	0.807	0.459	0.734	0.00179	13.8	0.049	0.0480
		0.512	0.3794	0.761	0.358	0.666	0.00213	23.0	0.029	0.0592
		0.321	0.6043	0.724	0.303	0.606	0.00235	30.9	0.020	0.0688
0.020	5	17.237	0.0113	0.845	0.958	0.729	0.00087	1.8	0.129	0.0512
		3.639	0.0534	0.738	0.567	0.652	0.00128	5.1	0.078	0.0620
		0.925	0.2100	0.653	0.356	0.561	0.00175	12.7	0.040	0.0763
		0.390	0.4986	0.588	0.259	0.475	0.00210	21.7	0.023	0.0891
		0.227	0.8560	0.539	0.207	0.408	0.00233	29.8	0.015	0.0986
0.050	5	19.210	0.0101	0.621	0.724	0.454	0.00077	1.2	0.100	0.0922
		2.154	0.0902	0.438	0.295	0.350	0.00124	4.5	0.046	0.1070
		0.273	0.7112	0.312	0.125	0.231	0.00185	15.0	0.016	0.1220
		0.113	1.7164	0.259	0.084	0.179	0.00216	23.8	0.010	0.1280
		0.063	3.0669	0.225	0.063	0.143	0.00237	31.3	0.007	0.1320
0.010	10	14.039	0.0138	0.977	0.885	0.887	0.00113	4.1	0.226	0.0508
		4.224	0.0460	0.906	0.608	0.830	0.00154	9.4	0.136	0.0646
		1.596	0.1217	0.851	0.448	0.770	0.00195	18.3	0.080	0.0836
		0.845	0.2300	0.809	0.363	0.711	0.00226	27.9	0.049	0.1029
		0.567	0.3427	0.777	0.316	0.659	0.00247	36.0	0.033	0.1194

Table 33. Condensation of Water Vapor From a Water Vapor and Air Mixture, Summary of Results: $D' = 0.16667$ ft., $\bar{u}' = 25$ ft./sec., $Re_g = 18435$, $Pr_\ell = 1.79$, $Sc_g = 0.600$

W_{air_o}	$\Delta T'$ ^oF	Fr_L	z' ft	h'_m ratio	$\frac{h'_m}{\Phi'}$	h'_{loc} ratio	$\frac{2\delta'}{D'}$	Film Re	τ^*	W_{air_q}
0.005	10	138.29	0.140	1.191	0.604	1.040	0.00187	29	1.329	0.0290
		52.25	0.372	1.100	0.438	0.992	0.00249	55	1.038	0.0297
		17.63	1.102	1.020	0.309	0.927	0.00343	116	0.697	0.0353
		7.13	2.723	0.963	0.233	0.877	0.00437	215	0.424	0.0455
		4.21	4.612	0.928	0.197	0.832	0.00499	307	0.280	0.0577
0.010	10	50.70	0.383	0.996	0.394	0.871	0.00250	51	0.846	0.0637
		21.95	0.885	0.935	0.299	0.852	0.00312	90	0.681	0.0656
		13.83	1.405	0.907	0.259	0.830	0.00354	123	0.556	0.0691
		7.76	2.504	0.873	0.216	0.774	0.00416	183	0.419	0.0801
		3.63	5.346	0.815	0.167	0.697	0.00499	302	0.257	0.1015
0.020	10	41.57	0.467	0.901	0.339	0.743	0.00259	54	0.713	0.0991
		17.02	1.141	0.819	0.246	0.718	0.00323	95	0.553	0.1051
		10.39	1.869	0.783	0.208	0.690	0.00366	132	0.442	0.1147
		5.60	3.470	0.737	0.168	0.614	0.00431	197	0.320	0.1285
		2.42	8.024	0.655	0.121	0.501	0.00517	328	0.177	0.1578
0.050	10	23.63	0.822	0.686	0.224	0.481	0.00282	62	0.470	0.1660
		11.33	1.714	0.594	0.161	0.455	0.00329	94	0.361	0.1742
		6.08	3.195	0.536	0.125	0.419	0.00376	135	0.272	0.1832
		3.47	5.599	0.488	0.099	0.374	0.00423	187	0.197	0.1935
		2.15	9.035	0.444	0.079	0.296	0.00470	243	0.149	0.2089

Table 34. Condensation of Water Vapor From a Water Vapor and Air Mixture, Summary of Results: $D' = 0.16667$ ft., $\bar{u}' = 2.5$ ft./sec., $Re_g = 1843$, $Pr_\ell = 1.79$, $Sc_g = 0.600$

W_{air_o}	$\Delta T'$ ^oF	Fr_L	z' ft	h'_m ratio	$\frac{h'_m}{\Phi'}$	h'_{loc} ratio	$\frac{2\delta'}{D'}$	Film Re	τ^*	W_{air_q}
0.010	5	16.853	0.0115	0.931	1.050	0.841	0.00090	2.1	0.142	0.0330
		3.428	0.0567	0.842	0.637	0.772	0.00135	6.1	0.084	0.0419
		1.013	0.1918	0.778	0.434	0.697	0.00181	14.1	0.046	0.0541
		0.468	0.4147	0.726	0.334	0.622	0.00214	23.4	0.027	0.0662
		0.290	0.6687	0.685	0.280	0.558	0.00237	31.5	0.018	0.0763
0.020	5	15.909	0.0122	0.814	0.904	0.695	0.00088	1.9	0.122	0.0566
		3.284	0.0592	0.703	0.526	0.613	0.00129	5.3	0.073	0.0682
		0.814	0.2387	0.612	0.323	0.515	0.00177	13.1	0.036	0.0833
		0.335	0.5802	0.542	0.229	0.426	0.00212	22.4	0.020	0.0962
		0.191	1.0151	0.491	0.181	0.360	0.00235	30.7	0.013	0.1053
0.050	5	16.616	0.0117	0.581	0.652	0.416	0.00079	1.3	0.091	0.0974
		1.763	0.1102	0.396	0.254	0.310	0.00126	4.7	0.041	0.1121
		0.403	0.4817	0.309	0.137	0.232	0.00168	11.1	0.020	0.1218
		0.115	1.6844	0.240	0.078	0.167	0.00210	21.7	0.010	0.1293
		0.047	4.1399	0.192	0.050	0.121	0.00241	33.1	0.006	0.1344
0.010	10	18.936	0.0103	0.974	0.951	0.875	0.00104	3.3	0.238	0.0562
		5.136	0.0378	0.894	0.630	0.815	0.00146	8.0	0.147	0.0704
		2.328	0.0834	0.848	0.490	0.767	0.00177	13.8	0.098	0.0846
		1.454	0.1336	0.819	0.421	0.732	0.00198	18.9	0.074	0.0958
		0.938	0.2072	0.789	0.363	0.691	0.00219	25.2	0.053	0.1088

Table 35. Condensation of Water Vapor From a Water Vapor and Air Mixture, Summary of Results: $D' = 0.03825$ ft., $\overline{u}' = 25$ ft./sec., $Re_g = 4231$, $Pr_\ell = 1.79$, $Sc_g = 0.500$

W_{air_o}	$\Delta T'$ ^oF	Fr_L	z' ft	h'_m ratio	$\frac{h'_m}{\Phi'}$	h'_{loc} ratio	$\frac{2\delta'}{D'}$	Film Re	τ^*	W_{air_q}
0.050	10	55.87	0.348	0.815	0.330	0.570	0.0101	38.8	0.704	0.145
		40.04	0.485	0.758	0.282	0.540	0.0109	46.3	0.593	0.152
		29.23	0.665	0.709	0.244	0.510	0.0117	54.9	0.492	0.159
		21.60	0.899	0.666	0.212	0.476	0.0126	64.7	0.403	0.167
		16.06	1.210	0.624	0.185	0.436	0.0134	75.7	0.324	0.176

Table 36. Condensation of Ethanol Vapor From an Ethanol Vapor and Air Mixture, Summary of Results: $D' = 0.16667$ ft., $\bar{u}' = 200$ ft./sec., $Re_g = 360793$, $Pr_\ell = 8.03$, $Sc_g = 0.537$

W_{air_o}	$\Delta T'$ ^oF	Fr_L	z' ft	h'_m ratio	$\frac{h'_m}{\Phi'}$	h'_{loc} ratio	$\frac{2\delta'}{D'}$	Film Re	τ^*	W_{air_q}
0.010	10	371.05	3.351	1.422	0.464	1.250	0.00382	130	5.841	0.0152
		255.84	4.859	1.354	0.402	1.086	0.00477	163	3.906	0.0164
		183.23	6.785	1.289	0.352	1.037	0.00540	199	3.308	0.0168
		113.93	10.912	1.207	0.293	0.988	0.00636	266	2.758	0.0174
		83.22	14.940	1.159	0.260	0.967	0.00699	323	2.469	0.0178

Table 37. Condensation of Ethanol Vapor From an Ethanol Vapor and Air Mixture, Summary of Results: $D' = 16667$ ft., $\overline{u}' = 100$ ft./sec., $Re_g = 180397$, $Pr_\ell = 8.03$, $Sc_g = 0.537$

W_{air_o}	$\Delta T'$ ^oF	Fr_L	z' ft	h'_m ratio	$\frac{h'_m}{\Phi'}$	h'_{loc} ratio	$\frac{2\delta'}{D'}$	Film Re	τ^*	W_{air_q}
0.001	10	51.10	6.083	1.189	0.334	1.068	0.00575	169	1.733	0.00211
		40.87	7.604	1.168	0.310	1.034	0.00628	197	1.368	0.00218
		31.39	9.901	1.143	0.284	1.019	0.00680	234	1.180	0.00226
		24.11	12.890	1.120	0.261	1.010	0.00732	280	1.053	0.00232
		18.72	16.599	1.101	0.241	1.003	0.00785	333	0.951	0.00238
0.010	10	438.35	0.709	1.477	0.710	1.285	0.00252	42	4.466	0.01486
		229.04	1.357	1.338	0.547	1.052	0.00358	62	2.461	0.01648
		59.69	5.207	1.115	0.326	0.949	0.00547	141	1.499	0.01811
		28.71	10.824	1.037	0.252	0.916	0.00673	227	1.126	0.01927
		18.63	16.682	1.002	0.219	0.899	0.00757	303	0.944	0.02067
0.010	20	83.30	3.731	1.180	0.315	0.999	0.00590	195	2.082	0.02769
		50.06	6.209	1.116	0.263	0.963	0.00688	270	1.687	0.02973
		31.07	10.005	1.067	0.223	0.943	0.00786	369	1.430	0.03130
		24.94	12.461	1.048	0.207	0.934	0.00835	427	1.316	0.03215
		20.24	15.353	1.031	0.194	0.925	0.00884	491	1.209	0.03309

Table 38. Condensation of Ethanol Vapor From an Ethanol Vapor and Air Mixture, Summary of Results: $D' = 0.16667$ ft., $\bar{u}' = 25$ ft./sec., $Re_g = 45099$, $Pr_\ell = 8.03$, $Sc_g = 0.537$

W_{air_o}	$\Delta T'$ °F	Fr_L	z' ft	h'_m ratio	$\frac{h'_m}{\Phi'}$	h'_{loc} ratio	$\frac{2\delta'}{D'}$	Film Re	τ^*	W_{air_q}
0.001	10	32.97	0.589	1.144	0.576	1.023	0.00335	28	0.600	0.00225
		11.48	1.692	1.069	0.413	0.996	0.00447	58	0.388	0.00251
		5.09	3.820	1.033	0.326	0.974	0.00558	104	0.290	0.00285
		2.46	7.898	1.009	0.265	0.970	0.00670	174	0.217	0.00331
		1.33	14.591	0.994	0.224	0.964	0.00782	272	0.154	0.00395
0.005	10	30.32	0.641	1.097	0.541	0.964	0.00340	29	0.564	0.01077
		13.23	1.468	1.029	0.412	0.940	0.00425	50	0.394	0.01184
		6.50	2.990	0.990	0.332	0.928	0.00509	83	0.304	0.01283
		3.06	6.358	0.957	0.266	0.901	0.00623	141	0.231	0.01489
		1.55	12.526	0.932	0.219	0.823	0.00736	228	0.165	0.01744
0.010	10	27.26	0.713	1.042	0.500	0.894	0.00346	30	0.523	0.02064
		11.58	1.677	0.948	0.374	0.869	0.00432	52	0.361	0.02283
		5.60	3.471	0.922	0.298	0.852	0.00518	86	0.276	0.02479
		2.59	7.507	0.883	0.235	0.815	0.00633	147	0.207	0.02871
		1.29	15.078	0.850	0.190	0.783	0.00749	238	0.144	0.03348
0.020	10	21.82	0.890	0.941	0.427	0.767	0.00358	32	0.451	0.03858
		8.76	2.217	0.846	0.306	0.736	0.00447	56	0.302	0.04282
		5.19	3.741	0.808	0.256	0.720	0.00507	80	0.248	0.04523
		2.76	7.035	0.769	0.208	0.678	0.00596	122	0.194	0.04996
		1.24	15.675	0.718	0.159	0.630	0.00716	207	0.135	0.05710
0.050	10	26.37	0.737	0.768	0.366	0.503	0.00317	22	0.435	0.07546
		9.21	2.110	0.608	0.223	0.457	0.00396	39	0.257	0.08259
		5.08	3.824	0.550	0.174	0.437	0.00486	55	0.205	0.08583
		2.51	7.746	0.496	0.131	0.391	0.00528	84	0.160	0.09123
		1.03	18.899	0.434	0.092	0.344	0.00633	143	0.112	0.09756

Table 39. Condensation of Ethanol Vapor From an Ethanol Vapor and Air Mixture, Summary of Results: $D' = 0.16667$ ft., $\bar{u}' = 25$ ft./sec., $Re_g = 45099$, $Pr_\ell = 8.03$, $Sc_g = 0.537$

W_{air_o}	$\Delta T'$ ^oF	Fr_L	z' ft	h'_m ratio	$\frac{h'_m}{\Phi'}$	h'_{loc} ratio	$\frac{2\delta'}{D'}$	Film Re	τ^*	W_{air_q}
0.010	5	53.67	0.362	1.119	0.757	0.870	0.00237	11	0.651	0.0138
		19.16	1.014	0.967	0.505	0.821	0.00315	21	0.348	0.0153
		5.49	3.539	0.869	0.332	0.789	0.00434	49	0.228	0.0170
		2.03	9.573	0.821	0.245	0.765	0.00552	98	0.154	0.0188
		1.16	16.684	0.799	0.207	0.745	0.00631	144	0.120	0.0203
0.010	20	66.32	0.293	1.147	0.579	0.981	0.00317	28	0.930	0.0288
		30.10	0.645	1.063	0.441	0.944	0.00396	47	0.710	0.0316
		15.30	1.270	1.012	0.354	0.922	0.00475	74	0.565	0.0340
		5.21	3.727	0.946	0.253	0.871	0.00633	155	0.383	0.0427
		2.81	6.907	0.913	0.209	0.840	0.00739	238	0.276	0.0506
0.050	5	12.55	1.548	0.453	0.213	0.201	0.00275	13.7	0.264	0.0567
		4.59	4.237	0.315	0.115	0.185	0.00321	20.2	0.163	0.0583
		2.10	9.258	0.255	0.077	0.175	0.00367	29.3	0.123	0.0592
		1.50	12.922	0.237	0.066	0.169	0.00390	34.9	0.111	0.0596
		1.11	17.547	0.223	0.057	0.164	0.00413	41.2	0.102	0.0599
0.050	20	13.39	1.450	0.744	0.252	0.559	0.00454	60	0.390	0.1347
		6.55	2.965	0.661	0.187	0.525	0.00530	91	0.295	0.1450
		4.77	4.076	0.631	0.165	0.509	0.00567	110	0.258	0.1497
		3.54	5.491	0.605	0.147	0.491	0.00605	132	0.226	0.1546
		2.67	7.277	0.582	0.132	0.472	0.00643	157	0.197	0.1598

Table 40. Condensation of Ethanol Vapor from an Ethanol Vapor and Air Mixture, Summary of Results: $D' = 0.03825$ ft., $\bar{u}' = 25$ ft./sec., $Re_g = 10350$, $Pr_\ell = 8.03$, $Sc_g = 0.537$

W_{air_o}	$\Delta T'$ °F	Fr_L	z' ft	h'_m ratio	$\frac{h'_m}{\Phi'}$	h'_{loc} ratio	$\frac{2\delta'}{D'}$	Film Re	τ^*	W_{air_q}
0.010	5	268.86	0.0723	1.345	1.360	1.143	0.00534	4.1	1.760	0.0128
		109.59	0.177	1.172	0.947	0.935	0.00802	7.0	0.907	0.0137
		19.21	1.011	0.954	0.499	0.841	0.01336	21.0	0.486	0.0152
		3.72	5.220	0.847	0.294	0.774	0.02049	64.0	0.255	0.0183
		1.94	10.004	0.810	0.239	0.726	0.02405	99.6	0.184	0.0213

Table 41. Velocity, Concentration and Temperature Profiles in the Vapor Phase: Water Vapor and Air, $D' = 0.16667$ Ft., $\bar{u}' = 25$ ft./sec., $Re_g = 18435$, $Pr_\ell = 1.79$, $T'_o = 212^o$ F, $T'_w = 202^o$ F, $W_{air_o} = 0.05$, $Sc_g = 0.600$.

z' in ft.	R = 0.0				R = 0.45				R = 0.75			
	U	V	T	C	U	V	T	C	U	V	T	C
0.409	1.014	0.00000	1.000	0.0500	1.014	-0.00063	1.000	0.0500	1.014	-0.00105	1.000	0.0501
1.714	0.990	0.00000	1.000	0.0500	0.990	0.00054	1.000	0.0500	0.989	0.00091	0.999	0.0509
5.599	0.906	0.00000	1.000	0.0500	0.906	0.00035	1.000	0.0502	0.887	0.00060	0.983	0.0612

$\frac{\rho'-\rho'_o}{\rho'_{j+1,o}\overline{u'^2}}$	R = 0.90				R = 0.96				Interface			
	U	V	T	C	U	V	T	C	R	U	T	C
0.0073	0.999	-0.00119	0.984	0.0562	0.821	-0.00046	0.857	0.0867	0.99765	0.012	0.449	0.1553
0.0980	0.879	0.00126	0.931	0.0757	0.528	0.00160	0.704	0.1232	0.99671	0.017	0.373	0.1742
0.3789	0.655	0.00089	0.795	0.1119	0.335	0.00102	0.539	0.1575	0.99577	0.026	0.294	0.1935

Table 42. Velocity, Concentration and Temperature Profiles in the Vapor Phase: Water Vapor and Air, $D' = 0.03825$ Ft., $\bar{u}' = 25$ ft./sec., $Re_g = 4231$, $Pr_\ell = 1.79$, $T'_o = 212^o$ F, $T'_w = 202^o$ F., $W_{air_o} = 0.05$, $Sc_g = 0.500$.

	R = 0.0				R = 0.45				R = 0.75			
z′ in ft.	U	V	T	C	U	V	T	C	U	V	T	C
0.204	1.049	0.00000	1.000	0.0500	1.048	-0.00103	0.999	0.0508	1.011	-0.00149	0.971	0.0613
0.665	1.017	0.00000	1.000	0.0507	1.008	0.00064	0.999	0.0557	0.837	0.00154	0.905	0.0855
2.217	0.840	0.00000	1.000	0.0757	0.753	0.00052	0.999	0.0986	0.464	0.00107	0.732	0.1464

$\frac{p'-p'_o}{\rho'_{j+1,o}\bar{u}'^2}$	R = 0.90				R = 0.93				Interface			
	U	V	T	C	U	V	T	C	R	U	T	C
-0.0385	0.755	-0.00024	0.832	0.0907	0.606	0.00064	0.763	0.1021	0.99162	0.010	0.533	0.1338
0.0190	0.441	0.00231	0.686	0.1255	0.314	0.00241	0.613	0.1360	0.98827	0.012	0.436	0.1587
0.2397	0.199	0.00123	0.457	0.1805	0.137	0.00123	0.391	0.1879	0.98492	0.017	0.260	0.2017

Table 43. Velocity, Concentration and Temperature Profiles in the Vapor Phase: Water Vapor and Air, $D' = 0.16667$ Ft., $\bar{u}' = 2.5$ ft./sec., $Re_g = 1843$, $Pr_\ell = 1.79$, $T'_o = 212^\circ$ F, $T'_w = 207^\circ$ F, $W_{air_o} = 0.01$, $Sc_g = 0.600$.

	R = 0.0				R = 0.45				R = 0.75			
z′ in ft.	U	V	T	C	U	V	T	C	U	V	T	C
0.00238	1.004	0.00000	1.000	0.0100	1.004	-0.03183	1.000	0.0100	1.004	-0.05305	1.000	0.0100
0.00681	1.004	0.00000	1.000	0.0100	1.004	0.01571	1.000	0.0100	1.004	0.02619	1.000	0.0100
0.0183	0.993	0.00000	1.000	0.0100	0.993	0.01724	1.000	0.0100	0.993	0.02874	1.000	0.0100
0.0791	0.942	0.00000	1.000	0.0100	0.942	0.01418	1.000	0.0100	0.942	0.02364	1.000	0.0100
0.251	0.839	0.00000	1.000	0.0100	0.839	0.01018	1.000	0.0100	0.839	0.01697	1.000	0.0102
0.669	0.660	0.00000	1.000	0.0100	0.660	0.00714	1.000	0.0101	0.654	0.01194	0.995	0.0136

$\frac{p'-p'_o}{\rho'_{j+1,o}\bar{u}'^2}$	R = 0.90				R = 0.96				Interface			
	U	V	T	C	U	V	T	C	R	U	T	C
0.0082	1.004	-0.06367	1.000	0.0100	1.003	-0.06773	1.000	0.0102	0.99944	0.008	0.814	0.0286
0.0308	1.004	0.03143	1.000	0.0100	0.994	0.03504	0.999	0.0107	0.99921	0.011	0.795	0.0315
0.101	0.993	0.03449	1.000	0.0100	0.952	0.03951	0.997	0.0126	0.99898	0.016	0.774	0.0346
0.464	0.937	0.02854	0.999	0.0111	0.785	0.03351	0.969	0.0206	0.99853	0.030	0.707	0.0446
1.44	0.793	0.02102	0.983	0.0173	0.554	0.02404	0.885	0.0343	0.99808	0.050	0.617	0.0578
3.73	0.547	0.01487	0.909	0.0329	0.341	0.01594	0.733	0.0548	0.99763	0.076	0.488	0.0763

Table 44. Velocity and Temperature Profiles in the Liquid Phase: Water Vapor and Air, $D' = 0.16667$ ft., $\bar{u}' = 2.5$ ft./sec., $Re_{go} = 1843$, $Pr_{\ell} = 1.79$, $T'_o = 212^{o}$ F., $T'_w = 207^{o}$ F, $Sc_g = 0.600$, $W_{air_o} = 0.01$

z′ in feet	R	Ux10^5	Vx10^9	T
0.00238	0.999944	126	742	0.082
	0.999774	448	9513	0.326
	0.999549	751	25615	0.651
	0.999492	805	28141	0.733
	0.999436	849	29816	0.814
0.00681	0.999944	137	97	0.057
	0.999774	496	1554	0.227
	0.999549	849	6217	0.454
	0.999323	1059	13992	0.681
	0.999210	1111	18948	0.795
0.0183	0.999944	167	49	0.043
	0.999774	615	776	0.172
	0.999549	1088	3103	0.344
	0.999323	1418	6982	0.516
	0.998984	1646	15664	0.774
0.0791	0.999887	446	69	0.054
	0.999661	1232	616	0.163
	0.999210	2377	3356	0.381
	0.998759	2951	8289	0.599
	0.998533	3024	11510	0.707
0.251	0.999887	580	27	0.036
	0.999661	1633	244	0.1093
	0.999210	3313	1328	0.2546
	0.998759	4422	3281	0.3996
	0.998081	5017	7811	0.6169
0.669	0.999887	717	12	0.024
	0.999661	2044	104	0.071
	0.998759	5929	1393	0.257
	0.998307	7017	2590	0.349
	0.997630	7579	5067	0.488

Table 45. Velocity, Concentration and Temperature Profiles in the Vapor Phase: Ethanol Vapor and Air, $D' = 0.16667$ Ft., $\bar{u}' = 25$ ft./sec., $Re_g = 45099$, $Pr_\ell = 8.08$, $T'_o = 173.3^\circ$ F, $T'_w = 153.3^\circ$ F, $W_{air_o} = 0.05$, $Sc_g = 0.537$

z' in ft.	R = 0.0				R = 0.45				R = 0.75			
	U	V	T	C	U	V	T	C	U	V	T	C
0.750	1.017	0.00000	1.000	0.0500	1.017	-0.00044	1.000	0.0500	1.017	-0.00073	1.000	0.0500
2.965	1.028	0.00000	1.000	0.0500	1.028	0.00007	1.000	0.0500	1.027	0.00013	1.000	0.0505
9.521	0.997	0.00000	1.000	0.0500	0.997	0.00008	1.000	0.0500	0.979	0.00015	0.996	0.0571

$\frac{p'-p'_o}{\rho'_{j+1,o}\bar{u}'^2}$	R = 0.90				R = 0.9525				Interface			
	U	V	T	C	U	V	T	C	R	U	T	C
0.0212	1.008	-0.00085	0.993	0.0539	0.897	-0.00065	0.929	0.0701	0.99622	0.014	0.533	0.1232
0.1248	0.909	0.00032	0.961	0.0690	0.596	0.00058	0.812	0.1002	0.99470	0.021	0.449	0.1450
0.4936	0.711	0.00034	0.870	0.0979	0.403	0.00043	0.666	0.1310	0.99319	0.032	0.370	0.1652

Table 46. Velocity, Concentration and Temperature Profiles in the Vapor Phase: Ethanol Vapor and Air, $D' = 0.16667$ Ft., $\bar{u}' = 100$ ft./sec., $Re_g = 180397$, $Pr_\ell = 8.03$, $T'_o = 173.3^\circ$ F, $T'_w = 153.3^\circ$ F, $W_{air_o} = 0.01$, $Sc_g = 0.537$

z' in ft.	R = 0.0				R = 0.45				R = 0.75			
	U	V	T	C	U	V	T	C	U	V	T	C
2.645	1.013	0.00000	1.000	0.0100	1.013	-0.00009	1.000	0.0100	1.013	-0.00016	1.000	0.0100
6.209	1.020	0.00000	1.000	0.0100	1.020	0.00002	1.000	0.0100	1.020	0.00004	1.000	0.0100
15.353	0.997	0.00000	1.000	0.0100	0.997	0.00005	1.000	0.0100	0.997	0.00008	1.000	0.0102

$\frac{p'-p'_o}{\rho'_{j+1,o}\bar{u}'^2}$	R = 0.90				R = 0.9525				Interface			
	U	V	T	C	U	V	T	C	R	U	T	C
-0.00462	1.006	-0.00018	0.999	0.0107	0.907	-0.00013	0.987	0.0144	0.99509	0.011	0.897	0.0275
0.00019	0.981	0.00007	0.997	0.0121	0.718	0.00017	0.974	0.0184	0.99312	0.013	0.889	0.0297
0.00523	0.885	0.00012	0.992	0.0152	0.564	0.00017	0.956	0.0231	0.99116	0.017	0.876	0.0331

Table 47. Velocity, Concentration and Temperature Profiles in the Vapor Phase: Ethanol Vapor and Air, $D' = 0.16667$ ft., $\bar{u}' = 25$ ft./sec., $Re_g = 45099$, $Pr_\ell = 8.03$, $T_o' = 173.3^\circ$ F, $T_w' = 163.3^\circ$ F, $W_{air_o} = 0.05$, $Sc_g = 0.537$

z' in ft.	R = 0.0				R = 0.45				R = 0.75			
	U	V	T	C	U	V	T	C	U	V	T	C
0.464	1.024	0.00000	1.000	0.0500	1.024	-0.00098	1.000	0.0500	1.024	-0.00163	1.000	0.0500
1.514	1.072	0.00000	1.000	0.0500	1.072	-0.00050	1.000	0.0500	1.072	-0.00084	1.000	0.0500
5.000	1.100	0.00000	1.000	0.0500	1.100	-0.00009	1.000	0.0500	1.090	-0.00014	0.998	0.0510
28.152	1.147	0.00000	1.000	0.0501	1.138	-0.00002	1.000	0.0516	0.943	0.00004	0.905	0.0650

$\frac{p'-p_o'}{\rho_{j+1,o}'\bar{u}'^2}$	R = 0.90				R = 0.96				Interface			
	U	V	T	C	U	V	T	C	R	U	T	C
-0.00026	1.022	-0.00194	0.994	0.0507	0.925	-0.00180	0.899	0.0564	0.99736	0.009	0.458	0.0720
0.00350	0.976	-0.00071	0.958	0.0545	0.552	0.00012	0.731	0.0669	0.99631	0.011	0.392	0.0807
0.153	0.807	0.00008	0.865	0.0633	0.384	0.00025	0.597	0.0770	0.99525	0.016	0.341	0.0873
1.29	0.500	0.00013	0.602	0.0844	0.215	0.00015	0.384	0.0947	0.99314	0.031	0.239	0.1008

Table 48. Velocity and Temperature Profiles in the Liquid Phase: Ethanol Vapor and Air, $D' = 0.16667$ ft., $\overline{u}' = 25$ ft./sec., $Re_g = 45099$, $Pr_\ell = 8.03$, $T'_o = 173.3^\circ$ F, $T'_w = 163.3^\circ$ F, $Sc_g = 0.537$, $W_{air_o} = 0.05$

z′ in feet	R	Ux10^5	Vx10^9	T
0.464	0.999736	133	18	0.046
	0.998945	475	219	0.185
	0.997889	797	526	0.368
	0.997625	854	534	0.413
	0.997361	901	510	0.458
1.514	0.999736	138	2	0.028
	0.998945	494	27	0.112
	0.997889	837	108	0.224
	0.996834	1026	242	0.336
	0.996570	1050	285	0.364
	0.996306	1064	329	0.392
5.000	0.999736	171	1	0.019
	0.998945	625	13	0.076
	0.997889	1099	51	0.152
	0.996834	1420	116	0.228
	0.995778	1589	206	0.303
	0.995514	1607	232	0.322
	0.995250	1616	259	0.341
28.152	0.999472	465	1	0.018
	0.998417	1282	7	0.055
	0.996306	2459	42	0.128
	0.994195	3028	104	0.202
	0.993667	3075	124	0.220
	0.993139	3084	145	0.239

APPENDIX G

BINARY VAPOR CONDENSATION RESULTS

This appendix contains the numerical results described in Chapter V for the condensation of binary vapors.

Table 49. Condensation of Ethanol-Water Vapors, Summary of Results: $D' = 0.03825$ ft., $\bar{u}' = 25$ ft./sec., $Re_g = 4941$, $Pr_\ell = 4.17$, $Sc_g = 0927$, $Sc_\ell = 276$, $T'_{dp} = 206.25^\circ$ F, $T'_{bp} = 186.5^\circ$ F, a = Ethanol

W_{a_o}	$\Delta T'_{o_F}$	Fr_L	z' ft	$\frac{h'_m}{\Phi'}$	$\frac{2\delta'}{D'}$	Film Re	τ^*	T'_q $^\circ F$	wt. % cond.	Avg.wt. % a in liq.
0.25	14.25	354.7	0.0548	0.771	0.00633	71	1.307	198.3	4.4	8.3
		74.0	0.263	0.347	0.01012	172	0.702	197.5	10.9	9.2
		21.6	0.900	0.199	0.01392	359	0.382	196.5	22.9	10.1
		10.4	1.870	0.142	0.01645	548	0.235	195.6	35.2	10.9
		5.0	3.883	0.098	0.01898	801	0.126	194.4	52.0	12.2

Table 50. Condensation of Ethanol-Water Vapors, Summary of Results: $D' = 0.03825$ ft., $\bar{u}' = 50$ ft./sec., $Re_g = 9882$, $Pr_\ell = 4.17$, $Sc_g = 0.927$, $Sc_\ell = 276$, $T'_{dp} = 206.25^\circ$ F, $T'_{bp} = 186.5^\circ$ F, a = Ethanol.

W_{a_o}	$\Delta T'$ °F	Fr_L	z' ft	$\frac{h'_m}{\Phi'}$	$\frac{2\delta'}{D'}$	Film Re	τ^*	T'_q °F	wt. % cond.	Ave.wt. % a in liq.
0.25	14.25	273.8	0.284	0.476	0.00958	23	1.783	198.1	7.1	8.6
		91.9	0.846	0.272	0.01341	43	1.130	197.5	13.4	9.2
		36.5	2.127	0.176	0.01724	73	0.711	196.8	23.1	9.8
		15.8	4.923	0.118	0.02107	117	0.413	195.7	37.5	10.8
		6.5	11.875	0.073	0.02490	180	0.195	193.9	58.3	12.7

Table 51. Condensation of Ethanol-Water Vapors, Summary of Results: $D' = 0.03825$ ft., $\bar{u}' = 100$ ft./sec., $Re_g = 19763$, $Pr_\ell = 4.17$, $Sc_g = 0.927$, $Sc_\ell = 276$, $T'_{dp} = 206.25^\circ$ F, $T'_{bp} = 186.5^\circ$ F, a = Ethanol

W_{a_o}	$\Delta T'$ °F	Fr_L	z' ft	$\frac{h'_m}{\Phi'}$	$\frac{2\delta'}{D'}$	Film Re	τ^*	T'_q °F	wt. % cond.	Ave. wt. % a in liq.
0.25	10.0	341.4	0.910	0.416	0.0108	41.8	2.806	200.6	6.5	6.6
		185.7	1.674	0.301	0.0135	59.3	2.220	200.1	9.2	7.0
		58.9	5.278	0.167	0.0189	112.2	1.373	199.5	17.6	7.5
		35.1	8.859	0.129	0.0216	149.5	1.085	199.2	23.5	7.8
		21.3	14.627	0.100	0.0243	195.6	0.848	198.7	31.0	8.2
0.25	14.25	691.4	0.450	0.556	0.0095	39.2	3.840	199.0	6.1	7.8
		230.7	1.347	0.307	0.0142	72.7	2.483	198.1	11.3	8.6
		92.3	3.367	0.193	0.0190	122.0	1.620	197.5	19.1	9.1
		41.0	7.582	0.130	0.0237	193.3	1.035	196.7	30.4	9.9
		18.9	16.402	0.088	0.0285	292.2	0.595	195.5	46.4	11.0
0.25	24.25	782.8	0.397	0.531	0.0109	61.7	4.879	194.7	9.6	11.7
		223.4	1.391	0.277	0.0174	127.3	2.833	194.4	19.9	12.3
		117.9	2.637	0.203	0.0217	184.9	1.900	193.7	28.9	12.8
		66.0	4.708	0.155	0.0261	259.1	1.191	192.8	40.7	13.7
		38.2	8.135	0.119	0.0304	354.8	0.629	191.6	56.1	15.0
0.25	29.25	833.2	0.373	0.541	0.0110	73.1	5.838	193.4	11.5	13.2
		357.7	0.869	0.350	0.0154	120.1	4.112	193.4	18.8	13.5
		192.4	1.616	0.258	0.0198	172.6	2.740	193.0	27.0	13.8
		109.6	2.837	0.197	0.0242	239.2	1.775	192.3	37.5	14.4
		64.9	4.787	0.154	0.0286	323.9	1.034	191.3	51.0	15.4
0.25	34.25	1421.7	0.219	0.724	0.0088	64.0	8.411	192.9	10.1	14.2
		557.6	0.557	0.444	0.0133	112.8	5.908	192.7	17.7	14.4
		298.4	1.041	0.325	0.0178	162.4	3.888	192.7	25.5	14.4
		172.7	1.799	0.248	0.0222	221.8	2.535	192.0	34.7	14.9
		102.9	3.021	0.193	0.0267	297.8	1.582	191.2	46.7	15.6

Table 52. Condensation of Ethanol-Water Vapors, Summary of Results: $D' = 0.03825$ ft., $Pr_\ell = 4.17$, a = Ethanol, $W_{a_o} = 0.50$, $Sc_g = 0.762$, $Sc_\ell = 276$, $T'_{dp} = 197.2^\circ$ F, $T'_{bp} = 179.9^\circ$ F, $\Delta T' = 25.2^\circ$ F.

$\bar{u}'$ ft./sec.	Re_g	Fr_L	z' ft.	$\frac{h'_m}{\Phi'}$	$\frac{2\delta'}{D'}$	Film Re	τ^*	T'_q $^\circ$F	Ave. wt. % a cond.	Ave. wt. % a in liq.
50	12027	210.7	0.369	0.321	0.0120	44	2.156	182.2	11.7	38.4
		93.5	0.831	0.219	0.0159	73	1.419	181.9	19.7	39.1
		46.1	1.685	0.160	0.0199	115	0.883	181.6	31.0	40.3
		24.4	3.182	0.123	0.0239	172	0.480	181.1	46.9	42.0
		13.6	5.699	0.097	0.0279	249	0.164	180.5	68.6	44.4
100	24054	529.7	0.587	0.353	0.0118	70	4.449	182.3	9.3	38.0
		232.4	1.337	0.232	0.0166	118	3.036	182.2	15.8	38.2
		116.7	2.664	0.167	0.0213	181	2.034	182.0	24.3	38.8
		63.1	4.929	0.126	0.0261	264	1.295	181.6	35.6	40.0
		35.9	8.651	0.099	0.0308	374	0.717	181.2	50.8	41.7

Table 53. Condensation of Ethanol-Water Vapors, Summary of Results: $D' = 0.03825$ ft., $\bar{u}' = 100$ ft./sec., $Re_g = 30{,}726$, $Pr_\ell = 4.17$, $Sc_g = 0.596$, $Sc_\ell = 276$, $T'_{dp} = 180.9^\circ$ F, $T'_{bp} = 175.5^\circ$ F, a = Ethanol

W_{a_o}	$\Delta T'$ $^\circ F$	Fr_L	z' ft	$\frac{h'_m}{\Phi'}$	$\frac{2\delta'}{D'}$	Film Re	τ^*	T'_q $^\circ F$	wt. % cond.	Ave.wt. % a in liq.
0.75	5.9	654.0	0.475	0.672	0.00702	22.0	4.250	177.4	2.3	63.9
		275.5	1.128	0.410	0.01053	38.8	2.783	177.3	4.0	64.5
		121.9	2.549	0.266	0.01404	64.0	2.033	177.3	6.7	64.9
		59.2	5.266	0.187	0.01755	100.2	1.570	177.2	10.4	65.4
		31.1	10.008	0.141	0.02106	149.5	1.240	177.1	15.6	66.0
0.75	15.9	421.7	0.737	0.552	0.01348	96.0	4.594	176.2	10.0	70.9
		148.4	2.095	0.323	0.02022	182.0	2.732	176.2	19.1	71.3
		63.4	4.904	0.218	0.02696	307.7	1.581	176.0	32.4	71.9
		38.6	8.056	0.177	0.03146	421.1	1.008	175.9	44.5	72.6
		24.5	12.665	0.147	0.03595	563.2	0.526	175.8	59.9	73.1

Table 54. Condensation of Benzene-Toluene Vapors, Summary of Results: $D' = 0.03825$ ft., $\bar{u}' = 2$ ft./sec., $Re_g = 2270$, $Pr_\ell = 4.11$, $Sc_g = 0.633$, $Sc_\ell = 8.79$, $T'_{dp} = 193.1^\circ$ F, $T'_{bp} = 184.7^\circ$ F, a = Toluene

W_{a_o}	$\Delta T'$ °F	Fr_L	z' ft	$\frac{h'_m}{\Phi'}$	$\frac{2\delta'}{D'}$	Film Re	τ^*	T'_q °F	wt. % cond.	Ave. wt. % a in liq.
0.25	10.0	8.353	0.0149	0.617	0.00541	3.1	0.145	188.2	4.6	33.6
		3.654	0.0340	0.466	0.00676	5.3	0.113	188.0	7.9	33.1
		1.644	0.0756	0.360	0.00811	9.0	0.086	187.8	13.6	32.6
		0.843	0.1475	0.293	0.00945	14.2	0.060	187.5	21.7	32.0
		0.467	0.2662	0.244	0.01081	21.1	0.037	187.2	32.7	31.3

Table 55. Condensation of Benzene-Toluene Vapors, Summary of Results: $D' = 0.03825$ ft., $\bar{u}' = 25$ ft./sec., $Re_g = 28378$, $Pr_\ell = 4.11$, $Sc_g = 0.633$, $Sc_\ell = 8.79$, $T'_{dp} = 193.1^\circ$ F, $T'_{bp} = 184.7^\circ$ F, a = Toluene

W_{a_o}	$\Delta T'$ °F	Fr_L	z' ft	$\frac{h'_m}{\Phi'}$	$\frac{2\delta'}{D'}$	Film Re	τ^*	T'_q °F	wt. % cond.	Ave.wt. % a in liq.
0.25	5.0	91.52	0.212	0.423	0.00794	15.2	1.027	190.2	1.8	38.2
		14.63	1.327	0.191	0.01270	43.2	0.530	189.8	5.1	37.4
		5.51	3.526	0.129	0.01588	77.4	0.383	189.6	9.3	36.8
		2.37	8.200	0.091	0.01906	127.8	0.285	189.3	15.4	36.3
		1.10	17.643	0.066	0.02223	197.5	0.213	189.1	23.9	35.7
0.25	10.0	72.09	0.269	0.364	0.01057	33.1	1.133	188.5	3.9	34.2
		15.83	1.227	0.204	0.01586	84.5	0.674	188.1	10.1	33.3
		5.03	3.863	0.136	0.02115	177.8	0.394	187.6	21.5	32.2
		1.96	9.910	0.098	0.02643	326.7	0.195	187.1	39.9	30.9
		1.12	17.335	0.079	0.02996	464.3	0.095	186.7	57.3	29.9
0.25	20.0	54.12	0.359	0.329	0.01377	78.7	1.747	186.8	9.4	30.2
		24.02	0.809	0.246	0.01771	132.6	1.202	186.6	15.9	29.8
		11.98	1.621	0.194	0.02164	209.2	0.801	186.4	25.3	29.3
		6.50	2.989	0.158	0.02558	314.7	0.496	186.2	38.3	28.6
		3.77	5.149	0.132	0.02951	454.5	0.248	185.9	55.9	28.0
0.25	30.0	144.61	0.134	0.481	0.01053	63.9	3.708	186.3	7.6	28.9
		41.89	0.464	0.305	0.01685	139.7	1.984	186.0	16.8	28.3
		15.13	1.284	0.210	0.02316	266.7	1.051	185.8	32.3	27.8
		8.44	2.302	0.172	0.02737	391.3	0.618	185.7	47.8	27.4
		5.03	3.865	0.145	0.03159	553.7	0.253	185.5	68.3	26.9

Table 56. Condensation of Benzene-Toluene Vapors, Summary of Results: $D' = 0.16667$ ft., $\bar{u}' = 25$ ft./sec., $Re_g = 123650$, $Pr_\ell = 4.11$, $Sc_g = 0.633$, $Sc_\ell = 8.79$, $T'_{dp} = 193.1^\circ$ F, $T'_{bp} = 184.7^\circ$ F, a = Toluene

W_{a_o}	$\Delta T'$ °F	Fr_L	z' ft	$\frac{h'_m}{\Phi'}$	$\frac{2\delta'}{D'}$	Film Re	τ^*	T'_q °F	wt. % cond.	Ave. wt. % a in liq.
0.25	10.0	19.10	1.017	0.231	0.00358	79	0.676	188.8	2.1	35.0
		10.46	1.858	0.188	0.00418	118	0.537	188.4	3.2	34.0
		5.95	3.266	0.155	0.00478	170	0.459	188.1	4.7	33.3
		2.59	7.487	0.117	0.00597	296	0.359	187.9	8.1	32.8
		1.17	16.660	0.090	0.00716	509	0.273	187.7	14.1	32.3

Table 57. Condensation of Benzene-Toluene Vapors, Summary of Results: $D' = 0.03825$ ft., $Pr_\ell = 4.11$, a = Toluene, $W_{a_o} = 0.50$, $Sc_g = 0.621$, $Sc_\ell = 8.79$, $T'_{dp} = 207.3^\circ$ F, $T'_{bp} = 195.8^\circ$ F, $\Delta T' = 27.3^\circ$ F.

$\bar{u}'$ ft./sec.	Re_g	Fr_L	z' ft.	$\frac{h'_m}{\Phi'}$	$\frac{2\delta'}{D'}$	Film Re	τ^*	T'_q °F	wt. % cond.	Ave.wt. % a in liq.
25	28967	142.0	0.137	0.451	0.0105	58	3.197	199.0	6.7	56.4
		37.5	0.518	0.274	0.0168	132	1.779	198.7	15.5	55.9
		13.2	1.472	0.187	0.0231	257	0.934	198.4	30.5	55.3
		7.2	2.683	0.152	0.0273	382	0.547	198.1	45.7	54.7
		4.2	4.581	0.127	0.0315	545	0.227	197.6	66.0	53.9
100	115867	459.1	0.677	0.365	0.0134	226	9.386	199.0	6.6	56.6
		114.7	2.710	0.207	0.0234	519	5.293	198.5	15.2	55.5
		57.4	5.414	0.156	0.0300	784	3.549	198.3	23.0	55.2
		30.9	10.043	0.122	0.0367	1141	2.347	198.1	33.6	54.8
		17.8	17.451	0.099	0.0434	1610	1.406	197.9	47.7	54.3
200	231734	621.5	2.000	0.297	0.0168	543	14.86	199.0	7.9	56.5
		239.7	5.187	0.198	0.0252	948	10.10	198.5	13.9	55.5
		116.6	10.667	0.145	0.0336	1434	6.86	198.2	21.0	55.0
		84.9	14.645	0.127	0.0377	1722	5.66	198.2	25.2	54.8
		62.9	19.755	0.112	0.0419	2050	4.66	198.1	30.0	54.7

Table 58. Condensation of Benzene-Toluene Vapors, Summary of Results: $D' = 0.03825$ ft., $\bar{u}' = 25$ ft./sec., $Re_g = 29581$, $Pr_\ell = 4.11$, $Sc_g = 0.608$, $Sc_\ell = 8.79$, $T'_{dp} = 219.9^\circ$ F, $T'_{bp} = 210.5^\circ$ F, a = Toluene

W_{a_o}	$\Delta T'_{o_F}$	Fr_L	z' ft	$\frac{h'_m}{\Phi'}$	$\frac{2\delta'}{D'}$	Film Re	τ^*	T'_{q_F}	wt. % cond.	Ave.wt. % a in liq.
0.75	10.0	22.43	0.866	0.256	0.0153	80	0.824	216.5	9.2	83.6
		10.98	1.768	0.207	0.0187	133	0.638	216.4	15.4	83.4
		7.98	2.434	0.188	0.0204	167	0.545	216.3	19.3	83.2
		5.90	3.291	0.171	0.0221	206	0.457	216.1	23.9	83.0
		4.43	4.385	0.156	0.0238	250	0.375	215.9	29.1	82.8

Table 59. Velocity, Temperature, and Concentration Profiles in the Liquid Phase: Ethanol-Water, $D' = 0.03825$ ft., $\overline{u}' = 100$ ft./sec., $Re_g = 19763$, $Pr_\ell = 4.17$, $W_{EtOH_o} = 0.25$, $T'_o = T'_{dp} = 206.25^\circ$ F, $T'_w = 182^\circ$ F, $Sc_g = 0.927$, $Sc_\ell = 276$, C = Weight fraction ethanol, q = interface.

z′ in feet	R	Ux10^5	Vx10^{10}	T	C
0.397	0.997829	163	-225	0.105	0.11386
	0.995658	314	-897	0.210	0.11416
	0.993487	456	-2012	0.315	0.11516
	0.991316	586	-3563	0.419	0.11747
	0.989145_q	706	-5337	0.524	0.12122
1.391	0.997829	144	-18	0.063	0.12147
	0.993487	401	-166	0.191	0.12169
	0.991316	514	-296	0.254	0.12201
	0.986974	707	-671	0.382	0.12316
	0.982632_q	857	-1181	0.510	0.12503
2.637	0.997829	143	1	0.048	0.12579
	0.991316	510	16	0.193	0.12623
	0.986974	700	36	0.290	0.12729
	0.982632	847	63	0.387	0.12926
	0.978290_q	951	95	0.484	0.13232
4.708	0.997829	148	5	0.037	0.13268
	0.991316	527	79	0.148	0.13312
	0.986974	727	178	0.223	0.13418
	0.982632	883	317	0.297	0.13614
	0.973948_q	1065	709	0.447	0.14338
8.135	0.997829	156	5	0.028	0.14360
	0.991316	560	77	0.112	0.14406
	0.982632	948	308	0.225	0.14714
	0.973948	1162	695	0.338	0.15465
	0.969606_q	1204	943	0.395	0.16035

Table 60. Velocity, Concentration and Temperature Profiles in the Vapor Phase: Ethanol-Water, $D' = 0.03825$ ft., $\bar{u} = 100$ ft./sec., $Re_g = 19{,}763$, $Pr_\ell = 4.17$, $T'_o = 206.25^\circ$ F, $T'_w = 182^\circ$ F, $W_{EtOH_o} = 0.25$, $Sc_g = 0.927$, $Sc_\ell = 276$, C = weight fraction ethanol.

	R = 0.0				R = 0.45				R = 0.75			
z′ in ft.	U	V	T	C	U	V	T	C	U	V	T	C
0.397	1.032	0.00000	1.000	0.250	1.032	0.00007	1.000	0.250	1.029	0.00013	0.999	0.251
1.391	0.975	0.00000	1.000	0.250	0.975	0.00023	1.000	0.250	0.935	0.00041	0.984	0.266
2.637	0.918	0.00000	1.000	0.250	0.915	0.00020	1.000	0.251	0.812	0.00038	0.951	0.294
4.708	0.830	0.00000	1.000	0.251	0.814	0.00019	1.000	0.259	0.631	0.00037	0.895	0.339
8.135	0.692	0.00000	1.000	0.258	0.640	0.00018	1.000	0.286	0.411	0.00032	0.828	0.400

$\frac{p'-p'_o}{\rho'_{j+1,o}\bar{u}^2}$	R = 0.84				R = 0.93				Interface		
	U	V	T	C	U	V	T	C	R	U	T
-0.0312	0.993	0.00023	0.986	0.263	0.692	0.00083	0.862	0.355	0.98915	0.0071	0.524
0.0296	0.813	0.00053	0.928	0.310	0.440	0.00068	0.739	0.432	0.98263	0.0086	0.510
0.0892	0.643	0.00048	0.861	0.357	0.296	0.00055	0.661	0.476	0.97829	0.0095	0.484
0.1735	0.456	0.00042	0.781	0.410	0.184	0.00044	0.584	0.517	0.97395	0.0106	0.447
0.2851	0.272	0.00035	0.694	0.470	0.098	0.00034	0.502	0.559	0.96961	0.0120	0.395

Table 61. Velocity, Temperature, and Concentration Profiles in the Liquid Phase: Benzene-Toluene, $D' = 0.03825$ ft., $\bar{u}' = 25$ ft./sec., $Re_g = 28967$, $Pr_\ell = 4.11$, $W_{Tol_o} = 0.50$, $T'_o = T'_{dp} = 207.3^\circ$ F, $T'_w = 180^\circ$ F, $Sc_g = 0.621$, $Sc_\ell = 8.79$, C = Weight fraction toluene, q = Interface

z′ in feet	R	Ux10^5	Vx10^{10}	T	C
0.137	0.997902	521	-843	0.139	0.56390
	0.995805	995	-3381	0.279	0.56387
	0.993707	1418	-7627	0.419	0.56380
	0.991610	1792	-13599	0.557	0.56365
	0.989512_q	2117	-20455	0.695	0.56343
0.518	0.995805	1008	389	0.172	0.55963
	0.991610	1817	1553	0.344	0.55958
	0.989512	2148	2422	0.430	0.55953
	0.985317	2659	4733	0.601	0.55935
	0.983219_q	2840	6083	0.687	0.55923
1.472	0.995805	1137	517	0.122	0.55291
	0.989512	2470	3240	0.306	0.55285
	0.985317	3110	6363	0.428	0.55275
	0.983219	3355	8318	0.490	0.55268
	0.976926_q	3790	15641	0.673	0.55235
2.683	0.997902	654	94	0.051	0.54689
	0.991610	2320	1503	0.203	0.54686
	0.983219	3845	6035	0.407	0.54669
	0.976926	4464	11440	0.560	0.54640
	0.972731_q	4625	15913	0.661	0.54611
4.580	0.995805	1395	266	0.086	0.53944
	0.989512	3117	1666	0.215	0.53940
	0.976926	5215	8108	0.474	0.53901
	0.972731	5513	11345	0.560	0.53875
	0.968536_q	5610	15066	0.646	0.53843

Table 62. Velocity, Concentration and Temperature Profiles in the Vapor Phase: Benzene-Toluene, $D' = 0.03825$ ft., $\bar{u}' = 25$ ft./sec., $Re_g = 28967$, $Pr_\ell = 4.11$, $T'_o = 207.3^\circ$ F., $T'_w = 180^\circ$ F, $W_{Tol_o} = 0.50$, $Sc_g = 0.621$, $Sc_\ell = 8.79$, C = Weight fraction toluene.

	R = 0.0				R = 0.45				R = 0.75			
z′ in ft.	U	V	T	C	U	V	T	C	U	V	T	C
0.137	0.976	0.00000	1.000	0.500	0.976	0.00101	1.000	0.500	0.976	0.00169	1.000	0.500
0.518	0.911	0.00000	1.000	0.500	0.911	0.00066	1.000	0.500	0.911	0.00110	1.000	0.500
1.472	0.778	0.00000	1.000	0.500	0.778	0.00058	1.000	0.500	0.775	0.00097	0.997	0.496
2.683	0.626	0.00000	1.000	0.500	0.626	0.00053	1.000	0.500	0.613	0.00089	0.988	0.487
4.580	0.407	0.00000	1.000	0.500	0.406	0.00049	1.000	0.497	0.379	0.00083	0.971	0.472

$\frac{p'-p'_o}{\rho'_{j+1,o}\bar{u}'^2}$	R = 0.84				R = 0.935				Interface		
	U	V	T	C	U	V	T	C	R	U	T
0.0307	0.976	0.00189	1.000	0.500	0.947	0.00220	0.986	0.488	0.98951	0.0212	0.695
0.1128	0.908	0.00124	0.997	0.496	0.757	0.00159	0.925	0.449	0.98322	0.0284	0.687
0.2771	0.746	0.00112	0.978	0.480	0.476	0.00137	0.849	0.411	0.97693	0.0379	0.673
0.4521	0.561	0.00103	0.952	0.462	0.306	0.00118	0.803	0.390	0.97273	0.0463	0.661
0.6748	0.324	0.00094	0.918	0.441	0.162	0.00102	0.758	0.369	0.96854	0.0561	0.646

LITERATURE CITED

1. E. F. Carpenter and A. P. Colburn, "The Effect of Vapor Velocity on Condensation Inside Tubes," Proceedings of the General Discussion on Heat Transfer, The Institution of Mechanical Engineers and The American Society of Mechanical Engineers, July, 1951, p. 20.

2. W. Nusselt, "Die Oberflächenkondensation des Wasserdampfes," Zeitschrift des Vereinen Deutscher Ingeinieure, 60, 541, 569 (1916).

3. M. Jakob, Heat Transfer, Vol. I, John Wiley and Sons, Inc., New York, 1949.

4. H. Hartmann,"Wärmeübergang bei der Kondensation strömender Sattdämpfe in senkrechten Rohren," Chemie Ingenieur Technik, 33, 343 (1961).

5. W. M. Rohsenow, J. H. Webber, and A. T. Ling,"Effect of Vapor Velocity on Laminar and Turbululent-Film Condensation," Transactions of the American Society of Mechanical Engineers, 78, 1637 (1956).

6. A. H. Shapiro, The Dynamics and Thermodynamics of Compressible Fluid Flow, Vol. II, The Ronald Press Company, New York, 1954,p. 1131.

7. D. C. Cronauer, "Condensation of Mixed Vapors in a Vertical Tube," Carnegie Institute of Tehnology, Ph.D. Thesis, 1961.

8. R. B. Bird, W. E. Stewart, and E. N. Lightfoot, Transport Phenomena, John Wiley and Sons, Inc., New York, 1960.

9. S. J. Friedman and C. O. Miller, "Liquid Films in the Viscous Flow Region," Industrial and Engineering Chemistry, 33, 885 (1941).

10. C. Stirba and D. M. Hurt, "Turbulence in Falling Liquid Films," Journal of the American Institute of Chemical Engineers, 1, 178 (1955).

11. R. E. Emmert and R. L. Pigford, "Interfacial Resistance; A Study of Gas Absorption in Falling Liquid Films," Chemical Engineering Progress; 50, 87 (1954).

12. C. M. Cooper, T. B. Drew, and W. H. McAdams, "Isothermal Flow of Liquid Layers," Industrial and Engineering Chemistry, 26, 428 (1934).

13. W. L. McCabe and J. C. Smith, Unit Operations of Chemical Engineering, McGraw-Hill Book Company, Inc., New York, 1956, p. 477.

14. W. M. Rohsenow, "Heat Transfer and Temperature Distribution in Laminar-Film Condensation," Transactions of the American Society of Mechanical Engineers, 78, 1645 (1956).

15. E. M. Sparrow and J. L. Gregg, "A Boundary-Layer Treatment of Laminar-Film Condensation," Journal of Heat Transfer, Transactions of the American Society of Mechanical Engineers, Series C, 81, 13 (1959).

16. J. C. Y. Koh, E. M. Sparrow, and J. P. Hartnett, "The Two Phase Boundary Layer in Laminar Film Condensation," International Journal of Heat and Mass Transfer, 2, 69 (1961).

17. T. Mizushina, M. Nakajima, and T. Oshima, "Study on Cooler Condensers for Gas-Vapour Mixtures," Chemical Engineering Science, 13, 7 (1960).

18. R. C. Cairns, "The Condensation of Vapour from Gas-Vapour Mixtures," Chemical Engineering Science, 2, 127 (1953).

19. W. D. Baasel, "The Application of Boundary-Layer Theory to the Condensation of Vapors From Noncondensing Gases," Cornell University, Ph.D. Thesis, 1962.

20. D. F. Othmer, "The Condensation of Steam," Industrial and Engineering Chemistry, 21, 576 (1929).

21. A. P. Colburn and O. A. Hougen, "Design of Cooler Condensers for Mixtures of Vapors with Noncondensing Gases," Industrial and Engineering Chemistry, 26, 1178 (1934).

22. J. C. Smith, "Condensation of Vapors from Noncondensing Gases," Industrial and Engineering Chemistry, 34, 1248, 1495 (1942).

23. B. Hulden, "Condensation of Vapours from Gas-Vapor Mixtures. An approximate Method of Design," Chemical Engineering Science, 7, 60 (1957).

24. E. M. Sparrow and S. H. Lin, "Condensation Heat Transfer in the Presence of a Noncondensable Gas," Journal of Heat Transfer, Transactions of the American Society of Mechanical Engineers, Series C, 86, 430 (1964).

25. W. D. Baasel and J. C. Smith,"A Mathematical Solution for the Condensation of Vapors from Noncondensing Gases in Laminar Flow inside Vertical Cylinders," Journal of the American Institute of Chemical Engineers, 9, 826 (1963).

26. A. P. Colburn and T. B. Drew, "The Condensation of Mixed Vapors," Transactions of the American Institute of Chemical Engineers, 33, 197 (1937).

27. A. P. Colburn, "Problems in Design and Research on Condensation of Vapours and Vapour Mixtures," Clayton Lecture, Proceedings of the General Discussion of Heat Transfer, The Institution of Mechanical Engineers and the Americal Society of Mechanical Engineers, July, 1951, p. 1.

28. J. P. van Es and P. M. Heertjes, "On the Condensation of a Vapour of a Binary Mixture in a Vertical Tube," Chemical Engineering Science, 5, 217 (1956).

29. D. Q. Kern, Process Heat Transfer, McGraw-Hill Book Company, Inc. New York, 1950.

30. W. H. McAdams, Heat Transmission 3rd Edition, McGraw-Hill Book Company, Inc., New York, 1954.

31. G. G. Haselden and W. A. Platt, "Heat Transfer Accompanying the Condensation of Mixed Vapours," British Chemical Engineering, 5, 37 (1960).

32. J. L. Wallace and A. W. Davison, "Condensation of Mixed Vapors," Industrial and Engineering Chemistry, 30, 948 (1938).

33. B. S. Pressburg and J. B. Todd, "Heat Transfer Coefficients for Condensing Organic Vapors of Pure Components and Binary Mixtures," Journal of the American Institute of Chemical Engineers, 3, 348 (1957).

34. V. V. Mirkovich and R. W. Missen,"A Study of the Condensation of Binary Vapors of Miscible Liquids," The Canadian Journal of Chemical Engineering, 41, 73 (1963).

35. W. J. Lee, "A Theoretical Study of Nonisothermal Flow and Heat Transfer in Vertical Tubes for Fluids with Variable Physical Properties," Georgia Institute of Technology, Ph.D. Thesis, 1962.

36. E. M. Sparrow and E. R. G. Eckert, "Effects of Superheated Vapor and Noncondensable Gases on Laminar Film Condensation," Journal of the American Institute of Chemical Engineers, 7, 473 (1961).

37. B. Wilkins, "Nonisothermal Laminar Flow and Heat Transfer with Temperature Dependent Physical Properties," Georgia Institute of Technology, Ph.D. Thesis, 1965.

38. M. Jakob, "Die Kondensation von Satt-und Heissdampf im Anfang einer Rohrstrecke," Centralblatt für die Zuckerindustrie, 42, 474 (1934).

39. F. G. Carpenter, "Heat Transfer and Pressure Drop for Condensing Pure Vapors Inside Vertical Tubes at High Vapor Velocities," University of Delaware, Ph.D. Thesis, 1948.

40. R. W. Hornbeck, W. T. Rouleau, and F. Osterle, "Laminar Entry Problem in Porous Tubes," The Physics of Fluids, 6, 1649 (1963).

41. W. H. Dorrance, Viscous Hypersonic Flow, McGraw-Hill Book Company, Inc., New York, 1962.

42. L. Lapidus, Digital Computation for Chemical Engineers, McGraw-Hill Book Company, Inc., New York, 1962.

43. O. A. Hougan, K. M. Watson, R. A. Ragatz, Chemical Process Principles, second edition, John Wiley and Sons, Inc., New York, 1959.

44. J. R. Bodoia, "The Finite Difference Analysis of Confined Viscous Flows," Carnegie Institute of Technology, Ph.D. Thesis, 1959.

45. J. W. Whatley, "Heat and Mass Transfer Effects in a Reacting Non-Newtonian Fluid in Laminar Flow in a Vertical Tube," Georgia Institute of Technology, Ph.D. Thesis, 1966.

46. P. D. Lax, "Difference Approximation to Solutions of Linear Differential Equations-An Operator Theoretical Approach," Lecture Series of the Symposium on Partial Differential Equations, University of Kansas Press, Lawrence, Kansas, 1960.

47. R. D. Richtmyer, Difference Methods for Initial Value Problems, Interscience Publishers, Inc., New York, 1964.

48. J. L. Shohet, "Errors and Stability of the Entry Problem Equations in Laminar Magnetohydrodynamic Flow," The Physics of Fluids, 6, 797 (1963).

49. P. Naur, "Report on the Algorithmic Language ALBOL 60," Communications of the Association for Computing Machinery, 3, 299 (1960).

50. D. D. McCracken, An Introduction to Algol Programming, John Wiley and Sons, New York, 1962.

51. Extended Algol Reference Manual for the Burroughs B-5000, Burroughs Corporation Bulletin 5000-21012, Detroit, Michigan, 1963.

52. E. W. Washburn, International Critical Tables of Numerical Data, Physics, Chemistry and Technology, Ed. Washburn, E. W., McGraw-Hill Book Company, Inc., New York, 1926.

53. J. H. Perry, Chemical Engineers' Handbook, Ed. Perry, J. H., McGraw-Hill Book Company, Inc., New York, 1963.

54. C. D. Hodgman, Handbook of Chemistry and Physics, Ed. Hodgman, C. D., Fortieth Edition, Chemical Rubber Publishing Company, Cleveland, 1958.

55. R. C. Reid and T. K. Sherwood, The Properties of Gases and Liquids, McGraw-Hill Book Company, Inc., New York, 1958.

56. O. A. Hougan, K. M. Watson, and R. A. Ragatz, Chemical Process Principles, Vol. 1, John Wiley and Sons, Inc., New York, 1954, p. 327.

57. J. Griswold and P. B. Stewart, "Rectification of Benzene-Toluene," Industrial and Engineering Chemistry, 39, 752 (1947).

VITA

William Arthur Burns, Jr. was born in Houston, Texas on November 25, 1939. He attended the Texas City, Texas, Dickinson, Texas, and Savannah, Georgia public school systems and graduated from Savannah High School in 1957.

He attended the Massachusetts Institute of Technology as a National Merit Scholar. He graduated in 1961 with a Bachelor of Science in Chemical Engineering. His Bachelor's thesis was entitled "Factors Affecting Ion Exchange Separation of Nickel and Cobalt." He helped finance his way through school with summer jobs in an oil refinery, a paint pigment plant, an asphalt roofing plant, and a molybdenum mine.

In the fall of 1961 he entered the Graduate Division of the Georgia Institute of Technology and received the Master of Science in Chemical Engineering in 1963. While at Georgia Tech he was recipient of the Dow Chemical Company Fellowship and the Ethyl Corporation Fellowship. In addition, he was a part time instructor in the School of Chemical Engineering, teaching junior level courses in Unit Operations and Transport Phenomena.

In August, 1961 he married the former Judith Warnock of Savannah, Georgia.